ANALYSIS AND OPTIMIZATION OF CRACKED COMPOSITE LAMINATES

by

Jianxiang Wang

Thesis presented for the Degree of
Doctor of Philosophy

School of Civil and Mining Engineering
The University of Sydney
AUSTRALIA

August, 1995

Dedicated to my parents

SYNOPSIS

This thesis deals with three inter-related topics. The first topic is concerned with the solution of a cracked transversely isotropic-orthotropic composite laminate of finite thickness. The transversely isotropic sublaminate which is sandwiched between orthotropic outer sublaminates contains a central crack or an array of periodically distributed cracks which are perpendicular to the interfaces between the two media. When the crack is wholly within the sublaminate, solutions are obtained for the stress intensity factors and the crack-induced interfacial stresses in three loading modes. When the crack tips touch the interfaces, the stress singularities are no longer the usual square-root type but are determined by the mechanical properties of the media. In this case, solutions are obtained for stress singularities and the corresponding stress intensity factors. The degenerate case when the outer sublaminates are also isotropic but dissimilar from the central sublaminate is also solved.

The second topic concerns the application of the above fracture mechanics solutions to crack problems of laminates composed of unidirectional fibre-reinforced composites. In view of the fact that unidirectional fibre-reinforced composites are prone to transverse cracking and that laminates made from unidirectional plies are prone to delamination, a cracked $[(\pm\theta)_{n_2}/(90^0)_{n_1}]_s$ symmetric laminate is studied with a view to examining the mutual constraining effect of plies on transverse cracking and the role of transverse cracks in causing delamination. The fracture mechanics framework is used to reveal the mechanisms behind the enhancement of the so-called *in situ* strengths of unidirectional laminae in multidirectional laminates. When the tips of a transverse crack touch the interfaces, the effect of the properties of the constraining sublaminates on the stress singularities and stress intensities at the tips of the crack is investigated.

The third topic is concerned with two types of optimum strength design of composites laminates. First, for a fibre-reinforced antisymmetric $[(\pm\theta^0)_{n_2}/(90^0)_{n_1}/(\mp\theta)_{n_2}]$ angle-ply laminate, the design variables of the laminate, viz. the ply angle θ and relative ply thickness, are chosen in such a way as to minimize the stress intensity factor at the crack tip in the $(90^0)_{n_1}$ lamina without exceeding the interfacial maximum principal tensile stress. Secondly, based upon the extensive fracture mechanics analysis (from topics one and two), a set of *in situ* strength parameters for unidirectional laminae in a multidirectional laminate is proposed. The *in situ* strength parameters take into account the influence of adjacent laminae and thickness of a particular lamina upon its transverse tensile and in-plane shear strengths when it is used in a multidirectional laminate. These strength parameters are then employed to calculate a stress norm which determines how close the stress state in the lamina is to its failure state. The stress norm is incorporated into the formalism of an optimization problem in order to enhance the load bearing capacity of multidirectional laminates.

PREFACE

This thesis is submitted to The University of Sydney, Australia, for the degree of Doctor of Philosophy. The work described in the thesis was carried out by the candidate during the years 1991 — 1995 in the School of Civil and Mining Engineering under the supervision of Professor Bhushan L. Karihaloo.

In accordance with the by-laws of The University of Sydney governing the requirements for the degree of Doctor of Philosophy, the candidate submits that the work presented in this thesis is original unless otherwise indicated in the text.

J Wang

Sydney
August, 1995

ACKNOWLEDGEMENTS

This work was carried out under the Equity and Merit Scholarship Scheme from AIDAB, Australia. The support of AIDAB is gratefully acknowledged.

I am indebted to my supervisor Professor B. L. Karihaloo for his inspiration, incisive guidance and friendliness throughout my studies. The support of the School of Civil and Mining Engineering, The University of Sydney, is deeply appreciated. I also like to take this opportunity to express my gratitude to the Institute of Mechanical Engineering, Aalborg University, Denmark, where I completed part of the work. The L. S. Hsu Memorial Scholarship awarded by The University of Sydney is warmly acknowledged. The supplementary scholarships by Professor B. L. Karihaloo have also been a great assistance to me.

Last, but never the least, I would like to thank my wife, Qingping, for her understanding, consistent support and love.

J Wang

Sydney
August, 1995

Contents

Synopsis I

Preface II

Acknowledgements III

Contents IV

List of Figures VIII

List of Tables XII

1 Introduction **1**

1.1 Introductory Remarks 1

1.2 Fibre-Reinforced Composite Materials 2

1.2.1 Transverse Cracking and Delamination 3

1.2.2 Lamination Effect and *In Situ* Strengths 5

1.3 Optimum Design of Laminates 6

1.4 Brief Outline of the Thesis 7

2 Optimum Strength Design of Composite Materials – A Review **10**

2.1 Failure Criteria of Composite Materials 10

2.2 Optimal Design with Respect to Failure Criteria 11

2.3 Optimal Design for Minimum Stress Irregularity 16

2.4 Optimum Stacking Sequence 18

2.5 Mixed-Variable Design 20

2.6 Concluding Remarks 21

3 Mathematical Preliminaries **23**

3.1 Introductory Remarks 23

3.2 Stress-Strain Relationships for a Transversely Isotropic Material 23

3.3 Fourier Transforms and Relevant Expressions 26
3.4 Basic Solution for an Infinite Plate with Crack 29
3.5 Basic Solution for an Isotropic Strip of Finite Thickness 33
3.6 Basic Solution for an Orthotropic Strip of Finite Thickness 35
3.7 Elements of Lamination Theory 38
3.7.1 Stress-Strain Relations of Unidirectional Lamina 39
3.7.2 Calculation of In-Plane Laminate Stresses 41
3.8 Elements of Optimization Techniques 44

4 Composite Laminate with Intralaminar Crack **48**
4.1 Introductory Remarks 48
4.2 Boundary-Value Problem for a Composite Laminate with a Single Crack 49
4.3 Solution for Opening Mode I 51
4.4 Solution for In-Plane Shear Mode II 60
4.5 Solution for Anti-Plane Shear Mode III 65
4.6 Solution for a Composite Laminate with Multiple Cracks 67
4.6.1 Solution for Mode I 67
4.6.2 Solution for Mode III 72
4.6.3 Remarks on Boundary and Symmetry Conditions 74

5 Composite Laminate with Interlaminar Crack **75**
5.1 Introductory Remarks 75
5.2 Solution for Mode I 77
5.2.1 Solution of Boundary-Value Problem 77
5.2.2 Stress Intensity Factor 87
5.2.3 Degenerate Case 92
5.3 Solutions for Mode II and Mode III 93
5.3.1 Solution of Boundary-Value Problem 93
5.3.2 Stress Intensity Factors 98
5.3.3 Degenerate Case 99
5.4 Relation between Stress Intensity Factor and Crack Opening Displacement . . . 99

6 Multiple Cracking in Fibre-Reinforced Angle-Ply Composite Laminates **102**
6.1 Introductory Remarks 102
6.1.1 Transverse (Matrix) Cracks and Interfacial Delamination 102
6.2 Boundary-Value Problem and Solution 105
6.2.1 Stress Intensity Factor in Mode I 105

6.2.2 Interfacial Stresses . . . 111
6.3 Mode III Stress Intensity Factor for Multiple Cracks . . . 114
6.4 Accuracy of the Numerical Scheme and Conclusions . . . 116
6.4.1 Remarks on the Constraining Effect . . . 116
6.4.2 Accuracy of Numerical Solution of the Fredholm Integral Equation . . . 117

7 Interlaminar Cracking in Angle-Ply Laminates 119
7.1 Introductory Remarks . . . 119
7.2 Elastic Properties of Composite Laminates . . . 120
7.3 Mode I Problem . . . 120
7.4 Mode II and Mode III Problems . . . 126
7.5 Extrema of Stress Singularities . . . 130

8 Design of Cracked Composite Laminates Least Prone to Delamination 132
8.1 Introductory Remarks . . . 132
8.1.1 Transverse (Matrix) Cracks and Interfacial Delamination . . . 132
8.1.2 Constraining Effect in Composite Laminates . . . 134
8.2 Mathematical Model and Solution . . . 135
8.2.1 An Idealized Model of Cracked Angle-Ply Laminate . . . 135
8.3 Optimization Problem and Solution . . . 140
8.4 Multicriterion Optimization . . . 143

9 Optimum *In Situ* Strength Design of Composite Laminates 147
9.1 Introductory Remarks . . . 147
9.2 Development of *In Situ* Strength Theory . . . 149
9.2.1 Analysis of a Cracked Laminate . . . 149
9.2.2 Calculation of *In Situ* Strength Parameters . . . 157
9.2.3 Failure Criterion of Lamina in Laminates . . . 168
9.3 Optimum Design of Multidirectional Laminates . . . 169
9.3.1 Problem Formulation . . . 169
9.3.2 Treatment of Non-differentiability of *In Situ* Strength Parameters . . . 170
9.3.3 Sensitivity Analysis . . . 172
9.3.4 Design Examples . . . 173
9.3.5 Sensitivity of Optimum Design . . . 182
9.4 Concluding Remarks . . . 184

10 Conclusions 186

Bibliography 191

Appendices 203

A 203

A.1 Determination of the Unknown Functions in Mode I 203

A.2 Determination of the Unknown Functions in Mode II 210

B Solution of the Dual Integral Equations 213

C Stiffness Parameters and Their Gradients 216

D Expressions for M_i When β_i Are Complex Conjugate 220

E Finiteness of $\frac{d}{d\xi}\left[\frac{\Phi(\xi)}{\xi^{1/2}}\right]$ 222

F Behaviour of the Smoothing Function 225

List of Figures

3.1 A transversely isotropic elastic body. The isotropy prevails in the plane perpendicular to z-axis, represented by xy-plane 24
3.2 An infinitely large plate containing a crack 29
3.3 An infinitely long strip of finite thickness without a crack 34
3.4 A fibre-reinforced unidirectional lamina. The on-axis coordinate system is denoted by L and T, and the off-axis by x and y 39
3.5 A fibre-reinforced multidirectional laminate. θ_1 and θ_2 indicate longitudinal directions of two constituent laminae in the laminate 41
3.6 Cross-section of a fibre-reinforced multidirectional laminate, showing a geometric mid-plane 42

4.1 A cracked composite laminate, showing the laminate configuration (a), and the opening (b), in-plane shear (c), and anti-plane shear (d) modes of crack face loading. The central layer is transversely isotropic in xy-plane, whilst the upper and lower layers are orthotropic 50
4.2 A multi-cracked composite laminate and coordinate axes 68

6.1 An illustration of the formation of a transverse crack. What concerns us is the constraining effect on the crack propagation at stage (b) supplied by the constraining sublaminates on the two sides (After Nairn, 1989) 104
6.2 The cracked composite laminate and coordinate axes 106
6.3 Variation of $\Phi(1)$ with θ and λ/d for multiple cracks each of length $a/d = 0.7$. 109
6.4 Variation of $\Phi(1)$ with a/d and θ for a single crack 110
6.5 Variation of the mode I stress intensity factor with a/d and θ for a single crack for $b/d = 2.0$ 111
6.6 Normalized interfacial normal stress: (a) $\theta = 0^0$; (b) $\theta = 45^0$ 115
6.7 Variation of $\Omega(1)$ with θ and λ/d for multiple cracks each of length $a/d = 0.7$. 116

7.1 Mode I stress singularity at a crack tip terminating at an isotropic-orthotropic bimaterial interface as a function of the orthotropic ply angle θ for the four material combinations of Table 7.1 121
7.2 Variation of μ_I with the ply angle θ for the four material combinations of Table 7.1 122
7.3 Variation of $H_I(1)/(-\sigma)$ for materials 1 (a) and 2 (b). The curves for $\theta = 45^0$ and 90^0 are indistinguishable on the scale of the figure for material 2 124
7.4 Normalized stress intensity factors for materials 1 (a) and 2 (b) 125
7.5 Stress singularities in (a) mode II and (b) mode III 127
7.6 Variation of (a) μ_{II} and (b) μ_{III} with θ for the materials in Table 7.1 128
7.7 (a) Mode II and (b) mode III normalized stress intensity factor for material 1 . . 129

8.1 A cross-ply composite laminate under transverse loading. The dark "Z"-shaped lines show the transverse cracks and areas of interfacial delamination (After Liu *et al.*, 1993) 133
8.2 The composite laminate and coordinate axes. The central crack is well removed from the edges of the laminate 135
8.3 Values of $\Psi(1)$ and $F(a/d)$. Value of θ is indicated on the graph. $b/d = 2$ . . . 137
8.4 Crack-induced interfacial principal tensile stress normalized by τ for $a/d = 0.4$ 140
8.5 The largest interfacial principal tensile stress normalized by τ for $y/d = 0.0$ and $b/d = 2.0$ 141
8.6 Minimization of $\Psi(1)$: $(b/d)_{opt} = \overline{b}$ 143
8.7 Minimization of σ_T: $(b/d)_{opt} = \overline{b}$ 144
8.8 Contours of the objective functions $f_1(\mathbf{x}) = \sigma_T$, $f_2(\mathbf{x}) = F_{II}$ and $f_3(\mathbf{x}) = \overline{D}$ for $a/d = 0.4$. Arrows indicate the direction in which the functions increase. The Pareto optimal design corresponding to $\rho = 50$ is indicated by an asterisk $(*)$. Maxima and minima of the three objective functions considered in isolation are also shown. **A**: max f_1, **B**: min f_1; **C**: max f_2, **D**: min f_2, **E**: max f_3, **F**: min f_3 145

9.1 A cracked composite laminate, showing the laminate configuration (a), and the opening (b) and anti-plane shear (c) modes of crack face loading 150
9.2(a) Variation of F_I with b/d and θ for half crack length $a = 0.4d$ 152
9.2(b) Variation of F_{III} with b/d and θ for half crack length $a = 0.4d$ 153
9.3(a) Variation of F_I with d/b and θ for half crack length $a = 0.4b$ 155
9.3(b) Variation of F_{III} with d/b and θ for half crack length $a = 0.4b$ 155
9.4(a) Variation of the mode I stress intensity factor with half crack length a and θ for $b/d = 2.0$ 156

9.4(b) Variation of the mode III stress intensity factor with half crack length a and θ for $b/d = 2.0$ 156
9.5(a) Variation of F_t with relative crack length a/d and θ for $b/d = 2.0$ 161
9.5(b) Variation of F_s with relative crack length a/d and θ for $b/d = 2.0$ 161
9.6(a) Typical variation of F_t with θ ($a/d = 0.7$). The solid line represents the calculated values of F_I^0/F_I from eqn (9.14), and the dotted line the approximate expression (9.20) 162
9.6(b) Typical variation of F_s with θ ($a/d = 0.7$). The solid line represents the calculated values of F_{III}^0/F_{III} from eqn (9.15), and the dotted line the approximate expression (9.21) 162
9.7(a) Variation of $\mathcal{A}$ with d/a, and of A/N^B with N 165
9.7(b) Variation of $\mathcal{C}$ with d/a, and of C/N^D with N 165
9.8 An elongated elliptic intralaminar transverse crack in a laminate. The coordinate system follows that in Figure 9.1. The direction of fibres in the central lamina (transverse lamina) is parallel to z-axis. It is assumed that the crack in z-direction is much longer than that in x-direction (After Dvorak & Laws, 1987) 166
9.9 The laminate configuration. The in-plane loading shown represents the resultant forces over the thickness 174
9.10 Evolution of load factor k for a symmetric laminate of 4 ply angles during optimization for four loading cases: (a) $[N_1^0, N_2^0, N_6^0]^T = [200, 200, 0]^T$ kN/m; (b) [200,0,200]^T kN/m; (c) [400,200,0]^T kN/m; and (d) [200,200,200]^T kN/m . 176
9.11 Evolution of load factor k for a symmetric laminate of 5 ply angles during optimization for four loading cases: (a) $[N_1^0, N_2^0, N_6^0]^T = [250, 250, 0]^T$ kN/m; (b) [250,0,250]^T kN/m; (c) [500,250,0]^T kN/m; and (d) [250,250,250]^T kN/m . 176
9.12 The stress state (a) referred to as loading case d in Figures 9.10–9.11, 9.13–9.16 and Tables 9.1–9.9 is equivalent to the unidirectional tension (b) 177
9.13 Evolution of load factor k for a symmetric laminate of 6 ply angles during optimization for four loading cases: (a) $[N_1^0, N_2^0, N_6^0]^T = [300, 300, 0]^T$ kN/m; (b) [300,0,300]^T kN/m; (c) [600,300,0]^T kN/m; and (d) [300,300,300]^T kN/m . 179
9.14 Evolution of load factor k for a symmetric laminate of 7 ply angles during optimization for four loading cases: (a) $[N_1^0, N_2^0, N_6^0]^T = [350, 350, 0]^T$ kN/m; (b) [350,0,350]^T kN/m; (c) [700,350,0]^T kN/m; and (d) [350,350,350]^T kN/m . 179
9.15 Evolution of load factor k for a symmetric laminate of 8 ply angles during optimization for four loading cases: (a) $[N_1^0, N_2^0, N_6^0]^T = [400, 400, 0]^T$ kN/m; (b) [400,0,400]^T kN/m; (c) [800,400,0]^T kN/m; and (d) [400,400,400]^T kN/m . 181

9.16 Evolution of load factor k for a symmetric laminate when ply angles and thicknesses are design variables during optimization for four loading cases: (a) $[N_1^0, N_2^0, N_6^0]^T = [1000, 1000, 0]^T$ kN/m; (b) [1000,0,1000]^T kN/m; (c) [2000,1000,0]^T kN/m; and (d) [1000,1000,1000]^T kN/m 182

A1 Variation of $\delta_s \times 10^{-3}$ with $s\frac{d}{a}$ for the material in Table 6.1 when $\theta = 0^0$, $b/d = 2.0$ and $a/d = 0.7$. The dotted line denotes its exact asymptotic value when $s \to +\infty$ (A.40) 209

F1(a) Comparison of F and $\mathcal{F}$ when A=100 226
F1(b) Comparison of F and $\mathcal{F}$ near a corner when A=100 on a magnified scale 226
F2(a) Comparison of F and $\mathcal{F}$ when A=2000 227
F2(b) Comparison of F and $\mathcal{F}$ near a corner when A=2000 on a magnified scale . . . 227

List of Tables

6.1 Material properties 109
6.2 Accuracy of mode III geometry factor ($\theta = 90^0$ and $b/d = 2.0$) for a single crack in a finite strip 117
6.3 Accuracy of mode III geometry factor for multiple cracks in an infinite body . . 118

7.1 Material properties 120
7.2 Stiffnesses of the sublaminates for $\theta = 30^0$ 121
7.3 Accuracy of mode III geometry factor ($\theta = 90^0$) 130
7.4 Strongest and weakest stress singularities 131

8.1 Functional (fe) and gradient (ge) evaluations 142
8.2 Minimum metric function $F^{(\rho)}(\mathbf{x})$ with corresponding optimum microstructural variables $(\theta, b/d)$ for two crack lengths (a/d) and various exponents (ρ); the upper half for $a/d = 0.4$ and the lower for $a/d = 0.7$. The corresponding values of objective functions $f_1(\mathbf{x})$, $f_2(\mathbf{x})$ and $f_3(\mathbf{x})$ are also given 146

9.1 Summary of optimized ply angles in a symmetric laminate of 4 ply angles . . . 175
9.2 Summary of optimized ply angles in a symmetric laminate of 5 ply angles . . . 175
9.3 Summary of 6 optimized ply angles in symmetric laminate 178
9.4 Summary of 7 optimized ply angles in symmetric laminate 180
9.5 Summary of 8 optimized ply angles in symmetric laminate. The prescribed loadings $[N_1^0, N_2^0, N_6^0]^T$ are twice those of example (i) 180
9.6 Summary of optimized ply angles and thicknesses in symmetric laminate. The prescribed loadings $[N_1^0, N_2^0, N_6^0]^T$ are 5 times those of example (i) 183
9.7 Nearly-optimum ply angles in a symmetric laminate of 4 ply angles. The mathematically optimized ply angles are given in Table 9.1 183
9.8 Nearly-optimum ply angles in a symmetric laminate of 5 ply angles. The mathematically optimized ply angles are given in Table 9.2 184

9.9 Nearly-optimum ply angles and thicknesses in symmetric laminate. The prescribed loadings $[N_1^0, N_2^0, N_6^0]^T$ are 5 times those in example (i). The mathematically optimized ply angles and thicknesses are given in Table 9.6 184

Chapter 1

Introduction

1.1 Introductory Remarks

In this Thesis composite materials refer to those heterogeneous materials which are composed of more than two homogeneous solids. These materials are nonhomogeneous and macroscopically anisotropic. Particularly, we are concerned with those fibre-reinforced composite materials which have been widely used in various structures in civil, mechanical, aeronautical and aerospace engineering. The primary function of the composite materials used in structures or substructures in engineering applications is to carry loads safely and reliably.

In order to fulfill the requirements arising from modern industry, advanced composite materials of more subtle and complicated compositions than hitherto are being developed. These compositions are made possible by the achievements of chemical industry and improvements in manufacturing techniques. The diversity of the compositions raises two difficulties in the design and application of these materials. The first is that the analysis of the mechanical response of the nonhomogeneous and anisotropic composite materials is very complicated. The high strength and high stiffness of these advanced composite materials usually means that they are highly prone to cracking under loading, so that we inevitably have to solve complicated boundary-value problems of a cracked body. Moreover, the many interfacial areas between the constituent phases in a composite can be sources of defects but can also serve as crack arrestors, depending on how we design the microstructure of the composite. The second difficulty is that when there are so many choices of compositions available, the materials technologists are faced with the difficult task of designing these materials without any sound guidelines. They often resort to empirical rules of thumb or design the material to suit a specific application utilising one of the performance indicators, e.g. high strength. In order to exploit the full potential of composite materials in different applications, guidelines based upon sound mechanical and mathematical knowledge are needed to assist the materials technologist.

It is the primary aim of this Thesis to develop such guidelines based on the analysis of cracked laminates and on mathematical optimization techniques. We begin with a brief overview of the materials and of the techniques found in the literature confining ourselves to only those materials and techniques which will be needed in achieving the aim of the Thesis.

1.2 Fibre-Reinforced Composite Materials

A fibre-reinforced composite material is composed of scattered fine fibres embedded in a continuous matrix. Because of their high strength, high modulus and low mass, fibres act as reinforcement in the composite materials. Matrices used today are mainly plastics (epoxy, polyester and resin, etc.), metals and ceramics. Obviously, the unconstrained sparse fibres neither have firm shapes nor bear compressive and bending loads from the standpoint of engineering application, so matrices are needed to play the part of adhesive and constraint material to the fibres. On the other hand, matrix materials, such as plastics, ceramics etc., generally have low strength and modulus, as well as small strength to weight ratio. However, the composition of fibres and matrices makes new materials which demonstrate unique mechanical properties. More important is that the diversity of the composition forms makes it possible to design the material properties suitable for various objectives.

A fibre-reinforced composite is macroscopically nonhomogeneous and anisotropic in nature. In addition, there are interfacial areas between the matrix and fibres. Strictly speaking, the properties of the interfacial areas are different from those of the constituents and the overall composite. These factors make the accurate solution of a boundary-value problem of a composite structure quite tedious. Thus, when we concentrate on one aspect of the behaviour of the material, we have to resort to some simplification and idealization of the material properties. Although the bonding condition of the interfacial areas has an important bearing upon the mechanical properties of the composite, it will not be discussed in this Thesis. However, the essential fact that the interfacial area is weak and prone to cracking when subjected to tensile and shear stresses will be accepted without further elaboration.

Most of the fibre-reinforced composite materials are used in the form of laminates consisting of unidirectional laminae with different fibre orientations. They are widely used as plate and shell substructures because of their high strength to weight ratio. They are also used to make boats, yachts and other items. The unidirectional fibre-reinforced composite has the strongest stiffness and strength along the fibre direction but it is weak in its transverse direction. This anisotropy is a great advantage when it is exploited in the design of a multidirectional angle-ply laminate. By varying the fibre orientations and thicknesses of the laminae, the property of a laminate can be tailored to suit a specific purpose.

The research into the mechanical properties and the structural response of fibre-reinforced composite laminates can be generally divided into two areas: the stiffness-based analysis and the strength-based analysis. In the former area, the stiffness properties calculated by classical lamination theory (CLT) (Tsai & Hahn, 1980) are widely applied. They have been used in the prediction of the traditional indicators such as stiffnesses, buckling load, vibration parameters and so on. They are also exploited in the optimum design of composite laminates with respect to these properties. Higher order analytical theories considering the shear deformation along the thickness direction of the laminate have also been developed (Reddy, 1984; Reddy & Robbins, 1994).

In the area of strength prediction of fibre-reinforced composites, the situation is different. Because of the complexity of the compositions, the development of failure criteria has to face the multimodal nature of the failure forms. A unidirectional lamina has several failure modes depending on how it is loaded. These modes include matrix cracking, fibre-matrix shearing, fibre breakage, matrix compression failure, and fibre buckling (Chang *et al.*, 1991). The damage of a multidirectional laminate is characterized by those modes of the unidirectional laminae, as well as by interfacial delamination. When there are several failure modes, the stress redistribution after one or several failure modes and the interaction among them make the stress evaluation quite complicated. In order to study the load carrying capacity of the composite, it is necessary to trace the development of damage in it. Through an examination of the relationship between the imperfections and the macroscopic strength indicators, we can more accurately predict the load carrying capability of composite structures from the properties of the basic constituents or substructures. Another difficulty in predicting the strength of a multidirectional laminate arises from the influence of the laminate configuration on the basic strength properties of an individual unidirectional lamina. This lamination effect can play a positive or a negative role in determining the strength of the whole laminate. The understanding of lamination effect is also instructive in the design of the composite laminates. The work in this Thesis will focus on the stress analysis of fibre-reinforced laminates. This analysis will be used to judge the strength of the material through the establishment of relationships among the laminate configuration, the applied external loads and the stress field in the material. In view of the myriad of the damage forms in composite materials, we confine our attention to two of them only, and namely to the transverse cracking and the delamination. Thus, the strength and/or load carrying capacity of the laminates will be defined with respect to these two damage forms.

1.2.1 Transverse Cracking and Delamination

A fibre-reinforced unidirectional lamina is weak in the transverse direction when subjected to tensile or shear loading. As a result, laminae in multidirectional laminates often crack in the

transverse direction, especially when thick unidirectional laminae are used. In most laminates the first failure mode is transverse cracking of the laminae along fibre directions (Herakovich, 1982; Crossman & Wang, 1982; Talreja, 1987). The development of these transverse cracks results in the redistribution of the stresses in a laminate and reduces its stiffness. Transverse cracks also directly contribute to the delamination of plies. The eventual failure of a laminate is caused by extensive delamination and/or fibre breakage (Herakovich, 1982).

Because of the inherent weakness of fibre-reinforced composites in the transverse direction, microcracks are likely to occur in component laminae, possibly from the residual stress of processing and the debonding between the fibres and matrix or matrix cracking. Upon being loaded, the transverse cracks may also form at very low load levels or after only a few load cycles under fatigue loading. Therefore, it is recognized that the transverse cracking of the unidirectional laminae in a laminate originates as microcracks or inherent flaws, which propagate under increasing load until they reach the interfaces, resulting in the complete rupture of the laminae (Bailey *et al.*, 1979; Wang & Crossman, 1980; Bailey & Parvizi, 1981; Dvorak & Laws, 1987; etc.). Moreover, because the adjacent plies do not offer a strong constraint against the crack growth, the initial microcracks are most likely to form away from the interfaces so that they are wholly within the lamina at the early stage of loading. More details about the transverse cracking will be given in Chapters 6, 8 and 9.

The other damage mechanism, namely the delamination between constituent laminae, is the most common and fatal form of failure in laminates resulting in loss of both their strength and stiffness. Under compression, the delaminated sublaminates may buckle leading to overall failure of the laminate. The mechanism of delamination has been widely investigated both theoretically and experimentally (Wang, 1980; Crossman & Wang, 1982; Chatterjee *et al.*, 1984; Reddy *et al.*, 1984; O'Brien, 1985; Murri & Guynn, 1988; Kim, 1989; Fish & Lee, 1990; Liu *et al.* 1993 and Doxsee *et al.* 1993). The delamination often occurs at the free-edges of laminates and at the interface in front of a transverse lamina crack. As the free-edge effect, so also the transverse cracking in the laminae, can result in interfacial delamination (Crossman & Wang, 1982; Kim, 1989; Fish & Lee, 1990; Liu *et al.* 1993 and Doxsee *et al.* 1993). The severity of the free-edge induced delamination can be reduced by varying the stacking sequence and ply thickness. In $[0^0/\pm\theta^0]_s$ angle-ply laminates the free-edge induced stress singularity can be minimized or even eliminated (Christensen & DeTeresa, 1992).

It has been found for some composite laminates that when intralaminar transverse cracks approach the interfaces, they can cause delamination. Experimental observations show (Kim, 1989) that under tensile loading delamination in laminates, especially those containing 90^0 plies, is preceded by transverse cracks, and that its location is related to the location of cracks. When a laminate is subjected to transverse loading (perpendicular to the laminate plane), matrix

cracks in any one lamina also cause delamination. Liu *et al.* (1993) made detailed studies of the interaction between transverse cracking and delamination in composite laminates under transverse loading. Both experimental and analytical results showed that a transverse crack in 90^0 lamina perpendicular to the interfaces in a $[0^0_{n_2}/90^0_{n_1}]_s$ laminate resulted in interfacial delamination at the intersection of the crack tips and the interfaces between the 0^0 and 90^0 laminae. It was also concluded that the delamination induced by an intraply crack under shear loading is very unstable and catastrophic. Doxsee *et al.* (1993) studied the delamination of a $[0^0_4/90^0_4]_s$ laminate under transverse loading. It was shown that when there was a delamination starter, the transverse cracks along the fibre directions in 0^0 and 90^0 laminae even occurred before the delamination began to extend beyond the starter delamination. As the loading increased, the delamination occurred at the intersection of crack tip and interface.

1.2.2 Lamination Effect and *In Situ* Strengths

It has been widely observed in tests that the transverse tensile and shear strengths of a fibre-reinforced unidirectional lamina, when it is situated in an angle-ply laminate, are functions of the thickness of the lamina itself and the ply angles of its neighbouring laminae (Parvizi *et al.*, 1978; Flaggs & Kural, 1982; Crossman & Wang, 1982; Yamada & Sun, 1979; Chang & Chen, 1987). These strengths of a lamina in a laminate are different from (generally larger than) those measured by using a thick unidirectional laminate. As a consequence, it is recognized that the transverse and in-plane shear strengths of a lamina cannot be regarded as its intrinsic property (Flaggs & Kural, 1982; Chang & Chen, 1987). Because of this observation, the transverse and in-plane shear strengths of a unidirectional lamina are referred to as *in situ* strengths, when this lamina is situated in a laminate. Since this phenomenon occurs when a lamina is put into a multidirectional laminate, it is also considered to be a sort of lamination effect.

Experiments by Flaggs & Kural (1982) indicated that the transverse tensile strength of the 90^0 lamina in $[\pm\theta/90^0_{n_1}]_s$ laminates was a function of θ and n ($\theta = 0^0,\ 30^0,\ 60^0$; $n_1 = 1, 2, 4, 8$). When n_1 is small the strength could differ significantly from the one measured using a unidirectional $(90^0_{n_2})_s$ ($n_2 = 8$) lamina. It was also observed that the tensile strength decreased with θ. The shear strength of a lamina in cross-ply laminates was also observed to be a function of the thickness of the lamina (Yamada & Sun, 1979; Chang & Chen, 1987).

A comprehensive literature survey can be found in Chang & Lessard (1991). From experiments and the literature survey, two important features of the *in situ* strengths emerge, as was pointed by Chang & Lessard (1991): (1) as the thickness of a group of identical plies increases, the *in situ* strength of this group of plies will decrease; and (2) the ply orientation of an adjacent ply will strengthen a ply according to the "adjacent ply constraint" effect, as long as it is different from that of the ply under consideration.

Since the strengths of a unidirectional lamina form the basis of the failure criteria for general multidirectional laminates, much effort has been spent on the prediction of the failure condition for a lamina in cross- and angle-ply laminates (Parvizi *et al.*, 1978; Bailey *et al.*, 1979; Flaggs & Kural, 1982; Tan & Nuismer, 1989; Chang & Lessard, 1991). These works examined the conditions at which a through-thickness transverse crack appears in a unidirectional lamina in these laminates. They certainly predicted the correlation between the strengths and thickness and the properties of neighbouring laminae. However, these conditions have not been formulated in a manner suitable for a general strength calculation of multidirectional laminates. An exception is the set of concise formulae proposed by Chang & Lessard (1991) for calculating the *in situ* transverse and in-plane shear strengths of a unidirectional lamina in multidirectional laminates.

1.3 Optimum Design of Laminates

Composite materials are themselves a kind of optimum usage of constituent phases. The aim of designing a composite material is to take advantage of the merits of the constituent phases. Therefore, one advantage of composite materials over the traditional ones is that they can demonstrate certain novel mechanical properties which are desired in some specific engineering applications but which cannot be expected from their constituent phases alone.

As the development and application of composite materials were initiated by the needs of the aeronautical industry, the research on the optimum design of composite material structures also started from the airplane design field. In view of the fact that composite materials have high strength/weight ratio and offer wide tailoring possibilities, the early optimum design schemes mainly concentrated on the minimum weight design. The earliest attempt in composite optimization seems to be due to Foye (1968), who studied the minimum weight design of laminated materials for strength and membrane stiffness. In his design procedure, multiple in-plane loading conditions were considered, and a random search method was used to find ply orientation angles, such that the strength and stiffness requirements would be satisfied with the least number of plies. Another procedure for the optimization of the design of laminates was reported by Waddoups (1969). Minimum weight design was obtained by considering strength constraint under multiple distinct loading conditions. Either the Tsai-Hill or the maximum strain criterion was used as constraint. The search procedure for optimization was a grid technique. Since then, optimization techniques have been widely applied to the design of laminates with respect to weight and stiffness-based structural responses, such as buckling, frequency etc.

The minimum weight design of composite materials is a theme directly inherited from optimization of structures made of isotropic materials. The minimum weight design is just one of the many tailoring possibilities offered by composite materials. The methods used for

optimizing the design of isotropic structures with respect to weight, buckling strength, frequency etc., can also be used for structures made of anisotropic materials. Of course there are major differences in the choice of design variables and analysis techniques. The former does not present a major obstacle. The main difficulty arises from the latter. If the optimum design of the composite laminates stays only at the macro-level and does not include the micromechanical characteristics of the composite material itself, it is evident that the advantages of formal optimization techniques are brought to bear upon the design at a late stage (at the structural level) using basic units which are not optimally designed. As a matter of fact, response of a structure made out of a composite material is strongly influenced by the microstructure of the basic unit. It is the aim of this Thesis to unify the optimum design of the basic composite unit cell with that of the structural unit.

1.4 Brief Outline of the Thesis

The main body of original research in this Thesis is divided into two parts. The first part consisting of Chapters 4 and 5 presents solutions to the boundary-value problems of cracked composite laminates. Although these problems are motivated by the failure characteristics of fibre-reinforced composites, the solutions are of general nature. They are the extension of elastostatic solutions to crack problems in finite regions made up of dissimilar subregions. The second part consisting of Chapters 6 to 9 inclusive specializes the solutions obtained in the first part to fibre-reinforced composite laminates. The basic theoretical tools necessary in both parts of the Thesis are introduced in Chapter 3. A brief overview of the contents of various Chapters follows.

Chapter 2 gives a review of the published works on optimum design of composite laminates with respect to their strength. Although the optimization techniques have been extensively applied to the optimum design of laminates with respect to the stiffness-based properties, as was mentioned before, these works will not be reviewed in detail because of the scope of this Thesis. On the other hand, for the strength optimization which is based on stress analysis and failure criteria, a description of optimum strength design will be preceded by a brief overview of the available failure criteria for composites. A description will also be given of the optimum stacking sequence design of laminates and of the mixed-variable (integer-continuous, integer-discrete) design. These two topics remain particularly challenging and also of great practical significance.

In order not to interrupt the exposition in the main body of the Thesis, Chapter 3 presents some mathematical preliminaries essential to the work in this Thesis. In particular, a brief description of the application of Fourier transforms to crack problems and of the classical

lamination theory (CLT) is presented.

In the framework of linear elastic fracture mechanics (LEFM), basic solutions of a boundary-value problem for a cracked composite laminate of finite thickness will be given in Chapter 4. The composite laminate is made of three-sublaminates in which the central one is a transversely isotropic medium and outer ones are orthotropic. The solutions are obtained when the central layer contains a single crack, as well as a periodic distribution of cracks in all three modes of loading - modes I, II and III in the terminology of fracture mechanics.

The solutions obtained in Chapter 4 are extended in Chapter 5 to the cases where the crack tips touch the interfaces. In these cases the interfacial stress singularities and the corresponding *in situ* stress intensity factors are calculated, again under all three modes of loading. The degenerate case when the outer sublaminates are also isotropic, but dissimilar from the central sublaminate, is also discussed.

The general solutions obtained in Chapter 4 are specialized in Chapter 6 to study a multiple crack problem in fibre-reinforced composite laminates. Such cracking is often observed in experiments. The influence of the ply angles, thicknesses and the crack spacing upon the stress field is depicted.

Chapter 7 specializes the general solutions obtained in Chapter 5 to the fibre-reinforced composite laminates. The stress singularities and stress intensity factors in the three loading modes are calculated when the tips of the crack touch the interfaces. Their variations with the ply angle and thickness of the constraining sublaminates are depicted.

In Chapter 8, the variations of the stress intensity factor and the *crack-induced* interfacial stresses are examined in an angle-ply laminate under transverse shear loading and found to show opposite trends with respect to the ply angle. To resolve the conflict, an optimization problem is formulated with a view to minimizing the risk of crack propagation and of interfacial delamination in the laminate. The optimization problem is solved using nonlinear mathematical programming techniques.

Chapter 9 investigates first in detail the mechanisms of lamination effect and *in situ* strength in fibre-reinforced composite laminates. Based upon this investigation, a set of *in situ* strength parameters for unidirectional laminae in a multidirectional laminate is proposed. The *in situ* strength parameters take into account the influence of adjacent laminae and thickness of a particular lamina upon its transverse tensile and in-plane shear strengths when it is used in a multidirectional laminate. These strength parameters are then employed to calculate a stress norm which determines how close the stress state in the lamina is to its failure state. Secondly, the stress norm is incorporated into the formalism of an optimization problem in order to enhance the load bearing capacity of multidirectional laminates. The optimization problem is solved for symmetric laminates subjected to any combination of in-plane loads.

Chapter 10 summarizes the main conclusions reached on the basis of the research work embodied in Chapters 4 to 9 inclusive.

References to works in the literature have been listed in an alphabetical order at the end of the Thesis. Most of the work described in this Thesis has been published or accepted for publication in Journals and presented at conferences. For easy reference, these publications are listed below:

1. Wang, J. & Karihaloo, B. L. 1993 Design of crack-insensitive composite laminates. *Optimal design with advanced materials – Proc. IUTAM Symp. Advanced Materials, Lyngby, Denmark, August 1992* (ed. P. Pedersen), pp. 207–219. London: Elsevier.
2. Wang, J. & Karihaloo, B. L. 1994a Cracked composite laminates least prone to delamination. *Proc. Roy. Soc. London* A**444**, 17–35.
3. Wang, J. & Karihaloo, B. L. 1994b Mode II and mode III stress singularities and intensities at a crack tip terminating on a transversely isotropic-orthotropic bimaterial interface. *Proc. Roy. Soc. London* A**444**, 447–460.
4. Thomsen, N. B., Wang, J. & Karihaloo, B. L. 1994 Optimization – a tool in advanced material technology. *Structural Optimization* **8**, 9–15.
5. Wang, J., Thomsen, N. B. & Karihaloo, B. L. 1994 Multicriterion optimization – a tool in advanced materials technology. In *Proc. of Fifth AIAA/USAF/NASA/ISSMO Symposium on Multidisciplinary Analysis and Optimization* Part I (ed. J. Soebieski, C. Borland, V. Venkayya, L. Berke & G. Rozvany), pp. 54–63. Panama City, September, 1994.
6. Wang, J. & Karihaloo, B. L. 1995a Multiple cracking in angle-ply composite laminates. *J. Compos. Mater.* **29**, 1321–1336.
7. Wang, J. & Karihaloo, B. L. 1995b Mode I stress singularity and intensity factor at a crack tip terminating at a transversely isotropic-orthotropic bimaterial interface. *J. Appl. Mech.* (To appear).
8. Wang, J. & Karihaloo, B. L. 1995c Fracture mechanics and optimization – a useful tool for fibre-reinforced composite design. *Composite Structures* **31**, 151–162.
9. Wang, J. & Karihaloo, B. L. 1995d Optimum *in situ* strength design of composite laminates. *J. Compos. Mater.* (Submitted).

We end this brief introduction by quoting a statement by Savage (1991) who describes the objectives of a project (worth 2 million pounds) ever taken by YARD (Glasgow) and its partners: *This project has two levels of focus in terms of damage type: (a) delamination; (b) matrix cracking. The output of the research will be a predictive system for the residual strength of fibre reinforced epoxy (FRE) composite materials, that is already extensively used in aircraft structures.*

Chapter 2

Optimum Strength Design of Composite Materials – A Review

2.1 Failure Criteria of Composite Materials

Since the stress field and strength properties of the laminae in a fibre-reinforced multidirectional composite laminate are all functions of the laminate configuration, it is evident that under a given loading condition, the risk of failure of the composite laminate also depends on the laminate configuration. For given material and loading conditions, it is favourable to design the laminate so that the risk of failure is minimized. In this way, the strength of the laminate is maximized, and the material is exploited to the best of its capacity.

The failure of a multidirectional laminate is of a multimodal nature. The optimum design can be pursued with respect to one or several of the strength indicators that reflect the overall strength of the laminate. Irrespective of the objective, it is necessary to determine the stress field in the laminate and to establish proper failure (strength) criteria, before any optimization procedure can be applied. The progress made in the development of the failure criteria of fibre-reinforced composite materials does not match the progress made in the analysis of their structural response. This situation has come about because of two factors. One is the difficulty in making an accurate assessment of the stress fields in the composite structures, and the other is attributable to the scatter in the strength parameters themselves. The failure criteria available in the literature, such as maximum stress (strain) criterion, Tsai-Hill failure criterion and Hoffman criterion, can attain fairly good accuracies in predicting the strength of unidirectional continuous fibre-reinforced laminae under uniaxial loading. On the other hand, the strength theory for laminates with multiple ply angles, which is obviously the more practical, is still a continuing research topic.

The main factors that need to be taken into account when developing strength theories for multidirectional laminates are the failure mode(s) likely to occur at given load conditions

and the laminate configuration. It is also important to know how to use the basic strength parameters obtained from unidirectional laminae to determine the strength of the multidirectional laminates. The failure modes are related to the stress distribution in the laminates and the relative strength of a lamina in different failure modes. The unidirectional lamina strengths are emphasized here because of the following reason. The basic strength parameters used in the failure criteria available in the literature for fibre-reinforced laminates are based on tests conducted on unidirectional laminae. The knowledge that the *in situ* strength of laminae is different from their unidirectional strength casts doubt on the validity of these failure criteria. It means that in determining the strength of a lamina in a multidirectional laminate, the mutual influence, viz. the layup or lamination effect, between adjacent plies and the dimensions of the lamina under consideration must be taken into account. Herakovich (1982) experimentally demonstrated the influence of layer thickness upon the ultimate strength of angle-ply laminates. Chang & Lessard (1991) have proposed a set of *in situ* transverse tensile strength and in-plane shear strength formulae. These formulae include the mutual influence between the adjacent laminae as well as the dimension factor.

Chang & Lessard (1991), and Chang *et al.* (1991) have applied these formulae to the damage analysis of laminates containing an open hole.

2.2 Optimal Design with Respect to Failure Criteria

The optimum strength design of fibre-reinforced composites has been pursued since the introduction of these materials and the development of failure criteria. For example, Sandhu (1969) used a parametric study to investigate the fibre orientation of a unidirectional lamina yielding maximum strength under in-plane stress conditions. Because of the simplicity of the stress evaluation and the laminate configuration, the strength of a unidirectional lamina under in-plane stresses can be maximized analytically with respect to the fibre orientation (Brandmaier, 1970). The results based on Tsai-Hill failure criterion indicated that the optimum fibre orientation depends on the stress state and the relative value of the transverse and in-plane shear strengths of the lamina. The intuitive design that the optimum fibre orientation for maximum strength corresponds to the principal stress direction was found not to be applicable to the case of the graphite/epoxy composite studied in that work.

When the strength of a multidirectional composite laminate is to be maximized, more complicated and explicit optimization techniques are needed. The work of Chao *et al.* (1975a) is the earliest study dealing with the optimal strength design of composite laminates using a failure criterion. They designed a cylindrical shell composed of alternate $+\theta$ and $-\theta$ undirectional fibre-reinforced laminae. The ply angles were symmetric with respect to the middle plane of the

shell wall. The optimum ply angle θ was sought when the shell was under the combined action of axial tension/compression, lateral pressure and torque. The yield criterion for orthotropic material was written as (Tsai, 1968)

$$\left(\frac{\sigma_L}{X}\right)^2 + \left(\frac{\sigma_T}{Y}\right)^2 - \left(\frac{\sigma_L}{X}\right)\left(\frac{\sigma_T}{Y}\right) + \left(\frac{\tau_{LT}}{S}\right)^2 = 1 \tag{2.1}$$

where X, Y and S are the longitudinal, transverse and in-plane shear strengths, respectively, and σ_L, σ_T and τ_{LT} are the corresponding stresses. This failure criterion predicts the initial failure in one of the laminae. If the failure progress is to be traced, it is necessary to consider the degradation of the material properties and the stress redistribution after each failure mode. Substitution of the stresses in kth lamina led to a "performance index"

$$P = \left\{\left(\frac{\sigma_L^k}{X}\right)^2 + \left(\frac{\sigma_T^k}{Y}\right)^2 - \left(\frac{\sigma_L^k}{X}\right)\left(\frac{\sigma_T^k}{Y}\right) + \left(\frac{\tau_{LT}^k}{S}\right)^2\right\}^{-1/2} \tag{2.2}$$

The optimization problem was to maximize the performance index

$$\text{Max } IP \equiv \text{Max } P\left(\theta^k, \xi, L_1, L_2, L_6\right) \tag{2.3}$$

Here, ξ designates the position of a lamina in the laminate, and L_i $(i = 1, 2, 6)$ are the loads.

In this optimization problem, there is actually only one design variable, i.e. θ. When the laminate is composed of several laminae, the stresses are generally different from one lamina to the next, as is P. Based on physical intuition and experimental observations, the optimization problem was simplified so as to consider the stress state in the inner and outer laminae, respectively. The optimization problem was solved by using a golden-section search, preceded by a pseudo-random search in order to circumvent the multimodality, i.e. multiple failure modes.

A similar optimization problem for a symmetric laminate was later solved to obtain the maximum buckling load (Chao *et al.*, 1975b). It was found that when the size of the laminate exceeded a certain "marginal" size, only then should it be designed with a buckling constraint. However, when its size is below this "marginal" value, it is enough to design it with respect to strength alone.

The optimum strength design of six groups of antisymmetric angle-ply laminates was considered by Park (1982). These laminates were $[-\phi^0/+\phi^0]$, $[-\phi^0/0^0/+\phi^0]$, $[-\phi^0/90^0/+\phi^0]$, $[-\phi/0^0/90^0/+\phi^0]$, $[-\phi^0/\mp 45^0/+\phi^0]$ and a laminate with continuously varying ply angle from the middle plane to the top. Under in-plane loads N_1, N_2 and N_6, the first-ply-failure (FPF) criterion of Tsai & Hahn (1980) was written as

$$\epsilon_1^2 + \epsilon_2^2 + \frac{1}{2}\epsilon_6^2 = 2b^2, \tag{2.4}$$

where b is a material parameter. If the left side of eqn (2.4) reaches a critical value, the lamina is said to have failed. As ϵ_i $(i = 1, 2, 6)$ are determined by the laminate configuration and the load condition, it is expected that under certain load conditions, there would be an optimal angle ϕ_{opt} which would minimize the left side of eqn (2.4).

Denoting

$$Q = \epsilon_1^2 + \epsilon_2^2 + \frac{1}{2}\epsilon_6^2, \tag{2.5}$$

the FPF optimality criterion is to minimize Q with respect to ϕ under given loading condition N_1, N_2 and N_6. Park gave results under various load combinations for T300/5208 composite material. It was found that the design angle ϕ is very sensitive to the load ratio under this criterion. Sudden jumps (discontinuities) were observed in the optimal design angle ϕ in the neighborhood of certain load combinations but no explanation was provided. It is likely that the jumps were caused by the switch of failure modes. This is the nature of multimodality of the strength optimization, as had been previously pointed out by Chao *et al.* (1975a).

Ikegami *et al.* (1982) used Hoffman failure criterion (Hoffman, 1967) in the optimal design of composite laminates

$$\frac{\sigma_L^2 - \sigma_L\sigma_T}{F_{cL}F_{tL}} + \frac{\sigma_T^2}{F_{cT}F_{tT}} + \frac{F_{cL} - F_{tL}}{F_{cL}F_{tL}}\sigma_L + \frac{F_{cT} - F_{tT}}{F_{cT}F_{tT}}\sigma_T + \frac{\tau_{LT}^2}{F_{sLT}^2} = 1 \tag{2.6}$$

where subscripts L and T denote the fibre and transverse directions, and c, t and s denote tension, compression and shear, respectively. F and σ denote strength and stress, respectively. The strength constants in this criterion are determined experimentally by subjecting tubular specimens respectively to axial load, torsion and to a combination of the two. The optimal ply angles θ_1 and θ_2 were sought for $[\theta_1/\theta_2]$ laminates under various in-plane load ratios by maximizing the lengths of load vectors to the failure surface. Under most load ratios the optimal configurations were found to be only symmetric or antisymmetric laminates, viz. $[-\theta^0/-\theta^0]$ or $[+\theta^0/-\theta^0]$. They applied the optimal fibre orientations to the design of rotating discs. The optimal fibre directions that maximized the strain energy of laminates were also reported.

Although there are only two design variables θ_1 and θ_2 here, the determination of their optimal values is not very straightforward because of their mutual influence when calculating the stresses in each layer. The mathematical procedure for obtaining optimal values was not described.

Adali (1985) optimized the configuration of a symmetric angle-ply laminate under in-plane cyclic loads for maximum fatigue failure loads. Fibre orientation, layer thickness and fibre content of the laminate were regarded as design variables. The maximum failure load was determined by using a fatigue failure criterion formulated by Hashin & Rotem (1973) (see also Rotem & Hashin, 1976).

The first failure mode in this criterion is related to the fibre breakage. The failure criterion is

$$\sigma_1 \leq S_L \, f_1(N) \tag{2.7}$$

where S_L denotes the tensile strength of the composite material in the fibre direction. $f_1(N)$ is a function of the number of cycles to failure denoted by N, as well as the stress ratio and frequency of cycling. The second mode of failure is the fracture of the matrix for which the condition is

$$\left(\frac{\sigma_2}{S_T f_2}\right)^2 + \left(\frac{\tau_{12}}{S_\tau f_{12}}\right)^2 \leq 1 \tag{2.8}$$

where S_T and S_τ are the transverse tensile and in-plane shear strengths, and σ_2 and τ_{12} are the corresponding stresses, respectively. f_2 and f_{12} play the same role as f_1 in (2.7). Design is obtained for a fixed number of cycles to failure.

Under out-of-plane bending load, the strength of a symmetric fibre-reinforced laminate was optimized based upon the FPF criterion by Tauchert & Adibhatla (1985). The strain field in the laminate was analysed by Rayleigh-Ritz method using thin plate theory. The first-ply-failure criterion was taken as the objective, and the following optimization problem was solved

$$\underset{t_i,\,\theta_i}{\text{Min}} \quad (\epsilon_x^2 + \epsilon_y^2 + \frac{1}{2}\epsilon_{xy}^2)_{max} \tag{2.9}$$

subject to

$$\sum_{i=1}^{N} t_i = t \tag{2.10}$$

$$0^0 \leq \theta_i \leq \frac{\pi}{2} \tag{2.11}$$

$$t_{min} \leq t_i \leq t_{max} \tag{2.12}$$

The criterion (2.9) is the same as that of Park (1982) (eqn (2.4)), except that the subscripts x, y and xy, instead of 1, 2 and 12, are used here in the specification of the strains. θ_i and t_i are ply angles and thicknesses, respectively.

The optimization was performed via a quasi-Newton technique modified to handle linear constraints. They concluded that a substantial increase in the failure load and stiffness of laminate was possible. However, the improvement in stiffness was normally less than that in strength.

Webber (1988) presented a parametric investigation through an interactive computer programme for the optimal configuration of symmetric laminates under combined in-plane loads. The stress field was calculated by classical lamination theory. The first-ply-failure and the corresponding load were determined by the maximum allowable failure strain criterion. For a

laminate subjected to a general loading system involving N_x, N_y and N_{xy}, two approaches to the design problem were taken. In the first place, the fibres were arranged in the direction of the principal load and the angles were varied about this initial position to find the optimum values. The second approach used the common $0^0/90^0/\pm 45^0$ lay-up to sustain the loads, but this lay-up is not as efficient as the design based on the principal load direction.

The effect of change in the ply thickness was considered for the $0^0/90^0/\pm 45^0$ laminate. It was shown that increasing the thickness of 90^0 ply is not an efficient way of raising the failure loads; rather, it is better to increase the thickness of the 0^0 layers because it dictates to a large extent the transverse strain in the 90^0 ply. Webber also pointed out that the sudden discontinuity in Park's work (1982) was most likely due to a switching from one set of maximum failure loads to another, fairly close to it in magnitude.

Through an analysis of the strain transformation from reference axes to material principal axes, Fukunaga & Chou (1988) presented a particular class of angle-ply laminates which could be obtained under certain in-plane loads. In these laminates, all the laminae would fail simultaneously. Moreover, a diagram which describes the variation of the two lamination parameters (Miki, 1982)

$$\left\{ \begin{array}{c} \xi_1 \\ \xi_2 \end{array} \right\} = \sum_{i=1}^{n} h_i \left\{ \begin{array}{c} \cos 2\theta_i \\ \cos^2 2\theta_i \end{array} \right\}, \tag{2.13}$$

was used to determine the laminate configuration with the highest failure strains as per the Tsai-Wu first-ply-failure criterion. A comparison between the laminates in which all laminae failed simultaneously and the optimum laminates showed that the configuration of the former was the optimum one for the loading condition $N_1 = N_2$. For all other loading conditions it was pointed out that the simultaneous-failure laminate configuration either did not exist or was not optimal.

Miravete (1989) using a quadratic failure criterion obtained the fully-stressed lightest design of rectangular angle-ply laminates under uniform transverse load. He considered first symmetric and balanced laminates restricting the ply angles to practical values $0^0, +45^0, -45^0$ and 90^0. Lamina thicknesses and fibre directions were treated as design variables which were modified at each iterative step. A finite element method accounting for in-plane and interlaminar stresses was used to carry out the stress analysis. This design procedure was then (Miravete, 1990) applied to find the lightest design of thick plates, sandwich panels and cantilever plates of fibre-reinforced composite material under other load conditions. An experimental study was made to assess the accuracy of the theoretical strain and displacement results. Good agreement was found. Through optimization, large weight savings were found to be possible in all design cases mentioned above.

The maximum strain energy density in an object can be used to assess how far the material

used in this object is away from its failure state. Minimization of the strain energy density is identical to maximization of the strength. Pedersen *et al.* (1991) have solved a shape design problem of an orthotropic plate with a central hole bearing in-plane loading by minimizing the maximum strain energy density in it. Parameters describing the shape of the hole were treated as design variables. The solution to this minimax problem was obtained in three stages, viz. finite element strain analysis for a given shape, followed by sensitivity analysis and optimal search by linear programming with move limits. The combined shape, sizing (thickness) and orientation optimization was also reported by Pedersen (1991).

The strength optimization of multidirectional laminates was converted into a thickness (weight) optimization problem in the work by Fukunaga & Vanderplaats (1991). Considering the optimum design problem of a symmetric laminate under in-plane loading, the optimization problem was cast into the form min$W$=min $\sum_{i=1}^{I} h_i$, where h_i are the ply thicknesses. The original design variables were the ply angles and/or the thicknesses. The constraints were the Tsai-Wu first failure criterion plus the bounds on the design variables. In order to overcome the difficulty caused by the many local minima because of the high nonlinearity of the failure criterion with respect the ply angles, the transformed design variables $x_i = \sin 2\theta_i$ or $x_i = \cos 2\theta_i$ $(i = 1, \cdots, I)$ were used instead of θ_i. The actual choice of transformed variables depends on the value of θ_i. Another feature of the optimization is the automatic deletion of the constraint (failure criterion) corresponding to layers of zero thickness. The deletion is accomplished by assigning a large negative value to the constraint corresponding to the layer of zero thickness.

Fukunaga & Sekine (1993) proposed a two-stage optimization procedure to minimize the strain energy of a multidirectional laminate under in-plane loading. In the first stage, an explicit optimal relation was derived for layer angles and layer thickness ratios in a single-element laminate, based on the minimum strain energy criterion. It was found that this optimum laminate is a cross-ply laminate in the principal load directions. In the second stage, the optimality criterion was applied to the multidirectional laminate under in-plane loading. The design variables were the ply angles and thicknesses. A strength constraint was imposed during the search for the optimum design.

2.3 Optimal Design for Minimum Stress Irregularity

It is common to encounter local stress concentrations in some areas of a composite material. These stress irregularities are caused by the mismatch of the material properties of the constituent phases or by local cracking. If these local irregularities are not properly smoothened out, they can cause rupture of the composite structure. In order to delay the damage or retard the crack propagation induced by stress concentration, it is necessary to choose proper composition forms

so as to minimize the risk of the failure. This can be done by incorporating the results of stress analysis of composites into the formalism of optimization. Although the optimization methodology has the same potential in this area of the design of composite materials, as in the stiffness and strength design justed described, it has not been widely applied. The following works present some implicit and/or explicit aspects of the optimum design of composite materials against local damage or cracking.

In applying fracture mechanics results to optimal design of fibre-reinforced composite materials, Budiansky *et al.* (1986) have analysed matrix cracking strength of fibre-reinforced ceramics, through an examination of the cracking process of the matrix at a microstructural level. The pre-existent mismatch between the fibre and matrix strains during fabrication influences the matrix cracking strength. An optimal strain match is found to exist which maximizes the matrix cracking strength, if the Coulomb friction law between the fibre and matrix is operative. Gao & Mai (1989) investigated a similar model. Considering the fact that the matrix of some composite materials usually contains microcracks even before loading, e.g. fibre-cementitious materials and fibre-reinforced ceramics, a fracture mechanics model was proposed and the stress field, as well as the failure process was investigated. The stress at which the matrix cracking began was maximized subject to the condition of the simultaneous failure of the fibre and matrix. This optimization procedure led to a formula which matches the properties of the fibre and the matrix.

On the experimental side, the work of Jones and co-workers (1990) illustrated how knowledge of the temperature and energy fields can be used to assess damage and to develop an optimum local redesign or repair strategy. The methodology was based on the fact that areas experiencing a high energy field also experience rises in the local temperature field. The temperature changes can be measured with an infra-red camera. Their report presented a new method enabling the energy field to be computed from the knowledge of the surface temperature profile. A damaged stabilizer of a fighter aircraft was used as an example, whose wing pivot fitting plate was a boron/epoxy angle-ply laminate. The above method was applied to assess the repair strategy to the damaged area.

Free-edge effects in fibre-reinforced composite laminates have received extensive attention, because they play an important part in the free-edge delamination failure. Delamination can be regarded as the most fatal failure form which damages the integrity of a laminate and therefore results in the loss of its stiffness and load carrying capability. In an angle-ply laminate, there are two sources of delamination between plies. One is the free-edge region; another is the interfacial area right in front of a transverse crack (Crossman & Wang, 1982; Murri & Guynn, 1988; Kim, 1989).

Free-edge stress irregularity is caused by the mismatch of the mechanical properties of

adjacent constituent plies of a laminate. The anisotropic nature of composite materials will inevitably bring out this kind of problem which is not encountered in traditional homogeneous and isotropic materials. The reduction of the free-edge effect was first studied by Pagano (1971). It is evident from the literature that the research in this field has continued during the last two decades. Recently, Christensen & DeTeresa (1992) proposed that for $[0^0/\pm\theta^0]_s$ laminate the free-edge induced stress irregularity can be minimized or even be eliminated through a proper choice of the ply angles θ. Folias (1992) investigated the stress field in the neighborhood of the intersection of the free-edge of a hole and an interface in angle-ply laminates. Shiau & Chue (1991) presented a different approach for the reduction of the free-edge interlaminar stresses. They varied the fibre volume fraction in the free-edge region, which in turn minimized the mismatch of elastic properties between adjacent layers, and consequently reduced the interlaminar stresses. Parametric studies were conducted to evaluate the influence of fibre volume fraction on the free-edge induced stresses. The results showed that proper fibre volume reduction in the neighborhood of the free edge can reduce the stress concentration.

Although the reduction of the free-edge induced stress irregularity in angle-ply laminates has been a topic of wide concern for a long time, no attempt has been made to study it using optimization techniques. This is attributed to the difficulty in the determination of the stress field. The optimum design process does not include the mechanical analysis of composite materials at a microstructural level thereby limiting the scope of optimization in the design of composite structures.

2.4 Optimum Stacking Sequence

Stacking-sequence design of composite laminates is a difficult and challenging topic. If the lamina orientations in an angle-ply laminate are allowed to vary continuously, as has been done in many designs mentioned previously, the stacking-sequence design would seem not to be important. But in the practical design of composite laminates, only finite ply angles are available for design selection because of fabrication convenience and other commercial considerations. In addition, the strength and stiffness of a laminate depend strongly on its configuration under certain loading conditions. For example, the bending strength and stiffness of a $[0^0/90^0]_s$ laminate are vastly different from those of a $[90^0/0^0]_s$ laminate. As is shown by Pagano (1971), the free-edge stress irregularity could be reduced by a proper choice of the stacking sequence. The *in situ* strengths of laminae in a laminate are also determined by its neighbouring plies. In view of the above considerations, the stacking-sequence design or the layup design, plays an important role in the performance of composite laminates.

From a mathematical standpoint, stacking-sequence design of composite laminates is a

nonlinear, discontinuous programming problem. The programming techniques dealing with this kind of topological design problems are being explored. At present, it would appear that there are two available techniques.

One of the techniques is reported by Rao *et al.* (1991). It is a selection technique. Using the code representation of laminates developed by Tsai, the authors propose a procedure for the optimum design of fibre-reinforced composite laminates by a ranking process. Given that a symmetric laminate is made of repeated sublaminates, the ranking process selects the number and kind of sublaminates from a set of basic configurations composed of $0^0, 90^0$ and $\pm 45^0$ plies. The design aim is the achievement of minimum weight of the laminate, with the satisfaction of a prescribed failure criterion. The laminate can be subjected to in-plane and/or bending loads, and optionally hygrothermal loads. Various layup schemes are evaluated based on lamination theory and a quadratic failure criterion in strain space for given mechanical and hygrothermal loads. A ply-drop round-off scheme is adopted to arrive at the optimum laminate thickness.

Haftka & Walsh (1992) proposed a mathematically rigorous scheme for the stacking-sequence design of composite. It is based upon the usage of four sets of ply-orientation-identity variables. For a symmetric angle-ply laminate composed of a total of N plies of $0^0, 90^0$ and $\pm 45^0$ laminae, the ply stacking sequence is defined in terms of four sets of ply-orientation-identity variables o_i, n_i, f_i^p and f_i^m $(i = 1, 2, ..., N/2)$ which are zero-one binary integer variables. The variable o_i, n_i, f_i^p or f_i^m is equal to one if there is a $0^0, 90^0, +45^0$ or -45^0 ply, respectively, in the ith layer. Then the integral factors in the expressions of stiffness coefficients can be written as linear functions of these variables. An optimization problem of a laminate with respect to a mechanical property, for example, the buckling load λ, is formulated as

$$\text{Max} \quad \lambda^*(o_i, n_i, f_i^p, f_i^m) \tag{2.14}$$

subject to

$$\lambda^* \leq \lambda_{cr}(m, n), \quad m = 1, 2, .., m_f, \quad n = 1, 2, .., n_f \tag{2.15}$$

$$o_i + n_i + f_i^p + f_i^m = 1, \quad i = 1, 2, ..., N/2 \tag{2.16}$$

$$\sum_{i=1}^{N/2} (f_i^p - f_i^m) = 0, \tag{2.17}$$

where λ^* is the lowest buckling load over m and n – the number of half-waves in two directions, and $\lambda_{cr}(m, n)$ is the critical buckling load. o_i, n_i, f_i^p and f_i^m $(i = 1, 2, ..., N/2)$ are zero-one binary integer variables. The last constraint (2.17) ensures the laminate is a balanced one. Other constraints on the stacking sequence such as a limit on the number of contiguous plies of the same orientation and limits on the in-plane stiffnesses are easily accommodated. The former condition may be necessary from the strength point of view.

The authors give the design examples for graphite/epoxy laminates under uniaxial and biaxial compression using a software LINDO (Schrage, 1989) based on branch-and-bound algorithm.

Gürdal & Haftka (1991) have reviewed optimization strategies for design with discrete and integer valued variables leading to the stacking-sequence optimization. The graphic optimization method of Miki (1982), the penalty function approach for problems with discrete-valued variables (Shin *et al.*, 1990) and the use of ply-orientation-identity variables are discussed. It is pointed out that a difficulty in using flexural lamination parameters in designing laminates for maximum buckling load is that the half wave numbers in two directions depend on the design variables, as well as the aspect ratios and the applied loads. It is not always possible to predict them accurately. The penalty method has mathematical continuity; hence it is simple and straightforward to use. In some cases, it is unable to reach the global optimum, especially for laminates with large number of plies or for discrete sets with large number of choices.

2.5 Mixed-Variable Design

From a commercial point of view, a logical construction of a fibre-reinforced laminate involves integer numbers of unidirectional laminae, while the thicknesses of these laminae are discrete numbers. In the design of laminates one inevitably encounters the situation where continuous, integer and discrete variables are present. These mixed programming problems are highly complex mathematically but have been receiving a lot of attention.

Mesquita & Kamat (1987) solved a mixed integer programming problem for the maximization of frequencies of a stiffened laminate subject to frequency separation constraints and an upper bound on the weight. In this design, a symmetric laminate is constructed of n_1 plies of 90^0, n_2 plies of 60^0, n_3 plies of 45^0, n_4 plies of 30^0 and n_5 plies of 0^0. Along its two centrelines, the laminate is reinforced by two stiffeners placed symmetrically with respect to the laminate midplane. The frequencies are calculated using the finite element method.

The number n_i $(i = 1, 2, .., 5)$ of plies and the stiffener areas form the two sets of design variables and the problem belongs to the class of nonlinear mixed integer programming (NMP). Dakin's branch and bound algorithm (Dakin, 1965) was employed to discompose the original problem into a sequence of nonlinear programming sub-problems. These sub-problems were then solved with projected Lagrangian or variable metric method for constrained optimization (Powell, 1978). It was demonstrated that nonlinear mixed integer programming can be a viable structural optimization alternative to the conventional practice of rounding off a continuous optimization solution.

Hajela & Shih (1989) proposed a modification of the branch and bound approach to include nonlinear optimization problems involving continuous, integer and discrete design variables. A

mathematical formulation of optimization problem with mixed continuous, discrete and integer variables can be stated as follows

$$\text{Min} \quad F(\overline{x}) \tag{2.18}$$

subject to

$$g_j(\overline{x}) \leq 0; \quad j = 1, 2, ..., p \tag{2.19}$$

$$h_k(\overline{x}) = 0; \quad k = 1, 2, ..., s \tag{2.20}$$

$$x_i^l \leq x_i \leq x_i^u, \quad i = 1, 2, ..., n \tag{2.21}$$

where

$$\overline{x} = (x_1, x_2, ..., x_L, ..., x_m, ..., x_n)^T \tag{2.22}$$

is the design variable vector. The design variables involve L non-negative discrete variables which may be the thicknesses of the plies, $m - L$ non-negative integer variables which may be the number of plies, and $n - m$ positive real continuous variables , e.g. the ply angles. From a practical point of view, the ply angles can also take discrete values.

The basic solution strategy used in this work for the nonlinear mixed integer programming problems is a variant of the approach proposed by Garfinkel & Nemhauser (1974). The strategy consists of a systematic search of continuous solutions in which the discrete and integer variables are successively forced to assume specific values. As a first step, the requirement that appropriate variables be discrete or integer is relaxed, and a solution of the continuous problem is reached. If the solution is such that the original requirements on integrality and discreteness are satisfied, and the design is feasible, an optimum design is obtained. If some of the variables violate the conditions of being integer or discrete values, then they are branched and new bounds are put on them. The sub-problems thus created are solved again as continuous problems. This branch and bound procedure is successively applied until a feasible integer and discrete design set is obtained.

A design example was presented using this procedure. The design objective was the minimum weight of a cantilever composite laminate beam. Constraints were placed on strength, displacement and natural frequency. A modified feasible direction algorithm was used in the solution of the continuous nonlinear programming problem, with piecewise linear representation of the objective function and constraints.

2.6 Concluding Remarks

From the above brief review of the optimum strength design of fibre-reinforced composites, the potential of optimization techniques to the design of composite materials became apparent.

But at the same time it became also apparent, that most of the explicit optimum designs were obtained at the structural level that did not take into account the microstructural characteristics of the composites. For instance, the high sensitivity of fibre-reinforced composite materials to defects such as cracks in the transverse direction was not considered in the prediction of the strength of the material. The literature survey also showed that the detailed stress analysis of cracked composites was not incorporated into the mathematical formalism of optimization. On the other hand, the recent developments in both the stress analysis of the heterogeneous materials and in the optimization techniques have provided us with effective tools which can be used to overcome the above shortcomings.

Therefore, the primary aim of this Thesis is to provide guidelines for the design of composite materials through a combination of the state-of-the-art analysis of cracked fibre-reinforced composite laminates based on fracture mechanics with mathematical optimization techniques. The analysis of the cracked composite laminates using fracture mechanics will examine the interaction between cracks and the interfaces in these materials, whereas the optimization of their design will aim at minimizing the influence of cracks on interfacial stresses and at maximizing the constraining effect of laminae on one another.

Chapter 3

Mathematical Preliminaries

3.1 Introductory Remarks

In order not to interrupt the continuity of exposition in the main body of this Thesis, and also for the sake of completeness a brief overview of the mathematical techniques that will be repeatedly used in this Thesis is given in this Chapter. In particular, the Fourier transform technique will receive some attention, as will the lamination theory for composite laminates. But we begin with the presentation of the stress-strain relationships for a transversely isotropic solid.

3.2 Stress-Strain Relationships for a Transversely Isotropic Material

Figure 3.1 shows a homogeneous elastic medium which has the property of transverse isotropy in the plane perpendicular to the z-axis, for instance, the xy-plane. In the coordinate system shown in Figure 3.1, the stress-strain relationships are

$$\varepsilon_{xx} = \frac{1}{E_{xx}}\sigma_{xx} - \frac{\nu_{yx}}{E_{yy}}\sigma_{yy} - \frac{\nu_{zx}}{E_{zz}}\sigma_{zz} \tag{3.1}$$

$$\varepsilon_{yy} = -\frac{\nu_{xy}}{E_{xx}}\sigma_{xx} + \frac{1}{E_{yy}}\sigma_{yy} - \frac{\nu_{zy}}{E_{zz}}\sigma_{zz} \tag{3.2}$$

$$\varepsilon_{zz} = -\frac{\nu_{xz}}{E_{xx}}\sigma_{xx} - \frac{\nu_{yz}}{E_{yy}}\sigma_{yy} + \frac{1}{E_{zz}}\sigma_{zz} \tag{3.3}$$

$$\gamma_{xy} = \frac{1}{\mu_{xy}}\tau_{xy} \tag{3.4}$$

$$\gamma_{yz} = \frac{1}{\mu_{yz}}\tau_{yz} \tag{3.5}$$

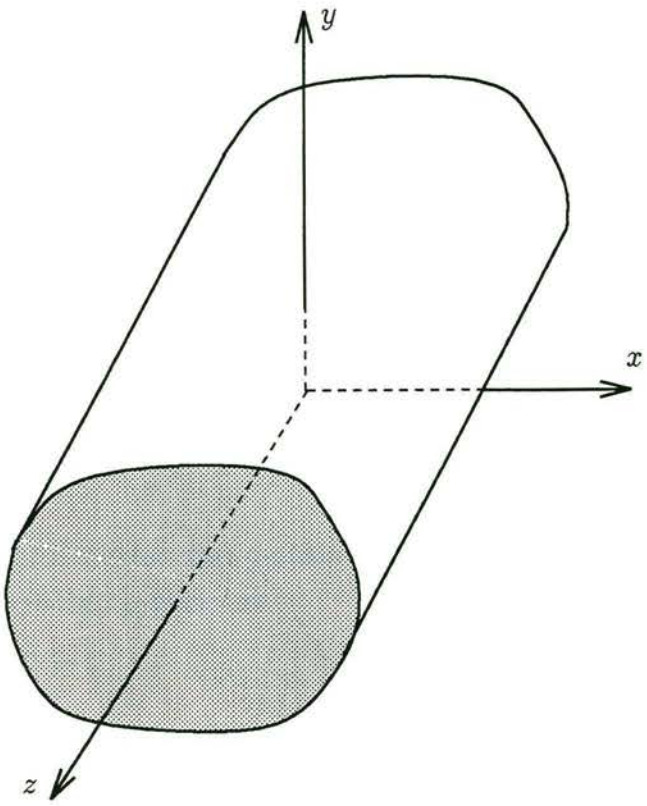

Figure 3.1: A transversely isotropic elastic body. The isotropy prevails in the plane perpendicular to z-axis, represented by xy-plane

$$\gamma_{zx} = \frac{1}{\mu_{zx}}\tau_{zx} \tag{3.6}$$

where E_{xx}, E_{yy} and E_{zz} denote Young's moduli along x, y and z-directions, respectively, and μ_{xy}, μ_{yz} and μ_{zx} represent the shear moduli in xy, yz and zx-planes, respectively. Because of the transversely isotropic nature of the body, we have the identities

$$E_{xx} = E_{yy} \equiv E \tag{3.7}$$

$$\mu_{xy} = \mu_{yx} \equiv \mu \tag{3.8}$$

$$\mu_{yz} = \mu_{zx} \tag{3.9}$$

$$\nu_{xy} = \nu_{yx} \equiv \nu \tag{3.10}$$

$$\nu_{xz} = \nu_{yz} \quad \nu_{zx} = \nu_{zy} \tag{3.11}$$

and

$$\mu = \frac{E}{2(1+\nu)} \tag{3.12}$$

In an elastostatic problem in which τ_{yz} and τ_{zx} are absent, eqns (3.1)–(3.6) using the notation of eqns (3.7)– (3.10) degenerate into

$$\varepsilon_{xx} = \frac{1}{E}\sigma_{xx} - \frac{\nu}{E}\sigma_{yy} - \frac{\nu_{zx}}{E_{zz}}\sigma_{zz} \tag{3.13}$$

$$\varepsilon_{yy} = -\frac{\nu}{E}\sigma_{xx} + \frac{1}{E}\sigma_{yy} - \frac{\nu_{zy}}{E_{zz}}\sigma_{zz} \tag{3.14}$$

$$\varepsilon_{zz} = -\frac{\nu_{xz}}{E}\sigma_{xx} - \frac{\nu_{yz}}{E}\sigma_{yy} + \frac{1}{E_{zz}}\sigma_{zz} \tag{3.15}$$

$$\gamma_{xy} = \frac{1}{\mu}\tau_{xy} \tag{3.16}$$

For a two-dimensional problem (in xy-plane) under general plane stress conditions ($\sigma_{zz} = 0$), the strain components in the xy-plane are

$$\varepsilon_{xx} = \frac{1}{2(1+\nu)\mu}\sigma_{xx} - \frac{\nu}{2(1+\nu)\mu}\sigma_{yy} \tag{3.17}$$

$$\varepsilon_{yy} = -\frac{\nu}{2(1+\nu)\mu}\sigma_{xx} + \frac{1}{2(1+\nu)\mu}\sigma_{yy} \tag{3.18}$$

$$\gamma_{xy} = \frac{1}{\mu}\tau_{xy} \tag{3.19}$$

where eqn (3.12) has been used.

On the other hand, for a problem under plane strain conditions ($\varepsilon_{zz} = 0$) and

$$\frac{1}{E_{zz}}\sigma_{zz} = \frac{\nu_{xz}}{E_{xx}}\sigma_{xx} + \frac{\nu_{yz}}{E_{yy}}\sigma_{yy} \tag{3.20}$$

the corresponding strain components are

$$\varepsilon_{xx} = \frac{1-\nu_{zx}\nu_{xz}}{2(1+\nu)\mu}\sigma_{xx} - \frac{\nu+\nu_{zx}\nu_{yz}}{2(1+\nu)\mu}\sigma_{yy} \tag{3.21}$$

$$\varepsilon_{yy} = -\frac{\nu+\nu_{zy}\nu_{xz}}{2(1+\nu)\mu}\sigma_{xx} + \frac{1-\nu_{zy}\nu_{yz}}{2(1+\nu)\mu}\sigma_{yy} \tag{3.22}$$

$$\gamma_{xy} = \frac{1}{\mu}\tau_{xy} \tag{3.23}$$

If we use the notation

$$\kappa = \begin{cases} \dfrac{3-\nu}{1+\nu} & \text{under general plane stress conditions} \\ \dfrac{3-\nu-4\nu_{xz(yz)}\nu_{zx(zy)}}{1+\nu} & \text{under plane strain conditions} \end{cases} \tag{3.24}$$

then eqns (3.17)–(3.19) and (3.21)–(3.23) can be expressed in the following unified form

$$\varepsilon_{xx} = \frac{1+\kappa}{8\mu}\sigma_{xx} - \frac{3-\kappa}{8\mu}\sigma_{yy} \tag{3.25}$$

$$\varepsilon_{yy} = -\frac{3-\kappa}{8\mu}\sigma_{xx} - \frac{1+\kappa}{8\mu}\sigma_{yy} \tag{3.26}$$

$$\gamma_{xy} = \frac{1}{\mu}\tau_{xy} \tag{3.27}$$

When the material degenerates into an isotropic medium, i.e. $\nu_{zx} = \nu_{zy} = \nu$ (which will automatically lead to $E_{zz} = E$), κ will become

$$\kappa = \begin{cases} \dfrac{3-\nu}{1+\nu} & \text{under general plane stress conditions} \\ 3-4\nu & \text{under plane strain conditions} \end{cases} \tag{3.28}$$

Combining eqns (3.24) with (3.28), the corresponding κ for both transversely isotropic and completely isotropic media under the two deformation modes can be explicitly written as

$$\kappa = \begin{cases} \dfrac{3-\nu}{1+\nu} & \text{isotropic or transversely isotropic in general plane stress} \\ 3-4\nu & \text{isotropic in plane strain} \\ \dfrac{3-\nu-4\nu_{xz(yz)}\nu_{zx(zy)}}{1+\nu} & \text{transversely isotropic in plane strain} \end{cases} \tag{3.29}$$

The first two values of κ for an isotropic medium are also called the Kolosov constants (Sokolnikoff, 1956; Markenscoff, 1993).

3.3 Fourier Transforms and Relevant Expressions

The purpose of this brief Section is to express the components of stresses and displacements of a two-dimensional elasticity problem in terms of relevant Fourier transforms. The exposition below follows closely that of Sneddon (1951) with a slight alteration to the notation.

In a two-dimensional problem of elasticity where body forces are absent, the stresses can be expressed as

$$\sigma_{\xi\xi} = \frac{\partial^2 \varphi}{\partial \eta^2} \quad \sigma_{\eta\eta} = \frac{\partial^2 \varphi}{\partial \xi^2} \quad \tau_{\xi\eta} = -\frac{\partial^2 \varphi}{\partial \xi \partial \eta} \tag{3.30}$$

where $\varphi = \varphi(\xi, \eta)$ is the Airy stress function. In the above expressions and in those to follow, the coordinates are denoted by ξ and η instead of the commonly used x and y. When these formulae are used later for detailed problems, ξ and η will be replaced by x and y or y and x, respectively, as desired.

The Airy stress function $\varphi(\xi, \eta)$ should satisfy the biharmonic equation

$$\nabla^4 \varphi(\xi, \eta) = 0 \tag{3.31}$$

This biharmonic equation can be solved using Fourier transforms. It is taken as granted that the Airy stress function and the resulting stresses and displacements all satisfy the conditions of Fourier transforms. If we denote the Fourier transform of $\varphi = \varphi(\xi, \eta)$ by

$$\overline{\varphi}(\xi, t) = \int_{-\infty}^{+\infty} \varphi(\xi, \eta)\, e^{it\eta}\, d\eta \tag{3.32}$$

then the inverse transform is

$$\varphi(\xi, \eta) = \frac{1}{2\pi} \int_{-\infty}^{+\infty} \overline{\varphi}(\xi, t)\, e^{-it\eta}\, dt \tag{3.33}$$

where $i = \sqrt{-1}$.

Substituting eqn (3.32) into (3.31), the general solution of the biharmonic equation where $\overline{\varphi}(\xi, t)$ is the unknown can be written as

$$\overline{\varphi}(\xi, t) = (C_1 + C_2\xi)\, e^{-|t|\xi} + (C_3 + C_4\xi)\, e^{|t|\xi} \tag{3.34}$$

where C_j $(j = 1, 2, 3, 4)$ are unknown functions of t which are to be determined from the proper boundary conditions.

From the relations (3.30), it is easily shown that

$$\int_{-\infty}^{+\infty} \sigma_{\xi\xi}\, e^{it\eta}\, d\eta = -t^2\, \overline{\varphi} \tag{3.35}$$

$$\int_{-\infty}^{+\infty} \sigma_{\eta\eta}\, e^{it\eta}\, d\eta = \frac{d^2 \overline{\varphi}}{d\xi^2} \tag{3.36}$$

$$\int_{-\infty}^{+\infty} \tau_{\xi\eta}\, e^{it\eta}\, d\eta = it \frac{d\overline{\varphi}}{d\xi} \tag{3.37}$$

The stresses are expressed as

$$\sigma_{\xi\xi} = -\frac{1}{2\pi}\int_{-\infty}^{+\infty} t^2\overline{\varphi}\, e^{-it\eta}\, dt \tag{3.38}$$

$$\sigma_{\eta\eta} = \frac{1}{2\pi}\int_{-\infty}^{+\infty} \frac{d^2\overline{\varphi}}{d\xi^2}\, e^{-it\eta}\, dt \tag{3.39}$$

$$\tau_{\xi\eta} = \frac{1}{2\pi}\int_{-\infty}^{+\infty} it\frac{d\overline{\varphi}}{d\xi}\, e^{-it\eta}\, dt \tag{3.40}$$

In order to calculate the displacements, we need the relations between the displacements and strains

$$\varepsilon_{\xi\xi} = \frac{\partial u_\xi}{\partial \xi} \tag{3.41}$$

$$\varepsilon_{\eta\eta} = \frac{\partial u_\eta}{\partial \eta} \tag{3.42}$$

$$\gamma_{\xi\eta} = \left(\frac{\partial u_\xi}{\partial \eta} + \frac{\partial u_\eta}{\partial \xi}\right) \tag{3.43}$$

where u_ξ and u_η represent the displacements along ξ and η directions, respectively.

From the constitutive equations (3.25)–(3.27) and eqn (3.42), we have

$$\frac{\partial u_\eta}{\partial \eta} = -\frac{3-\kappa}{8\mu}\sigma_{\xi\xi} + \frac{1+\kappa}{8\mu}\sigma_{\eta\eta} \tag{3.44}$$

Multiplying both sides by $e^{it\eta}$ and integrating from $-\infty$ to $+\infty$ gives

$$-it\int_{-\infty}^{+\infty} u_\eta\, e^{it\eta}\, d\eta = -\frac{3-\kappa}{8\mu}\int_{-\infty}^{+\infty} \sigma_{\xi\xi}\, e^{it\eta}\, d\eta + \frac{1+\kappa}{8\mu}\int_{-\infty}^{+\infty} \sigma_{\eta\eta}\, e^{it\eta}\, d\eta \tag{3.45}$$

Substituting eqns (3.35) and (3.36) into the above equation and inverting gives

$$u_\eta = \frac{1}{2\pi}\int_{-\infty}^{+\infty} \frac{1}{t}\left[\frac{3-\kappa}{8\mu}\, t^2\overline{\varphi} + \frac{1+\kappa}{8\mu}\,\frac{d^2\overline{\varphi}}{d\xi^2}\right] i\, e^{-it\eta}\, dt \tag{3.46}$$

Similarly, making use of eqn (3.43) and the proper integral of (3.37), the other component of displacement is obtained

$$u_\xi = \frac{1}{2\pi}\int_{-\infty}^{+\infty} \frac{1}{t^2}\left[\frac{1+\kappa}{8\mu}\,\frac{d^3\overline{\varphi}}{d\xi^3} - t^2\frac{5+\kappa}{8\mu}\,\frac{d\overline{\varphi}}{d\xi}\right] e^{-it\eta}\, dt \tag{3.47}$$

The expressions (3.46) and (3.47) were given in terms of Young's modulus and Poisson's ratio by Sneddon (1951) in his book. However, equation (29) on page 404 of that book corresponding to eqn (3.47) above has a typographical error.

Once a particular form of solution of $\overline{\varphi}$ is chosen, based upon the general solution (3.34), all the components of stresses and displacements can be obtained.

3.4 Basic Solution for an Infinite Plate with Crack

The basic solution for an infinitely large plate (shown in Figure 3.2) containing a crack which will be used later in this Thesis was given by Sneddon & Lowengrub (1969) in terms of Fourier transforms under mode I and mode II loadings. The solution for the combined mode I and II loading was given by Sneddon & Ejike (1969). Here the procedure first proposed by Sneddon (1951) is followed to arrive at the general solution (3.34) which is then specialized using the appropriate boundary conditions to determine the unknown functions C_j $(j = 1, .., 4)$.

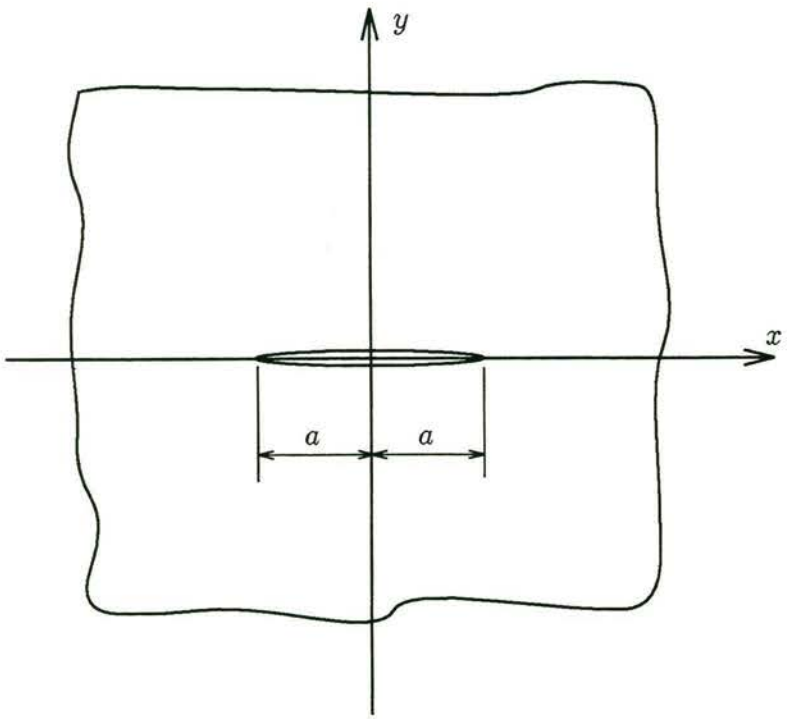

Figure 3.2: An infinitely large plate containing a crack

Let us consider first the mode I problem when the surfaces of the crack are subjected to a uniform pressure $-\sigma$. Because of symmetry, we consider only the upper half plane $y \geq 0$. The boundary conditions at $y = 0$ are

$$\tau_{xy}(x,0) = 0; \quad -\infty < x < +\infty \tag{3.48}$$

$$\sigma_{yy}(x,0) = -\sigma; \quad |x| < a \tag{3.49}$$

$$u_y(x,0) = 0; \quad |x| > a \tag{3.50}$$

Another necessary condition is that the stresses vanish when $y \to +\infty$, i.e.

$$\left.\begin{matrix}\sigma_{xx}(x,y)\\ \sigma_{yy}(x,y)\\ \tau_{xy}(x,y)\end{matrix}\right|_{y\to+\infty} \to 0; \quad -\infty < x < +\infty \tag{3.51}$$

Making use of the Fourier transforms (3.32) and (3.33) and expressions (3.35)–(3.40) after replacing ξ by y and η by x, we have

$$\overline{\varphi}(y,t) = \int_{-\infty}^{+\infty} \varphi(y,x)\, e^{itx}\, dx \tag{3.52}$$

$$\varphi(x,y) = \frac{1}{2\pi}\int_{-\infty}^{+\infty} \overline{\varphi}(y,t)\, e^{-itx}\, dt \tag{3.53}$$

$$\int_{-\infty}^{+\infty} \sigma_{yy}\, e^{itx}\, dx = -t^2\overline{\varphi} \tag{3.54}$$

$$\int_{-\infty}^{+\infty} \sigma_{xx}\, e^{itx}\, dx = \frac{d^2\overline{\varphi}}{dy^2} \tag{3.55}$$

$$\int_{-\infty}^{+\infty} \tau_{yx}\, e^{itx}\, dx = it\frac{d\overline{\varphi}}{dy} \tag{3.56}$$

$$\sigma_{yy} = -\frac{1}{2\pi}\int_{-\infty}^{+\infty} t^2\overline{\varphi}\, e^{-itx}\, dt \tag{3.57}$$

$$\sigma_{xx} = \frac{1}{2\pi}\int_{-\infty}^{+\infty} \frac{d^2\overline{\varphi}}{dy^2}\, e^{-itx}\, dt \tag{3.58}$$

$$\tau_{yx} = \frac{1}{2\pi}\int_{-\infty}^{+\infty} it\frac{d\overline{\varphi}}{dy}\, e^{-itx}\, dt \tag{3.59}$$

and from (3.46) and (3.47), we get

$$u_x \equiv u = \frac{1}{2\pi}\int_{-\infty}^{+\infty} \frac{1}{t}\left[\frac{3-\kappa}{8\mu}\, t^2\overline{\varphi} + \frac{1+\kappa}{8\mu}\,\frac{d^2\overline{\varphi}}{dy^2}\right] ie^{-itx}\, dt \tag{3.60}$$

$$u_y \equiv v = \frac{1}{2\pi}\int_{-\infty}^{+\infty} \frac{1}{t^2}\left[\frac{1+\kappa}{8\mu}\,\frac{d^3\overline{\varphi}}{dy^3} - t^2\frac{5+\kappa}{8\mu}\,\frac{d\overline{\varphi}}{dy}\right] e^{-itx}\, dt \tag{3.61}$$

In order to satisfy the conditions (3.51), it is necessary to set $C_3 = C_4 = 0$ in the general solution (3.34), and so giving

$$\overline{\varphi}(y,t) = (C_1 + C_2 y)\, e^{-|t|y} \tag{3.62}$$

and

$$\frac{d\overline{\varphi}}{dy} = (-|t|C_1 + C_2 - C_2|t|y)\, e^{-|t|y} \tag{3.63}$$

Substituting eqn (3.63) into (3.56) and imposing the first of the three conditions (3.48)–(3.50), we have

$$C_2 = |t|C_1, \tag{3.64}$$

so that (3.62) reduces to

$$\overline{\varphi}(y,t) = C_1(1 + |t|y)\, e^{-|t|y} \tag{3.65}$$

It is obvious that $\sigma_{xx}(x,y)$ and $\sigma_{yy}(x,y)$ are even functions of x and $\tau_{xy}(x,y)$ is an odd function of x. Therefore, from enqs (3.54)–(3.56) it follows

$$\overline{\varphi}(y,-t) = \overline{\varphi}(y,t) \tag{3.66}$$

In other words,

$$C_1(-t) = C_1(t) \tag{3.67}$$

Under this condition, the Airy stress function and the components of stresses and displacements can be written as

$$\varphi(x,y) = \frac{2}{\pi}\int_0^{+\infty} C_1(t)(1+ty)\, e^{-ty}\cos(tx)\, dt \tag{3.68}$$

$$\sigma_{xx} = -\frac{2}{\pi}\int_0^{+\infty} C_1(t)\, t^2\,(1-ty)\, e^{-ty}\,\cos(tx)\, dt \tag{3.69}$$

$$\sigma_{yy} = -\frac{2}{\pi}\int_0^{+\infty} C_1(t)\, t^2\,(1+ty)\, e^{-ty}\,\cos(tx)\, dt \tag{3.70}$$

$$\tau_{yx} = -\frac{2}{\pi}\int_0^{+\infty} C_1(t)\, t^3 y\, e^{-ty}\,\sin(tx)\, dt \tag{3.71}$$

$$u = \frac{2}{\pi}\frac{1}{4\mu}\int_0^{+\infty} C_1(t)t\,(1-\kappa+2ty)\, e^{-ty}\,\sin(tx)\, dt \tag{3.72}$$

$$v = \frac{2}{\pi}\frac{1}{4\mu}\int_0^{+\infty} C_1(t)t\,(1+\kappa+2ty)\, e^{-ty}\,\cos(tx)\, dt \tag{3.73}$$

Finally, the unknown function $C_1(t)$ is determined from the conditions (3.49)–(3.50).

Let us consider next the mode II case when the surfaces of the crack are subjected to a uniform shear stress $\tau_{xy} = -\tau$. We need again only consider the upper half of the body, $y \geq 0$.

Because of skew-symmetry, we have at the boundary of the half plane

$$\sigma_{yy}(x,0) = 0; \quad -\infty < x < +\infty \tag{3.74}$$

$$\sigma_{xy}(x,0) = -\tau; \quad |x| < a \tag{3.75}$$

$$u_x(x,0) = 0; \quad |x| > a \tag{3.76}$$

As the conditions (3.51) are also to be satisfied under the present form of loading, eqn (3.62) remains valid. Inserting the first of the three conditions (3.74)–(3.76) into the expression (3.57) gives

$$C_1 = 0 \tag{3.77}$$

so that $\overline{\varphi}$ reduces to

$$\overline{\varphi}(y,t) = C_2\, y\, e^{-|t|y} \tag{3.78}$$

and

$$\frac{d\overline{\varphi}}{dy} = C_2\,(1 - |t|y)\, e^{-|t|y} \tag{3.79}$$

In view of the skew-symmetry, we have $\overline{\varphi}(y,-t) = -\overline{\varphi}(y,t)$, i.e.

$$C_2(-t) = -C_2(t) \tag{3.80}$$

Because of the arbitrariness of function $C_2(t)$ and the homogeneous nature of the biharmonic equation, eqn (3.78) can be rewritten in the following form without altering the solution of the biharmonic equation

$$\overline{\varphi}(y,t) = C_2\, i\, y\, e^{-|t|y} \tag{3.81}$$

The corresponding Airy stress function and stresses and displacements can now be written as

$$\varphi(x,y) = \frac{2}{\pi}\int_0^{+\infty} C_2(t)\, y\, e^{-ty}\sin(tx)\, dt \tag{3.82}$$

$$\sigma_{xx} = \frac{2}{\pi}\int_0^{+\infty} C_2(t)\, t\,(-2+ty)\, e^{-ty}\sin(tx)\, dt \tag{3.83}$$

$$\sigma_{yy} = -\frac{2}{\pi}\int_0^{+\infty} C_2(t)\, t^2\, y\, e^{-ty}\sin(tx)\, dt \tag{3.84}$$

$$\tau_{yx} = -\frac{2}{\pi}\int_0^{+\infty} C_2(t)\, t\,(1-ty)\, e^{-ty}\cos(tx)\, dt \tag{3.85}$$

$$u = \frac{2}{\pi}\frac{1}{4\mu}\int_0^{+\infty} C_2(t)\,(1+\kappa-2ty)\,e^{-ty}\cos(tx)\,dt \tag{3.86}$$

$$v = \frac{2}{\pi}\frac{1}{4\mu}\int_0^{+\infty} C_2(t)\,(-1+\kappa+2ty)\,e^{-ty}\sin(tx)\,dt \tag{3.87}$$

The unknown function $C_2(t)$ is determined from the conditions (3.75)–(3.76).

3.5 Basic Solution for an Isotropic Strip of Finite Thickness

For an infinitely long strip of finite thickness, shown in Figure 3.3, the general solution of the biharmonic equation (3.31), using the Fourier transforms with respect to y, is taken in the form (Sneddon, 1951)

$$\overline{\varphi}(x,t) = (D_1 + D_2\,t\,x)\cosh(tx) + (D_3 + D_4\,t\,x)\sinh(tx) \tag{3.88}$$

where D_j $(j = 1,2,3,4)$ are functions of t which are to be determined from the boundary conditions. It is noted that the Fourier transforms are carried out here with respect to y in the coordinate system of Figure 3.3.

Following a similar procedure to that used in § 3.4, the general solution (3.88) can be reduced to specific forms for particular loading cases by enforcing appropriate symmetry and boundary conditions. For instance, Sneddon (1951) has given the solutions for a symmetric and an asymmetric loading condition. In the following, we shall give the expressions for the Airy stress function and the corresponding stresses and displacements for these two loading conditions without detail.

For symmetric loading, we have

$$\varphi(x,y) = \frac{2}{\pi}\int_0^{+\infty} [D_1(t) + D_4(t)\,t\,x\,\sinh(tx)]\cos(ty)\,dt \tag{3.89}$$

$$\sigma_{xx} = -\frac{2}{\pi}\int_0^{+\infty} t^2[D_1(t)\cosh(tx) + D_4(t)\,t\,x\sinh(tx)]\cos(ty)\,dt \tag{3.90}$$

$$\begin{aligned}\sigma_{yy} &= \frac{2}{\pi}\int_0^{+\infty} t^2\{D_1(t)\cosh(tx) + D_4(t)\,[2\cosh(tx)+\\ &+ t\,x\sinh(tx)]\}\cos(ty)\,dt\end{aligned} \tag{3.91}$$

$$\begin{aligned}\tau_{xy} &= \frac{2}{\pi}\int_0^{+\infty} t^2\{D_1(t)\sinh(tx) + D_4(t)\,[\sinh(tx)+\\ &+ t\,x\cosh(tx)]\}\sin(ty)\,dt\end{aligned} \tag{3.92}$$

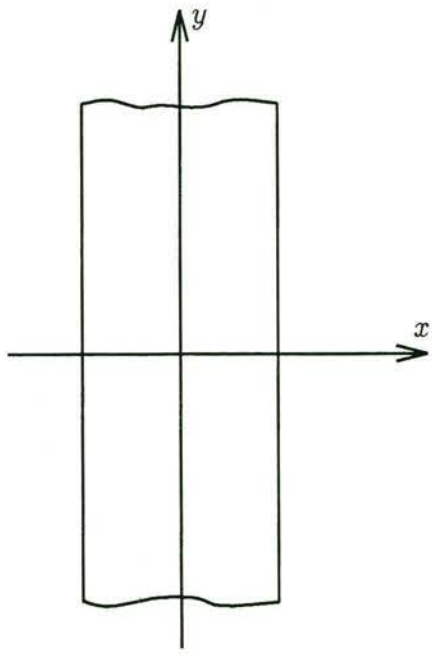

Figure 3.3: An infinitely long strip of finite thickness without a crack

$$u = -\frac{2}{\pi}\frac{1}{4\mu}\int_0^{+\infty} t\,\{2D_1(t)\sinh(tx) + D_4(t)\,[(1-\kappa)\sinh(tx) + \\ + \quad 2t\,x\cosh(tx)]\}\,\cos(ty)\,dt \tag{3.93}$$

$$v = \frac{2}{\pi}\frac{1}{4\mu}\int_0^{+\infty} t\,\{2D_1(t)\cosh(tx) + D_4(t)\,[(1+\kappa)\cosh(tx) + \\ + \quad 2t\,x\sinh(tx)]\}\,\sin(ty)\,dt \tag{3.94}$$

The expressions (3.90)–(3.94) have been incorporated into the solutions of crack problems under opening mode I in an isotropic strip by Sneddon & Lowengrub (1969) and Sneddon & Srivastav (1971), and in composites by Hilton & Sih (1971), Bogy (1973), Gupta (1973), Sih & Chen (1981), Fan *et al.* (1991), and Kaw & Besterfield (1992).

For skew-symmetric loading, the counterparts of the above formulae are

$$\varphi(x,y) = \frac{2}{\pi}\int_0^{+\infty} [D_2(t)\,t\,x\cosh(tx) + D_3(t)\sinh(tx)]\,\sin(ty)\,dt \tag{3.95}$$

$$\sigma_{xx} = -\frac{2}{\pi}\int_0^{+\infty} t^2[D_2(t)t\,x\cosh(tx) + D_3(t)\,\sinh(tx)]\sin(ty)\,dt \tag{3.96}$$

$$\begin{aligned}\sigma_{yy} &= \frac{2}{\pi}\int_0^{+\infty} t^2\{D_2(t)\,[2\sinh(tx) + t\,x\cosh(tx)] + \\ &+ D_3(t)\,\sinh(tx)\}\,\sin(ty)\,dt\end{aligned} \tag{3.97}$$

$$\begin{aligned}\tau_{xy} &= -\frac{2}{\pi}\int_0^{+\infty} t^2\{D_2(t)\,[\cosh(tx) + t\,x\sinh(tx)] + \\ &+ D_3(t)\,\cosh(tx)]\}\,\cos(ty)\,dt\end{aligned} \tag{3.98}$$

$$\begin{aligned}u &= -\frac{2}{\pi}\frac{1}{4\mu}\int_0^{+\infty} t\{D_2(t)\,[(1-\kappa)\cosh(tx) + 2t\,x\sinh(tx)] + \\ &+ 2D_3(t)\,\cosh(tx)\}\,\sin(ty)\,dt\end{aligned} \tag{3.99}$$

$$\begin{aligned}v &= -\frac{2}{\pi}\frac{1}{4\mu}\int_0^{+\infty} t\{D_2(t)\,[(1+\kappa)\sinh(tx) + 2t\,x\cosh(tx)] + \\ &+ 2D_3(t)\,\sinh(tx)\}\,\cos(ty)\,dt\end{aligned} \tag{3.100}$$

The expressions (3.96)–(3.100) have appeared in the solutions of crack problems for in-plane shear loading condition in the works of Hilton & Sih (1971), Bogy (1973) and Sih & Chen (1981).

In the next Chapter, the basic solutions given in §§ 3.4 and 3.5 will be utilised to solve the crack problems in composite laminates when the cracks appear in an infinitely long transversely isotropic strip of finite thickness.

3.6 Basic Solution for an Orthotropic Strip of Finite Thickness

In this Section, the basic solution for an infinitely long orthotropic strip of finite thickness is presented. The procedure is similar to that followed in the work of Konishi & Atsumi (1973). If the strip shown in Figure 3.3 is an orthotropic medium whose principal elastic axes (in two-dimensional case) are parallel with x- and y-axes, respectively, then the constitutive equations are as follows

$$\sigma_{xx} = c_{11}\,\varepsilon_{xx} + c_{12}\,\varepsilon_{yy} \tag{3.101}$$

$$\sigma_{yy} = c_{12}\,\varepsilon_{xx} + c_{22}\,\varepsilon_{yy} \tag{3.102}$$

$$\tau_{xy} = c_{66}\,\gamma_{xy} \tag{3.103}$$

where c_{ij} $(i,j = 1,2,6)$ $(c_{16} = c_{26} = 0)$ are the stiffness coefficients.

Substituting these expressions for stresses into the equilibrium equation and making use of strain-displacement relations (3.41)–(3.43) gives (Konishi & Atsumi, 1973)

$$c_{11}\frac{\partial^2 u}{\partial x^2} + c_{66}\frac{\partial^2 u}{\partial y^2} + (c_{12}+c_{66})\frac{\partial^2 v}{\partial xy} = 0 \tag{3.104}$$

$$c_{66}\frac{\partial^2 v}{\partial x^2} + c_{22}\frac{\partial^2 v}{\partial y^2} + (c_{12}+c_{66})\frac{\partial^2 u}{\partial xy} = 0 \tag{3.105}$$

The Fourier transforms of u and v with respect to y in the coordinate system of Figure 3.3 can be written as

$$\overline{u}(x,t) = \int_{-\infty}^{+\infty} u(x,y)\, e^{ity}\, dy \tag{3.106}$$

$$\overline{v}(x,t) = \int_{-\infty}^{+\infty} v(x,y)\, e^{ity}\, dy \tag{3.107}$$

Applying these transforms to (3.104)–(3.105) leads to the equations

$$c_{11}\frac{d^2\overline{u}}{dx^2} - c_{66}\,t^2\,\overline{u} - i\,t\,(c_{12}+c_{66})\frac{d\overline{v}}{dx} = 0 \tag{3.108}$$

$$c_{66}\frac{d^2\overline{v}}{dx^2} - c_{22}\,t^2\,\overline{v} - i\,t\,(c_{12}+c_{66})\frac{d\overline{u}}{dx} = 0 \tag{3.109}$$

The two unknown functions in the above two equations can be obtained by simple elimination. For instance, eliminating $\overline{v}$ from them by proper differentiation and substitution will lead to the following ordinary differential equation of the fourth order in $\overline{u}$ (see also Konishi & Atsumi, 1973)

$$\frac{d^4\overline{u}}{dx^4} - 2U_1\,t^2\,\frac{d^2\overline{u}}{dx^2} + U_2\,t^4\,\overline{u} = 0 \tag{3.110}$$

where U_1 and U_2 given by

$$2U_1 = \frac{c_{66}^2 + c_{11}c_{22} - (c_{12}+c_{66})^2}{c_{11}c_{66}} \tag{3.111}$$

$$U_2 = \frac{c_{22}}{c_{11}} \tag{3.112}$$

Let us discuss the solution of the differential equation (3.110). Its characteristic equation is

$$r^4 - 2U_1 t^2\, r^2 + U_2 t^4 = 0 \tag{3.113}$$

Generally, the roots of this quartic equation are

$$r^2 = \left(U_1 \pm \sqrt{U_1^2 - U_2}\right) t^2 \tag{3.114}$$

Denoting

$$\beta_1 = \sqrt{U_1 + \sqrt{U_1^2 - U_2}} \quad \beta_2 = \sqrt{U_1 - \sqrt{U_1^2 - U_2}} \tag{3.115}$$

and

$$x_1 = \beta_1 t\, x \quad x_2 = \beta_2 t\, x, \tag{3.116}$$

the general solution of the differential equation (3.110) can be expressed as

$$\overline{u}(x,t) = A_1 \sinh x_1 + B_1 \cosh x_1 + A_2 \sinh x_2 + B_2 \cosh x_2 \tag{3.117}$$

where A_1, B_1, A_2 and B_2 are functions of t to be determined from the boundary conditions of the problem.

However, eqn (3.117) is not the only possible form of solution. One minor alternative form of the solution is that when β_1 and β_2 are complex numbers. This case will be discussed later in the Thesis (Appendix D) when the above solution is applied to particular materials. Another form of solution will appear when $U_1^2 - U_2 = 0$, which has not been discussed in the work of Konishi & Atsumi (1973). Under this condition, eqn (3.113) will degenerate into a perfect square of a quadratic equation in r

$$\left(r^2 - U_1 t^2\right)^2 = 0 \tag{3.118}$$

so that it has two double roots

$$r_1 = +\beta_0 t \qquad r_2 = -\beta_0 t \tag{3.119}$$

where

$$\beta_0 = \sqrt{U_1} \tag{3.120}$$

As a result the solution of the differential equation (3.110) is

$$\overline{u}(x,t) = A_0 x_0 \sinh x_0 + B_0 x_0 \cosh x_0 + A_1 \sinh x_0 + B_1 \cosh x_0 \tag{3.121}$$

where

$$x_0 = \beta_0 x\, t \tag{3.122}$$

A_0, B_0, A_1 and B_1 are functions of t to be determined from the boundary conditions. For the sake of conciseness, the same notation A_1 and B_1 of two arbitrary functions has been used in the two solutions (3.117) and (3.121). Because these solutions will never be used simultaneously, this notation should not cause any confusion.

The components of stresses and displacements can now be obtained by substituting (3.117) or (3.121), as appropriate, into the following relations

$$\sigma_{xx} = \frac{1}{2\pi}\frac{1}{c_{22}(c_{12}+c_{66})}\int_{-\infty}^{+\infty}\frac{1}{t^2}\left\{-c_{11}c_{12}c_{66}\frac{d^3\overline{u}}{dx^3}+[c_{11}c_{22}(c_{12}+c_{66})- \right.$$
$$\left. - c_{12}^2(c_{12}+2c_{66})]\,t^2\frac{d\overline{u}}{dx}\right\}e^{-ity}\,dt \tag{3.123}$$

$$\sigma_{yy} = \frac{1}{2\pi}\frac{1}{c_{12}+c_{66}}\int_{-\infty}^{+\infty}\frac{1}{t^2}\left\{-c_{11}c_{66}\frac{d^3\overline{u}}{dx^3}+[c_{12}(c_{12}+c_{66})- \right.$$
$$\left. - c_{12}(c_{12}+2c_{66})]\,t^2\frac{d\overline{u}}{dx}\right\}e^{-ity}\,dt \tag{3.124}$$

$$\tau_{xy} = \frac{1}{2\pi}\frac{c_{66}}{c_{12}+c_{66}}\int_{-\infty}^{+\infty}\frac{1}{it}\left(c_{11}\frac{d^2\overline{u}}{dx^2}+c_{12}t^2\,\overline{u}\right)e^{-ity}\,dt \tag{3.125}$$

$$u = \frac{1}{2\pi}\int_{-\infty}^{+\infty}\overline{u}\,e^{-ity}\,dt \tag{3.126}$$

$$v = \frac{1}{2\pi}\frac{1}{c_{22}(c_{12}+c_{66})}\int_{-\infty}^{+\infty}\frac{1}{it^3}\left\{c_{11}c_{66}\frac{d^3\overline{u}}{dx^3}+c_{12}(c_{12}+2c_{66})t^2\frac{d\overline{u}}{dx}\right\}e^{-ity}dt \tag{3.127}$$

In eqns (3.123)–(3.127), the stresses and displacement v have been expressed in terms of $\overline{u}$ and its derivatives with respect to x instead of the integrals of $\overline{u}$, as has been done by Konishi & Atsumi (1973). Similarly, we can also solve $\overline{v}$ first and express other components in terms of $\overline{v}$ and its derivatives. Under certain conditions of symmetry, these expressions can be easily reduced to corresponding sine or cosine transforms, as was done above (see (3.68)–(3.73) or (3.82)–(3.87)).

3.7 Elements of Lamination Theory

This Section presents the calculation of the stiffness and stress field of fibre-reinforced composite laminates, following the book of Tsai & Hahn (1980). Again some notation here is different from that book. For instance, the notation x and y is used in the book to denote the directions along and perpendicular to the fibre, respectively, for a unidirectional lamina. Here, the notation L and T will be used to denote these two directions. In order to avoid confusion, all the symbols used in this Section will be defined where they appear first. The definition of a symbol introduced in this Section will remain in force throughout this Thesis, unless otherwise explicitly indicated. It should be pointed out that only a very short and simple part of the lamination theory is presented here. More details of the analysis of laminates can be found in the above-mentioned or other similar books.

3.7.1 Stress-Strain Relations of Unidirectional Lamina

A fibre-reinforced unidirectional lamina is regarded macroscopically as an isotropic and homogeneous medium in the plane parallel to the fibre. In this plane the two principal elastic axes are parallel and perpendicular to the fibre direction. These axes are designated by L and T in Figure 3.4, with L denoting the direction along the fibre. This direction is also called the longitudinal direction. T denotes the direction perpendicular to the fibre; it is also called the transverse direction. When the axes of a coordinate system coincide with the elastic principal axes, the coordinate system is called the on-axis system. Otherwise, it is called an off-axis system.

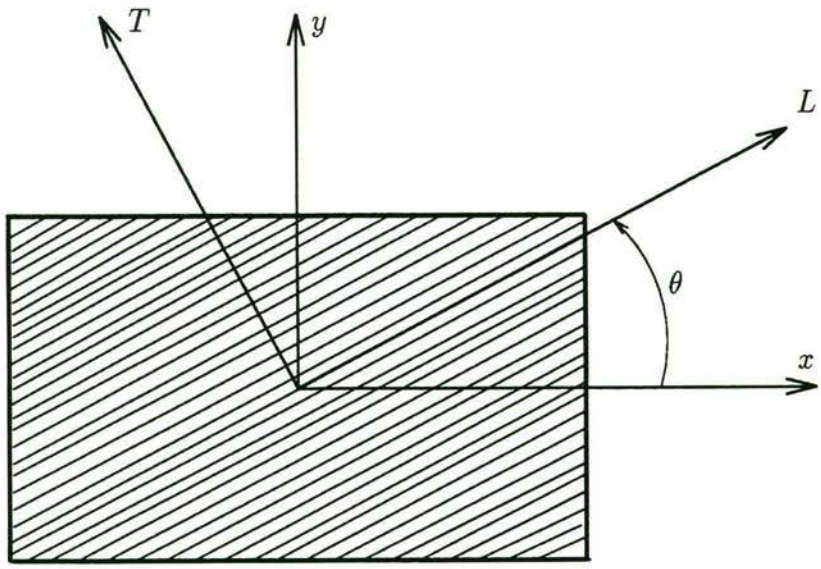

Figure 3.4: A fibre-reinforced unidirectional lamina. The on-axis coordinate system is denoted by L and T, and the off-axis by x and y

For the unidirectional lamina shown in Figure 3.4, the elastic constants in the LT plane are E_L, E_T, G_{LT} and ν_{LT}. Here E_L is the longitudinal Young's modulus, E_T is the transverse Young's modulus, G_{LT} the shear modulus in LT plane, and ν_{LT} is the Poisson ratio, defined as

$$\nu_{LT} = -\frac{\varepsilon_T}{\varepsilon_L} \tag{3.128}$$

where ε_L and ε_T are the strains in the longitudinal and transverse directions, respectively, when the lamina is subjected to a unidirectional load in the longitudinal direction.

The stress-strain relations in the on-axis system are

$$\begin{bmatrix} \sigma_{LL} \\ \sigma_{TT} \\ \tau_{LT} \end{bmatrix} = \begin{bmatrix} Q_{LL} & Q_{LT} & 0 \\ Q_{TL} & Q_{TT} & 0 \\ 0 & 0 & Q_{SS} \end{bmatrix} \begin{bmatrix} \varepsilon_{LL} \\ \varepsilon_{TT} \\ \gamma_{LT} \end{bmatrix} \tag{3.129}$$

where Q_{LL}, Q_{TT} and Q_{LT} $(= Q_{TL})$ are given by

$$Q_{LL} = \frac{E_L}{1 - \nu_{LT}\,\nu_{TL}} \tag{3.130}$$

$$Q_{LT} = \frac{E_L\,\nu_{TL}}{1 - \nu_{LT}\,\nu_{TL}} \tag{3.131}$$

$$Q_{TT} = \frac{E_T}{1 - \nu_{LT}\,\nu_{TL}} \tag{3.132}$$

$$Q_{SS} = G_{LT} \tag{3.133}$$

in which ν_{TL} can be expressed as

$$\nu_{TL} = \frac{E_T}{E_L}\nu_{LT} \tag{3.134}$$

When the lamina is considered in a general off-axis coordinate system where x and y are the reference axes as shown in Figure 3.4, the stress-strain relations are

$$\begin{bmatrix} \sigma_1 \\ \sigma_2 \\ \sigma_6 \end{bmatrix} = \begin{bmatrix} Q_{11} & Q_{12} & Q_{16} \\ Q_{21} & Q_{22} & Q_{26} \\ Q_{61} & Q_{62} & Q_{66} \end{bmatrix} \begin{bmatrix} \varepsilon_1 \\ \varepsilon_2 \\ \varepsilon_6 \end{bmatrix} \tag{3.135}$$

where σ_1 and σ_2 are the stresses along $x-$ and $y-$directions, respectively, and σ_6 denotes the shear stress in xy-plane. ε_i $(i = 1, 2, 6)$ are the corresponding strains. Q_{ij} $(i, j = 1, 2, 6)$ are expressed as

$$Q_{11} = U_1 + U_2 \cos 2\theta + U_3 \cos 4\theta \tag{3.136}$$

$$Q_{22} = U_1 - U_2 \cos 2\theta + U_3 \cos 4\theta \tag{3.137}$$

$$Q_{12} = U_4 - U_3 \cos 4\theta \tag{3.138}$$

$$Q_{16} = \frac{1}{2}U_2 \sin 2\theta + U_3 \sin 4\theta \tag{3.139}$$

$$Q_{26} = \frac{1}{2}U_2 \sin 2\theta - U_3 \sin 4\theta \tag{3.140}$$

$$Q_{66} = U_5 - U_3 \cos 4\theta \tag{3.141}$$

in which

$$U_1 = \frac{1}{8}[3Q_{LL} + 3Q_{TT} + 2Q_{LT} + 4Q_{SS}] \tag{3.142}$$

$$U_2 = \frac{1}{2}[Q_{LL} - Q_{TT}] \tag{3.143}$$

$$U_3 = \frac{1}{8}[Q_{LL} + Q_{TT} - 2Q_{LT} - 4Q_{SS}] \tag{3.144}$$

$$U_4 = \frac{1}{8}[Q_{LL} + Q_{TT} + 6Q_{LT} - 4Q_{SS}] \tag{3.145}$$

$$U_5 = \frac{1}{8}[Q_{LL} + Q_{TT} - 2Q_{LT} + 4Q_{SS}] \tag{3.146}$$

3.7.2 Calculation of In-Plane Laminate Stresses

A multidirectional laminate is composed of more than one unidirectional laminae each with its longitudinal axis in a different direction with respect to a reference system, e.g. the one shown in Figure 3.5. A typical cross-section of the multidirectional laminate is shown in Figure 3.6. Here, we consider only the in-plane (laminate plane) deformation of the laminate. It is assumed that the strain is constant across the laminate thickness (Tsai & Hahn, 1980). The components of the strains are denoted by

$$\varepsilon_1, \quad \varepsilon_2, \quad \varepsilon_6 \tag{3.147}$$

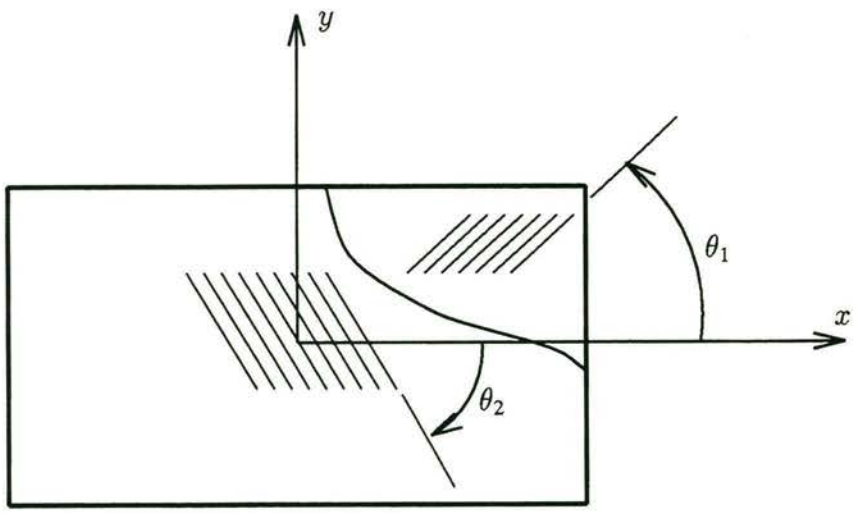

Figure 3.5: A fibre-reinforced multidirectional laminate. θ_1 and θ_2 indicate longitudinal directions of two constituent laminae in the laminate

Under this deformation, the components of the stress in a constituent lamina in the laminate are expressed by (3.135).

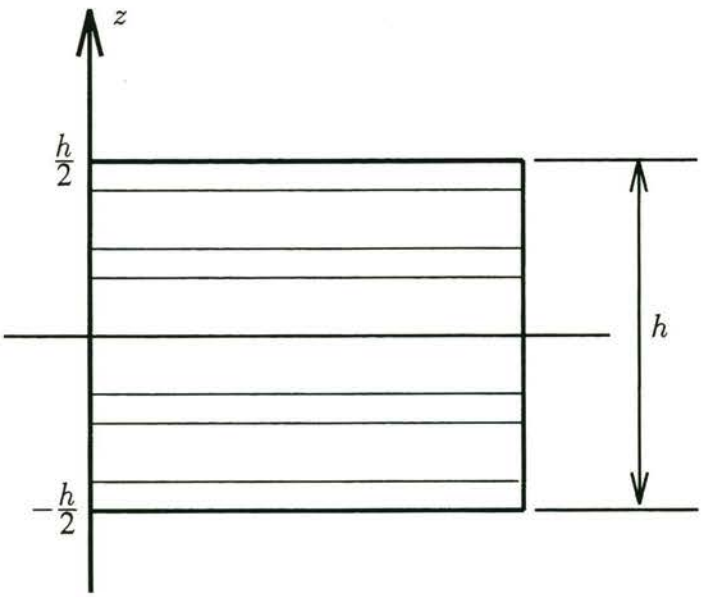

Figure 3.6: Cross-section of a fibre-reinforced multidirectional laminate, showing a geometric mid-plane

In the stress analysis of the laminate, as in the traditional analysis of thin plates, it is expedient to use the average stresses and stress resultants across the thickness. The average stresses are defined as

$$\overline{\sigma_1} = \frac{1}{h}\int_{-h/2}^{h/2} \sigma_1 \, dz \tag{3.148}$$

$$\overline{\sigma_2} = \frac{1}{h}\int_{-h/2}^{h/2} \sigma_2 \, dz \tag{3.149}$$

$$\overline{\sigma_6} = \frac{1}{h}\int_{-h/2}^{h/2} \sigma_6 \, dz \tag{3.150}$$

Substituting the stress-strain relations (3.135) into the above expressions, we get

$$\begin{bmatrix} \overline{\sigma_1} \\ \overline{\sigma_2} \\ \overline{\sigma_6} \end{bmatrix} = \frac{1}{h} \begin{bmatrix} A_{11} & A_{12} & A_{16} \\ A_{21} & A_{22} & A_{26} \\ A_{61} & A_{62} & A_{66} \end{bmatrix} \begin{bmatrix} \varepsilon_1 \\ \varepsilon_2 \\ \varepsilon_6 \end{bmatrix} \tag{3.151}$$

where

$$A_{ij} = \int_{-h/2}^{h/2} Q_{ij} \, dz, \quad i,j = 1,2,6 \tag{3.152}$$

If we further define the stress resultant as

$$N_i = h\,\overline{\sigma_i}, \quad i = 1,2,6 \tag{3.153}$$

we obtain the relations between the stress resultants and the strains in the laminate

$$\begin{bmatrix} N_1 \\ N_2 \\ N_6 \end{bmatrix} = \begin{bmatrix} A_{11} & A_{12} & A_{16} \\ A_{21} & A_{22} & A_{26} \\ A_{61} & A_{62} & A_{66} \end{bmatrix} \begin{bmatrix} \varepsilon_1 \\ \varepsilon_2 \\ \varepsilon_6 \end{bmatrix} \tag{3.154}$$

If the applied loads N_i $(i = 1, 2, 6)$ are known, it is easy to get the strain ε_i by the inversion of the above expressions. The stresses in the constituent laminae in the laminate can then be calculated by using eqn (3.135). These stresses are obtained with respect to the reference coordinate system xy. The components of the stresses in the on-axis system LT are obtained using the transformation matrix

$$\begin{bmatrix} \sigma_L \\ \sigma_T \\ \tau_{LT} \end{bmatrix} = \begin{bmatrix} m^2 & n^2 & 2mn \\ n^2 & m^2 & -2mn \\ -mn & mn & m^2 - n^2 \end{bmatrix} \begin{bmatrix} \sigma_1 \\ \sigma_2 \\ \sigma_6 \end{bmatrix} \tag{3.155}$$

where $m = \cos\theta$ and $n = \sin\theta$. The components of the stress in the LT system are useful in the strength prediction of the lamina.

For future reference, we present the average stress-strain relations for two angle-ply laminates. First, we consider an antisymmetric angle-ply $[(\pm\theta)_n/(\mp\theta)_n]$ laminate. Suppose that the ply thickness is t. Then the total thickness of the laminate is $h = 2nt$ (Figure 3.6). Since Q_{16} and Q_{26} in eqns (3.136)–(3.141) are odd functions of θ but the other coefficients are even functions, the in-plane moduli A_{ij} of this laminate may be formally written using (3.152)

$$\begin{bmatrix} A_{11} & A_{12} & A_{16} \\ A_{21} & A_{22} & A_{26} \\ A_{61} & A_{62} & A_{66} \end{bmatrix} = 2nt \begin{bmatrix} Q_{11} & Q_{12} & 0 \\ Q_{21} & Q_{22} & 0 \\ 0 & 0 & Q_{66} \end{bmatrix} \tag{3.156}$$

Substituting the above expressions into (3.151) and noting that $h = 2nt$, we get the relations between the average stresses and strains

$$\begin{bmatrix} \overline{\sigma_1} \\ \overline{\sigma_2} \\ \overline{\sigma_6} \end{bmatrix} = \begin{bmatrix} Q_{11} & Q_{12} & 0 \\ Q_{21} & Q_{22} & 0 \\ 0 & 0 & Q_{66} \end{bmatrix} \begin{bmatrix} \varepsilon_1 \\ \varepsilon_2 \\ \varepsilon_6 \end{bmatrix} \tag{3.157}$$

Therefore, the laminate behaves macroscopically like an orthotropic medium. Similarly, it can be shown that its overall flexural moduli are also like those of an orthotropic medium. However, there is an in-plane/out-of-plane coupling effect in an antisymmetric laminate. The details of this coupling can be found in the book of Tsai & Hahn (1980).

Secondly, we consider a symmetric $[(\pm\theta)_n]_s$ angle-ply laminate. Because of the equal number of plies in $+\theta$ and $-\theta$ directions and because Q_{16} and Q_{26} in eqns (3.136)–(3.141) are

odd functions of θ whereas the other coefficients are even functions, the in-plane moduli A_{ij} can also be written as (3.156). Following the same procedure that led to (3.157), the relations between the average stresses and strains for the symmetric angle-ply laminate can be written as

$$\begin{bmatrix} \overline{\sigma_1} \\ \overline{\sigma_2} \\ \overline{\sigma_6} \end{bmatrix} = \begin{bmatrix} Q_{11} & Q_{12} & 0 \\ Q_{21} & Q_{22} & 0 \\ 0 & 0 & Q_{66} \end{bmatrix} \begin{bmatrix} \varepsilon_1 \\ \varepsilon_2 \\ \varepsilon_6 \end{bmatrix} \tag{3.158}$$

which are identical to (3.157). Thus this symmetric laminate also behaves macroscopically like an orthotropic medium when subjected to in-plane loading. But its flexural moduli are different from those of the above antisymmetric laminate.

3.8 Elements of Optimization Techniques

This Section presents a brief introduction of the formulation of an optimization problem and optimization algorithms which will be used in this Thesis. A general mathematical optimization problem may be stated as follows

$$\text{Min } F(\mathbf{x}) \tag{3.159}$$

subject to

$$g_i(\mathbf{x}) = 0; \quad i = 1, ..., m_1 \tag{3.160}$$

$$g_j(\mathbf{x}) \leq 0; \quad j = 1, ..., m_2 \tag{3.161}$$

where $\mathbf{x}$ denotes the vector of design variables, and g_i and g_j describe the behavioural and other constraints.

The design variables can be grouped into size, geometry and topology. Optimal size design involves variables such as member cross-sectional parameters, e.g. thicknesses of laminae in a laminate. Geometrical design variables include positions of supports, shape of two- or three-dimensional continua etc. Topological optimization includes selection of the actual members of a structure or the structural model itself. In general, sizing optimization gives relatively limited results, whereas the inclusion of geometrical and topological design variables gives more flexibility and better designs, but the corresponding optimization problems are also more difficult to solve.

Objective functions may be either geometrical or physical quantities, i.e. weight, strength, toughness etc. which are desired to be minimized or maximized.

The constraints in (3.160)–(3.161) are given by limits and bounds on geometrical, physical quantities or follow from mathematical considerations. The physical quantities may include stresses, displacements, buckling loads, stress intensity factors, and so on.

Generally, the optimization problem described in (3.159)–(3.161) is a nonlinear one. It can be solved by a number of nonlinear programming (NLP) techniques. In the following a brief outline of five of the most common methods will be given (Karihaloo, 1993). They are: sequential unconstrained minimization technique, SUMT (Fiacco & McCormick, 1968); the augmented Lagrangian multiplier method, ALM (Rockafellar, 1973; Pierre & Lowe, 1975; Powell, 1978, and Imai & Schmit, 1981); sequential linear programming with move limits, SLP (Kelly, 1960; Moses, 1964, and Pedersen, 1981); sequential quadratic programming, SQP (Powell, 1978) and sequential convex programming, SCP (Fleury & Braibant, 1986).

In SUMT, the constraints are added to the objective using penalty terms to form unconstrained minimization sub-problems. Depending upon the penalty terms, there are many variants of SUMT.

The augmented Lagrangian multiplier method ALM differs from the conventional SUMT in that a quadratic term is added to the Lagrangian $L(\mathbf{x}, \mu)$ and not to the objective function $F(\mathbf{x})$

$$L(\mathbf{x}, \mu) = F(\mathbf{x}) - \sum_{i=1}^{m_1} \mu_i \, g_i(\mathbf{x}), \tag{3.162}$$

$$M(\mathbf{x}, \mu) = L(\mathbf{x}, \mu) + \frac{c}{2} \sum_{i=1}^{m_1} \mu_i \, g_i^2(\mathbf{x}), \tag{3.163}$$

where μ_i are uknown Lagrangian multipliers and $g_i(\mathbf{x})$ are equality constraints.

In SLP, the nonlinear objective and constraints are linearized at the current design $\mathbf{x^0}$ using only direct design variables. For instance ($n = m_1 + m_2$),

$$\tilde{\mathbf{g}}(\mathbf{x}) = \mathbf{g}(\mathbf{x^0}) + \sum_{i=1}^{n} \left. \frac{\partial \mathbf{g}(\mathbf{x})}{\partial x_i} \right|_{\mathbf{x^0}} dx_i \tag{3.164}$$

By this approach and using move limits, the original NLP is replaced with a sequence of linear sub-problems.

In SQP, the Lagrangian corresponding to the objective function is approximated by a quadratic function but the constraints are linearized. In this way the original NLP is replaced with a sequence of quadratic sub-problems. The convergence of the algorithm is forced by a line search with respect to an exact penalty function or an augmented Lagrangian merit function (3.163).

In SCP, the nonlinear objective and constraints are linearized at the current design $\mathbf{x^0}$ using mixed direct $(+)$ or reciprocal $(-)$ design variables depending on the sign of their gradients. For instance

$$\tilde{\mathbf{g}}(\mathbf{x}) = \mathbf{g}(\mathbf{x^0}) + \sum_{+} \left. \frac{\partial \mathbf{g}}{\partial x_i} \right|_{\mathbf{x^0}} (x_i - x_i^0) + \sum_{-} \left. \frac{\partial \mathbf{g}}{\partial x_i} \right|_{\mathbf{x^0}} \frac{x_i^0}{x_i} (x_i - x_i^0) \tag{3.165}$$

Thus the original NLP is replaced with a sequence of explicit, convex and separable linear sub-problems.

All the five methods are available in a general purpose package called ADS (Automated Design Synthesis) by Vanderplaats (1987).

PART I

The first part of the Thesis consists of Chapters 4 and 5. In these Chapters we obtain the solutions to the boundary-value problems of cracked composite regions. Although these problems are motivated by the failure characteristics of fibre-reinforced composites, the solutions can be applied to crack problems in finite regions made up of dissimilar subregions.

Chapter 4

Composite Laminate with Intralaminar Crack

4.1 Introductory Remarks

The elastostatic fracture problems involving composites made by bonding two dissimilar media have attracted continuing interest for a long time. Basically, there are two types of problems concerning the crack/inhomogeneity interaction, depending on the relative position of the crack(s) with respect to the interfaces between the media. The first type of problems relates to cracks that are within the interfaces, and the second type to cracks that are wholly within one material or touching the bimaterial interfaces at an angle. In the present exposition, we will only be concerned with the second type of crack configuration where the cracks are perpendicular to the bimaterial interfaces. The case when a crack (or cracks) is wholly within one homogeneous isotropic material and is lying perpendicular to a bimaterial interface between two dissimilar isotropic media has been attempted in the works of Cook & Erdogan (1972), Hilton & Sih (1971), Bogy (1973), Erdogan & Bakioglu (1976), Sih & Chen (1981), Ahmad (1991), and others. Kaw & Besterfield (1992) solved a more complicated crack problem arising from a bonded finite strip between two half-planes where the half planes contain multiple periodic cracks. For the combination of two dissimilar homogeneous orthotropic materials, Arin (1977), and Delale & Erdogan (1979) solved the second type of crack problems when the crack tip did not touch the interface. Erdogan *et al.* (1991a,b) solved two interesting crack problems of this type in bonded homogeneous/nonhomogeneous materials, in which one of the materials has variable elastic properties along one dimension. A common feature of the works cited above is that one of the bonded media is of infinite extent or the composite has a periodic structure.

Fan *et al.* (1989), and Bai (1989) considered the mode I crack problem in a cross-ply laminate of finite thickness. In a two-dimensional approximation, the materials forming the

laminate alternated between transversely isotropic and orthotropic media. Wu & Erdogan (1993) solved the crack problem in two bonded orthotropic layers of finite thickness. Solutions were given both when the crack is wholly within one medium and when it is touching the interface. The most recent work of Erdogan & Kadioglu (1994) considered the interaction of cracks in a bonded orthotropic/orthotropic composite. The cracked composite contained two interfacial cracks and one intralaminar crack perpendicular to the interface.

As mentioned in Chapter 3, a unidirectional fibre-reinforced lamina may be regarded macroscopically as an orthotropic medium in the plane parallel to the fibres. On the other hand, in the transverse direction, i.e. in the plane perpendicular to the fibres, it depicts macroscopically the mechanical properties of an isotropic material. In some sandwich plates, the core material is isotropic and weak. The facets bear the major flexural and/or tensile loads. They are stronger and may possess orthotropic properties so as to resist loads along the principal directions. These are just two examples of bonded isotropic/orthotropic composites in which the evaluation of influence of any cracks on the macroscopic response is of prime concern. Therefore, in this Chapter, we will first solve the boundary-value problem arising from a cracked bonded composite, shown in Figure 4.1. This is an idealized model of a single crack existing in the central layer of the composite. The physical background for this model is provided by experimental observations of cracking in composite laminates (Garrett & Bailey, 1977; Bailey & Parvizi, 1981; Highsmith & Reifsnider, 1982; Crossman & Wang, 1982). This simple model will be extended to the case of multiple cracks at the end of this Chapter. The major part of the work described in this Chapter has been published in two papers by Wang & Karihaloo (1994a; 1994b).

4.2 Boundary-Value Problem for a Composite Laminate with a Single Crack

The model of a symmetrically bonded composite laminate studied in this Chapter is shown in Figure 4.1. The central sublaminate is a homogeneous isotropic or transversely isotropic (in xy-plane) medium with elastic constants μ, κ which have been previously defined in Chapter 3. The two outer sublaminates of thickness b are made of an orthotropic material whose principal planes of elasticity are parallel to the coordinate planes. Their elastic properties in xy-plane are determined by the stiffness parameters c_{11}, c_{12}, c_{22} and c_{66} and those in yz- and zx-planes by c_{44}, c_{55}. The composite laminate is assumed to be infinitely long in the y-direction compared with its thickness. The inner sublaminate of thickness $2d$ contains a central transverse crack of length $2a$.

The model being studied is similar to that studied by Fan *et al.* (1989), and Bai (1989). The former authors were primarily concerned with the influence of the outer layers on the stress

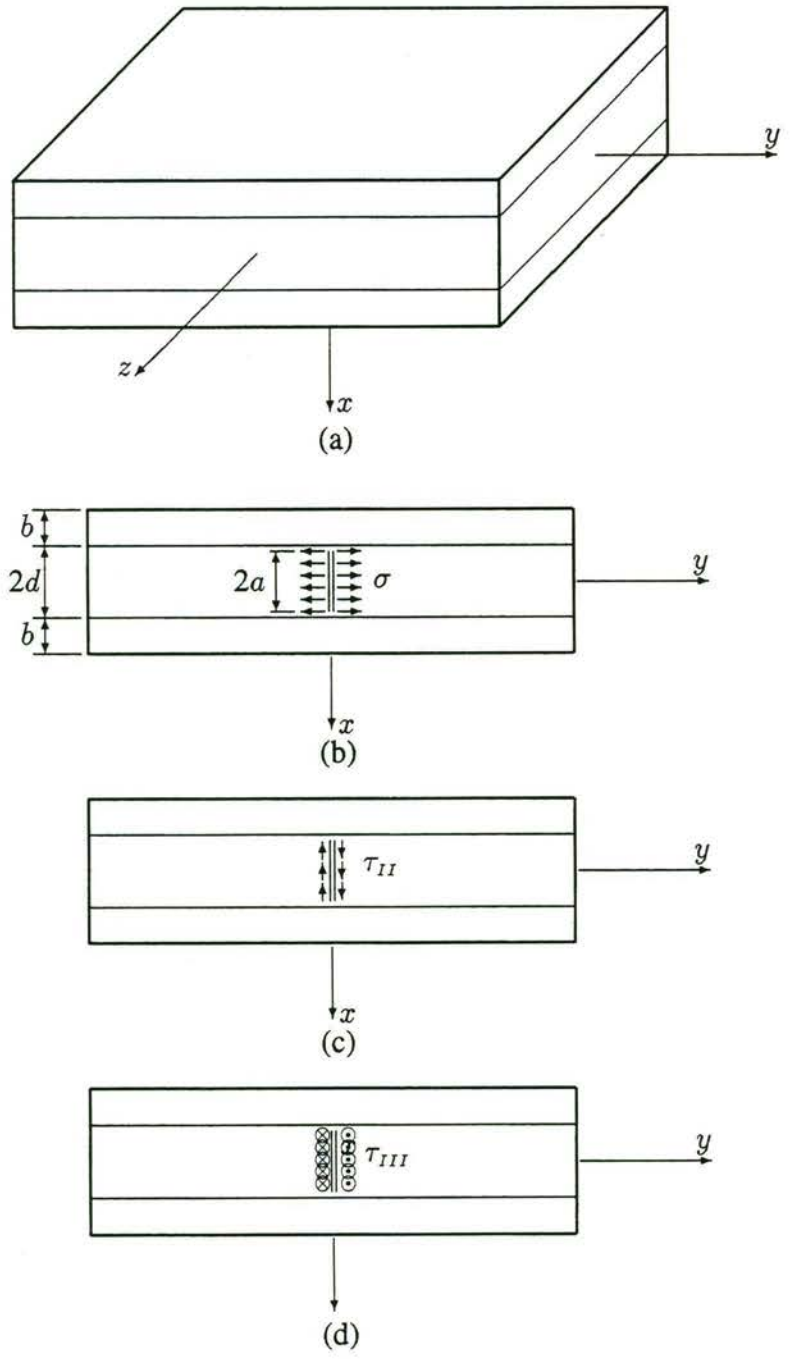

Figure 4.1: A cracked composite laminate, showing the laminate configuration (a), and the opening (b), in-plane shear (c), and anti-plane shear (d) modes of crack face loading. The central layer is transversely isotropic in xy-plane, whilst the upper and lower layers are orthotropic

intensity factor under tension at the crack tip in fibre-reinforced cross-ply laminates, whereas the latter author was concerned with the reduction in tensile stiffness due to the presence of multiple cracks.

In the following, we shall solve the two-dimensional boundary-value problems corresponding to the three loading cases shown in Figures 4.1(b), (c) and (d), when the crack faces are subjected to self-equilibrating tensile (opening), in-plane (crack plane) and antiplane shear stresses, respectively. These perturbation solutions can be superimposed on the uncracked body solution subjected to the corresponding external loadings, as is commonly done in the solution of cracked bodies. The solution under mode I loading has been given by Fan *et al.* (1989) for a $0^0/90^0/0^0$ (cross-ply) fibre-reinforced laminate. They obtained the solution to the orthotropic medium by using two displacement functions, following Sih & Chen (1981). The expressions for the stresses and displacements are similar to those which can be directly deduced from the solution of the equilibrium equations given in Chapter 3. However, the solution by Fan *et al.* (1989) did not discuss the degenerate case represented by the solution (3.121). Therefore, for completeness and for future use in the solution of multiple cracks and in Chapters 5 and 9, we shall also include the mode I solution, besides the mode II and mode III solutions that are not available in the literature.

4.3 Solution for Opening Mode I

Let us consider the opening mode crack problem, depicted in Figure 4.1(b). Because of symmetry, it is enough to consider a quarter of the laminate, say $x \geq 0, y \geq 0$. Since the central layer is (transversely) isotropic in xy-plane, we can directly use the basic solutions obtained in Chapter 3. We note that the central layer is a finite strip with a central crack. The solution to this configuration alone has been given by Sneddon & Lowengrub (1969), and Sneddon & Srivastav (1971). It can be obtained explicitly by superimposing the solution to the crack problem of an infinite plate given in § 3.3 and the solution to an uncracked finite strip given in § 3.4. This superposition technique was also used in the work of Nied (1987) for a cracked half-plane. The components of stresses and displacements are given by the summation of eqns (3.69)– (3.73) and (3.90)–(3.94).

If we rewrite the unknown functions in (3.69)–(3.73) and (3.90)–(3.94) as

$$C_1(t) = -\frac{1}{t^2} E(t) \tag{4.1}$$

$$D_1(t) = \frac{1}{t^2} A(t) \tag{4.2}$$

$$D_4(t) = \frac{1}{t^2} B(t) \tag{4.3}$$

then the expressions for the stress and displacement fields are

$$\sigma^1_{xx} = \frac{2}{\pi}\int_0^\infty (-1)\,[A(t)\cosh(tx) + B(t)\,t\,x\,\sinh(tx)]\,\cos(ty)\,dt + \\ +\frac{2}{\pi}\int_0^\infty E(t)(1-t\,y)e^{-ty}\cos(tx)\,dt \tag{4.4}$$

$$\sigma^1_{yy} = \frac{2}{\pi}\int_0^\infty \{A(t)\,\cosh(tx) + B(t)\,[2\cosh(tx) + t\,x\,\sinh(tx)]\}\,\cos(ty)\,dt + \\ +\frac{2}{\pi}\int_0^\infty E(t)\,(1+t\,y)\,e^{-ty}\,\cos(tx)\,dt \tag{4.5}$$

$$\tau^1_{xy} = \frac{2}{\pi}\int_0^\infty \{A(t)\,\sinh(tx) + B(t)[\sinh(tx) + t\,x\cosh(tx)]\}\,\sin(ty)dt + \\ +\frac{2}{\pi}\int_0^\infty E(t)\,t\,y\,e^{-ty}\sin(tx)\,dt \tag{4.6}$$

$$u^1 = \frac{2}{\pi}\frac{1}{4\mu}\int_0^\infty (-\frac{1}{t})\,\{2A(t)\sinh(tx) + B(t)[2t\,x\cosh(tx) - \tag{4.7}$$

$$-(\kappa-1)\sinh(tx)]\}\,\cos(ty)\,dt + \\ +\frac{2}{\pi}\frac{1}{4\mu}\int_0^\infty (\frac{1}{t})E(t)\,[(\kappa-1) - 2t\,y]\;e^{-ty}\sin(tx)\,dt \tag{4.8}$$

$$v^1 = \frac{2}{\pi}\frac{1}{4\mu}\int_0^\infty (\frac{1}{t})\,\{2A(t)\cosh(tx) + B(t)[(\kappa+1)\cosh(tx) + \tag{4.9}$$

$$+2t\,x\sinh(tx)]\}\,\sin(ty)\,dt + \\ +\frac{2}{\pi}\frac{1}{4\mu}\int_0^\infty (-\frac{1}{t})E(t)\,[(\kappa+1) + 2t\,y]\;e^{-ty}\cos(tx)\,dt \tag{4.10}$$

where the superscript 1 denotes the central layer. These expressions have already appeared in the works of Sneddon & Lowengrub (1969), Bogy (1973), and also Sih & Chen (1981), except for a slight difference in notation for unknown functions and elastic constants.

As each of the outer sublaminates is orthotropic, we shall use the solutions from § 3.6. Considering the symmetry and the two solution forms (3.117) and (3.121), the stresses and displacements can be written from eqns (3.123)–(3.127) as (superscript 2 denotes each of the outer layers)

$$\sigma^2_{xx} = \frac{2}{\pi}\int_0^{+\infty} t\,Q_1\big[A_1(t)\cosh x_1 + B_1(t)\sinh x_1\big]\cos(ty)\,dt + \\ +(1-\rho)\frac{2}{\pi}\int_0^{+\infty} t\,Q_2\big[A_2(t)\cosh x_2 + B_2(t)\sinh x_2\big]\cos(ty)\,dt + \\ +\rho\frac{2}{\pi}\int_0^{+\infty}\Big\{A_0(t)\big[(c_{11}\beta_0 - c_{12}Q_0)\sinh x_0 + \\ +(c_{11}\beta_0 + c_{12}Z_0)x_0\cosh x_0\big] + B_0(t)\big[(c_{11}\beta_0 - c_{12}Q_0)\cosh x_0 + \\ +(c_{11}\beta_0 + c_{12}Z_0)x_0\sinh x_0\big]\Big\}\cos(ty)\,dt \tag{4.11}$$

$$
\begin{aligned}
\sigma_{yy}^2 &= \frac{2}{\pi}\int_0^{+\infty} t\,T_1\big[A_1(t)\cosh x_1 + B_1(t)\sinh x_1\big]\cos(ty)\,dt + \\
&+(1-\rho)\frac{2}{\pi}\int_0^{+\infty} t\,T_2\big[A_2(t)\cosh x_2 + B_2(t)\sinh x_2\big]\cos(ty)\,dt + \\
&+\rho\,\frac{2}{\pi}\int_0^{+\infty} t\,\Big\{A_0(t)\big[(c_{12}\beta_0 - c_{22}Q_0)\sinh x_0 + T_0\,x_0\cosh x_0\big] + \\
&+B_0(t)\big[(c_{12}\beta_0 - c_{22}Q_0)\cosh x_0 + T_0\,x_0\sinh x_0\big]\Big\}\cos(ty)\,dt \qquad (4.12)\\
\tau_{xy}^2 &= \frac{2}{\pi}\int_0^{+\infty} t\,L_1\big[A_1(t)\sinh x_1 + B_1(t)\cosh x_1\big]\sin(ty)\,dt + \\
&+(1-\rho)\,\frac{2}{\pi}\int_0^{+\infty} t\,L_2\big[A_2(t)\sinh x_2 + B_2(t)\cosh x_2\big]\sin(ty)\,dt - \\
&-\rho\,\frac{2}{\pi}\int_0^{+\infty} t\,\Big\{A_0(t)\big[c_{66}\beta_0(Q_0 - Z_0)\cosh x_0 - L_0 x_0\sinh x_0\big] + \\
&+B_0(t)\big[c_{66}\beta_0(Q_0 - Z_0)\sinh x_0 - L_0 x_0\cosh x_0\big]\Big\}\sin(ty)\,dt \qquad (4.13)
\end{aligned}
$$

$$
\begin{aligned}
u^2 &= \frac{2}{\pi}\int_0^{+\infty}\big[A_1(t)\sinh x_1 + B_1(t)\cosh x_1\big]\cos(ty)\,dt + \\
&+(1-\rho)\,\frac{2}{\pi}\int_0^{+\infty}\big[A_2(t)\sinh x_2 + B_2(t)\cosh x_2\big]\cos(ty)\,dt + \\
&+\rho\,\frac{2}{\pi}\int_0^{+\infty}\big[A_0(t)x_0\sinh x_0 + B_0(t)x_0\cosh x_0\big]\cos(ty)\,dt \qquad (4.14)\\
v^2 &= \frac{2}{\pi}\int_0^{+\infty} Z_1\big[A_1(t)\cosh x_1 + B_1(t)\sinh x_1\big]\sin(ty)\,dt + \\
&+(1-\rho)\,\frac{2}{\pi}\int_0^{+\infty} Z_2\big[A_2(t)\cosh x_2 + B_2(t)\sinh x_2\big]\sin(ty)\,dt - \\
&-\rho\,\frac{2}{\pi}\int_0^{+\infty}\Big\{A_0(t)\big[Q_0\sinh x_0 - Z_0 x_0\cosh x_0\big] + \\
&+B_0(t)\big[Q_0\cosh x_0 - Z_0 x_0\sinh x_0\big]\Big\}\sin(ty)\,dt \qquad (4.15)
\end{aligned}
$$

In (4.11)-(4.15)

$$
x_l = \beta_l\,(x-d)\,t \qquad (l=0,1,2) \qquad (4.16)
$$

where β_l $(l=0,1,2)$ follow the definition introduced in § 3.6.

The introduction of the generalized fields (4.11)–(4.15) will enable us to recover the solution for the case when the orthotropic material 2 degenerates into an isotropic material (with elastic constants μ_2, κ_2), such that the laminate is now composed of two dissimilar isotropic materials. For this reason, the switching factor ρ has been used in (4.11)–(4.15) which is defined as

$$
\rho = \begin{cases} 0, & \text{if } \sqrt{U_1^2 - U_2} \neq 0 \\ 1, & \text{if } \sqrt{U_1^2 - U_2} = 0 \end{cases} \qquad (4.17)
$$

where U_1 and U_2 are given by (3.111)–(3.112). When $\rho = 1$, we define $x_1 = x_0 = \beta_0\,(x-d)\,t$.

The other constants in (4.11)–(4.15) are

$$Z_l = \frac{c_{66} - c_{11}\beta_l^2}{\beta_l(c_{12} + c_{66})} \tag{4.18}$$

$$L_l = c_{66}(\beta_l Z_l - 1) \quad (l = 0, 1, 2) \tag{4.19}$$

$$T_l = c_{12}\beta_l + c_{22}Z_l \tag{4.20}$$

$$Q_i = c_{11}\beta_i + c_{12}Z_i \quad (i = 1, 2) \tag{4.21}$$

$$Q_0 = \frac{c_{66} + c_{11}\beta_0^2}{\beta_0(c_{12} + c_{66})} \tag{4.22}$$

The above stress and displacement fields identically satisfy the symmetry conditions

$$\tau_{xy}^1(x, 0) = 0, \quad 0 \le x \le d \tag{4.23}$$

$$\tau_{xy}^1(0, y) = 0, \quad 0 \le y < +\infty \tag{4.24}$$

$$u^1(0, y) = 0, \quad 0 \le y < +\infty \tag{4.25}$$

$$\tau_{xy}^2(x, 0) = 0, \quad d \le x \le d + b \tag{4.26}$$

$$v^2(x, 0) = 0, \quad d \le x \le d + b \tag{4.27}$$

The arbitrary functions $A(t)$, $B(t)$, $E(t)$, $A_l(t)$ and $B_l(t)$ $(l = 0, 1, 2)$ in (4.4)–(4.15) are determined from the remaining symmetry, boundary and continuity conditions

$$v^1(x, 0) = 0; \quad x > a \tag{4.28}$$

$$\lim_{y \to 0^+} \sigma_{yy}^1(x, y) = -\sigma; \quad 0 \le x < a \tag{4.29}$$

and for $0 \le y < +\infty$,

$$\sigma_{xx}^1(d, y) = \sigma_{xx}^2(d, y) \tag{4.30}$$

$$\tau_{xy}^1(d, y) = \tau_{xy}^2(d, y) \tag{4.31}$$

$$u^1(d, y) = u^2(d, y) \tag{4.32}$$

$$v^1(d, y) = v^2(d, y) \tag{4.33}$$

$$\sigma_{xx}^2(d + b, y) = 0 \tag{4.34}$$

$$\tau_{xy}^2(d + b, y) = 0 \tag{4.35}$$

Substituting the expressions for the displacement (4.10) and the stress (4.5) into (4.28)–(4.29), respectively, and using the normalizations

$$t = \frac{s}{a} \tag{4.36}$$

$$x = r\,a, \tag{4.37}$$

we have

$$v^1(r,0) = -\frac{\kappa+1}{2\mu}\frac{1}{\pi}\int_0^{+\infty}\frac{1}{s}E(\frac{s}{a})\cos(sr)\,ds = 0; \quad r>1 \tag{4.38}$$

$$\begin{aligned}\lim_{y\to 0^+}\sigma^1_{yy}(r,y) &= \lim_{y\to 0^+}\left[\frac{2}{\pi a}\int_0^{+\infty}\left\{A(\frac{s}{a})\cosh(sr)+\right.\right.\\ &+ \left.\left.B(\frac{s}{a})\left[2\cosh(sr)+sr\sinh(sr)\right]\right\}\cos(s\frac{y}{a})+\right.\\ &+ \left.\frac{2}{\pi a}\int_0^{+\infty}E(\frac{s}{a})(1+\frac{y}{a})e^{-s\frac{y}{a}}\cos(sr)\,ds\right]\\ &= -\sigma, \quad 0\le r<1\end{aligned} \tag{4.39}$$

The functions $A(s/a)$ and $B(s/a)$ are determined from eqns (4.30)–(4.35) in a similar manner to that of Erdogan & Wu (1991) (see Appendix A) as

$$A(\frac{s}{a}) = \frac{1}{\Delta(\frac{s}{a})}\left[K_{11}F_1+K_{12}F_2+K_{13}F_3+K_{14}F_4\right] \tag{4.40}$$

$$B(\frac{s}{a}) = \frac{1}{\Delta(\frac{s}{a})}\left[K_{21}F_1+K_{22}F_2+K_{23}F_3+K_{24}F_4\right] \tag{4.41}$$

where $\Delta(\frac{s}{a})$, K_{ij} and F_j $(i=1,2; j=1,...,4)$ are listed in Appendix A ((A.33)–(A.35)).

Noting that

$$\cos(sr) \equiv \left(\frac{\pi sr}{2}\right)^{\frac{1}{2}}J_{-\frac{1}{2}}(sr) \tag{4.42}$$

where $J_{-1/2}$ is the Bessel function of the first kind, and denoting

$$F(s) = \left(\frac{\pi}{2s}\right)^{\frac{1}{2}}E(\frac{s}{a}) \tag{4.43}$$

the dual integral eqns (4.38)–(4.39) can be written in the form

$$\int_0^{\infty}F(s)\,J_{-\frac{1}{2}}(sr)\,ds = 0; \quad r>1 \tag{4.44}$$

$$\begin{aligned}\int_0^{\infty}s\,F(s)J_{-\frac{1}{2}}(sr)\,ds = -\frac{1}{\sqrt{r}}&\left[\frac{\pi a}{2}\sigma+\int_0^{\infty}\{A(\frac{s}{a})\cosh(sr)+\right.\\ &\left.+B(\frac{s}{a})[2\cosh(sr)+s\,r\sinh(sr)]\}\,ds\right];\ 0\le r<1\end{aligned} \tag{4.45}$$

As we have related the two unknown functions $A(s/a)$ and $B(s/a)$ to $E(s/a)$ through eqns (4.40) and (4.41), the only unknown function in the above dual integral equations is $F(s)$ which is related to $E(s/a)$ via eqn (4.43). This pair of dual integral equations can be solved by generalizing the procedure of Copson (1961) (see also Sih & Chen, 1981), after their reduction

to a Fredholm integral equation of the second kind. This reduction procedure has appeared elsewhere in the works of Sneddon & Srivastav (1971), Hilton & Sih (1971), and Bogy (1973). The solution of the integral equations is (Appendix B)

$$F(s) = s^{1/2} \int_0^1 \phi(\xi)\, J_0(s\xi)\, d\xi \tag{4.46}$$

where

$$\begin{aligned} \phi(\xi) &= -\left(\frac{2}{\pi}\right)^{1/2} \xi \int_0^{\xi} \frac{1}{\sqrt{\xi^2 - r^2}} \left\{ \frac{\pi a \sigma}{2} + \int_0^{+\infty} \left[A(\tfrac{s}{a}) + \right.\right. \\ &+ \left.\left. B(\tfrac{s}{a})[2\cosh(sr) + sr\sinh(sr)] \right] ds \right\} dr \end{aligned} \tag{4.47}$$

Interchanging the order of the integrations on the right hand side, we obtain

$$\begin{aligned} \phi(\xi) &= -\left(\frac{\pi}{2}\right)^{3/2} \xi\, a\, \sigma - \left(\frac{\pi}{2}\right)^{1/2} \xi \int_0^{+\infty} \left\{ A(\tfrac{s}{a})\, I_0(s\xi) + \right. \\ &+ \left. B(\tfrac{s}{a})[2I_0(s\xi) + s\xi\, I_1(s\xi)] \right\} ds \end{aligned} \tag{4.48}$$

where we have made use of the following identities

$$\int_0^{\xi} \frac{1}{\sqrt{\xi^2 - r^2}} \cosh(sr)\, dr = \frac{\pi}{2} I_0(s\xi) \tag{4.49}$$

$$\int_0^{\xi} \frac{1}{\sqrt{\xi^2 - r^2}} sr\, \sinh(sr)\, dr = \frac{\pi}{2} s\xi\, I_1(s\xi) \tag{4.50}$$

in which I_0 and I_1 are the modified Bessel functions of order zero and one, respectively.

Substituting (4.46) into (4.43) gives

$$E(\tfrac{\xi}{a}) = \left(\frac{2}{\pi}\right)^{1/2} \xi \int_0^1 \phi(\eta)\, J_0(\xi\eta)\, d\eta \tag{4.51}$$

Inserting the above expression into the formulae for F_i ((A.35), Appendix A) and using the identities (Gradshteyn & Ryzhik, 1965)

$$\int_0^{+\infty} \frac{x^{1-\nu}}{x^2 + \beta^2} \sin(\alpha x)\, J_\nu(\gamma x)\, dx = \frac{\pi}{2} \beta^{-\nu} e^{-\alpha\beta} I_\nu(\beta\gamma) \tag{4.52}$$

$$\int_0^{+\infty} \frac{x^{-\nu}}{x^2 + \beta^2} \cos(\alpha x)\, J_\nu(\gamma x)\, dx = \frac{\pi}{2} \beta^{-\nu-1} e^{-\alpha\beta} I_\nu(\beta\gamma) \tag{4.53}$$

we get

$$F_j = \left(\frac{2}{\pi}\right)^{1/2} s\, e^{-s\frac{d}{a}} \int_0^1 \phi(\eta)\, E_j(s,\eta)\, d\eta \quad (j = 1,2,3,4) \tag{4.54}$$

where

$$E_1(s,\eta) = (1 - s\frac{d}{a})\, I_0(s\eta) + s\eta\, I_1(s\eta) \tag{4.55}$$

$$E_2(s,\eta) = (2 - s\frac{d}{a})\, I_0(s\eta) + s\eta\, I_1(s\eta) \tag{4.56}$$

$$E_3(s,\eta) = \frac{1}{4\mu}\left[(\kappa - 3 + 2s\frac{d}{a})\, I_0(s\eta) - 2s\eta\, I_1(s\eta)\right] \tag{4.57}$$

$$E_4(s,\eta) = \frac{1}{4\mu}\left[(\kappa + 3 - 2s\frac{d}{a})\, I_0(s\eta) + 2s\eta\, I_1(s\eta)\right] \tag{4.58}$$

Substituting eqns (4.55)–(4.58) into (4.40)–(4.41) leads to

$$A(\frac{s}{a}) = \frac{1}{\Delta(\frac{s}{a})}\left(\frac{2}{\pi}\right)^{1/2} s\, e^{-s\frac{d}{a}} \sum_{j=1}^{4} K_{1j} \int_0^1 \phi(\eta)\, E_j(s,\eta)\, d\eta \tag{4.59}$$

$$B(\frac{s}{a}) = \frac{1}{\Delta(\frac{s}{a})}\left(\frac{2}{\pi}\right)^{1/2} s\, e^{-s\frac{d}{a}} \sum_{j=1}^{4} K_{2j} \int_0^1 \phi(\eta)\, E_j(s,\eta)\, d\eta \tag{4.60}$$

Substituting eqns (4.59)–(4.60) into the integral equation (4.48) gives

$$\phi(\xi) = -\left(\frac{\pi}{2}\right)^{3/2} \xi\, a\, \sigma - \sqrt{\xi} \int_0^1 \frac{\phi(\eta)}{\sqrt{\eta}}\, K(\xi,\eta)\, d\eta \tag{4.61}$$

in which the kernel $K(\xi,\eta)$ is

$$K(\xi,\eta) = \sqrt{\xi\eta} \int_0^{+\infty} \frac{s e^{-s\frac{d}{a}}}{\Delta(\frac{s}{a})} \left\{ I_0(s\xi) \sum_{j=1}^{4} K_{1j} E_j + [2I_0(s\xi) + s\xi I_1(s\xi)] \sum_{j=1}^{4} K_{2j} E_j \right\} ds \tag{4.62}$$

Dividing both sides of equation (4.61) by

$$-\left(\frac{\pi}{2}\right)^{3/2} \sqrt{\xi}\, a\, \sigma \tag{4.63}$$

and denoting

$$\Phi(\xi) = -\frac{\phi(\xi)}{\left(\frac{\pi}{2}\right)^{3/2} \sqrt{\xi}\, a\, \sigma} \tag{4.64}$$

$$\Phi(\eta) = -\frac{\phi(\eta)}{\left(\frac{\pi}{2}\right)^{3/2} \sqrt{\eta}\, a\, \sigma} \tag{4.65}$$

the integral equation (4.61) can be rewritten in a more concise form to read

$$\Phi(\xi) + \int_0^1 K(\xi,\eta)\, \Phi(\eta)\, d\eta = \sqrt{\xi} \tag{4.66}$$

After solving $\Phi(\xi)$ from the above Fredholm integral equation of second kind, $E(s/a)$ can be calculated from (4.51) and (4.64) to give

$$E(\frac{s}{a}) = -(\frac{\pi}{2})\, a\, \sigma\, s \int_0^1 \sqrt{\xi}\, \Phi(\xi)\, J_0(s\xi)\, d\xi \tag{4.67}$$

Integrating (4.67) by parts, we get

$$E(\frac{s}{a}) = -\frac{\pi a}{2}\, \sigma \left\{ \Phi(1)\, J_1(s) - \int_0^1 \xi\, J_1(s\xi)\, \frac{d}{d\xi} \left[\frac{\Phi(\xi)}{\sqrt{\xi}} \right] d\xi \right\} \tag{4.68}$$

Let us discuss the behaviour of the kernel $K(\xi, \eta)$ in the non-degenerate case when $\rho = 0$. The case when $\rho = 1$ can be similarly studied. First of all, we briefly examine its properties when $s = 0$ and $s \to +\infty$. Because of the term $\frac{s}{\Delta(\frac{s}{a})}$, the integrand in (4.62) has a removable singularity at $s = 0$. When s becomes large, we shall show in the next Chapter ((5.52)–(5.59)) that

$$\lim_{s \to \text{large}} \frac{K_{ij}}{\Delta(\frac{s}{a})} = \lim_{s \to \text{large}} \frac{K_{ij}\, e^{-2s\frac{d}{a}}\, e^{-(t_1+t_2)}}{\Delta(\frac{s}{a})\, e^{-2s\frac{d}{a}}\, e^{-(t_1+t_2)}} \Rightarrow \frac{1}{\delta}\, (a_{ij} + b_{ij}\, s)\, e^{-s\frac{d}{a}} \quad (i = 1, 2; j = 1, 2, 3, 4) \tag{4.69}$$

where $t_i = \beta_i s \frac{b}{a}$, and δ, a_{ij} and b_{ij} are constants determined by the elastic properties of the materials (see (5.52)–(5.59)). It is shown in Appendix A that for $s\frac{d}{a} > 0$, $\Delta(\frac{s}{a})\, e^{-2s\frac{d}{a}}\, e^{-(t_1+t_2)}$ never vanishes for the materials considered in this Thesis.

From the asymptotic behaviour of the deformed Bessel functions

$$\lim_{x \to +\infty} I_0(x) \approx \frac{1}{\sqrt{2\pi x}}\, e^x \tag{4.70}$$

$$\lim_{x \to +\infty} I_1(x) \approx \frac{1}{\sqrt{2\pi x}}\, e^x \tag{4.71}$$

it follows that as $s \to +\infty$ the integrand in (4.62) behaves as

$$\frac{1}{\delta \sqrt{\xi\eta}}\, f_k(s, \xi, \eta)\, e^{-(2\frac{d}{a} - \xi - \eta)s} \tag{4.72}$$

where $f_k(s, \xi, \eta)$ is a polynomial in s, and ξ and η are parameters. (4.72) shows that as $s \to +\infty$ the integrand in the infinite integral defining $K(\xi, \eta)$ (4.62) contains a negative exponential function provided that $d/a > 1$. The integral of such a function is obviously finite for any $\xi \in [0, 1]$ and $\eta \in [0, 1]$.

Next, we consider the behaviour of $K(\xi, \eta)$ from a physical point of view. For this, we rewrite the integral equation (4.66) in the following form

$$\Phi(\xi) = \sqrt{\xi} \left[1 - \int_0^1 K^*(\xi, \eta)\, \Phi(\eta)\, d\eta \right] \tag{4.73}$$

or

$$\frac{\Phi(\xi)}{\sqrt{\xi}} = 1 - \int_0^1 K^*(\xi,\eta)\,\Phi(\eta)\,d\eta \tag{4.74}$$

where

$$K^*(\xi,\eta) = \sqrt{\eta}\int_0^{+\infty} \frac{se^{-s\frac{d}{a}}}{\Delta(\frac{s}{a})}\left\{I_0(s\xi)\sum_{j=1}^{4} K_{1j}E_j + [2I_0(s\xi) + s\xi I_1(s\xi)]\sum_{j=1}^{4} K_{2j}E_j\right\} ds \tag{4.75}$$

When the central sublaminate is of infinite extent (i.e. $d/a \to +\infty$), the solution of the above integral equation is (Sneddon, 1951)

$$\Phi(\xi) = \sqrt{\xi} \tag{4.76}$$

A comparison of this solution with the equation (4.73) shows that the second term in the square brackets of (4.73) must be the perturbation due to the finite boundaries $|x| = d$ and the influence of the two sublaminates between $d \le |x| \le d + b$. The convergence of the integral (4.75) will therefore guarantee that this perturbation is finite.

Based upon the above observations, it is clear that the infinite integral in the kernel $K(\xi,\eta)$ (4.62) converges for any ξ and η provided $d/a > 1$, i.e. provided the crack tips do not touch the interfaces.

For the calculation of the mode I stress intensity factor at the tip of the crack, the relevant normal stress component near the crack tip is obtained from eqn (4.5), and is

$$\begin{aligned}\sigma^1_{yy}(x,0) = &\frac{2}{\pi a}\int_0^{+\infty} E(\frac{s}{a})\cos(s\frac{x}{a})ds + \\ &+\frac{2}{\pi a}\int_0^{+\infty}\left\{A(\frac{s}{a})\,\cosh(s\frac{x}{a}) + B(\frac{s}{a})\,[2\cosh(s\frac{x}{a}) + s\,\frac{x}{a}\sinh(s\frac{x}{a})]\right\} ds\end{aligned} \tag{4.77}$$

where we have used the normalized variables (4.36). Substituting eqn (4.68) into eqn (4.77) gives

$$\begin{aligned}\sigma^1_{yy}(x,0) = &-\sigma\,\Phi(1)\int_0^{+\infty} J_1(s)\cos(s\frac{x}{a})\,ds + \\ &+\sigma\int_0^{+\infty}\left\{\int_0^1 \xi J_1(s\xi)\frac{d}{d\xi}\left[\frac{\Phi(\xi)}{\sqrt{\xi}}\right] d\xi\right\}\cos(s\frac{x}{a})ds + \\ &+\frac{2}{\pi a}\int_0^{+\infty}\left\{A(\frac{s}{a})\,\cosh(s\frac{x}{a}) + B(\frac{s}{a})\,[2\cosh(s\frac{x}{a}) + s\,\frac{x}{a}\sinh(s\frac{x}{a})]\right\} ds, \\ &\qquad\qquad x > a\end{aligned} \tag{4.78}$$

Making use of the integral

$$\int_0^{+\infty} J_1(\alpha s)\,\cos(\beta s)\,ds = -\frac{\alpha}{\sqrt{\beta^2-\alpha^2}\,(\beta + \sqrt{\beta^2-\alpha^2})}, \qquad \alpha > \beta \tag{4.79}$$

eqn (4.78) can be rewritten as

$$\begin{aligned}\sigma^1_{yy}(x,0) &= \frac{\Phi(1)\sigma\, a^2}{\sqrt{x^2-a^2}\,(x+\sqrt{x^2-a^2})} - \\ &- \sigma a^2 \int_0^1 \frac{\xi}{\sqrt{x^2-(a\xi)^2}(a+\sqrt{x^2-(a\xi)^2})} \frac{d}{d\xi}\left[\frac{\Phi(\xi)}{\sqrt{\xi}}\right] d\xi + \\ &+ \frac{2}{\pi a}\int_0^{+\infty}\left\{A(\frac{s}{a})\cosh(s\frac{x}{a}) + B(\frac{s}{a})\,[2\cosh(s\frac{x}{a}) + s\,\frac{x}{a}\sinh(s\frac{x}{a})]\right\} ds, \\ & \qquad\qquad x > a \qquad (4.80)\end{aligned}$$

The mode I stress intensity factor at the crack tip is given by

$$K_I = \lim_{x\to a^+} \sqrt{2(x-a)}\,\sigma^1_{yy}(x,0) \qquad (4.81)$$

Let us examine the asymptotic behaviour of $\sigma^1_{yy}(x,0)$ when $x \to a^+$. From eqn (4.74), it can be shown that $\frac{d}{d\xi}\left[\frac{\Phi(\xi)}{\sqrt{\xi}}\right]$ is finite (Appendix D). The integrand in the second integral term of the expression (4.80) has therefore an integrable singularity at $\xi = 1$, when $x = a$. From the expressions (4.59)–(4.60) for $A(s/a)$ and $B(s/a)$ and the asymptotic behaviour of $\frac{K_{ij}}{\Delta(\frac{s}{a})}$ (eqn (4.69)), it follows that the third integral in the expression (4.80) is also finite, when $x = a$.

Therefore, substituting eqn (4.80) into (4.81) gives

$$K_I = \Phi(1)\,\sigma\sqrt{a} \equiv F_I\,\sigma\sqrt{a} \qquad (4.82)$$

The above expression for the stress intensity factor was deduced from the asymptotic behaviour of the expression (4.78) for the stress $\sigma^1_{yy}(x,0)$. It can also be derived in an alternative manner, as shown by Sneddon & Srivastav (1971). The form of (4.82) is not new. It appears in a lot of solutions of crack problems (Sneddon & Srivastav, 1971; Hilton & Sih, 1971; Bogy, 1973; Sih & Chen, 1981, and Fan *et al.*, 1991).

4.4 Solution for In-Plane Shear Mode II

For the mode II problem, i.e. when the crack faces are subjected to self-equilibrating in-plane shear stress τ_{II} (with respect to crack faces but out-of-plane with respect to the laminate), shown in Figure 4.1(c), we superimpose the solutions (3.83)–(3.87) and (3.96)–(3.100). Defining the unknown functions in these solutions via

$$C_2(t) = -\frac{1}{t}\,E(t) \qquad (4.83)$$

$$D_2(t) = \frac{1}{t^2} A(t) \tag{4.84}$$

$$D_3(t) = \frac{1}{t^2} B(t) \tag{4.85}$$

the stress and displacement components in the central, transversely isotropic layer can be written as

$$\begin{aligned}
\sigma^1_{xx} &= \frac{2}{\pi}\int_0^\infty (-1)\big[A(t)t\,x\cosh(tx) + B(t)\sinh(tx)\big]\sin(ty)\,dt + \\
&\quad + \frac{2}{\pi}\int_0^\infty E(t)(2 - t\,y)e^{-ty}\sin(tx)\,dt
\end{aligned} \tag{4.86}$$

$$\begin{aligned}
\sigma^1_{yy} &= \frac{2}{\pi}\int_0^\infty \Big\{A(t)[2\sinh(tx) + t\,x\cosh(tx)] + B(t)\sinh(tx)\Big\}\sin(ty)\,dt + \\
&\quad + \frac{2}{\pi}\int_0^\infty E(t)\,t\,y\,e^{-ty}\sin(tx)\,dt
\end{aligned} \tag{4.87}$$

$$\begin{aligned}
\tau^1_{xy} &= \frac{2}{\pi}\int_0^\infty (-1)\Big\{A(t)[\cosh(tx) + t\,x\sinh(tx)] + B(t)\cosh(tx)\Big\}\cos(ty)dt + \\
&\quad + \frac{2}{\pi}\int_0^\infty E(t)(1 - t\,y)e^{-ty}\cos(tx)\,dt
\end{aligned} \tag{4.88}$$

$$\begin{aligned}
u^1 &= -\frac{2}{\pi}\frac{1}{4\mu}\int_0^\infty (\frac{1}{t})\Big\{A(t)[2t\,x\sinh(tx) - (\kappa - 1)\cosh(tx)] + \\
&\quad + 2B(t)\cosh(tx)\Big\}\sin(ty)\,dt - \\
&\quad - \frac{2}{\pi}\frac{1}{4\mu}\int_0^\infty (\frac{1}{t})E(t)\big[\kappa + 1 - 2t\,y\big]e^{-ty}\cos(tx)\,dt
\end{aligned} \tag{4.89}$$

$$\begin{aligned}
v^1 &= -\frac{2}{\pi}\frac{1}{4\mu}\int_0^\infty (\frac{1}{t})\Big\{A(t)[(\kappa + 1)\sinh(tx) + 2t\,x\cosh(tx)] \\
&\quad + 2B(t)\sinh(tx)\Big\}\cos(ty)\,dt + \\
&\quad + \frac{2}{\pi}\frac{1}{4\mu}\int_0^\infty (\frac{1}{t})E(t)\big[1 - \kappa - 2t\,y\big]e^{-ty}\sin(tx)\,dt
\end{aligned} \tag{4.90}$$

In a like manner, the stress and displacement fields in the orthotropic material 2 follow from the general solution (3.123)–(3.127)

$$\begin{aligned}
\sigma^2_{xx} &= \frac{2}{\pi}\int_0^\infty t\,Q_1\,[A_1(t)\sinh x_1 + B_1(t)\cosh x_1]\,\sin(ty)\,dt + \\
&\quad + (1-\rho)\frac{2}{\pi}\int_0^\infty t\,Q_2\,[A_2(t)\sinh x_2 + B_2(t)\cosh x_2]\,\sin(ty)\,dt + \\
&\quad + \rho\frac{2}{\pi}\int_0^\infty t\,\{A_0\,[Q_0\,x_0\,\sinh x_0 + c_{11}\,\beta_0\,(Z_0 - T_0)\,\cosh x_0] + \\
&\quad + B_0\,[Q_0\,x_0\,\cosh x_0 + c_{11}\,\beta_0(Z_0 - T_0)\,\sinh x_0]\}\,\sin(ty)\,dt
\end{aligned} \tag{4.91}$$

$$\begin{aligned}
\sigma^2_{yy} &= \frac{2}{\pi}\int_0^\infty t\,L_1\,[A_1(t)\sinh x_1 + B_1(t)\cosh x_1]\,\sin(ty)\,dt + \\
&\quad + (1-\rho)\frac{2}{\pi}\int_0^\infty t\,L_2\,[A_2(t)\sinh x_2 + B_2(t)\cosh x_2]\,\sin(ty)\,dt +
\end{aligned}$$

$$+\rho\frac{2}{\pi}\int_0^\infty t\,\{A_0\,[L_0\,x_0\,\sinh x_0 + c_{12}\,\beta_0\,(Z_0 - T_0)\,\cosh x_0] +$$
$$+B_0\,[L_0\,x_0\,\cosh x_0 + c_{12}\,\beta_0(Z_0 - T_0)\,\sinh x_0]\}\,\sin(ty)\,dt \tag{4.92}$$

$$\tau^2_{xy} = \frac{2}{\pi}\int_0^\infty t\,c_{66}\,(Z_1+\beta_1)\,[A_1(t)\cosh x_1 + B_1(t)\sinh x_1]\,\cos(ty)\,dt +$$
$$+(1-\rho)\frac{2}{\pi}\int_0^\infty t\,c_{66}\,(Z_2+\beta_2)\,[A_2(t)\cosh x_2 + B_2(t)\sinh x_2]\,\cosh(ty)\,dt +$$
$$+\rho\frac{2}{\pi}\int_0^\infty t\,\{A_0\,[c_{66}\,(Z_0+\beta_0)\,x_0\,\cosh x_0 + c_{66}\,(\beta_0 - T_0)\,\sinh x_0] +$$
$$+B_0\,[c_{66}\,(Z_0+\beta_0)\,x_0\,\sinh x_0 + c_{66}\,(\beta_0 - T_0)\,\cosh x_0]\}\,\cos(ty)\,dt \tag{4.93}$$

$$u^2 = \frac{2}{\pi}\int_0^{+\infty} Z_1[A_1(t)\cosh x_1 + B_1(t)\sinh x_1]\sin(ty)\,dt +$$
$$+(1-\rho)\frac{2}{\pi}\int_0^{+\infty} Z_2[A_2(t)\cosh x_2 + B_2(t)\sinh x_2]\sin(ty)\,dt +$$
$$+\rho\frac{2}{\pi}\int_0^{+\infty}\{A_0(t)[Z_0x_0\cosh x_0 - T_0\sinh x_0]+$$
$$+B_0(t)\,[Z_0x_0\sinh x_0 - T_0\cosh x_0]\}\sin(ty)\,dt \tag{4.94}$$

$$v^2 = \frac{2}{\pi}\int_0^{+\infty}[A_1(t)\sinh x_1 + B_1(t)\cosh x_1]\cos(ty)\,dt +$$
$$+(1-\rho)\frac{2}{\pi}\int_0^{+\infty}[A_2(t)\sinh x_2 + B_2(t)\cosh x_2]\cos(ty)\,dt +$$
$$+\rho\frac{2}{\pi}\int_0^{+\infty}[A_0x_0\sinh x_0 + B_0x_0\cosh x_0]\cos(ty)\,dt, \tag{4.95}$$

where ρ and β_l $(l = 0, 1, 2)$ have the same meaning as in mode I, and

$$x_l = \beta_l(x-d)t \tag{4.96}$$
$$Z_l = \frac{c_{22} - c_{66}\beta_l^2}{\beta_l(c_{12}+c_{66})} \tag{4.97}$$
$$Q_l = c_{11}\,\beta_l\,Z_l - c_{12} \tag{4.98}$$
$$L_l = c_{12}\,\beta_l\,Z_l - c_{22} \quad (l = 0, 1, 2) \tag{4.99}$$
$$T_0 = \frac{c_{22} + c_{66}\beta_0^2}{\beta_0(c_{12}+c_{66})}. \tag{4.100}$$

The above expressions for the stress and displacement fields identically satisfy the skew-symmetry conditions of the problem

$$\sigma^1_{xx}(0,y) = 0, \quad 0 \le y < +\infty \tag{4.101}$$
$$\sigma^1_{yy}(x,0) = 0, \quad 0 \le x \le d \tag{4.102}$$

$$v^1(0,y) = 0, \quad 0 \le y < +\infty \tag{4.103}$$

$$\sigma^2_{yy}(x,0) = 0, \quad d \le x \le d+b \tag{4.104}$$

$$u^2(x,0) = 0, \quad d \le x \le d+b \tag{4.105}$$

The arbitrary functions $A(t)$, $B(t)$, $E(t)$, $A_l(t)$ and $B_l(t)$ $(l = 0,1,2)$ in eqns (4.86)–(4.95) are determined from the remaining boundary and continuity conditions

$$u^1(x,0) = 0; \quad x > a \tag{4.106}$$

$$\lim_{y\to 0^+} \tau^1_{xy}(x,0) = -\tau_{II}; \quad 0 \le x < a \tag{4.107}$$

and for $0 \le y < +\infty$

$$\sigma^1_{xx}(d,y) = \sigma^2_{xx}(d,y) \tag{4.108}$$

$$\tau^1_{xy}(d,y) = \tau^2_{xy}(d,y) \tag{4.109}$$

$$u^1(d,y) = u^2(d,y) \tag{4.110}$$

$$v^1(d,y) = v^2(d,y) \tag{4.111}$$

$$\sigma^2_{xx}(d+b,y) = 0 \tag{4.112}$$

$$\tau^2_{xy}(d+b,y) = 0 \tag{4.113}$$

From eqns (4.106)–(4.107), we get (vide (4.89), (4.88))

$$u^1(r,0) = -\frac{\kappa+1}{2\mu}\frac{1}{\pi}\int_0^{+\infty}\frac{1}{s}E(\frac{s}{a})\cos(sr)\,ds = 0; \quad r < 1 \tag{4.114}$$

$$\begin{aligned}\lim_{y\to 0^+} \tau^1_{xy}(r,y) &= \lim_{y\to 0^+}\left[-\frac{2}{\pi a}\int_0^{+\infty}\left\{A(\frac{s}{a})[\cosh(sr)+s\,r\,\sinh(sr)]+\right.\right.\\ &\quad \left.+B(\frac{s}{a})\cosh(sr)\right\}\cos(s\frac{y}{a})\,ds+\\ &\quad \left.+\frac{2}{\pi a}\int_0^{+\infty}E(\frac{s}{a})(1-\frac{y}{a})\,e^{-s\frac{y}{a}}\cos(sr)\,ds\right]\\ &= -\tau_{II}; \quad 0 \le r < 1\end{aligned} \tag{4.115}$$

where we have used the normalizations

$$t = \frac{s}{a} \tag{4.116}$$

$$x = r\,a \tag{4.117}$$

Denoting

$$F(s) = \left(\frac{\pi}{2s}\right)^{\frac{1}{2}} E(\frac{s}{a}), \tag{4.118}$$

the dual integral eqns (4.114)–(4.115) can be written in the form that we have discussed above in § 4.3

$$\int_0^\infty F(s)\, J_{-\frac{1}{2}}(sr)\, ds = 0; \quad r > 1 \tag{4.119}$$

$$\int_0^\infty s\, F(s) J_{-\frac{1}{2}}(sr)\, ds = -\frac{1}{\sqrt{r}}\left[\frac{\pi a}{2}\tau_{II} - \int_0^\infty \{A(\frac{s}{a})[\cosh(sr) + s\, r \sinh(sr)] + \right.$$
$$\left. + B(\frac{s}{a})\cosh(sr)\}\, ds\right]; \quad 0 \le r < 1 \tag{4.120}$$

where we have used the identity (4.42).

The functions $A(s/a)$ and $B(s/a)$ are determined from eqns (4.108)–(4.113) (see Appendix A)

$$A(\frac{s}{a}) = \frac{1}{\Delta(\frac{s}{a})}\left[K_{11}F_1 + K_{12}F_2 + K_{13}F_3 + K_{14}F_4\right] \tag{4.121}$$

$$B(\frac{s}{a}) = \frac{1}{\Delta(\frac{s}{a})}\left[K_{21}F_1 + K_{22}F_2 + K_{23}F_3 + K_{24}F_4\right] \tag{4.122}$$

where $\Delta(\frac{s}{a})$, K_{ij} and F_j $(i = 1, 2; j = 1, 2, 3, 4)$ are listed in Appendix A.

Using the same procedure as described in § 4.3, we obtain the mode II stress intensity factor at the crack tip

$$K_{II} = \lim_{x \to a^+} \sqrt{2(x-a)}\, \tau_{xy}^1(x, 0) = \Psi(1)\, \tau_{II}\, \sqrt{a} \equiv F_{II}\, \tau_{II}\, \sqrt{a} \tag{4.123}$$

Here, $\Psi(1)$ is calculated from the following Fredholm integral equation

$$\Psi(\xi) + \int_0^1 K(\xi, \eta)\, \Psi(\eta)\, d\eta = \sqrt{\xi} \tag{4.124}$$

in which the kernel $K(\xi, \eta)$ is given by

$$K(\xi, \eta) = -\sqrt{\xi\eta} \int_0^\infty \frac{s\, e^{-s\frac{d}{a}}}{\Delta(\frac{s}{a})} \left\{ I_0(s\xi) \sum_{j=1}^{4} (K_{1j} + K_{2j})\, E_j + s\xi\, I_1(s\xi) \sum_{j=1}^{4} K_{2j}\, E_j \right\} ds \tag{4.125}$$

where

$$E_1 = s\frac{d}{a}\, I_0(s\eta) - s\eta\, I_1(s\eta) \tag{4.126}$$

$$E_2 = (1 - s\frac{d}{a})\, I_0(s\eta) + s\eta\, I_1(s\eta) \tag{4.127}$$

$$E_3 = \left[\frac{\kappa + 1}{4\mu} + \frac{1}{2\mu}\, s\frac{d}{a}\right] I_0(s\eta) - \frac{1}{2\mu}\, s\eta\, I_1(s\eta) \tag{4.128}$$

$$E_4 = \left[\frac{\kappa + 1}{4\mu} - \frac{1}{2\mu}\, s\frac{d}{a}\right] I_0(s\eta) + \frac{1}{2\mu}\, s\eta\, I_1(s\eta) \tag{4.129}$$

4.5 Solution for Anti-Plane Shear Mode III

When the crack faces are subjected to a uniform anti-plane shear stress $\tau_{yz} = -\tau_{III}$, as shown in Figure 4.1(d), the only non-vanishing displacement component is in the z-direction

$$w = w(x, y), \tag{4.130}$$

so that for an orthotropic material the stress components are

$$\tau_{yz} = c_{44} \frac{\partial w}{\partial y} \qquad \tau_{zx} = c_{55} \frac{\partial w}{\partial x} \tag{4.131}$$

Here, c_{44} and c_{55} are the shear stiffnesses in yz- and zx-planes, respectively.

The only non-vanishing equilibrium equation in mode III is

$$c_{55} \frac{\partial^2 w}{\partial x^2} + c_{44} \frac{\partial^2 w}{\partial y^2} = 0 \tag{4.132}$$

For transversely isotropic material 1 of the central layer, $c^1_{44} = c^1_{55}$, and eqn (4.132) reduces to a harmonic equation whose solution may be written as

$$w^1 = \frac{2}{\pi} \int_0^{+\infty} \frac{1}{t} D(t) \cosh(tx) \sin(ty)\, dt + \frac{2}{\pi} \int_0^{+\infty} \frac{1}{t} E(t)\, e^{-ty} \cos(tx)\, dt \tag{4.133}$$

The stress components are

$$\tau^1_{yz} = \frac{2}{\pi} \int_0^{+\infty} c^1_{44}\, D(t)\, \cosh(tx)\, \cos(ty)\, dt - \frac{2}{\pi} \int_0^{+\infty} c^1_{44}\, E(t)\, e^{-ty} \cos(tx)\, dt \tag{4.134}$$

$$\tau^1_{zx} = \frac{2}{\pi} \int_0^{+\infty} c^1_{55}\, D(t)\, \sinh(tx)\, \sin(ty)\, dt - \frac{2}{\pi} \int_0^{+\infty} c^1_{55}\, E(t)\, e^{-ty} \sin(tx)\, dt \tag{4.135}$$

The solution of the equilibrium eqn (4.132) for the outer orthotropic layers is taken as

$$w^2 = \frac{2}{\pi} \int_0^{+\infty} [G(t)\, e^{-x^*} + H(t)\, e^{x^*}] \sin(ty)\, dt, \tag{4.136}$$

where

$$x^* = \beta_3 (x - d)\, t \qquad \beta_3 = \sqrt{\frac{c^2_{44}}{c^2_{55}}} \tag{4.137}$$

The stress components are

$$\tau^2_{yz} = \frac{2}{\pi} \int_0^{+\infty} c^2_{44}\, t\, [G(t)\, e^{-x^*} + H(t)\, e^{x^*}] \cos(ty)\, dt \tag{4.138}$$

$$\tau^2_{zx} = \frac{2}{\pi} \int_0^{+\infty} c^2_{55}\, \beta_3\, t\, [-G(t)\, e^{-x^*} + H(t)\, e^{x^*}] \sin(ty)\, dt, \tag{4.139}$$

The unknown functions $D(t)$, $F(t)$, $G(t)$ and $H(t)$ in the solutions (4.133) and (4.136) are determined from the boundary and continuity conditions

$$w^1(x,0) = 0; \quad x > a \tag{4.140}$$

$$\lim_{y\to 0^+} \tau^1_{yz}(x,y) = -\tau_{III}; \quad 0 \le x < a \tag{4.141}$$

and for $0 \le y < +\infty$

$$\tau^1_{zx}(d,y) = \tau^2_{zx}(d,y) \tag{4.142}$$

$$w^1(d,y) = w^2(d,y) \tag{4.143}$$

$$\tau^2_{zx}(d+b,y) = 0 \tag{4.144}$$

Substituting (4.133) and (4.134) into (4.140) and (4.141), respectively, gives

$$w^1(r,0) = \frac{2}{\pi}\int_0^{+\infty} \frac{1}{s} E(\frac{s}{a}) \cos(sr)\, ds = 0; \quad r > 1 \tag{4.145}$$

$$\lim_{y\to 0^+} \tau^1_{yz}(r,y) = \lim_{y\to 0^+} \left[\frac{2}{\pi a}\int_0^{+\infty} c^1_{44}\, D(\frac{s}{a}) \cosh(sr) \cos(s\frac{y}{a})\, ds - \right.$$
$$\left. -\frac{2}{\pi a}\int_0^{+\infty} c^1_{44}\, E(\frac{s}{a})\, e^{-s\frac{y}{a}} \cos(sr)\, ds\right] = -\tau_{III}; \quad 0 \le r < 1 \tag{4.146}$$

where we have used the normalizations

$$t = \frac{s}{a} \tag{4.147}$$

$$x = r\,a \tag{4.148}$$

From the continuity and free-surface conditions (4.142)–(4.144), the unknown function $D(\frac{s}{a})$ is solved

$$D(\frac{s}{a}) = \frac{1}{\Delta(\frac{s}{a})}\left[H_1\, F_1 + H_2\, F_2\right] \tag{4.149}$$

where

$$\Delta(\frac{s}{a}) = c^2_{55}\,\beta_3 \cosh(s\frac{d}{a}) + c^1_{55} \sinh(s\frac{d}{a}) +$$
$$+[c^1_{55} \sinh(s\frac{d}{a}) - c^2_{55}\,\beta_3 \cosh(s\frac{d}{a})]\, e^{-2t_3} \tag{4.150}$$

$$H_1 = c^2_{55}\beta_3(e^{-2t_3} - 1); \quad H_2 = c^1_{55}(e^{-2t_3} + 1) \tag{4.151}$$

$$t_3 = \beta_3 \frac{b}{a} s \tag{4.152}$$

and

$$F_1 = \frac{2}{\pi}\int_0^{+\infty} \frac{s^2}{\xi(\xi^2+s^2)} E(\frac{\xi}{a}) \cos(\xi\frac{d}{a})\, d\xi \tag{4.153}$$

$$F_2 = \frac{2}{\pi}\int_0^{+\infty} \frac{s}{\xi^2+s^2} E(\frac{\xi}{a}) \sin(\xi\frac{d}{a})\, d\xi \tag{4.154}$$

The dual integral equations (4.145)–(4.146) are solved using the same procedure as that used previously for mode I and II problems.

The mode III stress intensity factor is

$$K_{III} = \lim_{x\to a^+} \sqrt{2(x-a)}\, \tau^1_{yz}(x,0) = \Omega(1)\, \tau_{III}\sqrt{a} \equiv F_{III}\, \tau_{III}\sqrt{a} \tag{4.155}$$

where $\Omega(1)$ is calculated from a much simpler Fredholm integral equation than the equations in modes I and II (4.66) and (4.124)

$$\Omega(\xi) + \int_0^1 K(\xi,\eta)\, \Omega(\eta)\, d\eta = \sqrt{\xi} \tag{4.156}$$

The kernel is given by

$$K(\xi,\eta) = -\sqrt{\xi\eta}\int_0^{+\infty} \frac{s e^{-s\frac{d}{a}}}{\Delta(\frac{s}{a})} (H_1 + H_2)\, I_0(s\xi)\, I_0(s\eta)\, ds \tag{4.157}$$

where $\Delta(\frac{s}{a})$, H_1 and H_2 are given by (4.150) and (4.151), respectively.

We can show that $\frac{s}{\Delta(\frac{s}{a})}$ is finite for all $s \in [0, +\infty)$. First, we note that this expression has a removable singularity at $s = 0$. Secondly, we rewrite it as

$$\frac{s}{\Delta(\frac{s}{a})} = \frac{2se^{-s\frac{d}{a}}}{c^2_{55}\beta_3(1+e^{-2s\frac{d}{a}})(1-e^{-2t_3}) + c^1_{55}(1-e^{-2s\frac{d}{a}})(1+e^{-2t_3})} \tag{4.158}$$

It is seen that the two terms in the denominator of the above expression are always positive for $0 < s < +\infty$, and tend to a finite value $c^2_{55}\beta_3 + c^1_{55}$ when $s \to +\infty$. Therefore, (4.158) decays exponentially to zero as $s \to +\infty$.

It is seen that the mode III problem does not have a degenerate solution when the outer sublaminates tend to be an isotropic medium dissimilar to the central transversely isotropic medium. The basic solution (4.136) is therefore applicable irrespective of whether the outer sublaminates are orthotropic or transversely isotropic.

4.6 Solution for a Composite Laminate with Multiple Cracks

4.6.1 Solution for Mode I

In this Section, we shall extend the solution of the single crack problem obtained in § 4.3 to a multi-cracked composite laminate, shown in Figure 4.2. The exposition shall follow closely

the paper by Wang & Karihaloo (1995a). The solutions in modes II and III for multi-cracked laminate configuration can be obtained in a similar manner. As the tensile loading case is the most important one, we shall demonstrate the solution procedure on mode I, and then present the solution for mode III. We shall only need mode I and mode III solutions later in Chapter 9.

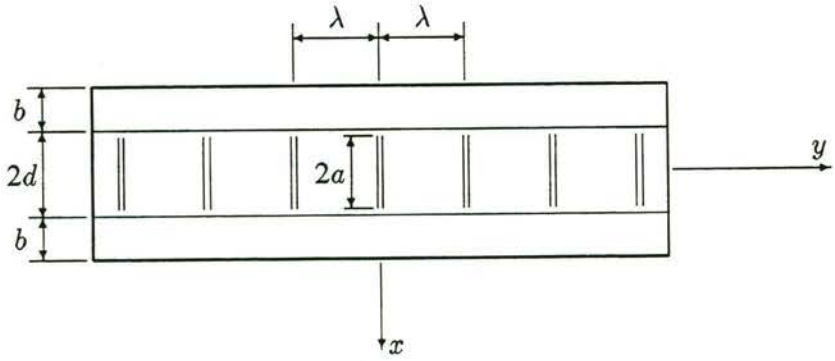

Figure 4.2: A multi-cracked composite laminate and coordinate axes

It is recognized that with an infinite cracked body, the concept of "remote" stress is not applicable, but the "average stress" is unique and it is equal to the uniform stress at the positions of the cracks when all the cracks are absent under the condition of unidirectional tension. This stress is sometimes called the solution of the homogeneous problem (e.g. Horii & Nemat-Nasser, 1985). Therefore, it is assumed that the composite laminate is subjected remotely to a uniform tensile deformation along y-direction when all the cracks are absent. From a mathematical point of view, one needs only to solve the problem of cancellation of a uniform stress over the faces of all the cracks. Because of symmetry, it is enough to consider a quarter of the laminate, say $x \geq 0, y \geq 0$.

The solution to the above problem must satisfy the following boundary, symmetry and periodicity conditions

$$\sigma^1_{yy}(x, n\lambda) = -\sigma; \quad 0 \leq x < a; \quad n = 0, 1, 2, ..., +\infty \tag{4.159}$$

$$v^1(x, n\lambda) = 0; \quad a < x \leq d \quad n = 0, 1, 2, ..., +\infty \tag{4.160}$$

$$v^2(x, n\lambda) = 0; \quad d \leq x \leq d + b; \quad n = 0, 1, 2, ..., +\infty \tag{4.161}$$

$$\tau^1_{xy}(x, n\lambda) = 0; \quad 0 \leq x \leq d; \quad n = 0, 1, 2, ..., +\infty \tag{4.162}$$

$$\tau^2_{xy}(x, n\lambda) = 0; \quad d \leq x \leq d + b; \quad n = 0, 1, 2, ..., +\infty \tag{4.163}$$

and the following continuity and free-surface conditions ($0 \leq y < +\infty$):

$$\sigma^1_{xx}(d, y) = \sigma^2_{xx}(d, y) \tag{4.164}$$

$$\tau^1_{xy}(d,y) = \tau^2_{xy}(d,y) \tag{4.165}$$

$$u^1(d,y) = u^2(d,y) \tag{4.166}$$

$$v^1(d,y) = v^2(d,y) \tag{4.167}$$

$$\sigma^2_{xx}(d+b,y) = 0 \tag{4.168}$$

$$\tau^2_{xy}(d+b,y) = 0 \tag{4.169}$$

The solution of the above boundary-value problem for multiple cracks is simplified by applying the superposition procedure of Nied (1987), and Kaw & Besterfield (1992) to the solution of the boundary-value problem for a single crack, given previously in § 4.3. For a single crack located at $y = 0$, the stress $\sigma^1_{yy}(x,y)$ and displacement $v^1(x,y)$ are given by (4.5) and (4.10), respectively,

$$\sigma^1_{yy}(r,y)|_{\text{single}} = \frac{2}{\pi a}\int_0^{+\infty} \mathcal{G}_1(\frac{s}{a},r)\cos(s\frac{y}{a})\,ds + \\ +\frac{2}{\pi a}\int_0^{+\infty} E(\frac{s}{a})\,(1+s\frac{y}{a})\,e^{-s\frac{y}{a}}\cos(sr)\,ds \tag{4.170}$$

$$v^1(r,y)|_{\text{single}} = \frac{2}{\pi}\int_0^{+\infty} \mathcal{G}_2(\frac{s}{a},r)\sin(s\frac{y}{a})\,ds - \\ -\frac{2}{4\mu\pi}\int_0^{+\infty} (\frac{1}{s})\,E(\frac{s}{a})\left[(\kappa+1)+2\,sy\right]e^{-s\frac{y}{a}}\cos(sr)\,ds, \tag{4.171}$$

where

$$\mathcal{G}_1(\frac{s}{a},r) = A(\frac{s}{a})\cosh(sr) + B(\frac{s}{a})\left[2\cosh(sr) + s\,r\sinh(sr)\right] \tag{4.172}$$

$$\mathcal{G}_2(\frac{s}{a},r) = \frac{1}{4\mu s}\Big\{2A(\frac{s}{a})\cosh(sr) + \\ +B(\frac{s}{a})\left[(\kappa+1)\cosh(sr) + 2\,s\,r\sinh(sr)\right]\Big\} \tag{4.173}$$

and we have introduced the normalized variables

$$x = ra, \quad t = \frac{s}{a} \tag{4.174}$$

The functions $A(s/a)$ and $B(s/a)$ are determined from the continuity and free-surface conditions (4.164)–(4.169). This has been done in Appendix A.

The perturbation of the stress and displacement fields caused by the infinite array of cracks can be obtained by superposing the contributions of cracks located at $y = \pm n\lambda, n = 0, ..., +\infty$. Therefore, we have

$$\sigma^1_{yy}(r,0) = \sum_{n=-\infty}^{+\infty} \sigma^1_{yy}(r,n\lambda)|_{\text{single}} \tag{4.175}$$

$$v^1(r,0) = \sum_{n=-\infty}^{+\infty} v^1(r,n\lambda)|_{\text{single}} \tag{4.176}$$

Substituting eqn (4.170) into (4.175) and noting that $\sigma^1_{yy}(r,y)|_{\text{single}}$ is an even function of y, we have

$$\sigma^1_{yy}(r,0) = \sigma^1_{yy}(r,0)|_{\text{single}} + 2\sum_{n=1}^{+\infty} \sigma^1_{yy}(r,n\lambda)|_{\text{single}} \tag{4.177}$$

From the solution (4.170) to an isolated crack, we know that the stress perturbation at $y = n\lambda$ caused by the crack located at $y = 0$ is

$$\begin{aligned}\sigma^1_{yy}(r,n\lambda)|_{\text{single}} &= \frac{2}{\pi a}\int_0^{+\infty} \mathcal{G}_1(\frac{s}{a},r)\cos(s\frac{n\lambda}{a})\,ds + \\ &+\frac{2}{\pi a}\int_0^{+\infty} E(\frac{s}{a})\,(1+s\frac{n\lambda}{a})\,e^{-s\frac{n\lambda}{a}}\cos(sr)\,ds\end{aligned} \tag{4.178}$$

Substituting (4.178) into (4.177) gives

$$\begin{aligned}\sigma^1_{yy}(r,0) &= \frac{2}{\pi a}\int_0^{+\infty} \mathcal{G}_1(\frac{s}{a},r)\,ds + \sum_{n=1}^{+\infty}\frac{2}{\pi a}\int_0^{+\infty} \mathcal{G}_1(\frac{s}{a},r)\,2\cos(sn\frac{\lambda}{a})\,ds + \\ &+ \frac{2}{\pi a}\int_0^{+\infty} E(\frac{s}{a})\left[1+\mathcal{G}(\frac{s}{a})\right]\cos(sr)\,ds\end{aligned} \tag{4.179}$$

where

$$\mathcal{G}(\frac{s}{a}) = \frac{2e^{-s\frac{\lambda}{a}}}{1-e^{-s\frac{\lambda}{a}}}\left[1+s\frac{\lambda}{a}\frac{1}{1-e^{-s\frac{\lambda}{a}}}\right]. \tag{4.180}$$

On the other hand, when we calculate the summation in (4.176), we should note that $v^1(r,y)|_{\text{single}}$ is an odd function of y, so that we can easily write (4.176) as

$$v^1(r,0) = -\frac{\kappa+1}{2\mu\pi}\int_0^{+\infty}(\frac{1}{s})\,E(\frac{s}{a})\cos(sr)\,ds, \tag{4.181}$$

Substituting (4.179) and (4.181) into (4.159) and (4.160), respectively, yields

$$\begin{aligned}&\int_0^{+\infty}\left[1+\mathcal{G}(\frac{s}{a})\right]E(\frac{s}{a})\cos(sr)ds = -\left\{\frac{\pi a}{2}\sigma + \int_0^{+\infty}\mathcal{G}_1(\frac{s}{a},r)\,ds + \right. \\ &\left. + \sum_{n=1}^{+\infty}\int_0^{+\infty}\mathcal{G}_1(\frac{s}{a},r)\,2\cos(sn\frac{\lambda}{a})\,ds\right\}; \qquad 0\le r<1\end{aligned} \tag{4.182}$$

$$\int_0^{+\infty}\frac{1}{s}E(\frac{s}{a})\cos(sr)\,ds = 0; \qquad r>1 \tag{4.183}$$

By denoting

$$F(s) = \left(\frac{\pi}{2s}\right)^{\frac{1}{2}}E(\frac{s}{a}) \tag{4.184}$$

the dual integral eqns (4.182)–(4.183) can be rewritten as

$$\int_0^{+\infty} s\left[1+\mathcal{G}(s)\right] F(s) J_{-\frac{1}{2}}(sr)\, ds = -\frac{1}{\sqrt{r}}\left\{\frac{\pi a}{2}\sigma + \int_0^{+\infty} \mathcal{G}_1(\frac{s}{a}, r)\, ds + \right.$$
$$\left. + \sum_{n=1}^{+\infty} \int_0^{+\infty} \mathcal{G}_1(\frac{s}{a}, r)\, 2\cos(sn\frac{\lambda}{a})\, ds\right\}; \quad 0 \le r < 1 \tag{4.185}$$

$$\int_0^{+\infty} F(s)\, J_{-\frac{1}{2}}(sr)\, ds = 0; \quad r > 1 \tag{4.186}$$

The first integral equation (4.185) is just a variation upon (4.45) which we met in § 4.3. Therefore, the dual integral equations can be solved following a similar procedure to that used in § 4.3 (see Appendix B) to give

$$E(\frac{s}{a}) = -\frac{\pi a}{2}\sigma\left\{\Phi(1)\, J_1(s) - \int_0^1 \xi\, J_1(s\xi)\, \frac{d}{d\xi}\left[\frac{\Phi(\xi)}{\sqrt{\xi}}\right] d\xi\right\}, \tag{4.187}$$

where $\Phi(\xi)$ is the solution of the following Fredholm integral equation

$$\Phi(\xi) + \int_0^1 \left[K_1(\xi,\eta) + K_2(\xi,\eta)\right]\Phi(\eta)\, d\eta = \sqrt{\xi} \tag{4.188}$$

The kernels $K_1(\xi,\eta)$ and $K_2(\xi,\eta)$ in eqn (4.188) are

$$K_1(\xi,\eta) = \sqrt{\xi\eta}\int_0^{+\infty} \frac{se^{-s\frac{d}{a}}}{\Delta(\frac{s}{a})}\left\{I_0(s\xi)\sum_{j=1}^4 K_{1j}E_j + [2I_0(s\xi) + s\xi I_1(s\xi)]\sum_{j=1}^4 K_{2j}E_j\right\} ds +$$
$$+2\sqrt{\xi\eta}\sum_{n=1}^{+\infty}\int_0^{+\infty} \frac{se^{-s\frac{d}{a}}}{\Delta(\frac{s}{a})}\left\{I_0(s\xi)\sum_{j=1}^4 K_{1j}E_j + [2I_0(s\xi) + s\xi I_1(s\xi)]\sum_{j=1}^4 K_{2j}E_j\right\}\cos(sn\frac{\lambda}{a})ds \tag{4.189}$$

$$K_2(\xi,\eta) = \sqrt{\xi\eta}\int_0^{+\infty} \frac{2se^{-s\frac{\lambda}{a}}}{1-e^{-s\frac{\lambda}{a}}}\left[1 + s\frac{\lambda}{a}\frac{1}{1-e^{-s\frac{\lambda}{a}}}\right] J_0(\xi s)J_0(\eta s)\, ds \tag{4.190}$$

where K_{ij} and E_j $(i = 1,2;\ j = 1,..,4)$ are defined by (Appendix A.34) and (4.55)–(4.58), respectively.

That the integrals in $K_1(\xi,\eta)$ are convergent follows from the integral

$$\int_0^{+\infty} s^m e^{-\beta s}\cos(n\alpha s)\, ds = (-1)^m \frac{\partial^m}{\partial\beta^m}\left(\frac{\beta}{n^2\alpha^2+\beta^2}\right). \tag{4.191}$$

The integral in $K_2(\xi,\eta)$ is evidently convergent.

We now calculate the mode I stress intensity factor at each crack tip. Substituting eqn (4.187) into eqn (4.179) gives

$$\sigma^1_{yy}(x,0) = -\sigma\int_0^{+\infty}\left[1+\mathcal{G}(\frac{s}{a})\right]\left\{\Phi(1)J_1(s) - \int_0^1 \xi J_1(s\xi)\frac{d}{d\xi}\left[\frac{\Phi(\xi)}{\sqrt{\xi}}\right]d\xi\right\}\cos(s\frac{x}{a})ds +$$
$$+\frac{2}{\pi a}\int_0^{+\infty}\mathcal{G}_1(\frac{s}{a}, x)\, ds + \frac{2}{\pi a}\sum_{n=1}^{+\infty}\int_0^{+\infty}\mathcal{G}_1(\frac{s}{a}, x)\, 2\cos(sn\frac{\lambda}{a})\, ds, \quad x > a \tag{4.192}$$

The mode I stress intensity factor at the tip of each crack is calculated from

$$K_I = \lim_{x \to a^+} \sqrt{2(x-a)}\, \sigma^1_{yy}(x,0) = \Phi(1)\, \sigma \sqrt{a} \tag{4.193}$$

where $\Phi(1)$ is calculated from the solution of the integral equation (4.188).

4.6.2 Solution for Mode III

When the surfaces of the cracks in Figure 4.2 are subjected to a uniform anti-plane shear stress $\tau_{yz} = -\tau$, the resulting boundary-value problem can be solved in a similar way to that used above for solving the mode I problem. Because of symmetry, it is enough to consider a quarter of the laminate, say $x \geq 0$, $y \geq 0$. Under this loading condition, the boundary and symmetry conditions are

$$\tau^1_{yz}(x, n\lambda) = -\tau; \quad 0 \leq x < a; \quad n = 0, 1, 2, ..., +\infty \tag{4.194}$$

$$w^1(x, n\lambda) = 0; \quad a < x \leq d; \quad n = 0, 1, 2, ..., +\infty \tag{4.195}$$

$$w^2(x, n\lambda) = 0; \quad d \leq x \leq d + b; \quad n = 0, 1, 2, ..., +\infty \tag{4.196}$$

and for $0 \leq y < +\infty$,

$$\tau^1_{zx}(d, y) = \tau^2_{zx}(d, y) \tag{4.197}$$

$$w^1(d, y) = w^2(d, y) \tag{4.198}$$

$$\tau^2_{zx}(d + b, y) = 0 \tag{4.199}$$

The superposition procedure used above for mode I problem will be recalled to solve the present boundary-value problem. For this, we need again the solution for a single crack. From eqns (4.134) and (4.133), we have

$$\begin{aligned} \tau^1_{yz}(r, y)|_{\text{single}} = {} & \frac{2}{\pi} \int_0^{+\infty} \frac{1}{a}\, c^1_{44}\, D(\frac{s}{a}) \cosh(sr) \cos(s\frac{y}{a})\, ds - \\ & - \frac{2}{\pi} \int_0^{+\infty} \frac{1}{a}\, c^1_{44}\, E(\frac{s}{a})\, e^{-s\frac{y}{a}} \cos(sr)\, ds \end{aligned} \tag{4.200}$$

$$\begin{aligned} w^1(r, y)|_{\text{single}} = {} & \frac{2}{\pi} \int_0^{+\infty} \frac{1}{s} D(\frac{s}{a}) \cosh(sr) \sin(s\frac{y}{a})\, dt + \\ & + \frac{2}{\pi} \int_0^{+\infty} \frac{1}{s} E(\frac{s}{a})\, e^{-s\frac{y}{a}} \cos(sr)\, ds \end{aligned} \tag{4.201}$$

where we have used the normalizations $t = s/a$ and $x = ra$.

The perturbation of the stress and displacement fields caused by the infinite array of cracks can be obtained by superposing the contributions of cracks located at $y = \pm n\lambda, n = 0, ..., +\infty$. Therefore, we have

$$\tau^1_{yz}(r,0) = \sum_{n=-\infty}^{+\infty} \tau^1_{yz}(r,n\lambda)|_{\text{single}} \tag{4.202}$$

$$w^1(r,0) = \sum_{n=-\infty}^{+\infty} w^1(r,n\lambda)|_{\text{single}} \tag{4.203}$$

Noting that $\tau^1_{yz}(r,y)|_{\text{single}}$ is an even function of y, eqn (4.202) can be rewritten as

$$\tau^1_{yz}(r,0) = \tau^1_{yz}(r,0)|_{\text{single}} + 2\sum_{n=1}^{+\infty} \tau^1_{yz}(r,n\lambda)|_{\text{single}} \tag{4.204}$$

Substituting eqn (4.200) into (4.204) gives

$$\tau^1_{yz}(r,0) = \frac{2c^1_{44}}{\pi a}\int_0^{+\infty} D(\frac{s}{a})\cosh(sr)\,ds + \frac{2c^1_{44}}{\pi a}\sum_{n=1}^{+\infty}\int_0^{+\infty} D(\frac{s}{a})\cosh(sr)\,2\cos(sn\frac{\lambda}{a})\,ds -$$
$$- \frac{2c^1_{44}}{\pi a}\int_0^{+\infty} E(\frac{s}{a})\left[1 + 2\frac{e^{-s\frac{\lambda}{a}}}{1-e^{-s\frac{\lambda}{a}}}\right]\cos(sr)\,ds \tag{4.205}$$

Because $w^1(r,y)|_{\text{single}}$ is an odd function of y, the summation in eqn (4.203) can be easily performed to give

$$w^1(r,0) = \frac{2}{\pi}\int_0^{+\infty} \frac{1}{s}E(\frac{s}{a})\cos(sr)\,ds \tag{4.206}$$

Substituting eqns (4.205) and (4.206) into (4.194) and (4.195), respectively, gives

$$\int_0^{+\infty} E(\frac{s}{a})\left[1 + 2\frac{e^{-s\frac{\lambda}{a}}}{1-e^{-s\frac{\lambda}{a}}}\right]\cos(sr)\,ds = \frac{\pi a\tau}{2c^1_{44}} + \int_0^{+\infty} D(\frac{s}{a})\cosh(sr)\,ds +$$
$$+\sum_{n=1}^{+\infty}\int_0^{+\infty} D(\frac{s}{a})\cosh(sr)\,2\cos(sn\frac{\lambda}{a})\,ds; \quad 0 \le r < 1 \tag{4.207}$$

$$\int_0^{+\infty} \frac{1}{s}E(\frac{s}{a})\cos(sr)\,ds = 0; \quad r > 1 \tag{4.208}$$

Eqns (4.207) and (4.208) are the counterparts of (4.182) and (4.183). They can be solved in a similar way. We shall therefore omit the details here and only give the result that we require later in Chapter 9.

The mode III stress intensity factor is also formally given by eqn (4.155) but with the geometry factor $\Omega(1)$ calculated from the solution of the following Fredholm integral equation

$$\Omega(\xi) + \int_0^1 [K_1(\xi,\eta) + K_2(\xi,\eta)]\,\Omega(\eta)\,d\eta = \sqrt{\xi} \tag{4.209}$$

in which the kernels are

$$K_1(\xi,\eta) = -\sqrt{\xi\eta}\int_0^{+\infty} \frac{se^{-s\frac{d}{a}}}{\Delta(\frac{s}{a})}(H_1+H_2)I_0(s\xi)\,I_0(s\eta)\,ds - \\ -2\sqrt{\xi\eta}\sum_{n=1}^{+\infty}\int_0^{+\infty}\frac{se^{-s\frac{d}{a}}}{\Delta(\frac{s}{a})}(H_1+H_2)I_0(s\xi)\,I_0(s\eta)\,\cos(sn\frac{\lambda}{a})\,ds \tag{4.210}$$

$$K_2(\xi,\eta) = \sqrt{\xi\eta}\int_0^{+\infty}\frac{2se^{-s\frac{\lambda}{a}}}{1-e^{-s\frac{\lambda}{a}}}J_0(s\xi)J_0(s\eta)\,ds \tag{4.211}$$

$\Delta(\frac{s}{a})$ is given by eqn (4.150), and H_1 and H_2 by (4.151).

4.6.3 Remarks on Boundary and Symmetry Conditions

In the solution to the crack problem in tensile mode I, we derived the solution by satisfying the major boundary and symmetry conditions (4.159) and (4.160) for the crack located at $y = 0$ (i.e. $n = 0$). The minor conditions (4.161)–(4.163) for this crack are identically satisfied by the basic solutions in view of the fact that $v^2(x,y)$ and $\tau^i_{xy}(x,y)$ $(i = 1,2)$ are all odd functions of y. If we consider an infinite extension of the body along the y-direction, then it is evident that by a suitable choice of the origin any crack can be made to coincide with $y = 0$ by translation. Therefore, the solution for the crack at $y = 0$ actually satisfies the conditions (4.159)–(4.163) for any crack in the array, i.e. any n (Kaw, 1992). The same discussion also holds for the anti-plane shear mode.

Chapter 5

Composite Laminate with Interlaminar Crack

5.1 Introductory Remarks

Interfacial areas between dissimilar media of a laminated composite material are the most critical locations for failure. A crack approaching transversely to an interface has been shown to increase the risk of delamination failure in fibre-reinforced angle-ply laminates. On the other hand, the interface area could be a crack arrestor preventing the crack from advancing further along its straight path (Gupta *et al.*, 1992).

For the configuration of dissimilar isotropic materials, the result obtained by Zak & Williams (1963) for determining the stress singularity under a symmetric stress field at a crack terminating at the interface is a widely cited result. Cook & Erdogan (1972) solved the boundary-value problem of a bonded isotropic/isotropic composite for the cases when a crack is wholly within one medium or is touching the interface at right angles. The stress intensity factors and crack surface displacements were obtained. For the same composition, Atkinson (1975) gave closed form expressions for the stresses at a crack tip in terms of a small parameter, the distance from or through the interface, when a crack is approaching the interface and when it has passed through the interface at a right angle. In both problems, the limiting case when the small parameter is identically zero was also discussed. Ashbaugh (1973) examined the behaviour of the stresses at a crack tip created by a broken layer of an isotropic material bonded between two semi-infinite planes of dissimilar isotropic materials. This problem was also solved by Gupta (1973), who reduced the boundary-value problem to a singular integral equation which could easily and accurately be solved by using a numerical Gauss-Jacobi integration technique (Erdogan *et al.*, 1973). Kaw & Besterfield (1992) gave the stress singularity and intensity factor when one tip of the multiple periodic cracks in a half-plane touches the interface between this half-plane and

a finite strip.

Regarding crack-interface interaction in anisotropic media, Arin (1974) studied the stress singularity and stress intensity factor at a crack tip in an orthotropic layer bonded to two half-planes of a different material. A similar characteristic equation for determining the stress singularity was also derived by Delale & Erdogan (1979). Wu & Erdogan (1993) solved the crack problem in two bonded orthotropic layers of finite thickness. Solutions were given both when the crack is wholly within one layer and when its tip is touching the interface. The expressions in these works for the displacement and stress fields do not include the degenerate case when one of the materials degenerates into an isotropic medium. They are only applicable to orthotropic/orthotropic configurations.

Ting & Hoang (1984) reported a solution for the stress singularities at the tip of a crack ending at an interface in an angle-ply laminated composite. The model used was that of two anisotropic bonded half planes, one of which contained a crack terminating at right angles to the interface. Their approach, although general in nature, leads to quite complicated results. The singularities have to be numerically computed from the determinant of an 18×18 matrix. The singularities for orthotropic configurations were given in a numerical form. Bai & Loo (1989), using Lekhnitskii's method of complex stress functions, calculated the stress singularities and stress intensity factors at the transverse crack tip intersecting an interface in fibre-reinforced cross-ply laminates under tension. Again, for determining the stress singularity the determinant of an 8×8 matrix has to be numerically resolved.

On the application of the solutions to the singular behaviour of stresses at interfaces, He & Hutchinson (1989) studied the crack deflection/penetration phenomenon at the interface of two dissimilar isotropic materials. The stress field (Zak & Williams, 1963; He & Hutchinson, 1989) around an interfacial crack tip was recently cited by Nakamura & Kamath (1992) in their three-dimensional computational analysis of a crack model for a film-substrate composite. Gupta *et al.* (1992) analysed the crack penetration/deflection at the interface between two aligned infinite orthotropic media, based upon the stress singularity and the angular functions of the singular stresses around the crack tip.

In this Chapter, the basic solutions presented in Chapter 4 will be applied to the corresponding boundary-value problems when the crack tip is touching the interface, i.e. $a \to d$. The procedure for solving the problems will follow that in the work of Gupta (1973). The fracture parameters of interest, i.e. the stress singularities and the *in situ* stress intensity factors at the crack tip terminating at a transversely isotropic-orthotropic bimaterial interface will be calculated. Since the basic solutions include the degenerate case when the outer sublaminates tend to be a dissimilar isotropic medium, those parameters are also given in this case and compared with the published results in the literature. A part of the work described in this Chapter has been

published in the paper by Wang & Karihaloo (1994b). Another part has been accepted for publication (Wang & Karihaloo, 1995b).

5.2 Solution for Mode I

5.2.1 Solution of Boundary-Value Problem

The basic solutions for inner (4.4)–(4.10) and outer sublaminates (4.11)–(4.15) obtained in Chapter 4 are all applicable, as are the continuity and free-surface conditions (4.30)–(4.35). In order to solve the present problem with $a \to d$, we reproduce eqns (4.38)–(4.39) here

$$v^1(r,0) = -\frac{\kappa+1}{2\mu}\frac{1}{\pi}\int_0^{+\infty}\frac{1}{s}E(\frac{s}{a})\cos(sr)\,ds = 0; \quad r>1 \tag{5.1}$$

$$\begin{aligned}\lim_{y\to 0^+}\sigma^1_{yy}(r,y) &= \lim_{y\to 0^+}\left[\frac{2}{\pi a}\int_0^{+\infty}\left\{A(\frac{s}{a})\cosh(sr)+\right.\right.\\ &\quad \left.+B(\frac{s}{a})[2\cosh(sr)+s\,r\sinh(sr)]\right\}\cos(s\frac{y}{a})\,ds+\\ &\quad \left.+\frac{2}{\pi a}\int_0^{+\infty}E(\frac{s}{a})(1+\frac{y}{a})\,e^{-s\frac{y}{a}}\cos(sr)\,ds\right]\\ &= -\sigma; \quad 0\le r<1\end{aligned} \tag{5.2}$$

To simplify (5.1)–(5.2), we introduce an unknown function

$$R_I(r) = \frac{1}{a}\frac{\partial}{\partial r}v^1(r,0) = \frac{\kappa+1}{2\mu}\frac{1}{\pi a}\int_0^{+\infty}E(\frac{s}{a})\sin(sr)\,ds. \tag{5.3}$$

$R_I(r)$ would be the so-called dislocation distribution function, had we used the dislocation formalism to model the crack.

Inverting eqn (5.3) and using eqn (5.1), we get

$$E(\frac{s}{a}) = \frac{4\mu a}{\kappa+1}\int_0^{+1}R_I(r)\sin(sr)\,dr \tag{5.4}$$

In order to solve for $R_I(r)$, we need first to relate the relations $A(s/a)$ and $B(s/a)$ appearing in (5.2) to $R_I(r)$. It is seen from (5.3) that $R_I(r)$ is an odd function of r. This property will be used in the following deductions. Substituting eqn (5.4) into the expressions for F_j $(j=1,2,3,4)$ given by eqn (A.35) in Appendix A, we have

$$F_1 = -\frac{2\mu a}{\kappa+1}\int_{-1}^{+1}R_I(r)\,(\frac{d}{a}-r)s\,e^{-s(\frac{d}{a}-r)}\,dr \tag{5.5}$$

$$F_2 = \frac{2\mu a}{\kappa+1}\int_{-1}^{+1} R_I(r)\, e^{-s(\frac{d}{a}-r)}\, dr - \\ - \frac{2\mu a}{\kappa+1}\int_{-1}^{+1} R_I(r)\,(\frac{d}{a}-r)s\, e^{-s(\frac{d}{a}-r)}\, dr \tag{5.6}$$

$$F_3 = \frac{(\kappa-1)a}{2(\kappa+1)}\int_{-1}^{+1} R_I(r)\, e^{-s(\frac{d}{a}-r)}\, dr + \\ + \frac{a}{\kappa+1}\int_{-1}^{+1} R_I(r)\,(\frac{d}{a}-r)s\, e^{-s(\frac{d}{a}-r)}\, dr \tag{5.7}$$

$$F_4 = \frac{a}{2}\int_{-1}^{+1} R_I(r)\, e^{-s(\frac{d}{a}-r)}\, dr - \\ - \frac{a}{\kappa+1}\int_{-1}^{+1} R_I(r)\,(\frac{d}{a}-r)s\, e^{-s(\frac{d}{a}-r)}\, dr \tag{5.8}$$

In deriving (5.5)–(5.8) we changed the order of integrations in (A.35) and used the following identities

$$\int_0^{+\infty} \frac{\xi^2}{(\xi^2+s^2)^2}\cos(\frac{d}{a}\pm r)\xi\, d\xi = \frac{\pi}{4s}\left[1 - s(\frac{d}{a}\pm r)\right] e^{-s(\frac{d}{a}\pm r)} \tag{5.9}$$

$$\int_0^{+\infty} \frac{\xi}{(\xi^2+s^2)^2}\sin(\frac{d}{a}\pm r)\xi\, d\xi = \frac{\pi}{4s}(\frac{d}{a}\pm r)\, e^{-s(\frac{d}{a}\pm r)} \tag{5.10}$$

It should also be pointed out that the range of r has been extended to $(-1,+1)$ in (5.5)–(5.8) and in the deduction to follow, in view of the fact that $R_I(r)$ is an odd function of r.

In order to avoid confusion when F_j $(j = 1,2,3,4)$ are used in the following deductions, we change the variable of integration r in eqns (5.5)–(5.8) to t and denote

$$f_1 = \int_{-1}^{+1} R_I(t)\, e^{-s(\frac{d}{a}-t)}\, dt \tag{5.11}$$

$$f_2 = \int_{-1}^{+1} R_I(t)\,(\frac{d}{a}-t)s\, e^{-s(\frac{d}{a}-t)}\, dt \tag{5.12}$$

Equations (5.5)–(5.8) can now be rewritten as

$$F_1 = -\frac{2\mu a}{\kappa+1} f_2 \tag{5.13}$$

$$F_2 = \frac{2\mu a}{\kappa+1} f_1 - \frac{2\mu a}{\kappa+1} f_2 \tag{5.14}$$

$$F_3 = \frac{(\kappa-1)a}{2(\kappa+1)} f_1 + \frac{a}{\kappa+1} f_2 \tag{5.15}$$

$$F_4 = \frac{a}{2} f_1 - \frac{a}{\kappa+1} f_2 \tag{5.16}$$

Substituting the above equations into (4.40)–(4.41), we get

$$A(\frac{s}{a}) = \frac{2\mu a}{\kappa+1}(N_1 f_1 + N_2 f_2) \tag{5.17}$$

$$B(\frac{s}{a}) = \frac{2\mu a}{\kappa+1}(N_3 f_1 + N_4 f_2) \tag{5.18}$$

in which

$$N_1 = \frac{1}{\Delta(\frac{s}{a})}\left[K_{12} + \frac{\kappa-1}{4\mu}K_{13} + \frac{\kappa+1}{4\mu}K_{14}\right] \tag{5.19}$$

$$N_2 = \frac{1}{\Delta(\frac{s}{a})}\left[-K_{11} - K_{12} + \frac{1}{2\mu}K_{13} - \frac{1}{2\mu}K_{14}\right] \tag{5.20}$$

$$N_3 = \frac{1}{\Delta(\frac{s}{a})}\left[K_{22} + \frac{\kappa-1}{4\mu}K_{23} + \frac{\kappa+1}{4\mu}K_{24}\right] \tag{5.21}$$

$$N_4 = \frac{1}{\Delta(\frac{s}{a})}\left[-K_{21} - K_{22} + \frac{1}{2\mu}K_{23} - \frac{1}{2\mu}K_{24}\right] \tag{5.22}$$

Substituting eqns (5.4) and (5.17)–(5.18) into (5.2) and noting (Erdogan & Gupta, 1971)

$$\lim_{y\to 0+}\int_0^1 R_I(t)\left[\int_0^{+\infty} e^{-\frac{y}{a}s}\sin(st)\cos(sr)\,ds\right]dt = \frac{1}{2}\int_{-1}^{+1}\frac{R_I(t)}{t-r}\,dt \tag{5.23}$$

we obtain a Cauchy-type singular integral equation for $R_I(t)$

$$\frac{1}{\pi}\int_{-1}^{+1}\frac{R_I(t)}{t-r}\,dt + \frac{1}{\pi}\int_{-1}^{+1}\mathcal{K}_I(r,t)\,R_I(t)\,dt = -\frac{\kappa+1}{4\mu}\,\sigma, \tag{5.24}$$

where

$$\mathcal{K}_I = \int_0^{+\infty} k_I(r,t,s)\,e^{-(\frac{d}{a}-t)s}\,ds, \tag{5.25}$$

with

$$\begin{aligned} k_I(r,t,s) = \frac{1}{\Delta(\frac{s}{a})}\Bigg\{&[K_{12} + \frac{\kappa-1}{4\mu}K_{13} + \frac{\kappa+1}{4\mu}K_{14}] + [-K_{11} - K_{12} + \frac{1}{2\mu}K_{13} - \\ &-\frac{1}{2\mu}K_{14}]\left(\frac{d}{a} - t\right)s\Bigg\}\cosh(sr) + \\ &+\frac{1}{\Delta(\frac{s}{a})}\Bigg\{[K_{22} + \frac{\kappa-1}{4\mu}K_{23} + \frac{\kappa+1}{4\mu}K_{24}] + [-K_{21} - K_{22} + \frac{1}{2\mu}K_{23} - \\ &-\frac{1}{2\mu}K_{24}]\left(\frac{d}{a} - t\right)s\Bigg\}[2\cosh(sr) + s\,r\sinh(sr)] \end{aligned} \tag{5.26}$$

$\Delta(\frac{s}{a})$ and $K_{ij}(s)$ $(i = 1,2; j = 1,...,4)$ are given by (A.33)–(A.34) in Appendix A.

The solution of eqn (5.24) is subject to the single-valuedness condition

$$\int_{-1}^{+1} R_I(t)\,dt = 0 \tag{5.27}$$

It is seen from (5.25)–(5.26) that when $d/a \to 1$, i.e. the crack tip approaches the interface, $\mathcal{K}_I(r,t)$ becomes unbounded at $t = 1$ and $r = \pm 1$, because of the infinite integral in eqn (5.25).

It is therefore necessary to use the asymptotic value of $k_I(r,t,s)$ as $s \to +\infty$ in order to study the singular behaviour of $K_I(r,t)$. The asymptotic value of $k_I(r,t,s)$ as $s \to +\infty$ is obtained in two steps.

First, we calculate the asymptotic values of $K_{ij}/\Delta(\frac{s}{a})$ $(i = 1,2; j = 1,2,3,4)$ by letting s in K_{ij} tend to $+\infty$. In the following, we demonstrate this asymptotic analysis on the example of $K_{11}/\Delta(\frac{s}{a})$.

The two hyperbolic functions $\sinh(s\frac{d}{a})$ and $\cosh(s\frac{d}{a})$ in (A.33)–(A.34) in Appendix A can be written as

$$\sinh(s\frac{d}{a}) = \frac{1}{2}\left[1 - e^{-2s\frac{d}{a}}\right] e^{s\frac{d}{a}} \tag{5.28}$$

$$\cosh(s\frac{d}{a}) = \frac{1}{2}\left[1 + e^{-2s\frac{d}{a}}\right] e^{s\frac{d}{a}} \tag{5.29}$$

$$\sinh(s\frac{d}{a})\cosh(s\frac{d}{a}) = \frac{1}{4}\left[1 - e^{-4s\frac{d}{a}}\right] e^{2s\frac{d}{a}} \tag{5.30}$$

whence, we have

$$2e^{-s\frac{d}{a}} \sinh(s\frac{d}{a}) = \left[1 - e^{-2s\frac{d}{a}}\right] \tag{5.31}$$

$$2e^{-s\frac{d}{a}} \cosh(s\frac{d}{a}) = \left[1 + e^{-2s\frac{d}{a}}\right] \tag{5.32}$$

$$4e^{-2s\frac{d}{a}} \sinh(s\frac{d}{a})\cosh(s\frac{d}{a}) = \left[1 - e^{-4s\frac{d}{a}}\right] \tag{5.33}$$

Dropping the lower order terms $e^{-2s\frac{d}{a}}$ and $e^{-4s\frac{d}{a}}$ in the square brackets in (5.31)–(5.33), we obtain the following asymptotic expressions as $s \to +\infty$

$$\lim_{s\to+\infty} 2e^{-s\frac{d}{a}} \sinh(s\frac{d}{a}) \Rightarrow 1 \tag{5.34}$$

$$\lim_{s\to+\infty} 2e^{-s\frac{d}{a}} \cosh(s\frac{d}{a}) \Rightarrow 1 \tag{5.35}$$

$$\lim_{s\to+\infty} 4e^{-2s\frac{d}{a}} \sinh(s\frac{d}{a})\cosh(s\frac{d}{a}) \Rightarrow 1 \tag{5.36}$$

In order to calculate the asymptotic value of $K_{11}/\Delta(\frac{s}{a})$, we multiply its numerator and denominator with $4e^{-2s\frac{d}{a}}$ to give

$$\frac{K_{11}}{\Delta(\frac{s}{a})} = \frac{4e^{-2s\frac{d}{a}} K_{11}}{4e^{-2s\frac{d}{a}} \Delta(\frac{s}{a})} = \frac{2e^{-s\frac{d}{a}} K_{11}}{4e^{-2s\frac{d}{a}} \Delta(\frac{s}{a})} 2e^{-s\frac{d}{a}} \tag{5.37}$$

Using K_{11} of eqn (A.34) and $\Delta(\frac{s}{a})$ of eqn (A.33) in Appendix A, we have

$$2e^{-s\frac{d}{a}}K_{11} = 2e^{-s\frac{d}{a}}\left\{\left[\sinh(s\frac{d}{a}) + s\frac{d}{a}\cosh(s\frac{d}{a})\right]M_1 - \left[-\frac{1}{2\mu}s\frac{d}{a}\cosh(s\frac{d}{a}) + \right.\right.$$
$$\left.\left. + \frac{\kappa-1}{4\mu}\sinh(s\frac{d}{a})\right]M_4 - \left[\frac{\kappa+1}{4\mu}\cosh(s\frac{d}{a}) + \frac{1}{2\mu}s\frac{d}{a}\sinh(s\frac{d}{a})\right]M_5\right\} \quad (5.38)$$

$$4e^{-2s\frac{d}{a}}\Delta(\frac{s}{a}) = 4e^{-2s\frac{d}{a}}\left\{\left[s\frac{d}{a} + \sinh(s\frac{d}{a})\cosh(s\frac{d}{a})\right]M_1 + \left[-\frac{\kappa+1}{4\mu}\sinh^2(s\frac{d}{a})\right]M_2 + \right.$$
$$+ \left[\frac{1}{2\mu}s\frac{d}{a} - \frac{\kappa-1}{4\mu}\sinh(s\frac{d}{a})\cosh(s\frac{d}{a})\right](M_3+M_4) + \left[-\frac{\kappa+1}{4\mu}\cosh^2(s\frac{d}{a})\right]M_5 +$$
$$\left. + \left[-\frac{1}{4\mu^2}s\frac{d}{a} + \frac{\kappa}{4\mu^2}\sinh(s\frac{d}{a})\cosh(s\frac{d}{a})\right]M_6\right\} \quad (5.39)$$

Using (5.34)–(5.35) in the asymptotic analysis of (5.38), we get

$$\lim_{s\to+\infty} 2e^{-s\frac{d}{a}}K_{11} \Rightarrow \left[1 + s\frac{d}{a}\right]M_1 - \left[-\frac{1}{2\mu}s\frac{d}{a} + \frac{\kappa-1}{4\mu}\right]M_4 - \left[\frac{\kappa+1}{4\mu} + \frac{1}{2\mu}s\frac{d}{a}\right]M_5 \quad (5.40)$$

Substituting (5.36) into (5.39) and ignoring, as before, the terms containing $s\frac{d}{a}e^{-2s\frac{d}{a}}$, we get

$$\lim_{s\to+\infty} 4e^{-2s\frac{d}{a}}\Delta(\frac{s}{a}) \Rightarrow M_1 - \frac{\kappa+1}{4\mu}M_2 - \frac{\kappa-1}{4\mu}(M_3+M_4) - \frac{\kappa+1}{4\mu}M_5 + \frac{\kappa}{4\mu^2}M_6 \quad (5.41)$$

Substituting (5.40) and (5.41) into (5.37) gives

$$k'_{11} = \lim_{s\to+\infty}\frac{K_{11}}{\Delta(\frac{s}{a})} = \frac{2}{\delta'}\left[M_1 + \frac{1}{2\mu}M_4 - \frac{1}{2\mu}M_5\right]s\frac{d}{a}e^{-s\frac{d}{a}} +$$
$$+ \frac{2}{\delta'}\left[M_1 - \frac{\kappa-1}{4\mu}M_4 - \frac{\kappa+1}{4\mu}M_5\right]e^{-s\frac{d}{a}} \quad (5.42)$$

(5.43)

where

$$\delta' = M_1 - \frac{\kappa+1}{4\mu}M_2 - \frac{\kappa-1}{4\mu}M_3 - \frac{\kappa-1}{4\mu}M_4 - \frac{\kappa+1}{4\mu}M_5 + \frac{\kappa}{4\mu^2}M_6 \quad (5.44)$$

Using the same procedure, we get the following asymptotics of the remaining expressions in (5.26):

$$k'_{12} = \lim_{s\to+\infty}\frac{K_{12}}{\Delta(\frac{s}{a})} = \frac{2}{\delta'}\left[M_1 - \frac{1}{2\mu}M_2 + \frac{1}{2\mu}M_3\right] s\frac{d}{a}e^{-s\frac{d}{a}} +$$
$$+ \frac{2}{\delta'}\left[\frac{\kappa-1}{4\mu}M_2 + \frac{\kappa+1}{4\mu}M_3\right] e^{-s\frac{d}{a}} \tag{5.45}$$

$$k'_{13} = \lim_{s\to+\infty}\frac{K_{13}}{\Delta(\frac{s}{a})} = \frac{2}{\delta'}\left[-M_2 - M_4 + \frac{1}{2\mu}M_6\right] s\frac{d}{a}e^{-s\frac{d}{a}} +$$
$$+ \frac{2}{\delta'}\left[-M_2 + \frac{\kappa+1}{4\mu}M_6\right] e^{-s\frac{d}{a}} \tag{5.46}$$

$$k'_{14} = \lim_{s\to+\infty}\frac{K_{14}}{\Delta(\frac{s}{a})} = \frac{2}{\delta'}\left[M_3 + M_5 - \frac{1}{2\mu}M_6\right] s\frac{d}{a}e^{-s\frac{d}{a}} +$$
$$+ \frac{2}{\delta'}\left[M_3 + \frac{\kappa-1}{4\mu}M_6\right] e^{-s\frac{d}{a}} \tag{5.47}$$

$$k'_{21} = \lim_{s\to+\infty}\frac{K_{21}}{\Delta(\frac{s}{a})} = \frac{2}{\delta'}\left[-M_1 - \frac{1}{2\mu}M_4 + \frac{1}{2\mu}M_5\right] e^{-s\frac{d}{a}} \tag{5.48}$$

$$k'_{22} = \lim_{s\to+\infty}\frac{K_{22}}{\Delta(\frac{s}{a})} = \frac{2}{\delta'}\left[-M_1 + \frac{1}{2\mu}M_2 - \frac{1}{2\mu}M_3\right] e^{-s\frac{d}{a}} \tag{5.49}$$

$$k'_{23} = \lim_{s\to+\infty}\frac{K_{23}}{\Delta(\frac{s}{a})} = \frac{2}{\delta'}\left[M_2 + \frac{1}{2\mu}M_4 - \frac{1}{2\mu}M_6\right] e^{-s\frac{d}{a}} \tag{5.50}$$

$$k'_{24} = \lim_{s\to+\infty}\frac{K_{24}}{\Delta(\frac{s}{a})} = \frac{2}{\delta'}\left[-M_3 - M_5 + \frac{1}{2\mu}M_6\right] e^{-s\frac{d}{a}} \tag{5.51}$$

In the second step of the asymptotic analysis of $k_1(r,t,s)$, we note that M_n $(n = 1,\cdots,6)$ appear both in the numerator and denominator (via δ') of the expressions for k'_{ij} $(i = 1,2; j = 1,2,3,4)$, and that M_n contain hyperbolic functions $\sinh t_i$ and $\cosh t_i$ $(i = 1,2)$. Therefore, we use a similar procedure to that used above to obtain the asymptotic expressions for k'_{ij} in (5.42) and (5.45)–(5.51) when s in the hyperbolic functions $\sinh t_i$ and $\cosh t_i$ in M_n tends to $+\infty$. In this way, the asymptotic values of k'_{ij} can be finally written as, after dropping the prime on k_{ij} in the above intermediate process,

$$k_{11} = \lim_{s\to+\infty}\frac{K_{11}}{\Delta(\frac{s}{a})} = \frac{2}{\delta}\left[m_1 + \frac{1}{2\mu}m_4 - \frac{1}{2\mu}m_5\right] s\frac{d}{a}e^{-s\frac{d}{a}} +$$
$$+ \frac{2}{\delta}\left[m_1 - \frac{\kappa-1}{4\mu}m_4 - \frac{\kappa+1}{4\mu}m_5\right] e^{-s\frac{d}{a}} \tag{5.52}$$

$$k_{12} = \lim_{s\to+\infty}\frac{K_{12}}{\Delta(\frac{s}{a})} = \frac{2}{\delta}\left[m_1 - \frac{1}{2\mu}m_2 + \frac{1}{2\mu}m_3\right] s\frac{d}{a}e^{-s\frac{d}{a}} +$$
$$+ \frac{2}{\delta}\left[\frac{\kappa-1}{4\mu}m_2 + \frac{\kappa+1}{4\mu}m_3\right] e^{-s\frac{d}{a}} \tag{5.53}$$

$$k_{13} = \lim_{s\to+\infty}\frac{K_{13}}{\Delta(\frac{s}{a})} = \frac{2}{\delta}\left[-m_2 - m_4 + \frac{1}{2\mu}m_6\right] s\frac{d}{a}\, e^{-s\frac{d}{a}} +$$
$$+ \frac{2}{\delta}\left[-m_2 + \frac{\kappa+1}{4\mu}m_6\right] e^{-s\frac{d}{a}} \tag{5.54}$$

$$k_{14} = \lim_{s\to+\infty}\frac{K_{14}}{\Delta(\frac{s}{a})} = \frac{2}{\delta}\left[m_3 + m_5 - \frac{1}{2\mu}m_6\right] s\frac{d}{a}\, e^{-s\frac{d}{a}} +$$
$$+ \frac{2}{\delta}\left[m_3 + \frac{\kappa-1}{4\mu}m_6\right] e^{-s\frac{d}{a}} \tag{5.55}$$

$$k_{21} = \lim_{s\to+\infty}\frac{K_{21}}{\Delta(\frac{s}{a})} = \frac{2}{\delta}\left[-m_1 - \frac{1}{2\mu}m_4 + \frac{1}{2\mu}m_5\right] e^{-s\frac{d}{a}} \tag{5.56}$$

$$k_{22} = \lim_{s\to+\infty}\frac{K_{22}}{\Delta(\frac{s}{a})} = \frac{2}{\delta}\left[-m_1 + \frac{1}{2\mu}m_2 - \frac{1}{2\mu}m_3\right] e^{-s\frac{d}{a}} \tag{5.57}$$

$$k_{23} = \lim_{s\to+\infty}\frac{K_{23}}{\Delta(\frac{s}{a})} = \frac{2}{\delta}\left[m_2 + \frac{1}{2\mu}m_4 - \frac{1}{2\mu}m_6\right] e^{-s\frac{d}{a}} \tag{5.58}$$

$$k_{24} = \lim_{s\to+\infty}\frac{K_{24}}{\Delta(s)} = \frac{2}{\delta}\left[-m_3 - m_5 + \frac{1}{2\mu}m_6\right] e^{-s\frac{d}{a}} \tag{5.59}$$

where

$$\delta = m_1 - \frac{\kappa+1}{4\mu}m_2 - \frac{\kappa-1}{4\mu}m_3 - \frac{\kappa-1}{4\mu}m_4 - \frac{\kappa+1}{4\mu}m_5 + \frac{\kappa}{4\mu^2}m_6 \tag{5.60}$$
$$m_1 = (1-\rho)(Z_1 - Z_2) - \rho Q_0 \tag{5.61}$$
$$m_2 = (1-\rho)(Z_2Q_1 - Z_1Q_2) + \rho\left[Q_1Q_0 + Z_1(c_{11}\beta_0 - c_{12}Q_0)\right] \tag{5.62}$$
$$m_3 = (1-\rho)(Q_1 - Q_2) + \rho(c_{11}\beta_0 - c_{12}Q_0) \tag{5.63}$$
$$m_4 = m_3 \tag{5.64}$$
$$m_5 = (1-\rho)(L_2 - L_1) + \rho c_{66}\beta_0(Q_0 - Z_0) \tag{5.65}$$
$$m_6 = -(1-\rho)(Q_1L_2 - Q_2L_1) -$$
$$-\rho\left[L_1(c_{11}\beta_0 - c_{12}Q_0) + c_{66}\beta_0Q_1(Q_0 - Z_0)\right] \tag{5.66}$$

Substituting (5.52)–(5.59) into (5.26) gives

$$\underset{s\to+\infty}{k_I}(r,t,s) = 2\left[4n_0 + (4n_0+n_1)\,s\frac{d}{a} + (4n_0+n_1+2n_2)\,(\frac{d}{a}-t)\,s + \right.$$
$$\left. + 2n_2\frac{d}{a}\,(\frac{d}{a}-t)\,s^2\right]\cosh(sr)\,e^{-s\frac{d}{a}} - 2\,[4n_0 + n_1 +$$
$$+ 2n_2(\frac{d}{a}-t)\,s\Big]\,[2\cosh(sr) + sr\sinh(sr)]\;e^{-s\frac{d}{a}} \tag{5.67}$$

where

$$n_0 = \frac{1}{\delta}\left[\frac{\kappa+1}{8\mu}m_3 + \frac{\kappa^2-1}{32\mu^2}m_6\right] \tag{5.68}$$

$$n_1 = \frac{1}{\delta}\left[m_1 - \frac{\kappa+1}{4\mu}(m_2-m_5) - \frac{\kappa-1}{2\mu}m_3 - \frac{\kappa^2+1}{8\mu^2}m_6\right] \tag{5.69}$$

$$n_2 = \frac{1}{\delta}\left[-m_1 - \frac{1}{\mu}m_3 + \frac{1}{4\mu^2}m_6\right] \tag{5.70}$$

Substituting (5.67) into (5.25) yields

$$\begin{aligned}\mathcal{K}_I &= \int_0^{+\infty} 2\left[4n_0 + (4n_0+n_1)\,s\frac{d}{a} + (4n_0+n_1+2n_2)\,(\frac{d}{a}-t)\,s+\right.\\ &+ \left.2n_2\frac{d}{a}(\frac{d}{a}-t)\,s^2\right]\cosh(sr)\,e^{-s(2\frac{d}{a}-t)}\,ds -\\ &- \int_0^{+\infty} 2\left[4n_0+n_1+2n_2(\frac{d}{a}-t)\,s\right]\left[2\cosh(sr)+sr\sinh(sr)\right]\,e^{-s(2\frac{d}{a}-t)}\,ds\end{aligned} \tag{5.71}$$

Making use of the following identities (Erdelyi, 1953)

$$\begin{aligned}\int_0^{+\infty} s^m\,e^{-s(2\frac{d}{a}-t)}\left\{\begin{array}{c}\sinh(sr)\\ \cosh(sr)\end{array}\right\}ds &= \frac{d^m}{dt^m}\int_0^{+\infty} e^{-s(2\frac{d}{a}-t)}\left\{\begin{array}{c}\sinh(sr)\\ \cosh(sr)\end{array}\right\}ds =\\ &= \frac{d^m}{dt^m}\left[\frac{1}{(2\frac{d}{a}-t)^2-r^2}\left\{\begin{array}{c}r\\ 2\frac{d}{a}-t\end{array}\right\}\right]\end{aligned} \tag{5.72}$$

we can evaluate the infinite integrals in (5.71) and obtain

$$\begin{aligned}\mathcal{K}_I(r,t) &= \left[(n_1+2n_2)+6n_2(\frac{d}{a}+r)\frac{d}{dr}+2n_2(\frac{d}{a}+r)^2\frac{d^2}{dr^2}\right]\frac{1}{t-(2\frac{d}{a}+r)}+\\ &+\left[(n_1+2n_2)-6n_2(\frac{d}{a}-r)\frac{d}{dr}+2n_2(\frac{d}{a}-r)^2\frac{d^2}{dr^2}\right]\frac{1}{t-(2\frac{d}{a}-r)}\end{aligned} \tag{5.73}$$

Substituting the above expression into (5.24) gives

$$\begin{aligned}&\frac{1}{\pi}\int_{-1}^{+1}\frac{R_I(t)}{t-r}\,dt + \frac{1}{\pi}\int_{-1}^{+1}\left[(n_1+2n_2)+6n_2(\frac{d}{a}+r)\frac{d}{dr}+\right.\\ &+\left.2n_2(\frac{d}{a}+r)^2\frac{d^2}{dr^2}\right]\frac{R_I(t)}{t-(2\frac{d}{a}+r)}\,dt + \frac{1}{\pi}\int_{-1}^{+1}\left[(n_1+2n_2)-6n_2(\frac{d}{a}-r)\frac{d}{dr}+\right.\\ &+\left.2n_2(\frac{d}{a}-r)^2\frac{d^2}{dr^2}\right]\frac{R_I(t)}{t-(2\frac{d}{a}-r)}\,dt = -\frac{\kappa+1}{4\mu}\sigma, \quad |r|<1\end{aligned} \tag{5.74}$$

In common with the works of Gupta (1973), and Arin (1974), $R_I(t)$ is assumed to exhibit the following behaviour near $t = \pm 1$

$$R_I(t) = \frac{H_I(t)}{(1-t^2)^{\gamma_1}} = \frac{H_I(t)\, e^{i\gamma_1\pi}}{(t-1)^{\gamma_1}\,(t+1)^{\gamma_1}} \qquad |t| < 1 \tag{5.75}$$

where $0 < \mathrm{Re}(\gamma_1) < 1$, and $H_I(t)$ satisfies Hölder condition in the closed interval $[-1, +1]$.

Denote

$$\phi(z) = \frac{1}{\pi}\int_{-1}^{+1} \frac{R_I(t)}{t-z}\,dt = \frac{1}{\pi}\int_{-1}^{+1} \frac{H_I(t)\, e^{i\gamma_1\pi}}{(t-1)^{\gamma_1}\,(t+1)^{\gamma_1}\,(t-z)}\,dt, \tag{5.76}$$

where $\phi(z)$ is a sectionally holomorphic function. If z is on the integration path, $\phi(z)$ may be written as (Muskhelishvili, 1953, Chapter 4)

$$\phi(z) = \frac{\cot\gamma_1\pi}{2^{\gamma_1}}\left[\frac{H_I(-1)}{(1+z)^{\gamma_1}} - \frac{H_I(1)}{(1-z)^{\gamma_1}}\right] + \phi^*(z) \tag{5.77}$$

Here $\phi^*(z)$ is bounded everywhere except at $z = \pm 1$ where it may be of the form

$$|\phi^*(z)| \le \frac{M}{|z \pm 1|^{\gamma_0}}, \qquad 0 \le \mathrm{Re}(\gamma_0) < \mathrm{Re}(\gamma_1) \tag{5.78}$$

in which M is a Hölder constant of some function.

Substituting $r \in (-1, +1)$ into (5.77), we get

$$\phi(r) = \frac{\cot\gamma_1\pi}{2^{\gamma_1}}\left[\frac{H_I(-1)}{(1+r)^{\gamma_1}} - \frac{H_I(1)}{(1-r)^{\gamma_1}}\right] + \phi_1(r) \qquad |r| < 1 \tag{5.79}$$

A comparison of the second and third integrals of (5.74) with (5.76) shows that we need to calculate $\phi(z)$ for $z = 2\frac{d}{a} \pm r$. We note that when $d/a = 1$ (so that $2\frac{d}{a} \pm r = 2 \pm r$) and as $r \to \mp 1$, $2 \pm r$ is near one end of the integration path, i.e. near $+1$. However, $2 \pm r$ will never be on this path. Therefore, we need only know the variation of the function $\phi(z)$ in eqn (5.77) for the case when z is near, but not on the integration path. In this case, in view of the behaviour of $R_I(t)$ in (5.75), $\phi(z)$ in (5.76) is written as (Muskhelishvili, 1953, Chapter 4)

$$\phi(z) = \frac{e^{\gamma_1\pi i}}{\sin\gamma_1\pi}\,\frac{1}{(z+1)^{\gamma_1}}\,\frac{H_I(-1)\, e^{i\gamma_1\pi}}{(-2)^{\gamma_1}} - \frac{e^{-\gamma_1\pi i}}{\sin\gamma_1\pi}\,\frac{1}{(z-1)^{\gamma_1}}\,\frac{H_I(1)\, e^{i\gamma_1\pi}}{2^{\gamma_1}} + \phi'(z) \tag{5.80}$$

instead of (5.77), where

$$|\phi'(z)| \le \frac{C}{|z \pm 1|^{\gamma_0}} \tag{5.81}$$

in which C and γ_0 are real constants such that $\gamma_0 < \mathrm{Re}(\gamma_1)$

Therefore, in terms of (5.76) and (5.80), we have

$$\phi(2+r) = \frac{1}{\pi}\int_{-1}^{+1}\frac{R_I(t)}{t-(2+r)}\,dt = \frac{e^{\gamma_1\pi i}}{\sin\gamma_1\pi}\,\frac{1}{(3+r)^{\gamma_1}}\,\frac{H_I(-1)\,e^{i\gamma_1\pi}}{(-2)^{\gamma_1}} -$$
$$-\frac{e^{-\gamma_1\pi i}}{\sin\gamma_1\pi}\,\frac{1}{(1+r)^{\gamma_1}}\,\frac{H_I(1)\,e^{i\gamma_1\pi}}{2^{\gamma_1}} + \phi'(2+r) \quad |r|<1 \tag{5.82}$$

$$\phi(2-r) = \frac{1}{\pi}\int_{-1}^{+1}\frac{R_I(t)}{t-(2-r)}\,dt = \frac{e^{\gamma_1\pi i}}{\sin\gamma_1\pi}\,\frac{1}{(3-r)^{\gamma_1}}\,\frac{H_I(-1)\,e^{i\gamma_1\pi}}{(-2)^{\gamma_1}} -$$
$$-\frac{e^{-\gamma_1\pi i}}{\sin\gamma_1\pi}\,\frac{1}{(1-r)^{\gamma_1}}\,\frac{H_I(1)\,e^{i\gamma_1\pi}}{2^{\gamma_1}} + \phi'(2-r) \quad |r|<1 \tag{5.83}$$

Noting that the terms involving $3+r$ and $3-r$ in (5.82)–(5.83) will never be singular when $r \to \pm 1$, we can write (5.77) and (5.82)–(5.83) as follows, as far as their leading singular terms are concerned

$$\phi(r) = \frac{\cot\gamma_1\pi}{2^{\gamma_1}}\left[\frac{H_I(-1)}{(1+r)^{\gamma_1}} - \frac{H_I(1)}{(1-r)^{\gamma_1}}\right] + \phi_1(r), \quad |r|<1 \tag{5.84}$$

$$\phi(2+r) = -\frac{1}{2^{\gamma_1}}\,\frac{1}{\sin\gamma_1\pi}\,\frac{H_I(1)}{(1+r)^{\gamma_1}} + \phi_2(r), \quad 1<2+r<3 \tag{5.85}$$

$$\phi(2-r) = -\frac{1}{2^{\gamma_1}}\,\frac{1}{\sin\gamma_1\pi}\,\frac{H_I(1)}{(1-r)^{\gamma_1}} + \phi_3(r), \quad 1<2-r<3 \tag{5.86}$$

The functions $\phi_n(r)$ $(n=1,2,3)$ have the same behaviour as that of $\phi^*(z)$ of (5.78).

Substituting eqns (5.84)–(5.86) into (5.74) gives

$$\frac{1}{2^{\gamma_1}(1+r)^{\gamma_1}\sin\gamma_1\pi}\,[H_I(-1)\cos\gamma_1\pi - H_I(1)(n_1+2n_2) + 6H_I(1)n_2\gamma_1 -$$
$$-2H_I(1)n_2\gamma_1(\gamma_1+1)] - \frac{H_I(1)}{2^{\gamma_1}(1-r)^{\gamma_1}\sin\gamma_1\pi}\,[\cos\gamma_1\pi + (n_1+2n_2) -$$
$$-6n_2\gamma_1 + 2n_2\gamma_1(\gamma_1+1)] = \Lambda(r), \qquad |r|<1 \tag{5.87}$$

where $\Lambda(r)$ is a linear combination of $\phi_n(r)$ $(n=1,2,3)$ and σ. It is bounded everywhere except as $r \to \pm 1$, when it behaves as

$$\frac{M^*}{|1\pm r|^{\gamma^*}}, \quad \mathrm{Re}(\gamma^*) < \mathrm{Re}(\gamma_1) \tag{5.88}$$

This property follows immediately from that of $\phi_n(r)$.

From (5.75) it follows that $H_I(-1) = -H_I(1)$. Following the procedure presented in the work of Gupta (1973), we multiply eqn (5.87) by $(1+r)^{\gamma_1}$ and substitute $r=-1$ and then multiply it by $(1-r)^{\gamma_1}$ and substitute $r=1$. In this way, we obtain the following characteristic equation

$$\cos\gamma_1\pi + 2n_2(\gamma_1-1)^2 + n_1 = 0 \tag{5.89}$$

where n_1 and n_2 are given by (5.69)–(5.70).

The root of eqn (5.89) in the range $(0,1)$ is the crack tip stress singularity in mode I. It is noted that the mode I stress singularity is determined by two parameters only, n_1 and n_2, which are related to the material properties, although there are six material constants which characterize the transversely isotropic central layer and the orthotropic outer layers.

5.2.2 Stress Intensity Factor

To calculate the mode I stress intensity factor, we need the tensile stress in front of the crack tip. When the crack tip touches the interface, the central sublaminate is completely broken. Therefore, the relevant stress is σ_{yy} in the outer sublaminate. This stress for the case $\rho = 0$, is given by (4.12)

$$\begin{aligned}\sigma^2_{yy}(x,0) &= \frac{2}{\pi}\int_0^{+\infty} t\,T_1\big[A_1(t)\cosh x_1 + B_1(t)\sinh x_1\big]\,dt + \\ &\quad + \frac{2}{\pi}\int_0^{+\infty} t\,T_2\big[A_2(t)\cosh x_2 + B_2(t)\sinh x_2\big]\,dt \end{aligned} \tag{5.90}$$

where

$$x_i = \beta_i\,(x-d)\,t \quad (i=1,2) \tag{5.91}$$

Using the normalization

$$t = \frac{s}{d} \tag{5.92}$$

we rewrite eqn (5.90) as

$$\begin{aligned}\sigma^2_{yy}(r,0) &= \frac{2}{\pi}\frac{1}{d^2}\int_0^{+\infty} s\,T_1\big[A_1(\tfrac{s}{d})\cosh r_1 s + B_1(\tfrac{s}{d})\sinh r_1 s\big]\,ds + \\ &\quad + \frac{2}{\pi}\frac{1}{d^2}\int_0^{+\infty} s\,T_2\big[A_2(\tfrac{s}{d})\cosh r_2 s + B_2(\tfrac{s}{d})\sinh r_2 s\big]\,ds \end{aligned} \tag{5.93}$$

where

$$r_i = \beta_i\,\frac{x-d}{d} \quad (i=1,2) \tag{5.94}$$

In the following, we shall analyse the asymptotic behaviour of the stress $\sigma^2_{yy}(r,0)$ near the crack tip, i.e. when $r \to 0^+$. $A_i(s/d)$ and $B_i(s/d)$ $(i=1,2)$ can be determined from (A.1)–(A.6) in Appendix A in the same way as $A(s/a)$ and $B(s/a)$ were determined above, and so giving,

$$A_i\left(\frac{s}{d}\right) = \frac{d}{s\Delta(\frac{s}{d})}\sum_{i=1}^{4} M_{ij}\,F_j + \frac{d}{s\Delta(\frac{s}{d})}\sum_{i=1}^{4}\mathcal{A}_{ij}\,F_j \tag{5.95}$$

$$B_i\left(\frac{s}{d}\right) = \frac{d}{s\Delta(\frac{s}{d})}\sum_{i=1}^{4} N_{ij}\,F_j + \frac{d}{s\Delta(\frac{s}{d})}\sum_{i=1}^{4}\mathcal{B}_{ij}\,F_j \quad (i=1,2) \tag{5.96}$$

in which $\Delta(\frac{s}{d})$ is obtained by replacing a with d in the expression for $\Delta(\frac{s}{a})$ in eqn (A.33), and

$$M_{11} = -\frac{\kappa+1}{4\mu} Z_2\,\omega_1 \sinh^2 s - \frac{\kappa-1}{4\mu}\omega_3 \sinh s\cosh s - \frac{\kappa}{4\mu^2} L_2\,\omega_3 \sinh s\cosh s \quad (5.97)$$

$$M_{12} = -\frac{\kappa-1}{4\mu} Z_2\,\omega_1 \sinh s\cosh s - \frac{\kappa+1}{4\mu}\omega_3 \cosh^2 s - \frac{\kappa}{4\mu^2} Q_2\,\omega_1 \sinh s\cosh s \quad (5.98)$$

$$M_{13} = Z_2\,\omega_1 \sinh s\cosh s - \frac{\kappa-1}{4\mu} Q_2\,\omega_1 \sinh s\cosh s + \frac{\kappa+1}{4\mu} L_2\,\omega_3 \cosh^2 s \quad (5.99)$$

$$M_{14} = -\omega_3 \sinh s\cosh s - \frac{\kappa+1}{4\mu} Q_2\,\omega_1 \sinh^2 s + \frac{\kappa-1}{4\mu} L_2\,\omega_3 \sinh s\cosh s \quad (5.100)$$

$$M_{21} = \frac{\kappa+1}{4\mu} Z_1\,\omega_1 \sinh^2 s + \frac{\kappa-1}{4\mu}\omega_4 \sinh s\cosh s + \frac{\kappa}{4\mu^2} L_1\,\omega_4 \sinh s\cosh s \quad (5.101)$$

$$M_{22} = \frac{\kappa-1}{4\mu} Z_1\,\omega_1 \sinh s\cosh s + \frac{\kappa+1}{4\mu}\omega_4 \cosh^2 s + \frac{\kappa}{4\mu^2} Q_1\,\omega_1 \sinh s\cosh s \quad (5.102)$$

$$M_{23} = -Z_1\,\omega_1 \sinh s\cosh s + \frac{\kappa-1}{4\mu} Q_1\,\omega_1 \sinh s\cosh s - \frac{\kappa+1}{4\mu_1} L_1\,\omega_4 \cosh^2 s \quad (5.103)$$

$$M_{24} = \omega_4 \sinh s\cosh s + \frac{\kappa+1}{4\mu} Q_1\,\omega_1 \sinh^2 s - \frac{\kappa-1}{4\mu} L_1\,\omega_4 \sinh s\cosh s \quad (5.104)$$

$$N_{11} = \frac{\kappa+1}{4\mu} Z_2\,\omega_2 \sinh^2 s + \frac{\kappa-1}{4\mu}\omega_4 \sinh s\cosh s + \frac{\kappa}{4\mu^2} L_2\,\omega_2 \sinh s\cosh s \quad (5.105)$$

$$N_{12} = \frac{\kappa-1}{4\mu} Z_2\,\omega_4 \sinh s\cosh s + \frac{\kappa+1}{4\mu_1}\omega_2 \cosh^2 s + \frac{\kappa}{4\mu^2} Q_2\,\omega_4 \sinh s\cosh s \quad (5.106)$$

$$N_{13} = -Z_2\,\omega_4 \sinh s\cosh s + \frac{\kappa-1}{4\mu} Q_2\,\omega_4 \sinh s\cosh s - \frac{\kappa+1}{4\mu} L_2\,\omega_2 \cosh^2 s \quad (5.107)$$

$$N_{14} = \omega_2 \sinh s\cosh s + \frac{\kappa+1}{4\mu} Q_2\,\omega_2 \sinh^2 s - \frac{\kappa-1}{4\mu} L_2\,\omega_4 \sinh s\cosh s \quad (5.108)$$

$$N_{21} = -\frac{\kappa+1}{4\mu} Z_1\,\omega_2 \sinh^2 s - \frac{\kappa-1}{4\mu}\omega_3 \sinh s\cosh s - \frac{\kappa}{4\mu^2} L_1\,\omega_2 \sinh s\cosh s \quad (5.109)$$

$$N_{22} = -\frac{\kappa-1}{4\mu} Z_1\,\omega_3 \sinh s\cosh s - \frac{\kappa+1}{4\mu}\omega_2 \cosh^2 s - \frac{\kappa}{4\mu^2} Q_1\,\omega_3 \sinh s\cosh s \quad (5.110)$$

$$N_{23} = Z_1\,\omega_3 \sinh s\cosh s - \frac{\kappa-1}{4\mu} Q_1\,\omega_3 \sinh s\cosh s + \frac{\kappa+1}{4\mu} L_1\,\omega_2 \cosh^2 s \quad (5.111)$$

$$N_{24} = -\omega_2 \sinh s\cosh s - \frac{\kappa+1}{4\mu} Q_1\,\omega_2 \sinh^2 s + \frac{\kappa-1}{4\mu} L_1\,\omega_3 \sinh s\cosh s \quad (5.112)$$

In the above expressions,

$$\begin{Bmatrix} \omega_1 \\ \omega_2 \\ \omega_3 \\ \omega_4 \end{Bmatrix} = Q_1 L_2 \begin{Bmatrix} \sinh t_1 \cosh t_2 \\ \sinh t_2 \cosh t_1 \\ \sinh t_1 \sinh t_2 \\ \cosh t_1 \cosh t_2 \end{Bmatrix} - Q_2 L_1 \begin{Bmatrix} \sinh t_2 \cosh t_1 \\ \sinh t_2 \cosh t_1 \\ \sinh t_2 \sinh t_1 \\ \cosh t_2 \cosh t_1 \end{Bmatrix} \quad (5.113)$$

$\mathcal{A}_{ij}$ and $\mathcal{B}_{ij}$ $(i = 1,2; j = 1,2,3,4)$ in (5.95)–(5.96) have the following asymptotic behaviour

$$\lim_{s\to+\infty} \frac{\mathcal{A}_{ij}}{\Delta(\frac{s}{d})} \Rightarrow \mathcal{C}_{ij}\, e^{-(t_1+t_2)} \tag{5.114}$$

$$\lim_{s\to+\infty} \frac{\mathcal{B}_{ij}}{\Delta(\frac{s}{d})} \Rightarrow \mathcal{D}_{ij}\, e^{-(t_1+t_2)} \quad (i = 1,2; j = 1,2,3,4) \tag{5.115}$$

where

$$t_i = \beta_i \frac{b}{d} s \quad (i = 1,2) \tag{5.116}$$

and $\mathcal{C}_{ij}$ and $\mathcal{D}_{ij}$ are constants.

Because of the asymptotic behaviour of $\mathcal{A}_{ij}$ and $\mathcal{B}_{ij}$, it will be seen that they do not enter into the asymptotic singular term of the stress $\sigma^2_{yy}(r,0)$ near the crack tip.

Substituting eqns (5.13)–(5.16) into (5.95)–(5.96) gives

$$A_i\left(\frac{s}{d}\right) = \frac{d^2}{s\,\Delta(\frac{s}{d})} \sum_{j=1}^{2} P_{ij}\, f_j + \frac{d^2}{s\,\Delta(\frac{s}{d})} \sum_{j=1}^{2} \mathcal{A}'_{ij}\, f_j \tag{5.117}$$

$$B_i\left(\frac{s}{d}\right) = \frac{d^2}{s\,\Delta(\frac{s}{d})} \sum_{j=1}^{2} Q_{ij}\, f_j + \frac{d^2}{s\,\Delta(\frac{s}{d})} \sum_{j=1}^{2} \mathcal{B}'_{ij}\, f_j \tag{5.118}$$

where $\mathcal{A}'_{ij}$ and $\mathcal{B}'_{ij}$ have the same behaviour as $\mathcal{A}_{ij}$ and $\mathcal{B}_{ij}$, and

$$P_{i1} = \frac{2\mu}{\kappa+1} M_{i2} + \frac{\kappa-1}{2(\kappa+1)} M_{i3} + \frac{1}{2} M_{i4} \tag{5.119}$$

$$P_{i2} = -\frac{2\mu}{\kappa+1} M_{i1} - \frac{2\mu}{\kappa+1} M_{i2} + \frac{1}{\kappa+1} M_{i3} - \frac{1}{\kappa+1} M_{i4} \tag{5.120}$$

$$Q_{i1} = \frac{2\mu}{\kappa+1} N_{i2} + \frac{\kappa-1}{2(\kappa+1)} N_{i3} + \frac{1}{2} N_{i4} \tag{5.121}$$

$$Q_{i2} = -\frac{2\mu}{\kappa+1} N_{i1} - \frac{2\mu}{\kappa+1} N_{i2} + \frac{1}{\kappa+1} N_{i3} - \frac{1}{\kappa+1} N_{i4} \quad (i = 1,2) \tag{5.122}$$

f_1 and f_2 are given by eqns (5.11)–(5.12).

Inserting (5.117)–(5.118) into (5.93) yields

$$\sigma^2_{yy}(r,0) = \frac{2}{\pi} \sum_{i=1}^{2} T_i \int_0^{+\infty} \left\{ \frac{1}{\Delta(\frac{s}{d})} \sum_{j=1}^{2} (P_{ij} \cosh r_i s + Q_{ij} \sinh r_i s)\, f_j + \right.$$
$$\left. + \frac{1}{\Delta(\frac{s}{d})} \sum_{j=1}^{2} (\mathcal{A}'_{ij} \cosh r_i s + \mathcal{B}'_{ij} \sinh r_i s)\, f_j \right\} ds \tag{5.123}$$

Substituting f_1 and f_2 from (5.11)–(5.12) (note $a = d$) into the above expression and changing the order of integrations, we get

$$\sigma^2_{yy}(r,0) = \frac{1}{\pi} \int_{-1}^{+1} K_I(r,t)\, R_I(t)\, dt \tag{5.124}$$

Here

$$K_I(r,t) = \int_0^{+\infty} k_I(r,t,s)\, e^{-s(1-t)}\, ds \tag{5.125}$$

in which

$$k_I(r,t,s) = \frac{2}{\Delta(\frac{s}{d})} \sum_{i=1}^{2} T_i \left[P_{i1} \cosh r_i s + Q_{i1} \sinh r_i s + (P_{i2} \cosh r_i s + Q_{i2} \sinh r_i s)(1-t)s\right] + \\ + \frac{2}{\Delta(\frac{s}{d})} \sum_{i=1}^{2} T_i \left[\mathcal{A}'_{i1} \cosh r_i s + \mathcal{B}'_{i1} \sinh r_i s + (\mathcal{A}'_{i2} \cosh r_i s + \mathcal{B}'_{i2} \sinh r_i s)(1-t)s\right] \tag{5.126}$$

From the expressions for P_{ij}, Q_{ij} $(i,j = 1,2)$ and $\Delta(s/d)$, it is seen that

$$\lim_{s\to+\infty} \frac{P_{ij}}{\Delta(\frac{s}{d})} \;\Rightarrow\; p_{ij} \tag{5.127}$$

$$\lim_{s\to+\infty} \frac{Q_{ij}}{\Delta(\frac{s}{d})} \;\Rightarrow\; q_{ij} \quad (i,j = 1,2) \tag{5.128}$$

where p_{ij} and q_{ij} are constants.

From the properties of P_{ij}, Q_{ij}, $\mathcal{A}'_{ij}$ and $\mathcal{B}'_{ij}$, it follows that for any values of r_i and t, the second term in $k_I(r,t,s)$ (5.126) only makes a finite contribution to $K_I(r,t)$, and thus only a finite (non-singular) contribution to the stress $\sigma^2_{yy}(r,0)$. However, the first term of $k_I(r,t,s)$ will result in an infinite value of $K_I(r,t)$ because of the infinite integral. Therefore, in order to examine the singular behaviour of $K_I(r,t)$, it is necessary to use the asymptotic value of $k_I(r,t,s)$, as $s \to +\infty$. This value is obtained in much the same way as in § 5.2.1 (cf. eqns (5.25) and (5.26)).

Through an asymptotic analysis similar to that which led to (5.67) from (5.26), we have

$$\underset{s\to+\infty}{k_I}(r,t,s) = 2 \sum_{l=1}^{2} T_i[l_{i1} - l_{i2} + l_{i2}(1-t)\, s](\cosh r_i s - \sinh r_i s) \tag{5.129}$$

where

$$\begin{aligned} l_{i1} &= \frac{1}{\delta}\left[-\frac{2\mu}{\kappa+1} m_{i1} + \frac{1}{2} m_{i3} + \frac{\kappa-1}{2(\kappa+1)} m_{i4}\right] \\ l_{i2} &= \frac{1}{\delta}\left[-\frac{2\mu}{\kappa+1}(m_{i1}+m_{i2}) + \frac{1}{\kappa+1}(m_{i3}-m_{i4})\right] \end{aligned} \quad (i=1,2) \tag{5.130}$$

δ is given by eqn (5.60), and the other constants are

$$m_{11} = -\frac{\kappa+1}{4\mu} Z_2 - \frac{\kappa-1}{4\mu} - \frac{\kappa}{4\mu^2} L_2 \tag{5.131}$$

$$m_{12} = -\frac{\kappa-1}{4\mu} Z_2 - \frac{\kappa+1}{4\mu} - \frac{\kappa}{4\mu^2} Q_2 \tag{5.132}$$

$$m_{13} = Z_2 - \frac{\kappa-1}{4\mu}Q_2 + \frac{\kappa+1}{4\mu}L_2 \tag{5.133}$$

$$m_{14} = -1 - \frac{\kappa+1}{4\mu}Q_2 + \frac{\kappa-1}{4\mu}L_2 \tag{5.134}$$

$$m_{21} = \frac{\kappa+1}{4\mu}Z_1 + \frac{\kappa-1}{4\mu} + \frac{\kappa}{4\mu^2}L_1 \tag{5.135}$$

$$m_{22} = \frac{\kappa-1}{4\mu}Z_1 + \frac{\kappa+1}{4\mu} + \frac{\kappa}{4\mu^2}Q_1 \tag{5.136}$$

$$m_{23} = -Z_1 + \frac{\kappa-1}{4\mu}Q_1 - \frac{\kappa+1}{4\mu}L_1 \tag{5.137}$$

$$m_{24} = 1 + \frac{\kappa+1}{4\mu}Q_1 - \frac{\kappa-1}{4\mu}L_1 \tag{5.138}$$

Substituting eqn (5.129) into (5.125) gives

$$K_I(r,t) = 2\sum_{i=1}^{2} T_i \int_0^{+\infty} [l_{i1} - l_{i2} + l_{i2}(1-t)\,s](\cosh r_i s - \sinh r_i s)\, e^{-s(1-t)}\, ds \tag{5.139}$$

Performing the integrations, we get

$$K_I(r,t) = -2\sum_{i=1}^{2} T_i \left[l_{i1} + l_{i2} r_i \frac{d}{dr_i}\right] \frac{1}{t-(1+r_i)} \tag{5.140}$$

Inserting eqn (5.140) into (5.124) yields

$$\sigma_{yy}^2(r,0) = -\frac{2}{\pi}\int_{-1}^{+1} R_I(t) \sum_{i=1}^{2} T_i \left[l_{i1} + l_{i2} r_i \frac{d}{dr_i}\right] \frac{1}{t-(1+r_i)}\, dt \tag{5.141}$$

As we are examining the asymptotic behaviour of the stress near the crack tip, $x \to d^+$ (i.e. $r_i \to 0^+$ $(i = 1,2)$), $1 + r_i$ lie near, but outside of the integration path. Substituting the expression (5.75) for $R_I(t)$ into (5.141) and using the equations (5.82) and (5.85) (also see Muskhelishvili, 1953, Chapter 4), we have

$$\frac{1}{\pi}\int_{-1}^{+1} \frac{R_I(t)}{t-(1+r_i)}\, dt = -\frac{1}{2^{\gamma_1}}\frac{1}{\sin\gamma_1\pi}\frac{H_I(1)}{r_i^{\gamma_1}} + \Phi_i^*(r_i) \quad (i = 1,2) \tag{5.142}$$

$\Phi_i^*(r_i)$ $(i = 1,2)$ in (5.142) have a similar behaviour to that of $\phi^*(z)$ in (5.78) except that their singular points are now at 0.

Inserting (5.142) into (5.141), we get

$$\sigma_{yy}^2(r,0) = -\frac{2}{2^{\gamma_1}}\frac{H_I(1)}{\sin\gamma_1\pi}\sum_{i=1}^{2}\left[T_i(l_{i2}\gamma_1 - l_{i1})\frac{1}{r_i^{\gamma_1}} + \Phi_i^{**}(r_i)\right], \tag{5.143}$$

where $\Phi_1^{**}(r_1)$ and $\Phi_2^{**}(r_2)$ are linear combinations of $\Phi_1^*(r_1)$ and $\Phi_2^*(r_2)$, respectively.

In the commonly used notation, the mode I stress intensity factor is defined as

$$K_I = \lim_{x \to d^+} \sqrt{2}\,(x-d)^{\gamma_1}\,\sigma_{yy}^2(x,0) \tag{5.144}$$

Substituting (5.143) into (5.144) and taking the indicated limit gives

$$K_I = -2\sqrt{2}\left(\frac{d}{2}\right)^{\gamma_1} \mu_I H_I(1) \tag{5.145}$$

where μ_I is a mixed parameter with the dimension of stiffness

$$\mu_I = \frac{1}{\sin\gamma_1\pi} \sum_{i=1}^{2} \left[\frac{1}{\beta_i^{\gamma_1}}\, T_i\,(l_{i2}\gamma_1 - l_{i1})\right] \tag{5.146}$$

The other stress components can be obtained straightforwardly. They have the same singular behaviour as $\sigma_{yy}^2(r,0)$. As they are not relevant to the calculation of the stress intensity factor, they are not reproduced here. However, an examination of the behaviour of the stresses at two areas around the crack tip, namely the domain of the material 2 in front of the crack tip and the interfacial area perpendicular to the crack path, may be useful in judging whether the crack will penetrate the interface or deflect, as is done by Gupta *et al.* (1992).

Although the stress intensity factor K_I is a function of μ_I and $H_I(1)$, it will be seen later (Chapter 7) that generally μ_I is the dominant factor. $H_I(1)$ is related to the material properties and the geometry and is proportional to the magnitude of the stress. The characteristic equation (5.89) and the corresponding stress intensity factor (5.145) are derived for orthotropic material 2 only. When the outer constraining sublaminates degenerate into an isotropic medium (similar or dissimilar to the inner isotropic layer), the corresponding characteristic equation and the expression for the stress intensity factor can be derived following the same procedure as above, but with $\rho = 1$ in the basic solutions (4.11)–(4.15). The results are discussed in the next Subsection.

5.2.3 Degenerate Case

When the outer layers are also isotropic, the fourth order characteristic equation (3.113) necessary for the solution of the differential equations (3.108)–(3.109), degenerates into a perfect square of a second order equation (3.118). In this degenerate case, we should take $\rho = 1$ in the basic solutions (4.11)–(4.15). Through a similar asymptotic analysis to that in § 5.2.2, we can examine the features of the stress field near the tip of the crack when it touches the interface. The characteristic equation (5.89) for determining the stress singularity degenerates into

$$\cos\gamma_1\pi + 2\lambda_2(\gamma_1 - 1)^2 - \frac{1}{2}(\lambda_1 + \lambda_2) = 0 \tag{5.147}$$

where n_1 and n_2 of (5.89) given by (5.69)–(5.70) now simplify to λ_1 and λ_2

$$\lambda_1 = \frac{\mu_2\kappa_1 - \mu_1\kappa_2}{\mu_2 + \mu_1\kappa_2} \tag{5.148}$$

$$\lambda_2 = \frac{\mu_2 - \mu_1}{\mu_1 + \mu_2\kappa_1} \tag{5.149}$$

with the subscripts 1 and 2 with μ and κ now referring to materials 1 and 2, respectively.

The characteristic equation (5.147) is in the form reported by Gupta (1973) and is identical to the well-known formula obtained by Zak & Williams (1963). It can be written in an alternative form (He & Hutchinson, 1989) via Dundurs' parameters α and β (Dundurs, 1969) instead of λ_1 and λ_2,

$$\cos\gamma_1\pi - 2\frac{\beta-\alpha}{1+\beta}(\gamma_1 - 1)^2 - \frac{\alpha+\beta^2}{1-\beta^2} = 0 \tag{5.150}$$

Here, α and β are the two Dundurs' parameters

$$\alpha = \frac{\mu_2(\kappa_1+1) - \mu_1(\kappa_2+1)}{\mu_2(\kappa_1+1) + \mu_1(\kappa_2+1)} \tag{5.151}$$

$$\beta = \frac{\mu_2(\kappa_1-1) - \mu_1(\kappa_2-1)}{\mu_2(\kappa_1+1) + \mu_1(\kappa_2+1)} \tag{5.152}$$

For the isotropic combination, it can be shown following the procedure in § 5.2.2 that μ_I degenerates into the form

$$\mu_I = \frac{\mu_1\mu_2}{\sin\gamma_1\pi}\left[\frac{1+2\lambda_1(1-\gamma_1)}{\mu_1+\mu_2\kappa_1} + \frac{1-2\lambda_2(1-\gamma_1)}{\mu_2+\mu_1\kappa_2}\right] \tag{5.153}$$

which is consistent with the result of Cook & Erdogan (1972), and also of Gupta (1973).

5.3 Solutions for Mode II and Mode III

5.3.1 Solution of Boundary-Value Problem

Using the basic solutions (4.86)–(4.95) and (4.133)–(4.136) for mode II and mode III, respectively, the boundary-value problems for these two modes can be solved straightforwardly following the procedure adopted in the preceding Section (§ 5.2). As the asymptotic analyses for modes II and III completely parallel the analysis for mode I above, many intermediate steps will be omitted and only the key steps presented.

For mode II problem with $a \to d$, we reproduce eqns (4.114)–(4.115) here

$$u^1(r,0) = -\frac{\kappa+1}{2\mu}\frac{1}{\pi}\int_0^{+\infty}\frac{1}{s}E(\frac{s}{a})\cos(sr)\,ds = 0; \quad r<1 \tag{5.154}$$

$$\begin{aligned}\lim_{y\to 0^+}\tau^1_{xy}(r,y) &= \lim_{y\to 0^+}\left[-\frac{2}{\pi a}\int_0^{+\infty}\left\{A(\frac{s}{a})[\cosh(sr)+s\,r\,\sinh(sr)]+\right.\right.\\ &\quad \left.\left.+B(\frac{s}{a})\cosh(sr)\right\}\cos(s\frac{y}{a})\,ds+\right.\\ &\quad \left.+\frac{2}{\pi a}\int_0^{+\infty}E(\frac{s}{a})(1-\frac{y}{a})\,e^{-s\frac{y}{a}}\cos(sr)\,ds\right]\\ &= -\tau_{II}; \quad 0\le r<1\end{aligned} \tag{5.155}$$

To solve (5.154)–(5.155), we introduce an unknown function

$$R_{II}(r) = \frac{1}{a}\frac{\partial}{\partial r}u^1(r,0) = \frac{\kappa+1}{2\mu}\frac{1}{\pi a}\int_0^{+\infty}E(\frac{s}{a})\sin(sr)\,ds. \tag{5.156}$$

$R_{II}(r)$ would be the so-called dislocation distribution function, had we used the dislocation formalism to model the crack.

Inverting eqn (5.156) and noting eqn (5.154), we get

$$E(\frac{s}{a}) = \frac{4\mu a}{\kappa+1}\int_0^{+1}R_{II}(r)\sin(sr)\,dr \tag{5.157}$$

The solution procedure for (5.154)–(5.155) is the same as that for (5.1)–(5.2) in § 5.2.1 for mode I problem. First, we substitute (5.157) into $A(s/a)$ and $B(s/a)$ ((A.41)–(A.42) in Appendix A) and insert the resulting expressions into (5.155). These steps give

$$\frac{1}{\pi}\int_{-1}^{+1}\frac{R_{II}(t)}{t-r}\,dt - \frac{1}{\pi}\int_{-1}^{+1}\mathcal{K}_{II}\,R_{II}(t)\,dt = -\frac{\kappa+1}{4\mu}\tau_{II}, \tag{5.158}$$

where

$$\mathcal{K}_{II} = \int_0^{+\infty}k_{II}(r,t,s)\,e^{-(\frac{d}{a}-t)s}\,ds, \tag{5.159}$$

with

$$\begin{aligned}k_{II}(r,t,s) &= \frac{1}{\Delta(\frac{s}{a})}\left\{\left[\frac{\kappa+1}{4\mu}K_{11}+\frac{\kappa-1}{4\mu}K_{12}+K_{13}\right]+\right.\\ &\quad \left.+\left[\frac{1}{2\mu}K_{11}-\frac{1}{2\mu}K_{12}+K_{13}-K_{14}\right](\frac{d}{a}-t)s\right\}\\ &\quad [\cosh(sr)+s\,r\,\sinh(sr)]+\\ &\quad +\frac{1}{\Delta(s)}\left\{\left[\frac{\kappa+1}{4\mu}K_{21}+\frac{\kappa-1}{4\mu}K_{22}+K_{23}\right]+\right.\\ &\quad \left.+\left[\frac{1}{2\mu}K_{21}-\frac{1}{2\mu}K_{22}+K_{23}-K_{24}\right](\frac{d}{a}-t)s\right\}\cosh(sr).\end{aligned} \tag{5.160}$$

$\Delta(\frac{s}{a})$ and K_{ij} $(i=1,2;j=1,...,4)$ are given by (A.43)–(A.44) in Appendix A.

Using asymptotic analysis similar to that which led to (5.73) from (5.25), we get

$$\begin{aligned}\mathcal{K}_{II}(r,t) &= -\left[(n_1+2n_2)+6n_2(\frac{d}{a}+r)\frac{d}{dr}+2n_2(\frac{d}{a}+r)^2\frac{d^2}{dr^2}\right]\frac{1}{t-(2\frac{d}{a}+r)}- \\ &\quad -\left[(n_1+2n_2)-6n_2(\frac{d}{a}-r)\frac{d}{dr}+2n_2(\frac{d}{a}-r)^2\frac{d^2}{dr^2}\right]\frac{1}{t-(2\frac{d}{a}-r)} \qquad (5.161)\end{aligned}$$

Substituting (5.161) into (5.158) gives

$$\begin{aligned}&\frac{1}{\pi}\int_{-1}^{+1}\frac{R_{II}(t)}{t-r}\,dt+\frac{1}{\pi}\int_{-1}^{+1}\left[(n_1+2n_2)+6n_2(\frac{d}{a}+r)\frac{d}{dr}+\right. \\ &+\left.2n_2(\frac{d}{a}+r)^2\frac{d^2}{dr^2}\right]\frac{R_{II}(t)}{t-(2\frac{d}{a}+r)}\,dt+\frac{1}{\pi}\int_{-1}^{+1}\left[(n_1+2n_2)-6n_2(\frac{d}{a}-r)\frac{d}{dr}+\right. \\ &+\left.2n_2(\frac{d}{a}-r)^2\frac{d^2}{dr^2}\right]\frac{R_{II}(t)}{t-(2\frac{d}{a}-r)}\,dt=-\frac{\kappa+1}{4\mu}\tau_{II}, \qquad (5.162)\end{aligned}$$

The constants n_i $(i=1,2)$ are related to the elastic constants of the two media and to the switching factor ρ

$$n_1 = \frac{1}{\delta}\left[\frac{\kappa^2+1}{2\mu}m_1-2(\kappa-1)m_2-(\kappa+1)(m_3+m_4)-4\mu m_6\right] \qquad (5.163)$$

$$n_2 = \frac{1}{\delta}\left[-\frac{1}{\mu}m_1-4m_2+4\mu m_6\right] \qquad (5.164)$$

where

$$\begin{aligned}m_1 &= (1-\rho)\,c_{66}\big[Q_1(Z_2+\beta_2)-Q_2(Z_1+\beta_1)\big]+ \\ &\quad +\rho\left[c_{11}c_{66}\beta_0(Z_1+\beta_1)(Z_0-T_0)-c_{66}Q_1(\beta_0-T_0)\right] \qquad (5.165)\\ m_2 &= (1-\rho)\,c_{66}\big[(Z_1+\beta_1)-(Z_2+\beta_2)\big]+ \\ &\quad +\rho\,c_{66}(\beta_0-T_0) \qquad (5.166)\\ m_3 &= (1-\rho)\,(Q_2-Q_1)-\rho\,c_{11}\beta_0(Z_0-T_0) \qquad (5.167)\\ m_4 &= (1-\rho)\,c_{66}\big[Z_1(Z_2+\beta_2)-Z_2(Z_1+\beta_1)\big]-\rho\,c_{66}(Z_1\beta_0+\beta_1T_0) \qquad (5.168)\\ m_5 &= -m_2 \qquad (5.169)\\ m_6 &= (1-\rho)\,(Z_1-Z_2)-\rho\,T_0 \qquad (5.170)\\ \delta &= -\frac{\kappa}{\mu}m_1+(\kappa+1)(m_3-m_4)+2(\kappa-1)m_5-4\mu m_6 \qquad (5.171)\end{aligned}$$

with Z_i, Q_i $(i=1,2)$ and T_0 given by (4.97), (4.98) and (4.100), respectively.

As in the mode I case, $R_{II}(t)$ is assumed to exhibit the following behaviour near $t=\pm1$

$$R_{II}(t)=\frac{H_{II}(t)}{(1-t^2)^{\gamma_2}}=\frac{H_{II}(t)\,e^{i\gamma_2\pi}}{(t-1)^{\gamma_2}\,(t+1)^{\gamma_2}} \qquad |t|<1 \qquad (5.172)$$

where $0 < \mathrm{Re}(\gamma_2) < 1$, and $H_{II}(t)$ satisfies Hölder condition in the closed interval $[-1, +1]$.

Following the procedure for mode I, the characteristic equation for determining the stress singularity can be shown to be

$$\cos \gamma_2 \pi + 2n_2(\gamma_2 - 1)^2 + n_1 = 0 \tag{5.173}$$

The solution for mode III is obtained in a similar but simpler manner. For this, we reproduce here eqns (4.145)–(4.146) from § 4.5

$$w^1(r,0) = \frac{2}{\pi}\int_0^{+\infty} \frac{1}{s} E(\frac{s}{a}) \cos(sr)\, ds = 0; \quad r > 1 \tag{5.174}$$

$$\lim_{y\to 0^+} \tau^1_{yz}(r,y) = \lim_{y\to 0^+} \left[\frac{2}{\pi a}\int_0^{+\infty} c^1_{44}\, D(\frac{s}{a}) \cosh(sr) \cos(s\frac{y}{a})\, ds - \right.$$
$$\left. -\frac{2}{\pi a}\int_0^{+\infty} c^1_{44}\, E(\frac{s}{a})\, e^{-s\frac{y}{a}} \cos(sr)\, ds\right] = -\tau_{III}; \quad 0 \le r < 1 \tag{5.175}$$

We again introduce an unknown function

$$R_{III}(t) = \frac{1}{a}\frac{\partial}{\partial r} w^1(r,0) = -\frac{2}{\pi a}\int_0^{+\infty} E(\frac{s}{a}) \sin(sr)\, sr \tag{5.176}$$

Inverting eqn (5.176) and using eqn (5.174), we get

$$E(\frac{s}{a}) = -a\int_0^{+1} R_{III}(r) \sin(sr)\, dr \tag{5.177}$$

Substituting (5.177) into (4.153)–(4.154) and noting that $R_{III}(t)$ is an odd function, we get

$$F_1 = -\frac{a}{2}\int_{-1}^{+1} R_{III}(t)\, e^{-s(\frac{d}{a}-t)}\, dt \tag{5.178}$$

$$F_2 = -\frac{a}{2}\int_{-1}^{+1} R_{III}(t)\, e^{-s(\frac{d}{a}-t)}\, dt = F_1 \tag{5.179}$$

so that $D(\frac{s}{a})$ in eqn (4.149) can be written as

$$D(\frac{s}{a}) = -\frac{a}{2}\frac{1}{\Delta(\frac{s}{a})}[H_1 + H_2]\int_{-1}^{+1} R_{III}(t)\, e^{-s(\frac{d}{a}-t)}\, dt \tag{5.180}$$

Substituting eqns (5.177) and (5.180) into (5.175) and using (5.23), we get the following singular integral equation

$$\frac{1}{\pi}\int_{-1}^{+1} \frac{R_{III}(t)}{t-r}\, dt - \frac{1}{\pi}\int_{-1}^{+1} \mathcal{K}_{III}(r,t)\, R_{III}(t)\, dt = -\frac{1}{c^1_{44}}\tau_{III}, \tag{5.181}$$

where

$$\mathcal{K}_{III}(r,t) \;=\; = \int_0^{+\infty} k_{III}(r,t,s)\, e^{-s(\frac{d}{a}-t)}\, ds \tag{5.182}$$

with

$$k_{III}(r,t,s) = \frac{1}{\Delta(\frac{s}{a})}[H_1 + H_2]\, \cosh(sr) \tag{5.183}$$

$\Delta(\frac{s}{a})$, H_1 and H_2 are given by (4.150) and (4.151), respectively.

The solution of eqn (5.181) is subject to the single-valuedness condition

$$\int_{-1}^{+1} R_{III}(t)\, dt \;=\; 0 \tag{5.184}$$

It is seen from (5.182)–(5.183) that when $d/a \to 1$, i.e. the crack tip approaches the interface, $\mathcal{K}_{III}(r,t)$ becomes unbounded at $t = 1$ and $r = \pm 1$, because of the infinite integral in eqn (5.182). It is therefore necessary to use the asymptotic value of $k_{III}(r,t,s)$ as $s \to +\infty$ in order to study the singular behaviour of $\mathcal{K}_{III}(r,t)$. The asymptotic value of $k_{III}(r,t,s)$ as $s \to +\infty$ is easily obtained

$$\underset{s\to+\infty}{k_{III}}(r,t,s) = 2n_3\, e^{-s\frac{d}{a}}\, \cosh(sr) \tag{5.185}$$

where

$$n_3 = \frac{c_{55}^1 - \sqrt{c_{44}^2 c_{55}^2}}{c_{55}^1 + \sqrt{c_{44}^2 c_{55}^2}} \tag{5.186}$$

Substituting (5.185) into (5.182) gives

$$\mathcal{K}_{III}(r,t) \;=\; -n_3 \left[\frac{1}{t-(2\frac{d}{a}+r)} + \frac{1}{t-(2\frac{d}{a}-r)}\right] \tag{5.187}$$

Substituting (5.187) into (5.181) gives

$$\begin{aligned} &\frac{1}{\pi}\int_{-1}^{+1} \frac{R_{III}(t)}{t-r}\, dt + \\ &+n_3 \frac{1}{\pi}\int_{-1}^{+1} \mathcal{K}_{III}(r,t)\, R_{III}(t) \left[\frac{1}{t-(2\frac{d}{a}+r)} + \frac{1}{t-(2\frac{d}{a}-r)}\right] dt = -\frac{1}{c_{44}^1}\tau_{III} \end{aligned} \tag{5.188}$$

As in modes I and II cases, $R_{III}(t)$ is assumed to exhibit the following behaviour near $t = \pm 1$

$$R_{III}(t) = \frac{H_{III}(t)}{(1-t^2)^{\gamma_3}} = \frac{H_{III}(t)\, e^{i\gamma_3\pi}}{(t-1)^{\gamma_3}\,(t+1)^{\gamma_3}} \qquad |t| < 1 \tag{5.189}$$

where $0 < \mathrm{Re}(\gamma_3) < 1$, and $H_{III}(t)$ satisfies Hölder condition in the closed interval $[-1,+1]$.

Following the procedure for modes I and II, the characteristic equation for determining the stress singularity γ_3 in mode III can be simply written as

$$\cos \gamma_3 \pi + n_3 = 0 \tag{5.190}$$

which contains only one mixed material parameter n_3 given by (5.186).

5.3.2 Stress Intensity Factors

In the commonly used notation, the mode II and mode III stress intensity factors are written as

$$K_{II} = -2\sqrt{2}\left(\frac{d}{2}\right)^{\gamma_2} \mu_{II} H_{II}(1), \tag{5.191}$$

$$K_{III} = -2\sqrt{2}\left(\frac{d}{2}\right)^{\gamma_3} \mu_{III} H_{III}(1), \tag{5.192}$$

where

$$\mu_{II} = \frac{c_{66}}{\sin \gamma_2 \pi} \sum_{i=1}^{2} \frac{1}{\beta_i^{\gamma_2}} (Z_i + \beta_i)(l_{i2}\gamma_2 - l_{i1}) \tag{5.193}$$

$$\mu_{III} = \frac{c_{55}^1 c_{44}^2}{\sin \gamma_3 \pi} \left(\frac{c_{55}^2}{c_{44}^2}\right)^{\frac{\gamma_3}{2}} \frac{1}{\sqrt{c_{44}^2 c_{55}^2} + c_{55}^1}. \tag{5.194}$$

In eqns (5.191)–(5.192), $H_{II}(1)$ and $H_{III}(1)$ are the counterparts of $H_I(1)$ in eqn (5.145). The constants Z_i $(i = 1, 2)$ in (5.193) are given by (4.97), while l_{i1} and l_{i2} $(i = 1, 2)$ are

$$\begin{aligned} l_{i1} &= \frac{1}{\delta}\left[\frac{\kappa+3}{2(\kappa+1)} m_{i1} + \frac{\kappa-3}{2(\kappa+1)} m_{i2} + 2m_{i3} - m_{i4}\right] \\ l_{i2} &= \frac{1}{\delta}\left[\frac{1}{\kappa+1}(m_{i1} - m_{i2}) + m_{i3} - m_{i4}\right] \end{aligned} \qquad (i = 1, 2) \tag{5.195}$$

where δ is given by eqn (5.171) and

$$m_{11} = (\kappa+1)c_{66}(Z_2 + \beta_2) + (\kappa-1)Q_2 + 4\mu \tag{5.196}$$

$$m_{12} = (\kappa-1)c_{66}(Z_2 + \beta_2) + (\kappa+1)Q_2 + 4\mu Z_2 \tag{5.197}$$

$$m_{13} = \frac{2\kappa}{\kappa+1} c_{66}(Z_2 + \beta_2) - \frac{2(\kappa-1)\mu}{\kappa+1} Z_2 + 2\mu \tag{5.198}$$

$$m_{14} = \frac{2\kappa}{\kappa+1} Q_2 - \frac{2(\kappa-1)\mu}{\kappa+1} + 2\mu Z_2 \tag{5.199}$$

$$m_{21} = -(\kappa+1)c_{66}(Z_1 + \beta_1) - (\kappa-1)Q_1 - 4\mu \tag{5.200}$$

$$m_{22} = -(\kappa-1)c_{66}(Z_1 - \beta_1) + (\kappa+1)Q_1 - 4\mu Z_1 \tag{5.201}$$

$$m_{23} = -\frac{2\kappa}{\kappa+1} c_{66}(Z_1 + \beta_1) + \frac{2(\kappa-1)\mu}{\kappa+1} Z_1 - 2\mu \tag{5.202}$$

$$m_{24} = -\frac{2\kappa}{\kappa+1} Q_1 + \frac{2(\kappa-1)\mu}{\kappa+1} - 2\mu Z_1 \tag{5.203}$$

5.3.3 Degenerate Case

When the outer layers are also isotropic with elastic constants μ_2, κ_2 different from the central layer ($\rho = 1$ in the general solutions (4.91)–(4.95) for mode II; there is no degeneracy in mode III), the two characteristic equations (5.173) and (5.190) reduce to

$$\cos\gamma_2\pi + 2\lambda_2(\gamma_2 - 1)^2 - \frac{1}{2}(\lambda_1 + \lambda_2) = 0 \tag{5.204}$$

$$\cos\gamma_3\pi + \lambda_3 = 0 \tag{5.205}$$

where

$$\lambda_1 = \frac{\mu_2\kappa_1 - \mu_1\kappa_2}{\mu_2 + \mu_1\kappa_2} \tag{5.206}$$

$$\lambda_2 = \frac{\mu_2 - \mu_1}{\mu_1 + \mu_2\kappa_1} \tag{5.207}$$

$$\lambda_3 = \frac{\mu_1 - \mu_2}{\mu_1 + \mu_2} \tag{5.208}$$

The two mixed parameters, μ_{II} and μ_{III}, in the stress intensity factors (5.191) and (5.192), reduce to

$$\mu_{II} = \frac{\mu_1\mu_2}{\sin\gamma_2\pi}\left[\frac{1 - 2\lambda_1(1-\gamma_2)}{\mu_1 + \mu_2\kappa_1} + \frac{1 + 2\lambda_2(1-\gamma_2)}{\mu_2 + \mu_1\kappa_2}\right] \tag{5.209}$$

$$\mu_{III} = \frac{\mu_1\mu_2}{\sin\gamma_3\pi}\frac{1}{\mu_1 + \mu_2} \tag{5.210}$$

μ_{II} (5.209) is similar in form to that obtained in § 5.2.3 (eqn (5.153)) for the mode I stress intensity factor, but the signs before λ_1 and λ_2 are reversed. Thus, whilst the characteristic eqn (5.204) and the corresponding λ_1 and λ_2 in mode II are identical to those obtained in § 5.2.3 for mode I implying identical nature of stress singularity in both modes, the stress intensity factors are different in the two modes. The stress singularity for both isotropic-isotropic and isotropic-orthotropic configurations in anti-plane deformation is determined by an independent characteristic equation and a different mixed material parameter (λ_3 or n_3).

5.4 Relation between Stress Intensity Factor and Crack Opening Displacement

Equation (5.75) gives a relation between $H_I(t)$ (which is in turn related to the stress intensity factor K_I) and R_I which is related by definition (5.3) to the gradient of the crack surface displacement $v^1(x,0)$ $(0 \le x < a)$

$$H_I(t) = (1-t^2)^{\gamma_1} R(t) = (1-t^2)^{\gamma_1} \frac{\partial}{\partial x} v^1(x,0), \quad 0 \le x < a \tag{5.211}$$

Noting $t = x/a$ and $a = d$, we get

$$\begin{aligned} H_I(t) &= \left[1 - \left(\frac{x}{d}\right)^2\right]^{\gamma_1} \frac{\partial}{\partial x} v^1(x,0) \\ &= \frac{1}{d^{2\gamma_1}} (d+x)^{\gamma_1} (d-x)^{\gamma_1} \frac{\partial}{\partial x} v^1(x,0) \end{aligned} \tag{5.212}$$

Because $H_I(t)$ satisfies the Hölder condition in the closed interval $[-1,+1]$, it follows that

$$\begin{aligned} H_I(1) &= \lim_{t \to 1^-} H_I(t) \\ &= \lim_{x \to d^-} \frac{1}{d^{2\gamma_1}} (d+x)^{\gamma_1} (d-x)^{\gamma_1} \frac{\partial}{\partial x} v^1(x,0) \\ &= \left(\frac{2}{d}\right)^{\gamma_1} \lim_{x \to d^-} (d-x)^{\gamma_1} \frac{\partial}{\partial x} v^1(x,0) \end{aligned} \tag{5.213}$$

Substituting the expression (5.213) for $H_I(1)$ into the expression (5.145) gives the following relation between the stress intensity factor K_I and the crack opening displacement $v^1(x,0)$

$$K_I = -2\sqrt{2} \left(\frac{d}{2}\right)^{\gamma_1} \mu_I \lim_{x \to d^-} (d-x)^{\gamma_1} \frac{\partial}{\partial x} v^1(x,0) \tag{5.214}$$

The relation (5.214) was also obtained by Cook & Erdogan (1972), Kaw & Besterfield (1992).

In a like manner, the function $H_{II}(1)$ in mode II can be related to $u^1(x,0)$ and the function $H_{III}(1)$ in mode III to $w^1(x,0)$. When the functions so obtained are substituted into (5.191) and (5.192), respectively, the following relations emerge

$$K_{II} = -2\sqrt{2} \left(\frac{d}{2}\right)^{\gamma_2} \mu_{II} \lim_{x \to d^-} (d-x)^{\gamma_2} \frac{\partial}{\partial x} u^1(x,0) \tag{5.215}$$

$$K_{III} = -2\sqrt{2} \left(\frac{d}{2}\right)^{\gamma_3} \mu_{III} \lim_{x \to d^-} (d-x)^{\gamma_3} \frac{\partial}{\partial x} w^1(x,0) \tag{5.216}$$

PART II

In the second part of the Thesis comprising of Chapters 6 – 9 the elastostatic solutions for cracked transversely isotropic-orthotropic bonded layers obtained in Part I are specialized to specific glass or carbon fibre-reinforced resins (e.g. epoxies and polyesters, etc.). The ever-increasing range of application of these materials is the main motivation of the study presented in this Thesis, while the numerous experimental studies on these materials provide a proper frame of reference.

Chapter 6

Multiple Cracking in Fibre-Reinforced Angle-Ply Composite Laminates

6.1 Introductory Remarks

6.1.1 Transverse (Matrix) Cracks and Interfacial Delamination

The significance of the application of the solutions obtained in Chapters 4 and 5 to the fibre-reinforced composites is manifested in the following mechanical and structural properties of these composites. The strength and stiffness of unidirectional fibre-reinforced composite laminae are quite sensitive to the direction of the application of load with respect to the fibre orientation. For this reason, they are often used in the form of multidirectional laminates. In these laminates, because of the inherent weakness of the laminae in their transverse direction, multiple transverse cracks are the most frequently observed form of damage. They can be found in the very early loading stage or even before external service load is applied (Bailey & Parvizi, 1981). The propagation of these cracks results not only in the fracture of the laminae, but also in the delamination failure between the sublaminates. Experimental results and theoretical calculations (Crossman & Wang, 1982; Fish & Lee, 1990; Kim, 1989) have revealed that transverse cracks, especially when they are close to the interfaces, are directly responsible for the delamination failure.

In the sequel, the terms laminate, lamina and ply will be interpreted according to the following example laminate, unless otherwise stated. The whole structure of a $[\pm\theta/90_n^0]_s$ composite material is referred to as a laminate. The subscript s means "symmetric". A part of this laminate which has distinct interface(s) with other part(s) of the laminate and in which the fibres are oriented in the same direction is referred to as a lamina, e.g. the $+\theta^0$, $-\theta^0$ and $(90^0)_n$ parts in the above laminate. A lamina is composed of one or several plies. Thus, for instance,

$+\theta^0$ and $-\theta^0$ laminae are composed of one ply each, whereas the $(90^0)_n$ lamina is composed of n consecutive plies. When the term *in situ* strength is mentioned, it refers to the strength of a lamina in a laminate.

Recognizing the transverse cracks as a basic damage feature of fibre-reinforced angle-ply laminates, many studies have been devoted to estimating the perturbations induced in the stress fields and laminate properties by these cracks. Thus, for $[0^0/90^0]_s$ type cross-ply laminates, Garrett & Bailey (1977) used a one-dimensional shear-lag model to predict the stress redistribution due to multiple transverse cracks in the 90^0 ply. Using the energy criterion advanced by Aveston & Kelly (1973), Parvizi *et al.* (1978), and Bailey *et al.* (1979) have shown the dependence of the transverse failure strain of the 90^0 lamina on the geometric and mechanical properties of the 90^0 and 0^0 sublaminates. Crossman & Wang (1982) made detailed experimental observations of the phenomena of multiple transverse cracks in 90_n^0 and of delamination in $[\pm 25^0/90_n^0]_s$ angle-ply laminates. The stress redistribution and the stiffness reduction due to the existence of multiple transverse cracks were extensively investigated in the works of other researchers (Highsmith & Reifsnider, 1982; Hashin, 1985; Talreja, 1985; Tan & Nuismer, 1989; Nairn, 1989; Lee *et al.*, 1989; McCartney, 1992, and others). They studied composite laminates which contain pre-existing through-thickness transverse cracks in the 90^0 plies. The interesting statement made by Nairn (1989) and his illustration (Figure 6.1) perhaps encapsulates this feature : "*We must conclude that while the propagation step in Figure 1(b) is an interesting fracture mechanics problem (it has been studied by finite elements [19]), it is not relevant to the practical problem at hand which is the analysis of experimental composite microcracking data. We therefore concern ourselves with the fracture analysis of the process described by the direct transition from Figure 1(a) to Figure 1(c).*"

However, through-thickness cracks do not normally exist in laminates but originate as microcracks or small flaws in the 90^0 ply and propagate under increasing load until they reach the interfaces, resulting in the complete fracture of the 90^0 ply. The microcracks appear first in the form of fiber-matrix debonding in small areas. As the loading increases, these debonds join up to form the nuclei for the transverse cracks (Bailey *et al.*, 1979; Bailey & Parvizi, 1981). The propagation of these cracks at a later stage depends on the configuration of the laminate of which the lamina is just a small part. The most striking feature is that the further growth of these cracks which eventually leads to the formation of a through-thickness crack in the lamina depends strongly on the thickness of the lamina and on the constraining effect provided by the neighbouring sublaminates. Moreover, when a crack is wholly within one of the two bonded materials and is perpendicular the the interface, the stress intensity factor at the tip which is away from the interface is larger than that for the tip which is close to the interface (Kaw & Besterfield, 1992; Wu & Erdogan, 1993), if the constraining material is stiffer than the cracked

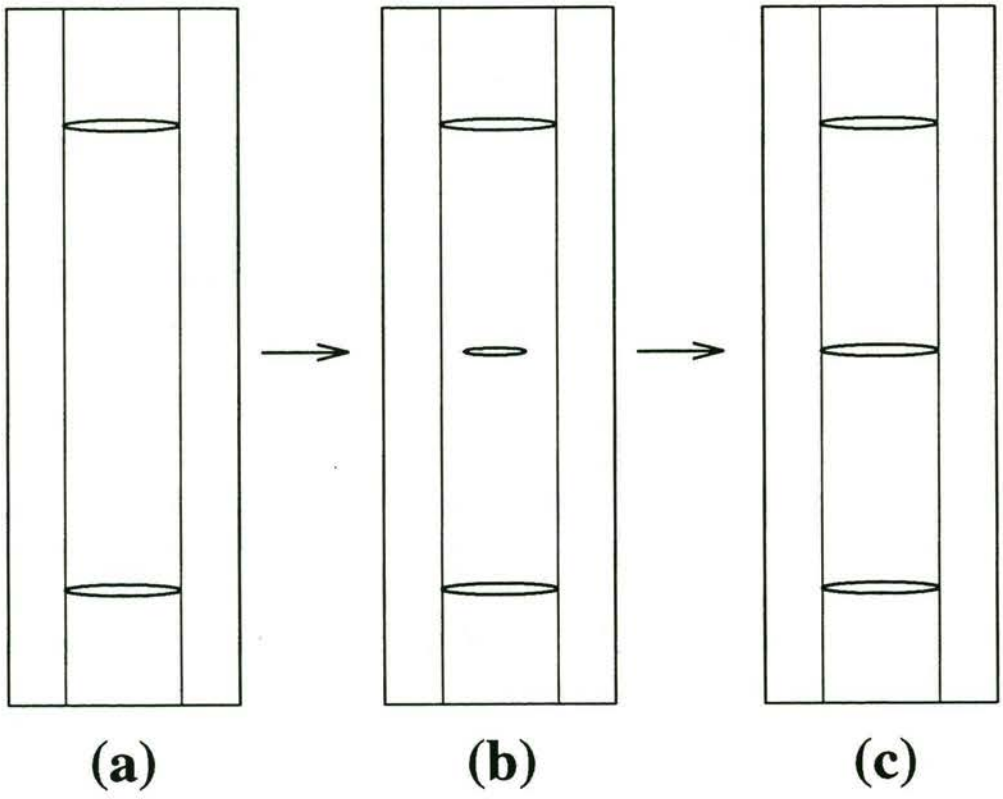

Figure 6.1: An illustration of the formation of a transverse crack. What concerns us is the constraining effect on the crack propagation at stage (b) supplied by the constraining sublaminates on the two sides (After Nairn, 1989)

one. Therefore, the initial microcracks are most likely to form away from the interfaces so that they are wholly within the 90^0 ply at the initial stage. The influence of the geometry of the cracks and the laminate configuration on the crack driving force will be examined in detail in Chapter 9.

On the aspect of the intralaminar crack problem, Wang & Crossman (1980) calculated the energy release rate at the tip of an intralaminar transverse crack using the finite element method. It was found that the energy release rate is a function of the relative size of the crack with respect to the thickness of the transverse ply and the laminate configuration. The stiffness reduction in laminates due to the development of multiple transverse cracks was predicted by Talreja (1985) using the stiffness-damage relationship developed by the author. Good agreement with experimental results was found. Dvorak & Laws (1987) calculated the strain energy release rates in two orthogonal directions of an elongated elliptic intralaminar transverse crack in a composite laminate. These strain energy release rates were used to judge the condition and sequence of propagation of the crack in the two directions. We shall discuss the results by Wang

& Crossman (1980), and Dvorak & Laws (1987) in Chapter 9. Fan *et al.* (1989) calculated the stress intensity factor at the tip of a single transverse crack in the 90^0 ply of a cross-ply laminate. Bai (1989) studied the tensile stiffness reduction of cross-ply laminates due to the existence of multiple intralaminar cracks in the 90^0 ply. Our primary concern in this Chapter is to investigate the constraining effect on the crack propagation at stage **(b)** (Figure 6.1) supplied by the neighbouring sublaminates on either side of the sublaminate under consideration. The major part of the work described in this Chapter has been published in the paper by Wang & Karihaloo (1995a).

6.2 Boundary-Value Problem and Solution

We consider a symmetric (or antisymmetric) angle-ply $[(\pm\theta^0)_{n_2}/(90^0)_{n_1}]_s$ fibre-reinforced laminate shown in Figure 6.2. It consists of a central sublaminate in which the fibres are oriented normal to the plane of the paper (90^0 ply) and two outer sublaminates which are composed of an equal number of $+\theta^0$ and $-\theta^0$ angle plies. The $(90^0)_{n_1}$ sublaminate of thickness $2d$ is transversely isotropic (in xy-plane) and is assumed to contain a series of parallel, periodically distributed transverse cracks of length $2a$. Each outer sublaminate of thickness b is treated as being homogeneous orthotropic with average elastic properties of $[\pm\theta^0]_s$ laminate, consistent with the classical lamination theory (Chapter 3). The random nature of the distribution of the defects in composites is not taken into account here. The neglect of this randomness does not invalidate the evaluation of the interaction between the cracks and sublaminates. We shall see that the density and the size of the cracks will only influence the magnitude of this interaction but not its basic features. In fact, experiments show that the transverse cracks are fairly evenly spaced in reality (Garrett & Bailey, 1977; Highsmith & Reifsnider, 1982; Crossman & Wang, 1982). The calculation of the elastic parameters of the sublaminates is given in Appendix C.

It is assumed that the composite laminate is subjected to a tensile load along y-direction so that the central sublaminate is subjected to a homogeneous tensile stress σ along this direction when the cracks are absent, as discussed at the beginning of § 4.6.1. Because of the orthotropy of the outer sublaminates, the 90^0 sublaminate also undergoes a uniform tensile deformation along y-direction except near the free edges. This free-edge effect is not considered here.

The solution of the boundary-value problem for multiple cracks is readily obtained from the general solutions of § 4.6.1.

6.2.1 Stress Intensity Factor in Mode I

The mode I stress intensity factor at the tips of each of the cracks is given by eqn (4.193)

$$K_I = \Phi(1)\,\sigma\sqrt{a} \tag{6.1}$$

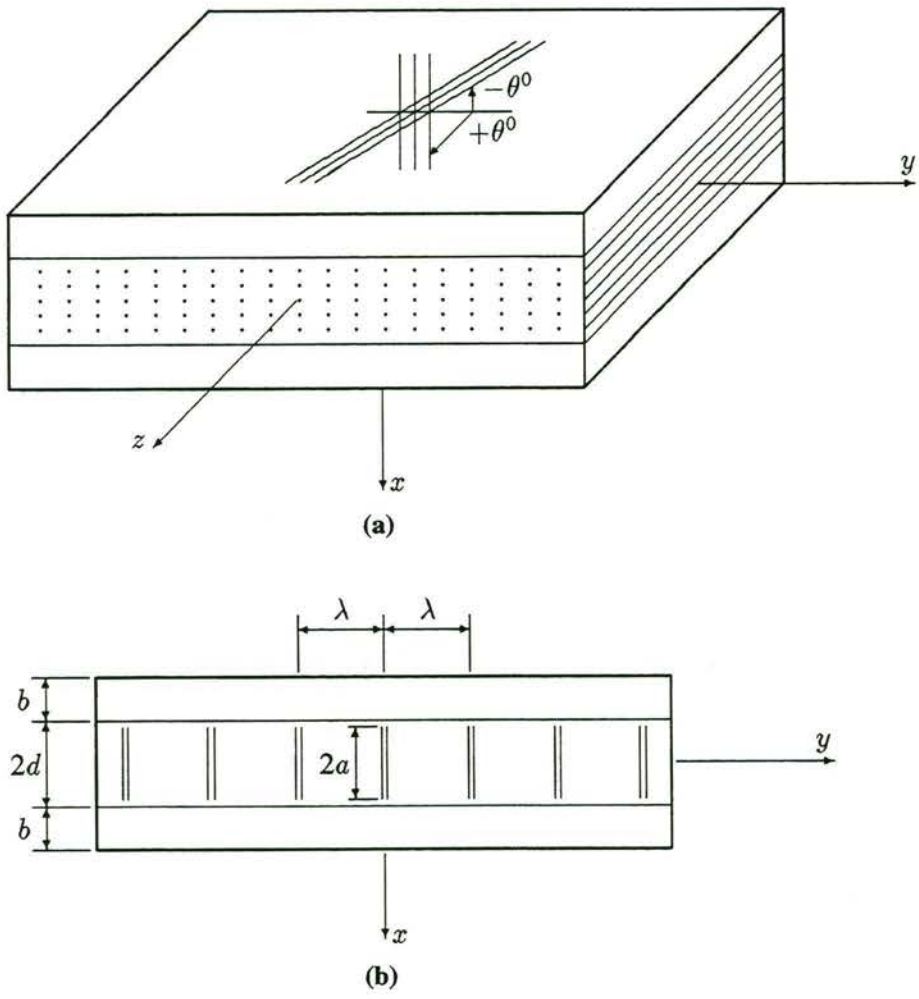

Figure 6.2: The cracked composite laminate and coordinate axes

where $\Phi(1)$ is given by the solution of the Fredholm integral equation (4.188).

Before we calculate the value of $\Phi(1)$ for some specific materials, let us comment briefly on the solution of the Fredholm integral equation (4.188) and on the evaluation of its kernels (4.189) and (4.190). The integral equation (4.188) is solved numerically by using the trapezoidal rule. In this way, the original integral equation is discretized into a system of linear equations

$$\sum_{j=1}^{n} a_{ij}\, \Phi(\xi_j) = \sqrt{\xi_i} \quad (i = 1, \cdots, n) \tag{6.2}$$

where ξ_i $(i = 1, \cdots, n)$ is a set of uniformly distributed discrete values in the interval $[0, 1]$. The value of n is chosen having regard to the desired accuracy and the CPU time spent on the computation, as the calculation of the complicated kernel (4.189) is very time consuming. In most of the computations, $n = 10$ was found to be quite adequate, although $n = 20$ was also tried to check the accuracy. It was found that when $\theta = 90^0$, i.e. the cracked composite laminate

degenerates into an isotropic strip with a periodic array of parallel central cracks, the parameter $\Phi(1)$ for a given crack spacing is in close agreement with the value given in the handbook of Tada *et al.* (1985).

The first kernel (4.189) contains both the summation of an infinite series and an infinite integral. Let us discuss the computation of the infinite integral. The integrand of this integral can be separated into two parts. The first part is given by eqn (4.62), and it does not contain the cosine function. The second part contains the cosine function. Having regard to the asymptotic behaviour of the first part of the integrand (eqn (4.72)), the Gauss-Laguerre quadrature was used to calculate the integral numerically. The number of quadrature points was chosen between 15 and 20. It was found that the integral for different number of quadrature points converged rapidly. The convergence of the second part of the infinite integral containing the cosine function is demonstrated by the integral (4.191). Because of the influence of the cosine function, the value of the integrand will oscillate. Therefore, in order to enhance the accuracy of the numerical integration, these infinite integrals are calculated using the following procedure. The term containing the cosine function in eqn (4.189) can be written as

$$\int_0^{+\infty} F(\xi,\eta,s)\cos(sn\frac{\lambda}{a})ds = \int_0^{s_N} F(\xi,\eta,s)\cos(sn\frac{\lambda}{a})ds + \int_{s_N}^{+\infty} F(\xi,\eta,s)\cos(sn\frac{\lambda}{a})ds \tag{6.3}$$

where

$$F(\xi,\eta,s) = \sqrt{\xi\,\eta}\,\frac{se^{-s\frac{d}{a}}}{\Delta(\frac{s}{a})}\left\{I_0(s\xi)\sum_{j=1}^{4}K_{1j}E_j + [2I_0(s\xi)+s\xi I_1(s\xi)]\sum_{j=1}^{4}K_{2j}E_j\right\} \tag{6.4}$$

and s_N is a large finite number.

The first integral in the right hand side of eqn (6.3) is evaluated using Simpson's quadrature, and the second by Gauss-Laguerre quadrature. Because the integrand contains a negative exponential term, the second integral only makes a minor contribution to the total, when s_N is large. In most of the computations, $s_N = 20$ was found adequate.

Next, we encounter the problem of the summation of an infinite series in the calculation of the kernel, i.e.

$$\sum_{n=1}^{+\infty}\int_0^{+\infty} F(\xi,\eta,s)\,\cos(sn\frac{\lambda}{a})\,ds \tag{6.5}$$

Because of its complexity, the summation of the infinite series in eqn (6.5) is approximated by a finite sum in the computations. Physically, each term in the summation gives a part of the perturbation in the stress field caused by a crack at a distance $n\lambda$ along the y-direction. A second part of the perturbation in the stress field is given by the sum of a second infinite series (i.e. the

sum of the second part of the expression (4.178) with respect to λ). However, this summation can be performed analytically and is given by (4.180) which appears in the kernel (4.190). So the finite series approximation of (6.5) can be expected to give a limited truncation error based on the convergence of the series resulting from the infinite integral of (4.191).

From the calculations, it was found that when λ is greater than approximately 6 times the half-thickness of 90^0 layer, the interaction among the cracks is not significant. This can be clearly seen from Figure 6.3. A comparison of this numerical result for the present composite laminate with the available results for other material configurations obtained by different techniques should give us some confidence in the acçuracy of the evaluation of interaction among multiple cracks by the present technique. The book by Tada *et al.* (1985) gives the stress intensity factor at the tips of an array of parallel cracks located centrally in an isotropic strip of finite thickness. When the spacing between the cracks is greater than twice the half-width of strip, the stress intensity factor is quite close to that for an isolated crack, i.e. the interaction among the cracks is not significant. On the other hand, for a multicracked $[0^0_m/90^0_n]_s$ laminate with interlaminar transverse cracks, Hashin (1985) evaluated the stress field by a variational approach. For an isolated transverse crack, he found that the stress perturbation caused by the crack decays rapidly with the distance away from the crack. Under uniaxial tension, the perturbation virtually vanishes at a distance equal to 6 times the half-thickness of the 90^0 sublaminate away from the crack. For the case of interacting multiple transverse cracks, he found that the crack interaction is not significant when the distance between the cracks is greater than 8 times the half-thickness of the 90^0 sublaminate. Therefore, the finite term approximation to the infinite sum in the calculation of the first kernel (4.189) would seem to be reasonably accurate.

The kernel (4.190) was also evaluated by Simpson's quadrature. Because the integrand decays rapidly when s tends to infinity (it contains a negative exponential term), a limited truncation error is expected as a result of numerical integration.

As a check on the accuracy of the numerical scheme described above, we compare some results for mode I problem with those available in the handbook of Tada *et al.* (1985). For example, for $\theta = 90^0$, $b/d = 1.0$ and $a/d = 0.7$, when $\lambda/d \geq 2.0$, the relative error of $\Phi(1)$ calculated above from the value read off the curves in the handbook was less than 3%. It is noted that the error of the value in the handbook is itself within 1%. For an isolated crack, the relative error of the present result from that calculated by the formulae in the handbook is around 1%. The error is even smaller for mode III problem, as will be demonstrated later in § 6.4.2.

$\Phi(1)$ alone is affected by the stiffness properties of the sublaminates, the density of the cracks and the laminate configuration, i.e. the ply angle θ and the relative thicknesses of the sublaminates. For the graphite/epoxy material properties (Tan & Nuismer, 1989) listed in Table 6.1, the variations of $\Phi(1)$ and $\Phi(1)\sqrt{a}/\sqrt{d}$ with a/d and θ for a single crack ($\lambda/d \to +\infty$)

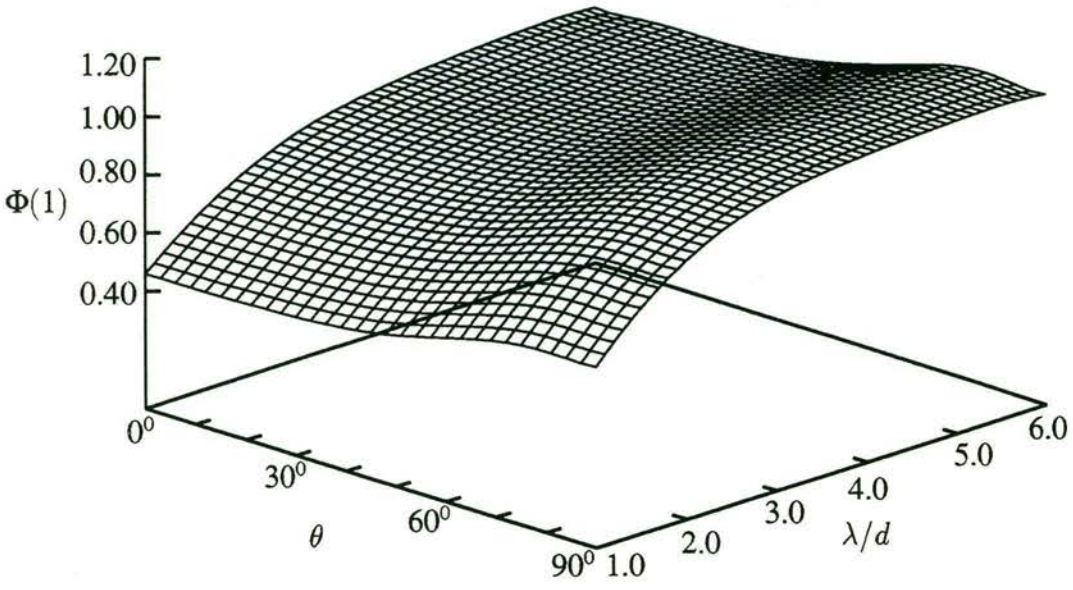

Figure 6.3: Variation of $\Phi(1)$ with θ and λ/d for multiple cracks each of length $a/d = 0.7$

are shown in Figure 6.4 and Figure 6.5, respectively, while that with θ and λ/d for multiple cracks is shown in Figure 6.3. For these calculations the ratio of sublaminate thicknesses b/d was chosen to be unity, unless otherwise indicated explicitly.

Table 6.1: Material properties

Properties & Material	E_L (GPa)	E_T (GPa)	G_{LT} (GPa)	G_{TT} (GPa)	ν_{LT} -	ν_{TT} -	Ply thickness(mm)
T300/934	138	11.7	4.56	4.18	0.29	0.40	0.132

We are now in a position to examine the constraining effect of the outer sublaminates on the inner 90^0 sublaminate. $\Phi(1)$ exhibits two notable features. First, it always increases with increasing θ, irrespective of the crack size. This means that the constraining effect of the outer plies decreases with increasing θ. In other words, transverse cracks in the 90^0 ply of $[\pm\theta^0/90^0]_s$ laminates will propagate at smaller stress levels, the larger the ply angle θ. This result agrees with experimental observations which show that *in situ* tensile strength of the 90^0_n layer in $[\pm\theta^0/90^0_n]_s$ laminates reduces with an increase in θ (Flaggs & Kural, 1982). It is also seen from Figure 6.5 that if the size of the initial cracks or flaws is less than a certain critical value, the *in situ* stress intensity factor increases with an increase in the thickness of the 90^0 sublaminate. Thus, the thicker the 90^0 layer, the smaller the *in situ* transverse tensile strength. This result also

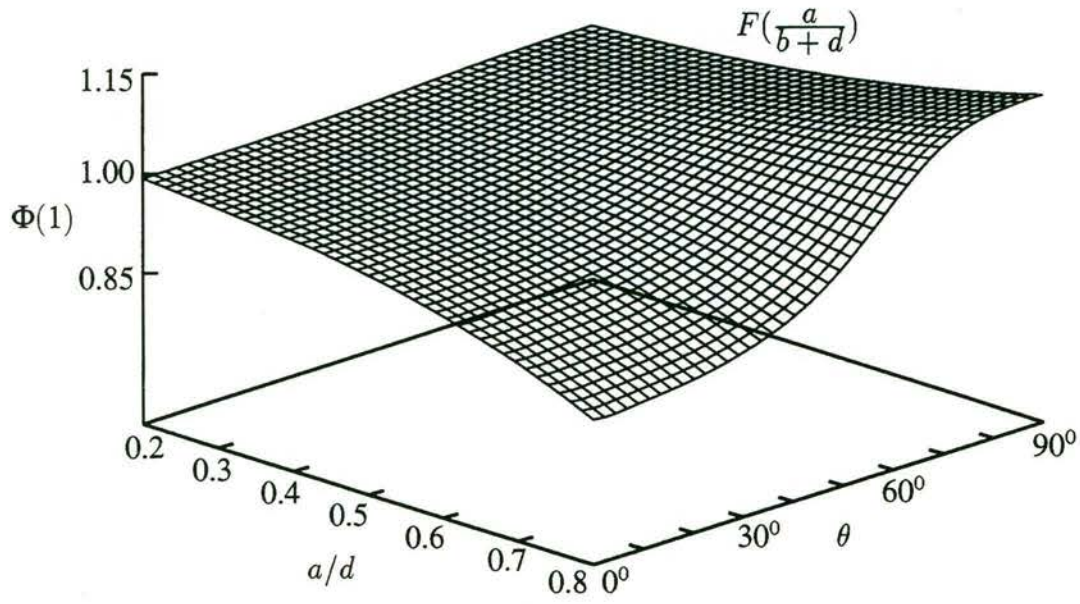

Figure 6.4: Variation of $\Phi(1)$ with a/d and θ for a single crack

confirms experimental observations made by Garrett & Bailey (1977), Parvizi *et al.* (1978), and Flaggs & Kural (1982).

Secondly, for $0^0 \leq \theta < 90^0$, $\Phi(1)$ is always less than $F(\frac{a}{b+d})$ — the corresponding geometry factor at each crack tip in a finite homogeneous isotropic strip (if the θ^0 sublaminates on the two sides are absent then the stress intensity factor is $K_{I0} = F(\frac{d}{a})\sigma\sqrt{a}$) otherwise there would be no point in using composite materials. It is also for this reason that the θ^0 sublaminates are regarded as constraints for the central layer. However, it is found that this constraining effect has the following important property which can be exploited in the design of laminates insensitive to cracks (flaws). As can be seen from Figure 6.4, when θ is less than a certain critical value θ_c, $\Phi(1)$ decreases with increasing crack length, so that the crack driving force decreases during the propagation of the crack. This suggests that for arbitrary multidirectional laminates, the difference between the fibre orientations in the adjacent plies should exceed a certain minimum value θ_m, if the laminae are going to play the role of mutual crack arrestors. For the material properties of Table 6.1, this critical value θ_c is around 70^0, i.e. the ply angle difference between the central sublaminate and the outer sublaminates should exceed $\theta_m = 20^0$. The configurations with smaller ply angle differences should be avoided in order not to exaggerate the crack growth in the central sublaminate.

Figure 6.3 shows the variation of $\Phi(1)$ with θ and λ/d. The interaction among the multiple cracks helps to reduce the value of the stress intensity factor at each crack tip. This effect comes from the stress relaxation caused by crack arrays on either side of a particular crack.

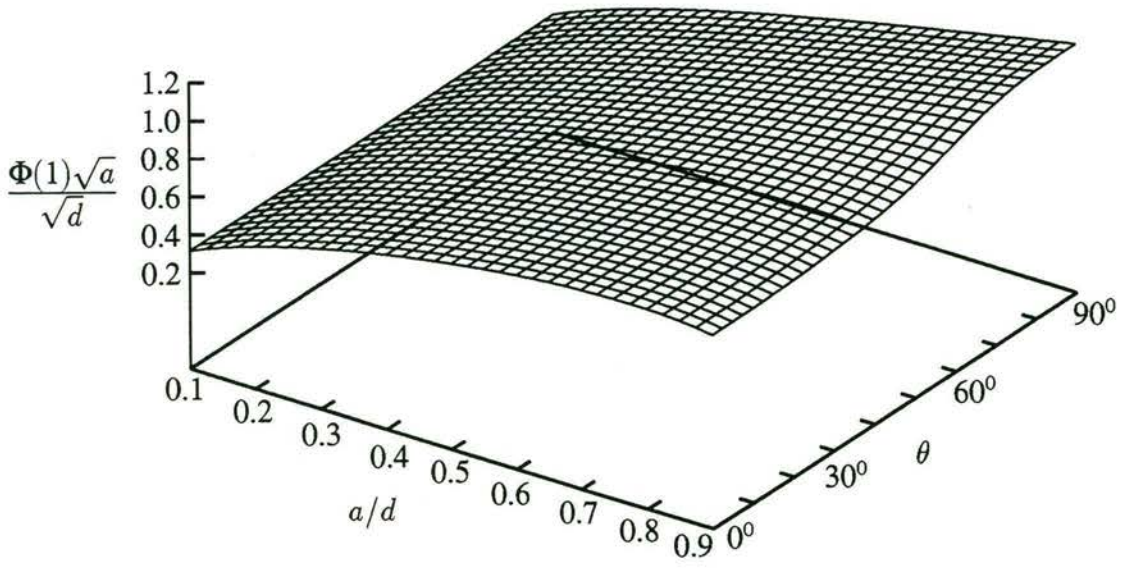

Figure 6.5: Variation of the mode I stress intensity factor with a/d and θ for a single crack for $b/d = 2.0$

Theoretically, when $\lambda/d \to 0$, $\Phi(1) \to 0$ (a paradoxical result from a practical view point). Experimental results (e.g. Highsmith & Reifsnider, 1982) reveal that the number of cracks (the crack density) in the 90^0 sublaminate increases with increasing tensile load, reaching a saturation value at a certain load level. This saturation phenomenon is evidently a result of the interplay between $\Phi(1)$ and λ/d just mentioned.

6.2.2 Interfacial Stresses

The evaluation of the interfacial stresses in composite laminates is also an important subject because high interfacial stresses can lead to delamination failure in laminates. Even though the overall integrity of the laminate may still be intact after the occurrence of transverse cracks in individual laminae, the delamination failure will profoundly destroy this integrity. As has been previously pointed out, experimental results show that when transverse cracks approach the interfaces, they can cause delamination failure (Crossman & Wang, 1982; Kim, 1989; and Fish & Lee, 1990). In this Section, we shall investigate the perturbation of the interfacial stresses due to the existence of transverse cracks, i.e. the *crack-induced* interfacial stresses, with a view to revealing the role of transverse cracks in the delamination failure of laminates.

In the preceding Section, we replaced each of the $[(\pm\theta^0)_{n_2}]$ outer sublaminates by a homogeneous orthotropic medium with average stiffness properties according to the classical lamination theory (CLT). However, as the central 90^0 layer is bonded from above and below to a $-\theta^0$ layer,

a question arises when we calculate the *crack-induced* interfacial stresses, namely, how does the local anisotropy of the $-\theta^0$ layer influence the nature of the *crack-induced* interfacial stresses calculated using the indicated homogenisation procedure? This question is directly related to applicability of the CLT and the complexity of the analysis of interfacial stresses in angle-ply laminates.

As we have seen in § 3.7, CLT is based upon thin plate approximation and macroscopic average elastic properties of laminates. For various angle-ply laminates under in-plane loading (e.g. tension), the problem posed above has been extensively investigated by many researchers (e.g. Pagano & Soni, 1983; Wang & Choi, 1982a,b; Jones, 1975; the paper by Wang & Choi (1982a) contains a brief review of this topic). These and other investigations show that the CLT cannot accurately predict the stress fields in the boundary regions near the free edges of a laminate. The mismatch in the elastic properties of plies indeed invalidates the stress prediction by CLT in these regions. However, they also show that away from the boundary regions, the stress fields converge to those predicted by CLT. For the problem under consideration, according to CLT, the interfacial stresses in xy-plane at the interface without the transverse cracks will be $\sigma_{xx} = 0$ and $\sigma_{yy} = \sigma$. (There is a discontinuity in σ_{yy} at the transition from the 90^0 layer to the outer layer. $\sigma_{yy} = \sigma$ is valid on the side of the weaker 90^0 layer). That is to say, the local anisotropy of the outer $+\theta^0$ (or $-\theta^0$) layer does not give rise to any additional interfacial stresses that would distort the stress field predicted by CLT. Therefore, as the dominant interfacial stresses will result from the existence of transverse cracks, the replacement of the $[(\pm\theta^0)_{n_2}]$ outer layer by an effective orthotropic medium should not invalidate the interfacial stress calculations except near the boundary regions.

The extent of this boundary region is generally one to several times the laminate thickness (about 2.2 times the thickness for a $[+45^0/-45^0]_s$ laminate according to Wang & Choi, 1982b). The width to thickness ratios of actual laminate components generally far exceed this boundary region. The investigation of the stress state in the boundary region is a continuing research topic (e.g. Christensen & DeTeresa, 1992; Folias, 1992; and Becker, 1994).

Following the principle of superposition (§ 4.6), the *crack-induced* interfacial stresses can be calculated by superimposing the perturbations from a single crack calculated in § 4.3. From the expressions of the stresses (4.4)–(4.6) and the symmetry of the problem, it is seen that only σ^1_{xx} and σ^1_{yy} exist at the interface just in front of the tip of a crack, i.e. $x = d,\ y = 0$. Therefore, following the procedure that led to the derivation of (4.179), the relevant interfacial stresses are

$$\sigma^1_{xx}(d,0) = -\frac{2}{\pi a}\int_0^{+\infty}[A(\frac{s}{a})\cosh(s\frac{d}{a}) + B(\frac{s}{a})\,s\frac{d}{a}\,\sinh(s\frac{d}{a})]\left[1+2\sum_{n=1}^{+\infty}\cos(sn\frac{\lambda}{a})\right]ds +$$
$$+\frac{2}{\pi a}\int_0^{+\infty}E(\frac{s}{a})\left[1+2\frac{e^{-s\frac{\lambda}{a}}}{1-e^{-s\frac{\lambda}{a}}}\left(1-s\frac{\lambda}{a}\frac{1}{1-e^{-s\frac{\lambda}{a}}}\right)\right]\cos(s\frac{d}{a})\,ds \qquad (6.6)$$

$$\sigma^1_{yy}(d,0) = \frac{2}{\pi a}\int_0^{+\infty}\left\{A(\frac{s}{a})\cosh(s\frac{d}{a}) + B(\frac{s}{a})[2\cosh(s\frac{d}{a})+\right.$$
$$\left. + \; s\frac{d}{a}\sinh(s\frac{d}{a})]\right\}\left[1+2\sum_{n=1}^{+\infty}\cos(sn\frac{\lambda}{a})\right]ds +$$
$$+\frac{2}{\pi a}\int_0^{+\infty} E(\frac{s}{a})\left[1+2\frac{e^{-s\frac{\lambda}{a}}}{1-e^{-s\frac{\lambda}{a}}}\left(1+s\frac{\lambda}{a}\frac{1}{1-e^{-s\frac{\lambda}{a}}}\right)\right]\cos(s\frac{d}{a})\,ds \tag{6.7}$$

Moreover, substituting (4.65) into (4.59) and (4.60) gives

$$A(\frac{s}{a}) = -\frac{\pi}{2}a\sigma\frac{1}{\Delta(\frac{s}{a})}se^{-s\frac{d}{a}}\sum_{j=1}^{4}K_{1j}G_j \tag{6.8}$$

$$B(\frac{s}{a}) = -\frac{\pi}{2}a\sigma\frac{1}{\Delta(\frac{s}{a})}se^{-s\frac{d}{a}}\sum_{j=1}^{4}K_{2j}G_j \tag{6.9}$$

where

$$G_j = \int_0^1 \sqrt{\eta}\Phi(\eta)\,E_j(s,\eta)\,d\eta \quad (j=1,2,3,4) \tag{6.10}$$

Substituting eqns (6.8)–(6.9) into the first integral in each of (6.6) and (6.7), and eqn (4.67) into the second integrals, we get

$$\frac{\sigma^1_{xx}(d,0)}{\sigma} = \int_0^{+\infty}\frac{se^{-s\frac{d}{a}}}{\Delta(s)}\left[\cosh(s\frac{d}{a})\sum_{j=1}^{4}K_{1j}G_j+\right.$$
$$\left.+\,s\frac{d}{a}\sinh(s\frac{d}{a})\sum_{j=1}^{4}K_{2j}G_j\right]\left[1+2\sum_{n=1}^{\infty}\cos(sn\frac{\lambda}{a})\right]ds +$$
$$+\int_0^1\Phi(\eta)\,G(\eta)\,d\eta - \int_0^{+\infty}K_5\,G_5\,ds \tag{6.11}$$

$$\frac{\sigma^1_{yy}(d,0)}{\sigma} = -\int_0^{+\infty}\frac{se^{-s\frac{d}{a}}}{\Delta}\left\{\cosh(s\frac{d}{a})\sum_{j=1}^{4}K_{1j}G_j+\right.$$
$$\left.+\left[2\cosh(s\frac{d}{a})+\frac{d}{a}\sinh(s\frac{d}{a})\right]\sum_{j=1}^{4}K_{2j}G_j\right\}\left[1+2\sum_{n=1}^{\infty}\cos(sn\frac{\lambda}{a})\right]ds +$$
$$+\int_0^1\Phi(\eta)\,G(\eta)\,d\eta - \int_0^{+\infty}K_6\,G_6\,ds \tag{6.12}$$

where

$$G(\eta) = \left(\frac{a}{d}\right)^2\frac{\sqrt{\eta}}{\sqrt{1-\left(\frac{a}{d}\eta\right)^2}\left[1+\sqrt{1-\left(\frac{a}{d}\eta\right)^2}\right]}\left\{2+\frac{\left(\frac{a}{d}\eta\right)^2\left[1+2\sqrt{1-\left(\frac{a}{d}\eta\right)^2}\right]}{\left[1-\left(\frac{a}{d}\eta\right)^2\right]\left[1+\sqrt{1-\left(\frac{a}{d}\eta\right)^2}\right]}\right\} \tag{6.13}$$

$$G_5 = G_6 = \int_0^1 \sqrt{\eta}\,\Phi(\eta)\,J_0(s\eta)\,d\eta$$

$$K_5 = 2s\frac{e^{-s\frac{\lambda}{a}}}{1-e^{-s\frac{\lambda}{a}}}\left[1 - s\frac{\lambda}{a}\frac{1}{1-e^{-s\frac{\lambda}{a}}}\right]\cos(s\frac{d}{a}) \tag{6.14}$$

$$K_6 = 2s\frac{e^{-s\frac{\lambda}{a}}}{1-e^{-s\frac{\lambda}{a}}}\left[1 + s\frac{\lambda}{a}\frac{1}{1-e^{-s\frac{\lambda}{a}}}\right]\cos(s\frac{d}{a}) \tag{6.15}$$

All the infinite integrals are computed by the numerical scheme described in § 6.2.1.

The tensile stress normal to the interface area is most likely to cause delamination. For the crack configuration and loading of Figure 6.2, the interfacial stresses σ_{xx} and σ_{yy} in front of each crack tip are found to be always positive. Therefore, under plane strain conditions, the interfacial area is subjected to an unfavourable three-dimensional tensile field. The variation of *crack-induced* interfacial normal stress σ_{xx} with λ/d and a/d for $\theta = 0^0$ and $\theta = 45^0$ is shown in Figures 6.6(a) and (b), respectively. The *crack-induced* interfacial stress σ_{yy} is almost of the same order as σ_{xx}. The total interfacial stress σ_{yy} is obtained by adding the applied homogeneous stress σ to the *crack-induced* value.

As the crack tip approaches the interface ($a/d \rightarrow 1$), the interfacial stresses increase rapidly for all θ. For small cracks though, the interfacial stresses are fairly insensitive to changes in θ, but as a/d increases so also does this sensitivity to outer ply angle θ, as is evident from a comparison of Figures 6.6(a) and (b).

6.3 Mode III Stress Intensity Factor for Multiple Cracks

When an angle-ply fibre-reinforced composite laminate is subjected to in-plane loads and if there exit no in-plane/out-of-plane coupling effects within the framework of classical lamination theory described in § 3.7, the stress components existing in a lamina of this laminate are σ_{yy}, σ_{zz} and $\tau_{zy(yz)}$ in the coordinate system of Figure 6.2. These stresses can be resolved into three components σ_L, σ_T and τ_{LT} in the system of the elastic principal axes L (longitudinal) and T (transverse) of the lamina. σ_L is the stress along the fibre direction, σ_T is normal to the fibres and τ_{LT} is the shear stress in LT plane. Since the transverse and in-plane shear strengths of the lamina are much smaller than its strength in the longitudinal direction, the stresses σ_T and τ_{LT} generally result in the failure of the lamina in the transverse direction. This failure is manifested through the appearance of transverse cracks. For a transverse crack in the 90^0 sublaminate in Figure 6.2, the transverse tensile stress σ_T results in mode I deformation, while the stress τ_{LT} causes a mode III (anti-plane shear) deformation. Therefore, in this Section, we shall give the results of the mode III stress intensity factor at the tips of the cracks of the cracked composite laminate shown in Figure 6.2, just as the mode I stress intensity factor was obtained in § 6.2.1.

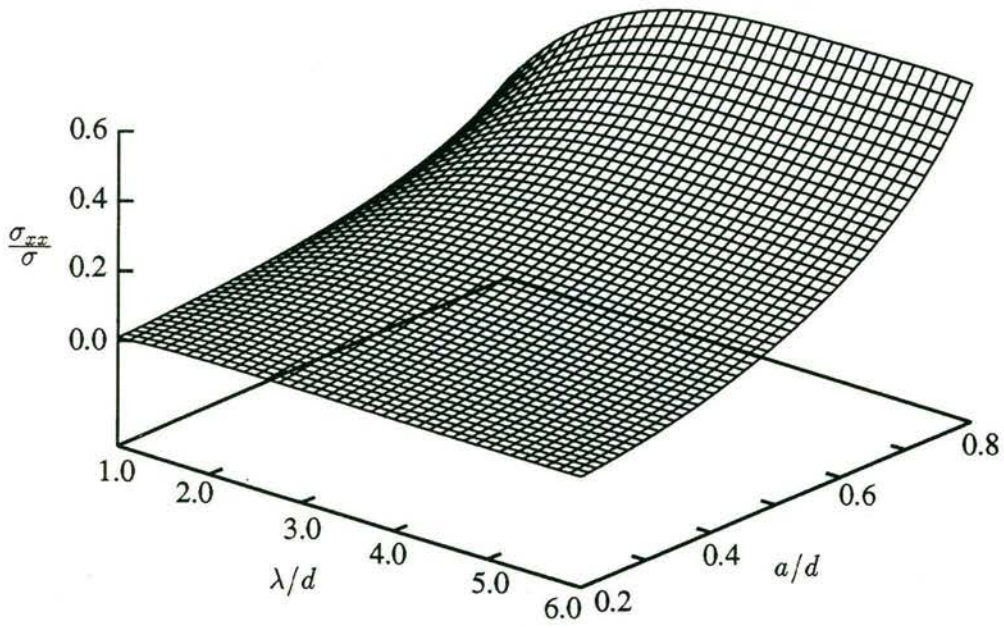

(a)

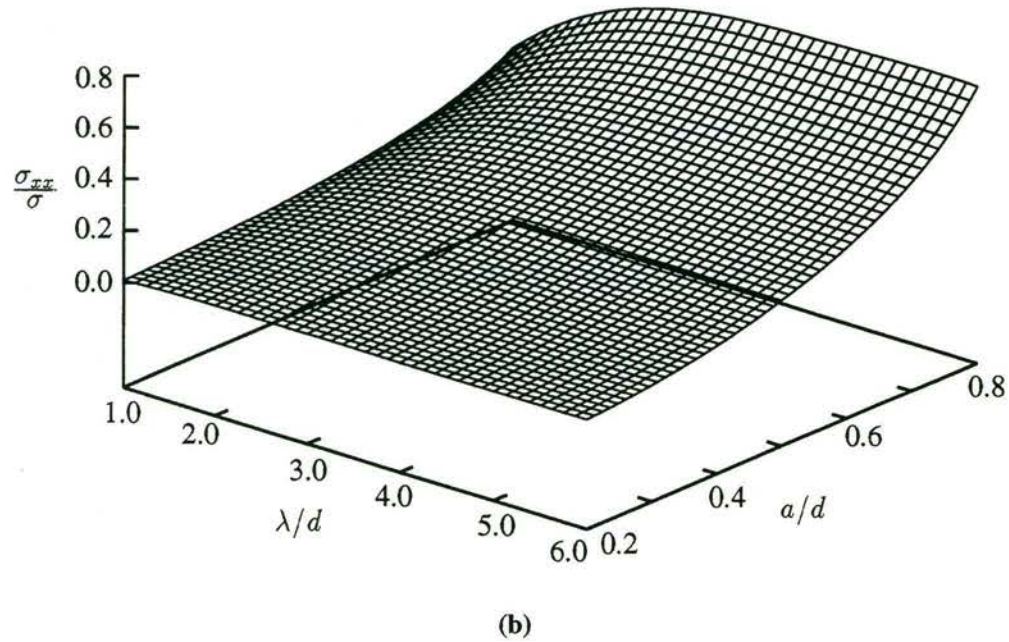

(b)

Figure 6.6: Normalized interfacial normal stress: (a) $\theta = 0^0$; (b) $\theta = 45^0$

For the material properties listed in Table 6.1, the integral equation (4.209) for mode III was solved, and the variation of $\Omega(1)$ with θ and λ/d is shown in Figure 6.7. $\Omega(1)$ depicts a variation with λ/d similar to that of $\Phi(1)$ in Figure 6.3. The interaction among the cracks also helps to reduce the value of the mode III stress intensity factor at each crack tip. When the cracks are fairly well apart, e.g. $\lambda/d > 6$, the influence of this interaction on the mode III SIF is not significant for the crack length under consideration.

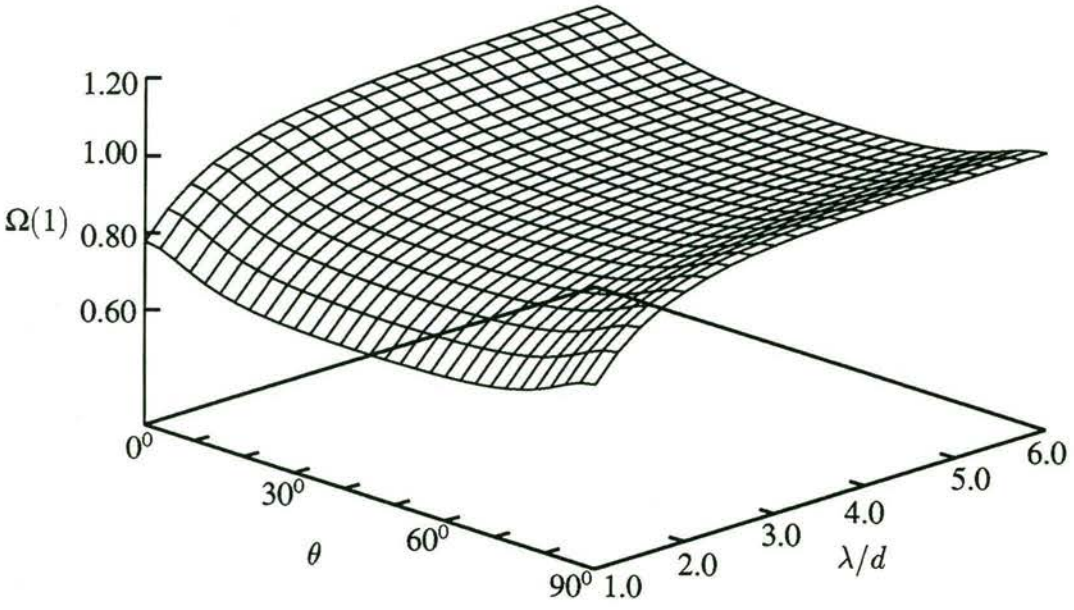

Figure 6.7: Variation of $\Omega(1)$ with θ and λ/d for multiple cracks each of length $a/d = 0.7$

6.4 Accuracy of the Numerical Scheme and Conclusions

6.4.1 Remarks on the Constraining Effect

In a $[(\pm\theta^0)_{n_2}/(90^0)_{n_1}]_s$ angle-ply laminate, the constraining effect of the outer $[(\pm\theta)_{n_2}]$ sublaminates on the inner $[(90^0)n_1]$ sublaminate is determined by the stiffness, geometry and ply angle θ, with the stiffness of the outer sublaminates playing the most dominant role. In order to retard the growth of transverse cracks in the inner sublaminate the difference in the fibre orientations in the adjacent laminae must exceed a certain critical value. For the same reason, the inner sublaminate should not be very thick. We shall return to this topic in Chapter 9.

Transverse cracks can induce high interfacial stresses, the more so when these cracks are close to the interface. This is a major cause of the *crack-induced* delamination in angle-ply laminates.

6.4.2 Accuracy of Numerical Solution of the Fredholm Integral Equation

In § 6.3, we described the numerical procedure for the solution of the Fredholm integral equation (4.188) that determines the stress intensity factor via $\Phi(1)$ for the case of the multiple cracks. This procedure was also used to solve the Fredholm integral equation (4.209) for the mode III problem. For the configuration of a single crack, the integral equations given by (4.66) for mode I, (4.124) for mode II and (4.156) for mode III are simpler and easier to handle. Moreover, as exact expressions of the geometry factors for mode III stress intensity factor exist for a single central crack in an isotropic strip of finite width and for multiple cracks in an infinite body (Tada *et al.*, 1985), we can judge the accuracy of the numerical scheme used here by comparing the numerical solutions of the integral equations (4.156) and (4.209) with the exact values for the two indicated configurations. The numerical results were computed by setting $\theta = 90^0$. Under this condition, the bonded composite laminate degenerates into an isotropic strip of width $2(b+d)$. For the case of a single crack, the geometry factor is determined by the relative length of the crack to the width of the strip, while for multiple cracks in an infinite body it is determined by the ratio of the spacing between the cracks to the length of the cracks. It is noted that the definitions of the stress intensity factors in this Thesis and those in the handbook of Tada *et al.* (1985) differ by the constant $\sqrt{\pi}$. The exact geometry factor for a single crack in a finite strip is compared in Table 6.2 with the numerical value for several a/d values. Similarly, the exact geometry factor for an array of periodic cracks (period λ) in an infinite isotropic body ($b + d \to \infty$) is compared in Table 6.3 with its numerical counterpart.

Table 6.2: Accuracy of mode III geometry factor ($\theta = 90^0$ and $b/d = 2.0$) for a single crack in a finite strip

$\frac{a}{d}$	0.20	0.30	0.40	0.50	0.60	0.70	0.80	0.90
Exact Solution	1.0018	1.0041	1.0074	1.0120	1.0170	1.0234	1.0310	1.0398
Numerical Solution	1.0019	1.0043	1.0077	1.0122	1.0177	1.0244	1.0323	1.0416

It is seen from Table 6.2 that the numerical solution for a single crack is in very good agreement with the exact value for all values of a/d. Although the accuracy for the multiple cracks is not as good as that for the single crack, the relative error is still less than 1% for the considered crack spacings. No exact solutions exist for modes I and II, but the numerical values of the geometry factors are also close to the data calculated using the approximate formulae given in the above mentioned handbook. For mode I, as was mentioned in § 6.2.1, the relative

error is less than 3% for multiple cracks ($\lambda/d \geq 2.0$), and around 1% for a single crack.

Table 6.3: Accuracy of mode III geometry factor for multiple cracks in an infinite body

$\frac{\lambda}{a}$	1.25	1.4286	1.6667	2.00	2.50	3.3333	5.00	10.0
Exact Solution	0.6267	0.6661	0.7118	0.7641	0.8225	0.8839	0.9414	0.9840
Numerical Solution	0.6207	0.6605	0.7068	0.7598	0.8191	0.8815	0.9402	0.9837

Chapter 7

Interlaminar Cracking in Angle-Ply Laminates

7.1 Introductory Remarks

In this Chapter, we shall apply the basic solutions given in Chapter 5 to fibre-reinforced composite laminates. Although the through-thickness crack problem, i.e. the problem where the tips of the transverse cracks touch the interfaces, would appear to have been well investigated, there is practically no information available in a useful form on the behaviour of the stress fields. Bai & Loo (1989) have come closest to providing such information. They used Lekhnitskii's method of complex stress functions for anisotropic media to solve the problem of a finite $[0^0/90^0]_s$ cross-ply fibre-reinforced composite laminate with a transverse through-thickness crack under tension. The stress singularity and stress intensity factor were calculated. However, their method led to very complicated expressions for the stress and displacement fields. The stress singularity had to be calculated from a complicated transcendental equation which is the determinant of an 8×8 matrix. Wu & Erdogan (1993) have solved the problem of bonded orthotropic/orthotropic composite when a crack is embedded in one layer and when one tip of the crack touches the interface. They have given characteristic equations for determining the stress singularities and expressions for stress intensity factors. It is the aim of this Chapter to examine the singular behaviour of the stresses for fibre-reinforced composite laminates and provide easily-accessible information, using the solutions from Chapter 5. In particular, we shall consider situations where both crack tips touch neighbouring interfaces and when the laminate consists of an inner transversely isotropic sublaminate of finite thickness surrounded by outer finite orthotropic sublaminates. A part of the work described in this Chapter has been published in the paper by Wang & Karihaloo (1994b). Another part has been accepted for publication (Wang & Karihaloo, 1995b).

7.2 Elastic Properties of Composite Laminates

In order that the basic solutions given in Chapter 5 are applicable to the problem at hand, it is necessary to restrict the structure of the composite laminates and to use certain homogeneity assumptions. Suppose that the central layer of the composite laminate shown in Figure 4.1 is composed of a fibre-reinforced unidirectional lamina in which the fibres are aligned parallel to the z-axis (material 1), while each of the outer layers (material 2) is an angle-ply sublaminate in which the fibres, in yz-plane, lie symmetrically at angles $+\theta^0$ and $-\theta^0$ with respect to the y-axis. For these fibre layouts, the central layer may be treated as a transversely isotropic material (in xy-plane) and the constraining sublaminates as orthotropic with their principal elastic axes parallel to the coordinate axes. From a manufacturing point of view, the angle-ply sublaminates can also have a $(\pm\theta^0)_n$ or $[(\pm\theta^0)_n]_s$ structure. When n is fairly large for a given thickness of the structure, such a sublaminate may also be approximated by an effective orthotropic medium whose elastic constants can be calculated by the classical lamination theory (CLT). In the following, we shall calculate the stress singularities and the *in situ* stress intensity factors using the four materials listed in Table 7.1. The properties of unidirectional laminae listed in Table 7.1 are reported by Tan & Nuismer (1989), and Talreja (1991). The elastic stiffness of the central and outer sublaminates are calculated using the procedure discussed in Appendix C. The consequences of the homogenisation are also discussed in that Appendix.

Table 7.1: Material properties

Materials / Property	E_L (GPa)	E_T (GPa)	G_{LT} (GPa)	G_{TT} (GPa)	ν_{LT} -	ν_{TT} -
1 T300/934 (Gr/Ep)	138.0	11.7	4.56	4.18	0.29	0.40
2 Glass/Ep	41.7	13.0	3.40	4.57	0.30	0.42
3 AS4/3501-6 (Gr/Ep)	140.1	8.36	4.31	3.20	0.253	0.297
4 AS4/Tactix 556 (Gr/Ep)	151.1	7.09	3.63	2.72	0.241	0.304

7.3 Mode I Problem

After calculating the elastic stiffnesses (and/or compliances) of the sublaminates following the procedure in Appendix C, the mode I stress singularity γ_1 can be directly obtained by solving the characteristic equation (5.89). The necessary elastic stiffnesses of the four materials of Table 7.1 are given in Table 7.2 for one representative value of $\theta = 30^0$.

Table 7.2: Stiffnesses of the sublaminates for $\theta = 30^0$

Material	Stiffnesses (GPa)					
	c_{11}	c_{12}	c_{22}	c_{44}	c_{55}	c_{66}
M1	20.80	30.22	127.46	28.13	4.27	4.47
M2	26.36	22.20	47.73	9.90	4.28	3.69
M3	10.91	13.89	101.33	28.23	3.48	4.03
M4	9.66	15.03	112.41	30.01	2.95	3.40

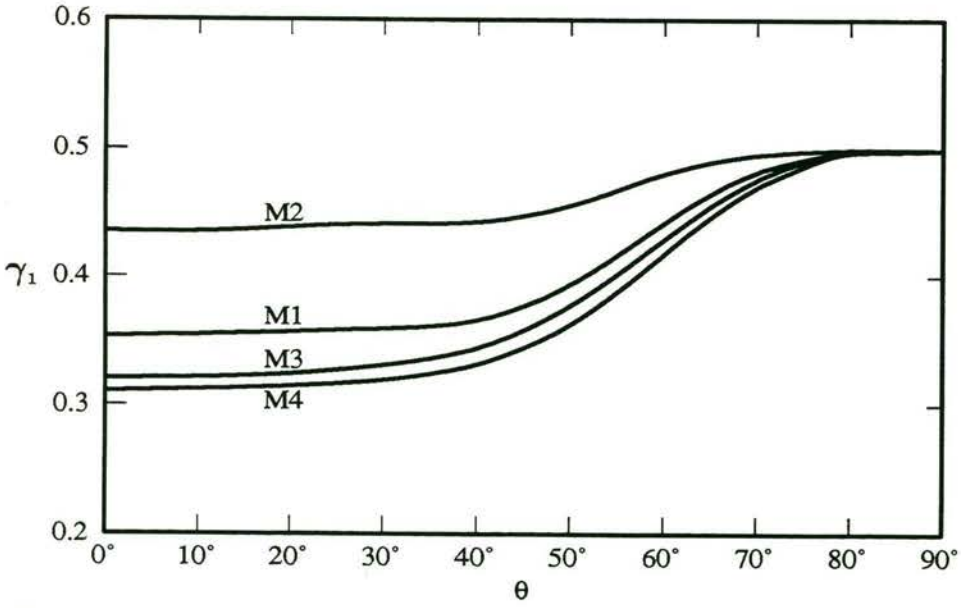

Figure 7.1: Mode I stress singularity at a crack tip terminating at an isotropic-orthotropic bimaterial interface as a function of the orthotropic ply angle θ for the four material combinations of Table 7.1

The variation of the stress singularity γ_1 with θ for the four materials is shown in Figure 7.1. For all four materials the weakest singularity always occurs when $\theta = 0^0$, i.e. for cross-ply laminates, because the highest modulus (but not necessarily the stiffness coefficient) of the $[\pm\theta^0]$ ply in y-direction is when $\theta = 0^0$. It seems that the reduction of the interfacial stress singularity from the usual value 0.5 is greatly assisted by the high anisotropy in the longitudinal (L) and transverse (T) directions of the unidirectional laminae. Materials 2 and 4 are two extreme cases in point. The ratio E_L/E_T of material 4 is the largest and that of material 2, glass/epoxy, the smallest among the four chosen materials. The values of γ_1 for these two materials therefore are also at the extreme ends; the larger the ratio E_L/E_T of the orthotropic layer the smaller the stress singularity at the interface.

It is seen from eqn (5.145) that the stress intensity factor at the crack tip when it reaches the interface is determined by two parameters, i.e. μ_I and $H_I(1)$. The former is a function of the elastic properties of the central and outer sublaminates (eqn (5.146)), while the latter is related to the material properties and geometry and is proportional to the applied stress. $H_I(1)$ is obtained by solving the singular integral equation (5.24) after substituting eqn (5.75) into it. Here, we first examine the influence of the ply angle θ on μ_1 assuming that the variation of θ only affects the stiffness of the outer sublaminates. The variation of μ_I with the ply angle θ is shown in Figure 7.2. The trend in μ_I is exactly the opposite of that in γ_1 (cf. Figures 7.1 and 7.2).

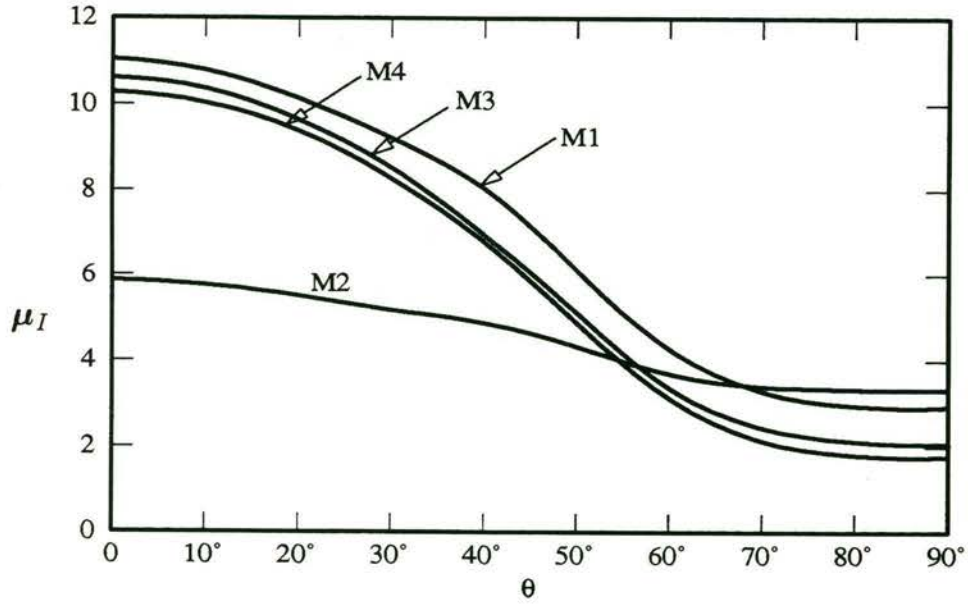

Figure 7.2: Variation of μ_I with the ply angle θ for the four material combinations of Table 7.1

Since the stress intensity factor is related to $H_I(1)$, we must solve the Cauchy-type singular integral equation (5.24). This can be done by using the Gauss-Jacobi quadrature (Erdogan *et al.*, 1973). But first, the Cauchy-type singular integral equation (5.24) is rewritten as

$$\frac{1}{\pi}\int_{-1}^{+1}\frac{R_I(t)}{t-r}\,dt+\frac{1}{\pi}\int_{-1}^{+1}\mathcal{K}_I^S(r,t)\,R_I(t)\,dt+\frac{1}{\pi}\int_{-1}^{+1}\mathcal{K}_I^F(r,t)\,R_I(t)\,dt=-\frac{\kappa+1}{4\mu}\,\sigma, \quad (7.1)$$

where the two kernels are

$$\mathcal{K}_I^S(r,t) = \int_0^{+\infty} \underset{s\to+\infty}{k_I}(r,t,s)\; e^{-(\frac{d}{a}-t)s}\,ds, \quad (7.2)$$

$$\mathcal{K}_I^F(r,t) = \int_0^{+\infty} \left[k_I(r,t,s)- \underset{s\to+\infty}{k_I}(r,t,s)\right] e^{-(\frac{d}{a}-t)s}\,ds, \quad (7.3)$$

In the above expressions for the kernels, $\overset{k_I}{{}_{s\to+\infty}}(r,t,s)$ and $k_I(r,t,s)$ are given by (5.67) and (5.26), respectively. From the asymptotic analysis in § 5.2.1, we know that when $a = d$, the kernel (7.2) is singular, and its asymptotic representation is given by (5.73); the kernel (7.3) on the other hand is of the Fredholm type. Subject to the condition that $R_I(t)$ behaves like (5.75) and that $0 < \mathrm{Re}(\gamma_1) < 1$ (which is evidently satisfied by all four materials under consideration, see Figure 7.1), the singular integral equation (7.1) can be readily solved by using the procedure of Erdogan *et al.* (1973). Following this procedure, the singular integral equation (7.1) and single-valuedness condition (5.27) are discretized into a system of N linear equations

$$\frac{1}{\pi}\sum_{k=1}^{N} H_I(t_k)\, W_k\left[\frac{1}{t_k - r_j} + \mathcal{K}_I^S(r_j,t_k) + \mathcal{K}_I^F(r_j,t_k)\right] = -\frac{\kappa+1}{4\mu}\sigma, \quad j = 1,\cdots,N-1 \tag{7.4}$$

$$\sum_{k=1}^{N} H_I(t_k)\, W_k = 0 \tag{7.5}$$

where t_k and r_j which vary in the interval $(-1,+1)$ are given by the roots of the following Jacobi polynomials

$$P_N^{(-\gamma_1,-\gamma_1)}(t_k) = 0 \quad k = 1,\cdots,N \tag{7.6}$$

$$P_{N-1}^{(1-\gamma_1,1-\gamma_1)}(r_j) = 0 \quad j = 1,\cdots,N-1 \tag{7.7}$$

W_k are the corresponding weights which are given by

$$W_k = -\frac{2(N-\gamma_1+1)}{(N+1)!(N-2\gamma_1+1)}\frac{[\Gamma(N-\gamma_1+1)]^2}{\Gamma(N-2\gamma_1+1)}\frac{2^{-2\gamma_1}}{P_N'^{(-\gamma_1,-\gamma_1)}(t_k)\, P_{N+1}^{(-\gamma_1,-\gamma_1)}(t_k)} \tag{7.8}$$

where a prime denotes derivative. Equations (7.4) and (7.5) are N linear equations for determining the N unknowns $H_I(t_k)$ $(k = 1,\cdots,N)$.

A discussion of the convergence of the above method will be found in the work of Erdogan *et al.* (1973). In the numerical computation of the present mode I problem, as well as of the mode II and mode III problems (§ 7.4) $N = 40$ was used. The accuracy was judged by comparing the geometry factor for $\theta = 90^0$ with that given in the book of Tada *et al.* (1985). Since an exact solution exists only for mode III, the comparison will be given in Table 7.3 of the next Section. In the other two modes, there are no exact solutions available for comparison. However, the numerical solutions obtained here are quite close to the approximate solutions given in the above handbook.

In order to examine the influence of both the stiffness and the geometry of the constraining layers on the behaviour of the stresses, we show the properties of μ_I and $H_I(1)$, respectively. The variation of μ_I with the ply angle θ is shown in Figure 7.2. It is found that when θ varies

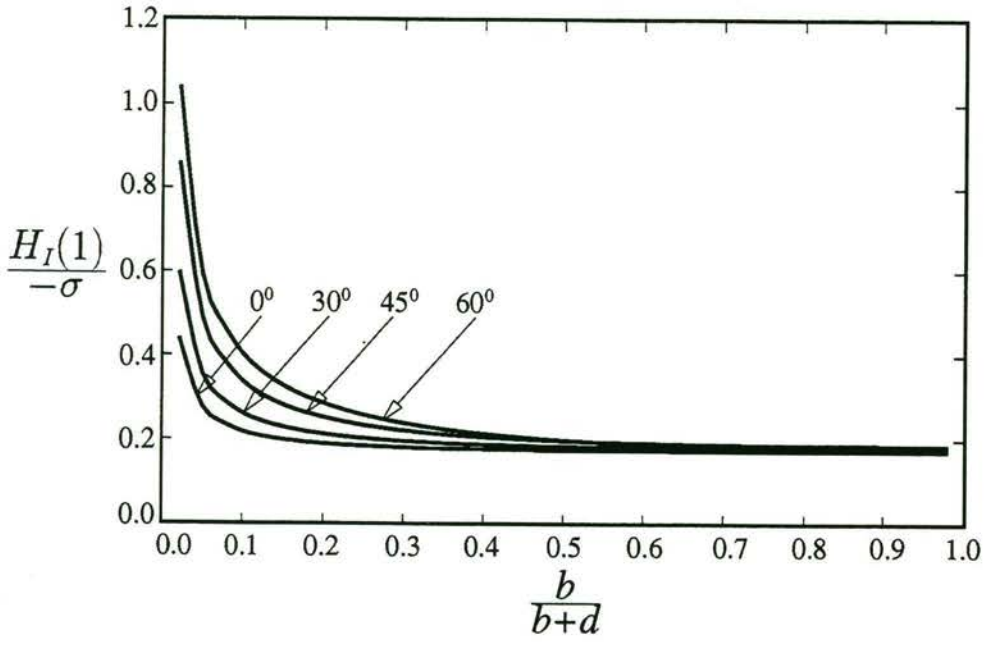

(a)

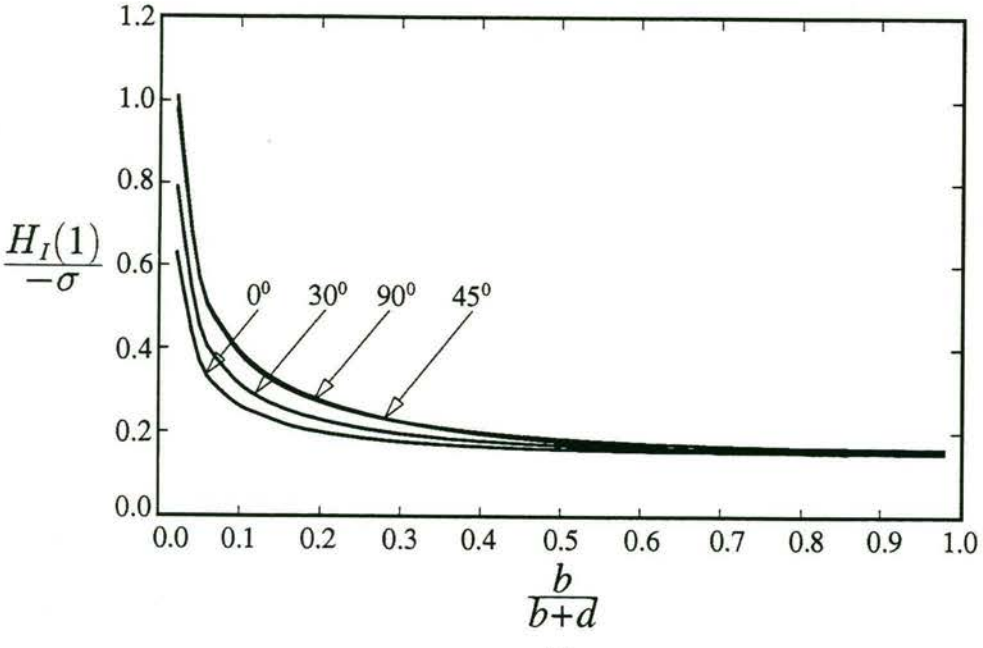

(b)

Figure 7.3: Variation of $H_I(1)/(-\sigma)$ for materials 1 (a) and 2 (b). The curves for $\theta = 45^0$ and 90^0 are indistinguishable on the scale of the figure for material 2

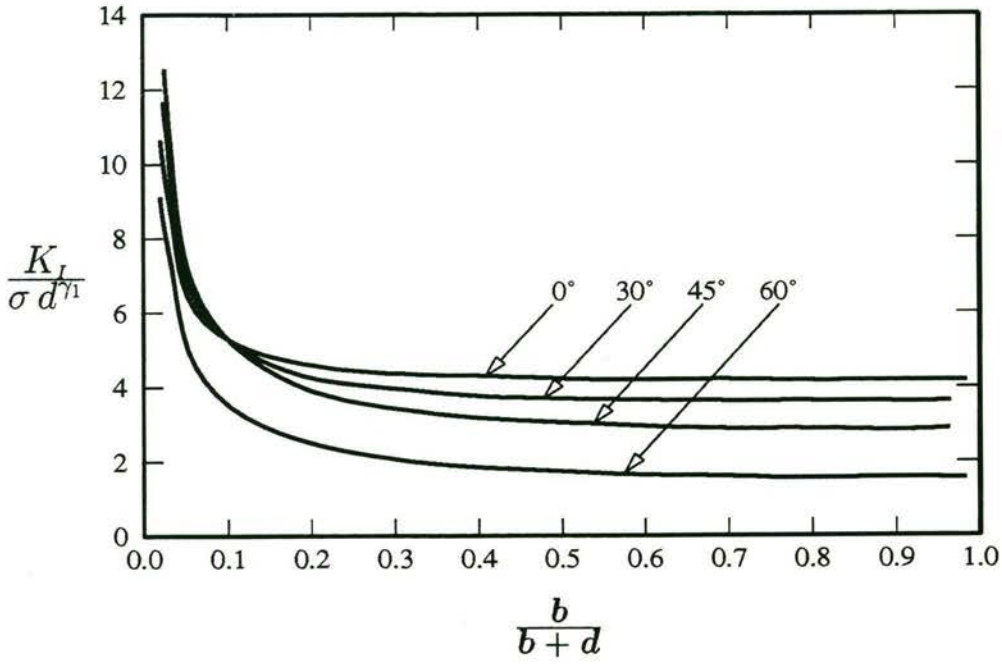

(a)

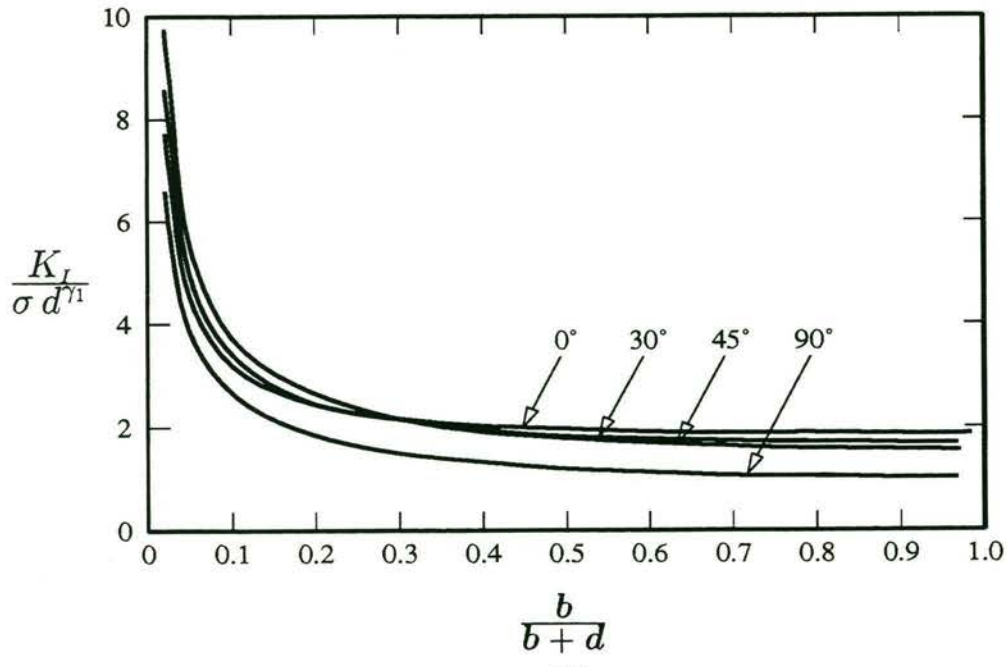

(b)

Figure 7.4: Normalized stress intensity factors for materials 1 (a) and 2 (b)

from 0^0 to 90^0, μ_I decreases greatly for graphite composites (materials 1, 3 and 4). It has a much larger value at $\theta = 0^0$ than at $\theta = 90^0$ (homogeneous isotropic material), as expected due to the high ratio of E_L/E_T.

$H_I(1)$ is a function of $b/(b+d)$ and θ, and is proportional to the applied stress $-\sigma$. We show the variations of $H_I(1)/(-\sigma)$ in Figures 7.3(a) and (b) for materials 1 and 2, respectively. This parameter shows two features. First, it decreases monotonically with the thickness of the constraining layers for all ply angles θ. Secondly, it is very sensitive to the change in $b/(b+d)$ when $b/(b+d)$ is small.

The normalized stress intensity factors $K_I/(\sigma d^{\gamma_1})$ for materials 1 and 2 are depicted in Figures 7.4(a) and (b), respectively, as a function of the ply angle and the relative thickness of the constraining layers. Corresponding figures for graphite/epoxy compositions of materials 3 and 4 have been omitted because of their similarity to the graphite/epoxy composition of material 1 shown in Figure 7.4(a). Due to the influence of $H_I(1)/(-\sigma)$, the normalized stress intensity factors have similar variation with $b/(b+d)$ to that of $H_I(1)/(-\sigma)$ in Figures 7.3(a) and (b). Therefore, when the constraining layers are thin, the stress intensity is equally influenced by both the geometry and the ply angle, but when they are thick, it is mostly influenced only by the ply angle via μ_I. This ought to be borne in mind in designing composite laminates which are least sensitive to interfacial delamination.

7.4 Mode II and Mode III Problems

The mode II and mode III stress singularities γ_2 and γ_3 are calculated from eqns (5.173) and (5.190), respectively. Their variation with the ply angle θ of the outer sublaminates is depicted in Figure 7.5, for the four materials of Table 7.1.

It is seen that the stress singularity in a particular loading mode for all four materials shows a similar trend with the ply angle θ of the constraining sublaminates. The singularities in both modes can be larger or smaller than the inverse square-root singularity in a homogeneous isotropic medium depending on the elastic properties of materials and on the ply angle θ.

To calculate the stress intensity factors K_{II} (5.191) and K_{III} (5.192), it only remains to determine $H_{II}(1)$ and $H_{III}(1)$, since μ_{II} and μ_{III} are already known from (5.193) and (5.194). The latter are related to the elastic properties of the two media and the respective crack tip singularity. $H_{II}(1)$ and $H_{III}(1)$, on the other hand are related to the elastic properties and geometry of the laminate and it is necessary to solve Cauchy-type singular integral equations to determine them. The singular integral equation for determining $H_{II}(1)$ is obtained after substituting $R_{II}(t)$ from (5.172) into (5.162). $H_{III}(1)$ is solved from the singular integral equation (5.181) which is much simpler than those for modes I and II.

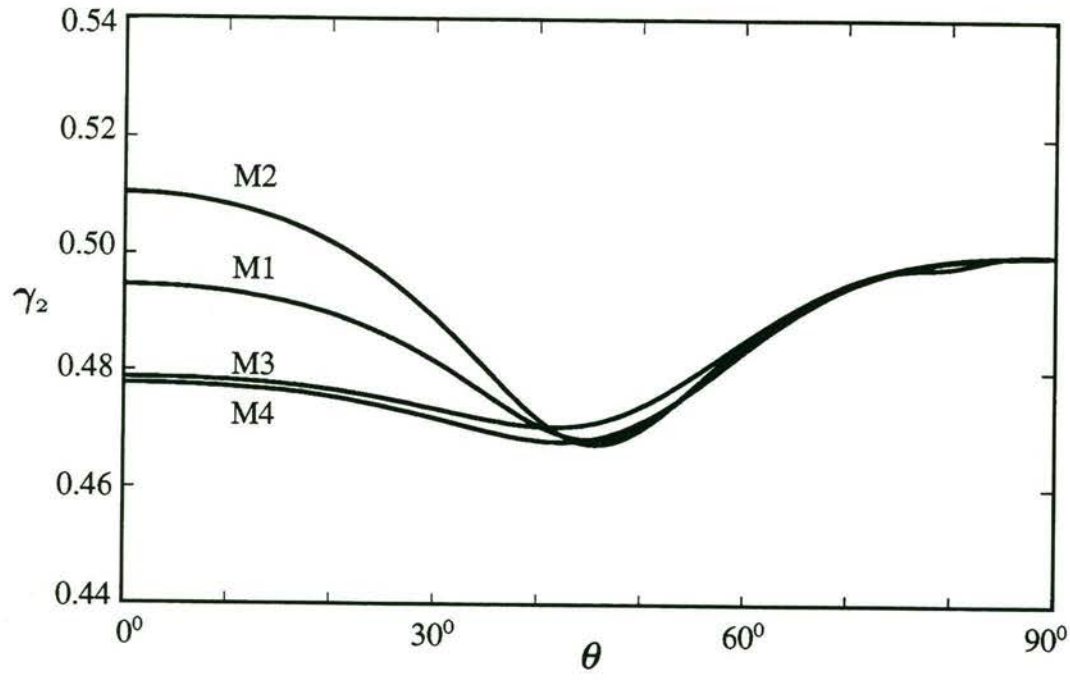

(a)

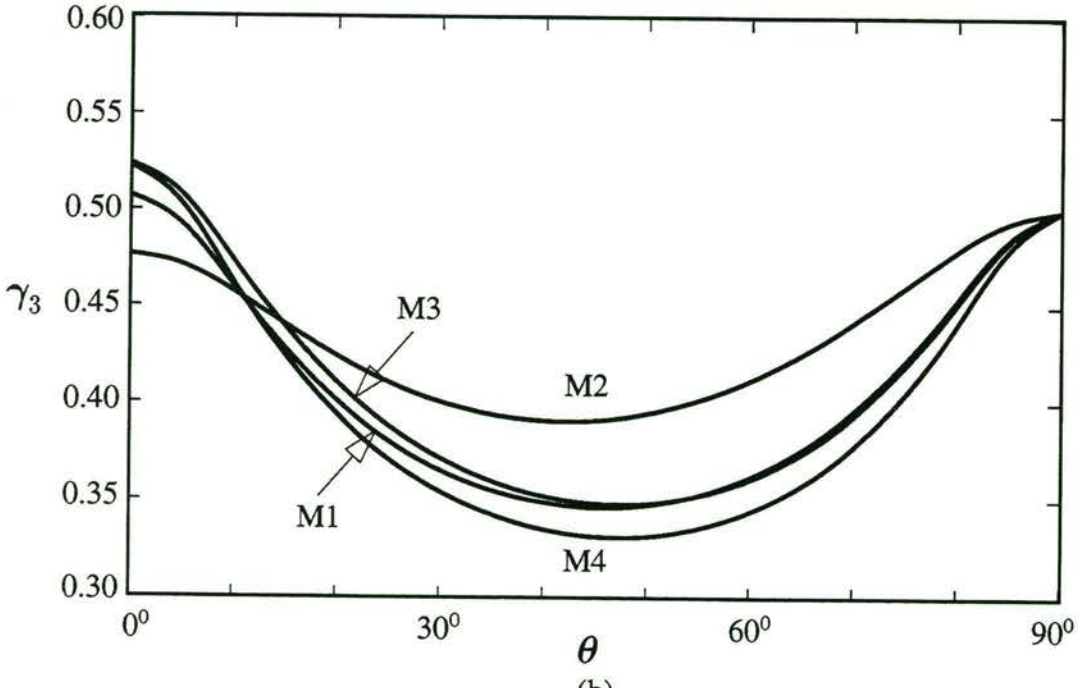

(b)

Figure 7.5: Stress singularities in (a) mode II and (b) mode III

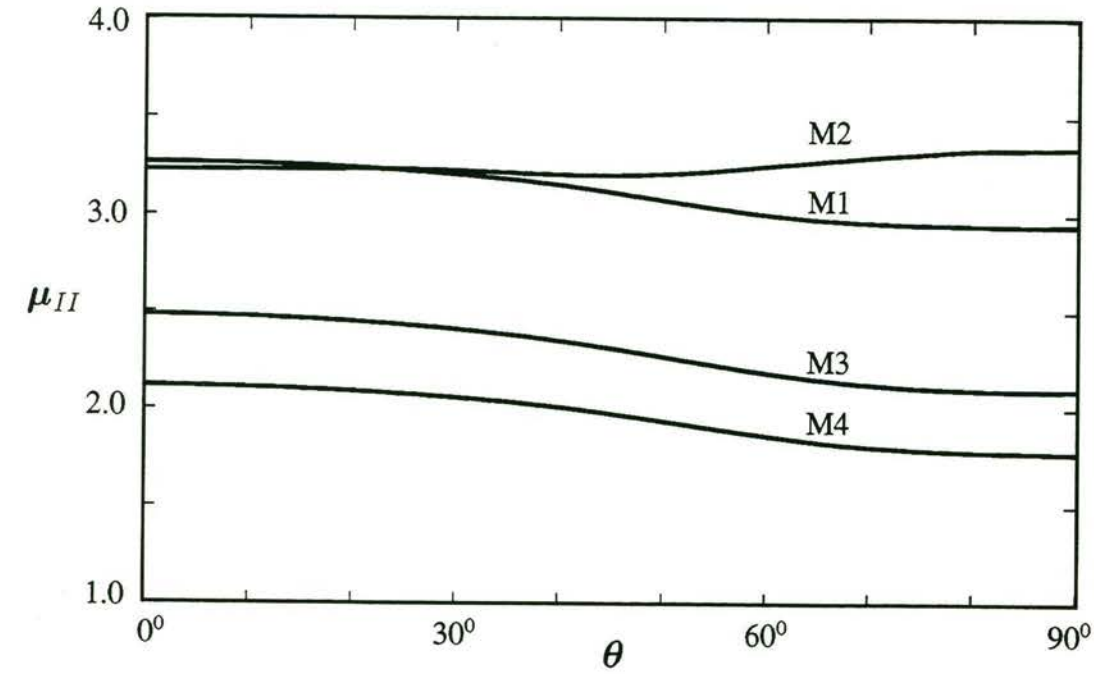

(a)

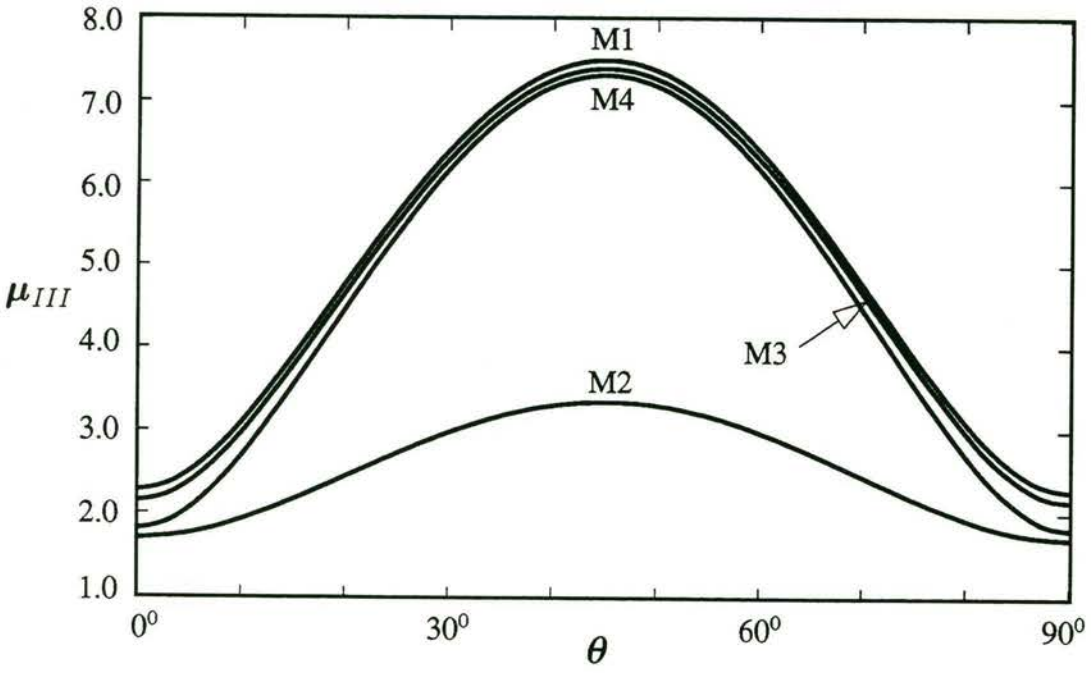

(b)

Figure 7.6: Variation of (a) μ_{II} and (b) μ_{III} with θ for the materials in Table 7.1

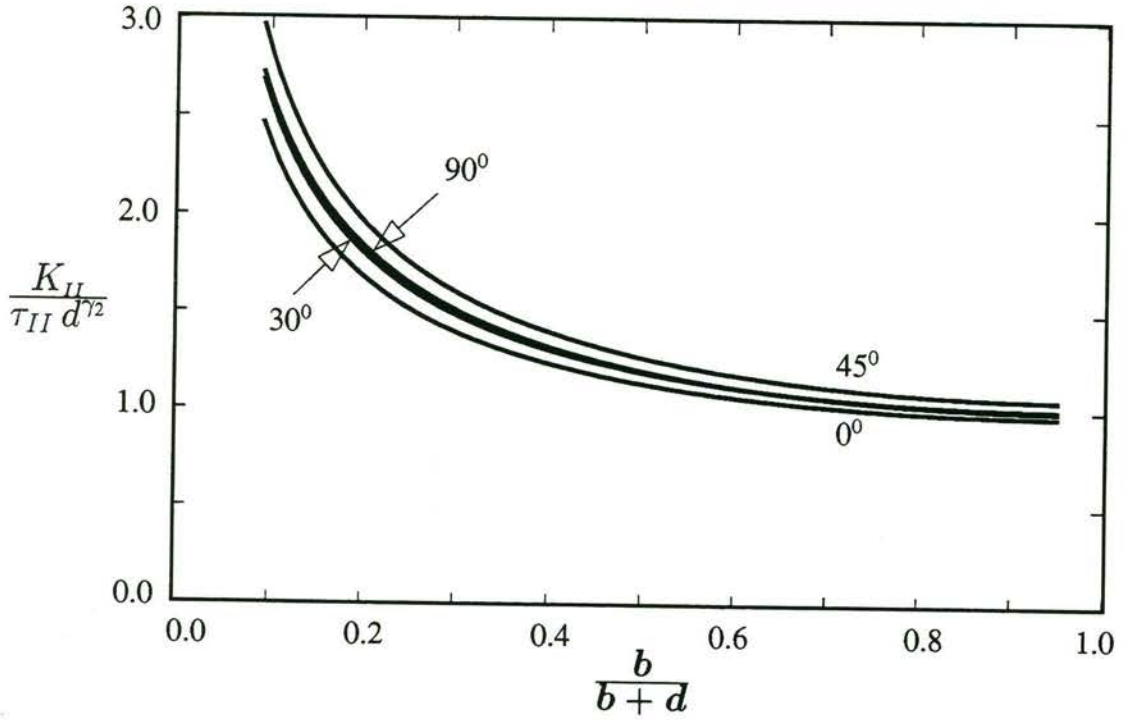

(a)

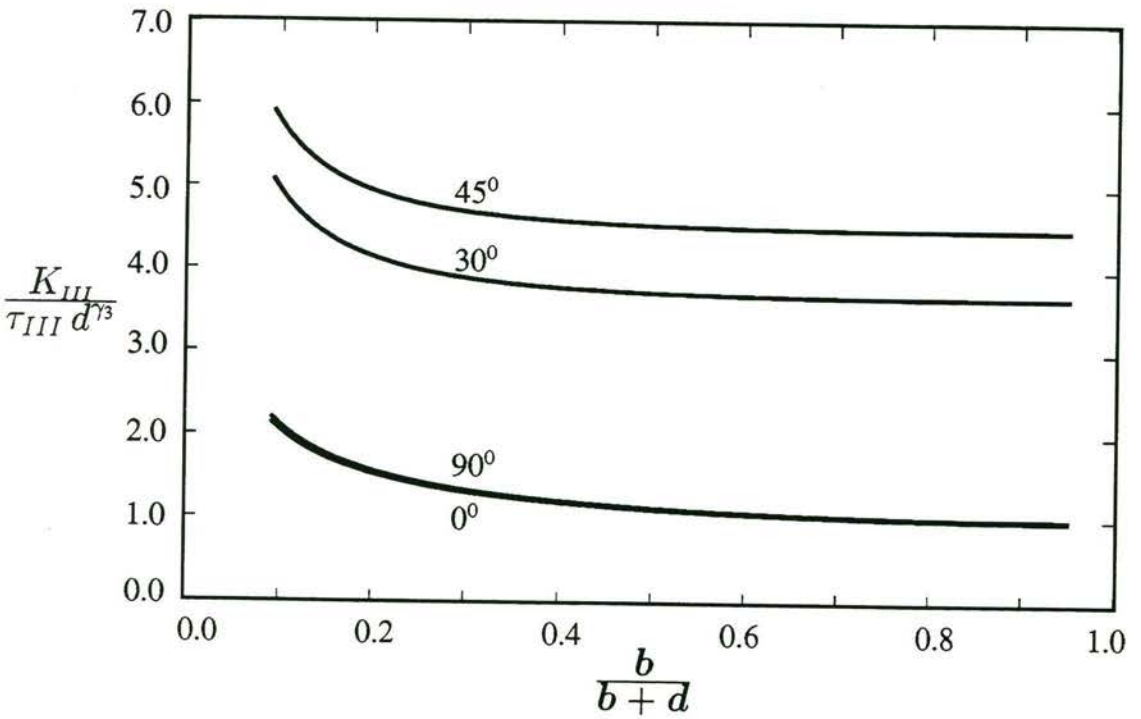

(b)

Figure 7.7: (a) Mode II and (b) mode III normalized stress intensity factor for material 1

Table 7.3: Accuracy of mode III geometry factor ($\theta = 90^0$)

$\frac{d}{b+d}$	0.20	0.30	0.40	0.50	0.60	0.70	0.80	0.90
Exact Solution	1.0170	1.0398	1.0753	1.1284	1.2085	1.3360	1.5650	2.1133
Numerical Solution	1.0171	1.0399	1.0754	1.1285	1.2086	1.3361	1.5651	2.1132

The variation of μ_{II} and μ_{III} with θ is shown in Figure 7.6. It is seen that whereas μ_{II} decreases with θ (except for glass/epoxy combination (material 2), when it is almost independent of θ), μ_{III} peaks at $\theta = 45^0$, contrary to the mode III stress singularity that has a minimum around this value of θ. This is a result of the fact that the shear stiffness c_{44} (G_{yz}) is the largest when $\theta = 45^0$.

Figure 7.7(a) shows the normalized stress intensity factor $K_{II}/(\tau_{II}d^{\gamma_2})$ for different values of θ as a function of the ratio of outer layer thickness to the laminate thickness. It decreases monotonically with increasing $b/(b+d)$. When b/d tends to infinity, it reaches a steady state value. When $\theta = 90^0$, it simply represents the geometry factor in the stress intensity factor at the tip of a central crack in a finite isotropic plate. The mode III counterpart $K_{III}/(\tau_{III}d^{\gamma_3})$ is depicted in Figure 7.7(b). Because of the indicated behaviour of μ_{III}, the normalized mode III stress intensity factor is maximum when $\theta = 45^0$.

The numerical algorithm was found to be quite accurate by comparing the computed results, i.e. the normalized stress intensity factor $K_{III}/(\tau_{III}\sqrt{d})$ for $\theta = 90^0$ with the exact solution of the geometry factor[1] for the mode III stress intensity factor for a centre cracked isotropic plate (Table 7.3). For mode II loading no exact solutions are available, but for isotropic materials, the computed results were found to be in very good agreement with those given in the handbook by Tada *et al.* (1985).

7.5 Extrema of Stress Singularities

The values of the strongest and weakest singularities are given in Table 7.4, as are the corresponding θ. The weakest and strongest stress singularities in mode I occur when $\theta = 0^0$ and

[1]When $\theta = 90^0$, the composite laminate degenerates into an isotropic strip with a central crack. The stress singularity is of the usual square-root type and the stress intensity factor at the crack tip is $K_{III} = F_{III}\tau_{III}\sqrt{d}$, where F_{III} is the geometry factor which is determined by the size of the crack relative to the width of the strip and is not related to elastic properties of the medium.

$\theta = 90^0$, respectively, for all the composites in Table 7.1. The strongest singularity in mode II occurs when $\theta = 90^0$ for all the graphite/epoxy compositions (materials 1,3 and 4). For all four materials, the singularities in modes II and III attain a minimum at almost the same value of θ^0 – around 45^0. For the glass/epoxy composition (materials 2) the mode III singularity has the largest value when $\theta = 90^0$, which may be attributed to the fact that its longitudinal shear modulus G_{LT} is smaller than transverse shear modulus G_{TT} (Table 7.1). An examination of the stress singularities and the stress intensity factors in three modes shows that they depict opposite variation with θ, that is, when the former attain the minimum, the latter reach the maximum.

Table 7.4: Strongest and weakest stress singularities

Material / Mode		M1	M2	M3	M4
Mode I	γ_{1max}	0.500	0.500	0.500	0.500
	θ_{max}	90^0	90^0	90^0	90^0
	γ_{1min}	0.355	0.436	0.321	0.312
	θ_{min}	0^0	0^0	0^0	0^0
Mode II	γ_{2max}	0.500	0.510	0.500	0.500
	θ_{max}	90^0	0^0	90^0	90^0
	γ_{2min}	0.468	0.468	0.470	0.468
	θ_{min}	45^0	45^0	41^0	42^0
Mode III	γ_{3max}	0.507	0.500	0.524	0.523
	θ_{max}	0^0	90^0	0^0	0^0
	γ_{3min}	0.346	0.390	0.348	0.331
	θ_{min}	46^0	42^0	47^0	47^0

Chapter 8

Design of Cracked Composite Laminates Least Prone to Delamination

8.1 Introductory Remarks

8.1.1 Transverse (Matrix) Cracks and Interfacial Delamination

Unidirectional fibre-reinforced laminae are typical orthotropic materials as far as their mechanical properties in the plane of the fibres are considered. The fibre-reinforced composite materials are commonly used in the form of laminates composed of laminae with different fibre directions. The most common and fatal form of failure in these laminates resulting in loss of both their strength and stiffness is delamination between constituent laminae. Under compression, the delaminated sublaminates may buckle leading to overall failure of the laminate; under transverse bending the extensive delamination caused by matrix cracking results in a significant drop in the applied load (Liu *et al.*, 1993). The mechanism of delamination has been widely investigated both theoretically and experimentally (Wang, 1980; Crossman & Wang, 1982; Chatterjee *et al.*, 1984; Reddy *et al.*, 1984; O'Brien, 1985; Murri & Guynn, 1988; Kim, 1989; Fish & Lee, 1990; Liu *et al.*, 1993; Doxsee *et al.*, 1993; Liu & Chang, 1994). The delamination often occurs at the free-edges of laminates and at the interface in front of transverse lamina cracks. The severity of the free-edge induced delamination can be reduced by varying the stacking sequence and ply thickness. In $[0^0/\pm\theta^0]_s$ laminates the free-edge induced stress singularity can be minimized or even deleted (Christensen & DeTeresa, 1992). Because of the inherent weakness of fibre-reinforced composites in the transverse direction, the pre-service microcracks are likely to occur in component laminae, possibly from the residual stress of processing and the debonding between the fibres and matrix. Upon being loaded, the transverse cracks may also form at very low load levels or after only a few load cycles under fatigue loading. It is the propagation of

these initial cracks that results in delamination when they approach the interfaces. Experimental observations show (Kim, 1989) that under tensile loading delamination in laminates, especially those containing 90^0 plies, is preceded by transverse cracks, and that its location is related to the location of cracks. Furthermore, the load at which delamination occurs is influenced by the crack size.

Similarly, under transverse (perpendicular to laminate plane) loading conditions, both experimental and theoretical calculations show that the matrix cracks in the 90^0 sublaminate in a $[0^0_{n_2}/90^0_{n_1}]_s$ laminate could directly result in delamination (Liu, *et al.*, 1993; Doxsee, *et al.*, 1993; Liu & Chang, 1994). Figure 8.1 clearly shows the relation between the matrix cracks in the 90^0 sublaminate and the interfacial delamination when the laminate is subjected to a transverse load. Calculations done by Liu *et al.* (1993) show that matrix cracks immediately produce an interfacial delamination which propagates instantly to the boundaries. In a load-displacement diagram, a sharp drop in the load is observed due to the extensive delamination resulting from the matrix cracks. The cracks in Figure 8.1 are called "shear matrix cracks" in the papers of Liu *et al.* (1993), and Liu & Chang (1994). The cracked areas are mainly subjected to shear deformation. Therefore, it was concluded by these authors that the delamination growth induced by intraply shear cracks is very unstable and catastrophic. Interfacial delamination induced by a transverse crack was also observed in the experiment by Doxsee *et al.* (1993) who subjected a cross-ply laminate to transverse loads.

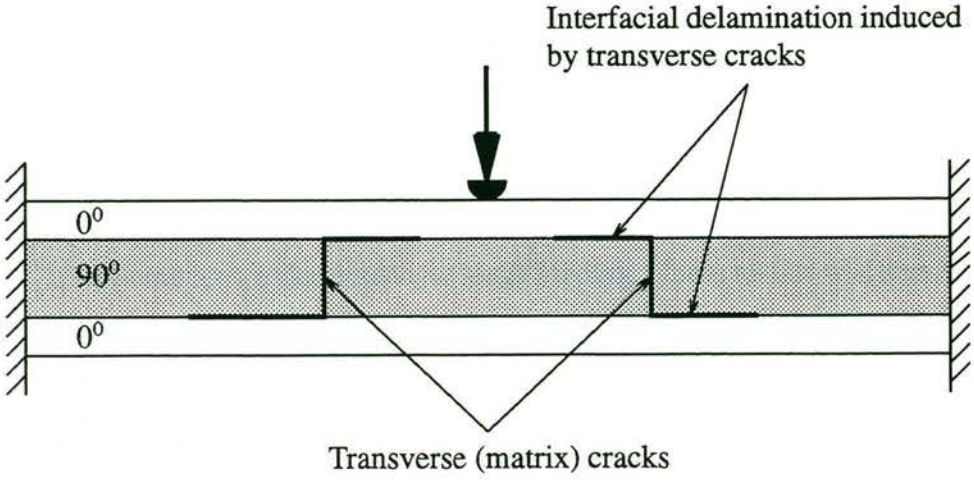

Figure 8.1: A cross-ply composite laminate under transverse loading. The dark "Z"-shaped lines show the transverse cracks and areas of interfacial delamination (After Liu *et al.*, 1993)

From the above mentioned experimental results, it is clear that transverse cracks are directly responsible for interfacial delamination when their tips approach the interfaces. The mechanisms

behind this phenomenon will be investigated in this Chapter by investigating the perturbation in the stress field induced by the existence of a transverse crack. It transpires that a transverse crack can induce high interfacial stresses when it is close to the interface. Theoretically, when the crack tip touches the interface the stress field is singular, but the singularity is different from that the usual square root type when the crack is wholly within one lamina. The problem when the crack tip terminates at the bimaterial interface was studied in Chapters 5 and 7.

8.1.2 Constraining Effect in Composite Laminates

It is known (Parvizi *et al.*, 1978; Bailey *et al.*, 1979; Flaggs & Kural 1982; Fan *et al.*, 1989) that crack propagation in the 90^0 sublaminate in angle-ply laminates under in-plane tension is constrained by the adjacent sublaminates. We have revealed in Chapter 6 the mechanisms of this constraining effect using fracture mechanics. This constraining effect results in the observed higher *in situ* strength of laminae in laminates. Because it is relatively easy to apply unidirectional in-plane tension in a laboratory, the constraining effect in laminates under this load condition has been widely studied both experimentally and theoretically. In this Chapter, we will show that this constraining effect also exists when a laminate is subjected to a transverse shear load. This effect influences the crack-driving force at the tip of a transverse crack in a unidirectional lamina in an angle-ply laminate.

Since the constraining effect on the crack propagation and the influence of the transverse crack on the interfacial stress field vary with the configuration of laminates, it may be possible that the risk of interfacial delamination and crack propagation can be reduced to a certain extent by varying the configuration of laminates.

It is the aim of this Chapter to explore this possibility. To this end, we will calculate the stress intensity factor for a transverse crack in the $(90^0)_{n_1}$ layer of a $[(\pm\theta^0)_{n_2}/(90^0)_{n_1}/(\mp\theta^0)_{n_2}]$ antisymmetric laminate and also the *crack-induced* interfacial stresses between the $(90^0)_{n_1}$ and $(\pm\theta^0)_{n_2}$ sublaminates under transverse shear loading. These results will then be used to optimize the configuration, that is, to choose the ply angle θ, the relative thickness of the constraining sublaminates and the commonly reported fibre-reinforced material properties, so as to minimize the tendency of crack growth in the $(90^0)_{n_1}$ sublaminate and therefore of delamination between this and $(\pm\theta^0)_{n_2}$ sublaminates under shear loading. The optimization problem is posed as a nonlinear programming problem whose solution is sought by several techniques. The design sensitivities required in these techniques are calculated by mixed analytical/numerical means. The results confirm the possibility of minimizing the crack driving force in the $(90^0)_{n_1}$ layer and of avoiding the risk of delamination by a judicious choice of ply angle θ and relative sublaminate thickness. The major part of the work described in this Chapter has been published in two papers by Wang & Karihaloo (1994a), and Wang *et al.* (1994).

8.2 Mathematical Model and Solution

8.2.1 An Idealized Model of Cracked Angle-Ply Laminate

The model being studied in this Chapter is shown in Figure 8.2. It consists of a central layer in which the fibres are oriented normal to the plane of the paper ($(90^0)_{n_1}$ layer) and two outer sublaminates which are composed of an equal number of $+\theta^0$ and $-\theta^0$ angle plies. They can also be regarded as a kind of woven structure with fibres intersecting at an angle of $2\theta^0$ (Figure 8.2(a)). The $(90^0)_{n_1}$ layer of thickness $2d$ is transversely isotropic (in xy-plane) and is assumed to contain a flaw in the form of a central transverse crack of length $2a$ well removed from the edges of the laminate. In the analysis, each outer sublaminate of thickness b is treated as being homogeneous orthotropic with average elastic properties of $[(\pm\theta^0)_{n_2}/(\mp\theta^0)_{n_2}]$ laminate, consistent with the classical lamination theory.

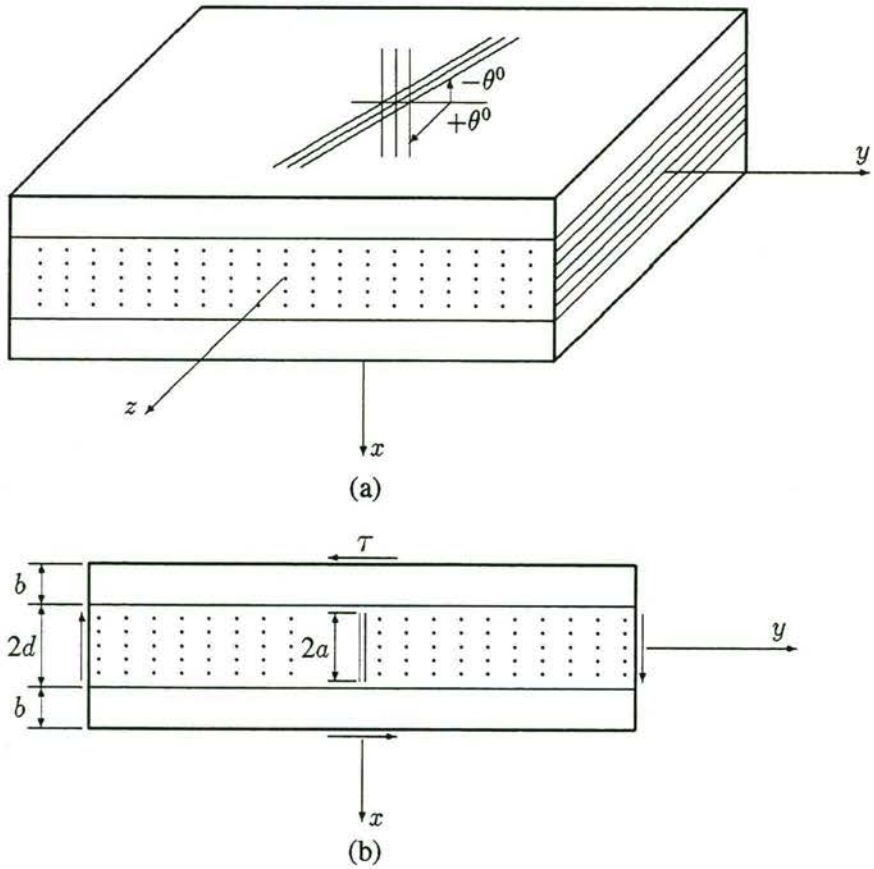

Figure 8.2: The composite laminate and coordinate axes. The central crack is well removed from the edges of the laminate

It is assumed that the composite laminate is subjected remotely to self-equilibrating shear

stress $\tau_{xy} = \tau$, so that from a mathematical point of view one needs only to solve the problem of cancellation of this stress over the crack faces. Using the basic solution for mode II problem given in § 4.4, the mode II stress intensity factor is

$$K_{II} = \lim_{x \to a^+} \sqrt{2(x-a)}\, \tau^1_{xy}(x,0) = \Psi(1)\, \tau \sqrt{a} \equiv F_{II}\, \tau \sqrt{a} \tag{8.1}$$

where $\Psi(1)$ is calculated from the solution of the integral equation (4.124).

If the $(\pm\theta^0)_{n_2}$ sublaminates on the two sides are absent then the stress intensity factor is

$$K_{II} = F(\tfrac{a}{d})\, \tau \sqrt{a}\,, \tag{8.2}$$

where the geometry factor $F(a/d)$ may be found in any standard handbook of stress intensity factors (e.g. Tada *et al.*, 1985).

For the graphite/epoxy material properties listed in Table 6.1, the variation of $\Psi(1)$ with a/d is shown in Figure 8.2. Also shown is the value of $F(a/d)$. $\Psi(1)$ is equal to $F[a/(b+d)]$ when $\theta = 90^0$.

It is seen that the magnitude of $\Psi(1)$ and its variation with a/d are different from those of $F(a/d)$ – the geometry factor for an isotropic material. $\Psi(1)$ is not only related to the geometry a/d and b/d, but is also influenced by the stiffness of the $(90^0)_{n_1}$ and $(\pm\theta^0)_{n_2}$ layers. Obviously, $\Psi(1) \leq F(a/d)$, otherwise there would be no point in using composite materials. It is also for this reason that the $(\pm\theta^0)_{n_2}$ sublaminates are regarded as constraints for central layer. It is noted that the degree of this constraint can be expressed solely in terms of $\Psi(1)$.

In the following, we shall calculate the *crack-induced* interfacial stresses. Before that let us discuss briefly the evaluation of interfacial stresses in composite laminates in view of the average elastic properties used in the classical lamination theory to determine the stress and strain fields in the laminates. We already discussed some aspects of these limitations of CLT in § 6.4.

In the present investigation, the outer sublaminates $[(\pm\theta^0)_{n_2}]$ are replaced by an effective orthotropic medium whose elastic stiffnesses are calculated following the CLT. In § 6.4 it was pointed out that under tension there are interfacial stresses caused by the mismatch of the elastic properties of the laminae in an angle-ply laminate. These stresses which are not predicted by the CLT, however, only exist in the boundary regions (edges) of the laminate and vanish in the area of the laminate away from the boundaries. On the other hand, as noted by Kassapoglou (1990), very little research has been done on the stress analysis of laminates, especially of angle-ply laminates, subjected to out-of-plane loads. However, the limited results for various symmetric angle-ply laminates that are available do show certain tendencies. Thus, for instance, Tang (1976) calculated analytically the stresses at the interface of $+\theta^0/-\theta^0$ plies in a four layer $[\pm\theta^0]_s$ angle-ply laminate under a uniform transverse load. The interior domain was assumed

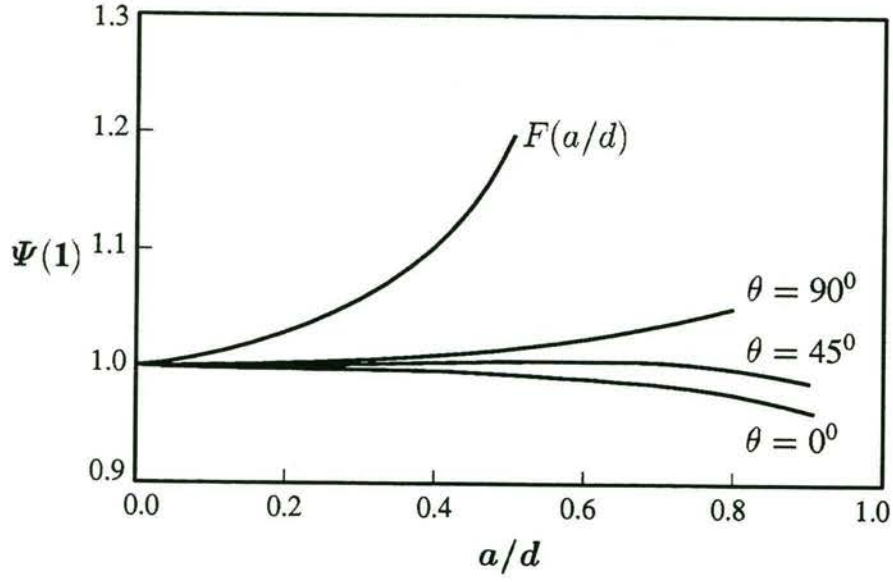

Figure 8.3: Values of $\Psi(1)$ and $F(a/d)$. Value of θ is indicated on the graph. $b/d = 2$

to be governed by CLT (as was also done by Kassapoglou, 1990), so that the interfacial shear stresses (τ_{xz} and τ_{yz}, which might otherwise exist at a micromechanical level) did not arise in this domain. Salamon (1978) solved the exact elasticity equations, using finite-difference approximations. The stresses at the interface between $+45^0$ and -45^0 plies in a four layer $[\pm 45^0]_s$ angle-ply laminate and at the interface between θ^0 and 0^0 plies in a four layer $[\theta^0/0^0]_s$ laminate were calculated in flexure. The interfacial shear stress (τ_{xz}) indeed tended to vanish in the area away from the boundary region, as would be expected if even a single lamina were assumed to behave orthotropically when it is situated in the symmetric laminate. It is recognized that whereas τ_{xz} and τ_{yz} are absent in an orthotropic medium under loads along its principal axes, the vanishing of τ_{xz} and τ_{yz} does not necessarily imply that the medium is orthotropic. However since these shear stresses vanish for different ply combinations, the assumption of orthotropy seems to be reasonable. It is worth noting that the maximum width/thickness ratio considered by Salamon (1978) was only 3.

The 3-D finite element calculations (Murthy & Chamis, 1987) for four layer symmetric $[+\theta^0/-\theta^0]_s$ angle-ply laminates under out-of-plane shear and bending also showed that the interfacial shear stresses τ_{xy} and τ_{zy} of the laminae were negligibly small away from the edges and practically disappeared in the central region of the laminate. Although an isotropic interply was added in this analysis, the results are still indicative.

It is noted that there is a coupling of bending and twisting in all symmetric $[\pm\theta^0]_s$ angle-ply laminates. They are macroscopically orthotropic only when bearing in-plane loads along their

principal axes, but not when bearing out-of-plane flexural loads ($D_{16} \neq 0$; $D_{26} \neq 0$, Tsai & Hahn, 1980). The local anisotropy of the laminae (or sublaminates) in the macroscopically orthotropic laminates referred to above does not seem to generate significant interfacial shear stresses. Salamon (1978) noted "....*While the magnitudes of these stresses are generally small, the distinguishing feature is the sharp rise near the free edge which affects a boundary region of the order of one laminate thickness (2t) inward.*" It is noted that the antisymmetric laminate in this exposition behaves macroscopically like an orthotropic medium under in-plane (laminate plane) and flexural loadings, respectively (cf. § 3.7.2).

From the above statements and the fact that under the present loading condition the dominant interfacial stress will be τ_{xy}, the replacement of the $[(\pm\theta^0)_{n_2}]$ layer by an effective orthotropic medium should not invalidate the interfacial stress calculations except in the boundary regions. The calculation of the stiffness parameters of the $[(\pm\theta^0)_{n_2}]$ layer is given in Appendix C.

Following the procedure for deriving the interfacial stresses (6.6)–(6.7) for the multicracked laminate under tensile load described in § 6.4, the non-dimensional normal and the shear stresses at the interface between the $(90^0)_{n_1}$ and $(\pm\theta^0)_{n_2}$ layers are written as

$$\begin{aligned}
\frac{\sigma_{xx}(d,y)}{\tau} &= \int_0^\infty \frac{s e^{-s\frac{d}{a}}}{\Delta(\frac{s}{a})}\Big\{[K_{11}G_1 + K_{12}G_2 + K_{13}G_3 + K_{14}G_4]s\frac{d}{a}\cosh(s\frac{d}{a}) + \\
&\quad + [K_{21}G_1 + K_{22}G_2 + K_{23}G_3 + K_{24}G_4]\sinh(s\frac{d}{a})\Big\}\sin(s\frac{y}{a})\,ds - \\
&\quad - \int_0^\infty e^{-s\frac{y}{a}} K_5\, G_5\, ds \qquad (8.3) \\
\frac{\sigma_{yy}(d,y)}{\tau} &= \int_0^\infty (-1)\frac{s e^{-s\frac{d}{a}}}{\Delta(\frac{s}{a})}\Big\{[K_{11}G_1 + K_{12}G_2 + K_{13}G_3 + \\
&\quad + K_{14}G_4][2\sinh(s\frac{d}{a}) + s\frac{d}{a}\cosh(s\frac{d}{a})] + \\
&\quad + [K_{21}G_1 + K_{22}G_2 + K_{23}G_3 + K_{24}G_4]\sinh(s\frac{d}{a})\Big\}\sin(s\frac{y}{a})\,ds - \\
&\quad - \int_0^\infty e^{-s\frac{y}{a}} K_6\, G_6\, ds \qquad (8.4) \\
\frac{\tau_{xy}(d,y)}{\tau} &= \int_0^\infty \frac{s e^{-s\frac{d}{a}}}{\Delta(\frac{s}{a})}\Big\{[K_{11}G_1 + K_{12}G_2 + K_{13}G_3 + \\
&\quad + K_{14}G_4][\cosh(s\frac{d}{a}) + s\frac{d}{a}\sinh(s\frac{d}{a})] + \\
&\quad + [K_{21}G_2 + K_{22}G_2 + K_{23}G_3 + K_{24}G_4]\cosh(s\frac{d}{a})\Big\}\cos(s\frac{y}{a})\,ds - \\
&\quad - \int_0^\infty e^{-s\frac{y}{a}} K_7\, G_7\, ds \qquad (8.5)
\end{aligned}$$

At the interfacial point right in front of the crack tip, where $y = 0, x = d$, the only non-vanishing

stress is

$$\frac{\tau_{xy}(d,0)}{\tau} = \int_0^\infty \frac{se^{-s\frac{d}{a}}}{\Delta(\frac{s}{a})}\Big\{[K_{11}G_1 + K_{12}G_2 + K_{13}G_3 + \\ +K_{14}G_4][\cosh(s\frac{d}{a}) + s\frac{d}{a}\sinh(s\frac{d}{a})] + \\ +[K_{21}G_1 + K_{22}G_2 + K_{23}G_3 + K_{24}G_4]\cosh(s\frac{d}{a})\Big\}\,ds + \\ + \int_0^1 \Phi(\xi)\,G_8(\xi)\,d\xi \tag{8.6}$$

In eqns (8.3)–(8.6)

$$G_i = \int_0^1 \sqrt{\eta}\,\Phi(\eta)\,E_i(s,\eta)\,d\eta \quad (i = 1,..,4)$$

$$G_5 = G_6 = G_7 = \int_0^1 \sqrt{\eta}\,\Phi(\eta)\,J_0(s\eta)\,d\eta$$

$$G_8 = (\frac{a}{d})^2 \frac{\sqrt{\xi}}{\sqrt{1-(\frac{a}{d}\xi)^2}\left[1+\sqrt{1-(\frac{a}{d}\xi)^2}\right]}\left\{2 + \frac{(\frac{a}{d}\xi)^2\left[1+2\sqrt{1-(\frac{a}{d}\xi)^2}\right]}{\left[1-(\frac{a}{d}\xi)^2\right]\left[1+\sqrt{1-(\frac{a}{d}\xi)^2}\right]}\right\}$$

$$K_5 = s(2 - s\frac{y}{a})\sin(s\frac{d}{a})$$

$$K_6 = s^2\frac{y}{a}\sin(s\frac{d}{a})$$

$$K_7 = s(1 - s\frac{y}{a})\cos(s\frac{d}{a})$$

The variation of *crack-induced* interfacial principal tensile stress (normalized by τ)

$$\sigma_t = \frac{\sigma_{xx}+\sigma_{yy}}{2\tau} + \sqrt{(\frac{\sigma_{xx}-\sigma_{yy}}{2\tau})^2 + (\frac{\tau+\tau_{xy}}{\tau})^2} \tag{8.7}$$

with y/d and a/d for $\theta = 0^0$ and $\theta = 45^0$ is shown in Figure 8.4. It is seen that the largest tensile stress σ_T (normalized by τ) occurs at $y/d = 0$ for different θ^0 and a/d. This largest stress is depicted in Figure 8.5, for $\theta = 0^0$, $\theta = 90^0$ and $\theta = 45^0$. As the crack tip approaches the interface (a/d increases), the largest interfacial tensile stress increases rapidly for all θ^0. For small cracks, this stress is fairly insensitive to changes in θ, but as a/d increases so also does its sensitivity to the ply angle θ. An examination of Figures 8.3 and 8.5 shows that for all a/d, the crack driving force takes on its minimum value, but the largest interfacial tensile stress (at $y/d = 0$) its maximum value when $\theta = 0^0$. There is thus a need for a compromise design which would ensure minimization of the crack driving force in the central layer without exceeding the interfacial strength of the laminate.

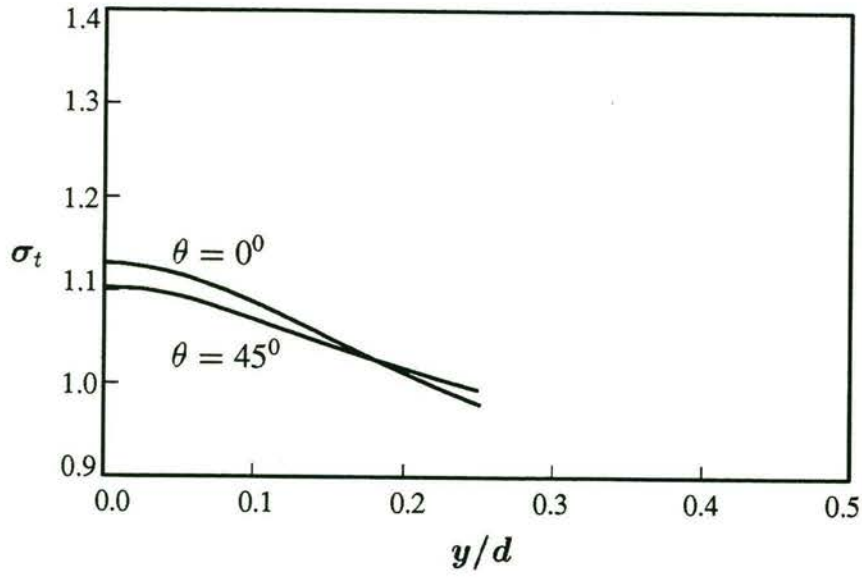

Figure 8.4: Crack-induced interfacial principal tensile stress normalized by τ for $a/d = 0.4$

8.3 Optimization Problem and Solution

To obtain the compromise design, we formulate the following minimization problem

$$\underset{c_{ij}^{\theta}, \frac{b}{d}, \theta}{\text{Min}} \quad \Psi(1)[c_{ij}^{\theta}, \frac{b}{d}, \theta; \frac{a}{d}] \tag{8.8}$$

subject to

$$\sigma_T \leq \sigma_0 = (1+\alpha) \tag{8.9}$$

$$\overline{D} \geq (1-\gamma)\, D_0 \tag{8.10}$$

$$\underline{b} \leq \frac{b}{d} \leq \overline{b} \tag{8.11}$$

$$0 \leq \theta \leq \frac{\pi}{2} \tag{8.12}$$

$\overline{D}$ is the normalized laminate modulus. For the transverse loading case, $\overline{D}$ is the normalized flexural modulus

$$\overline{D} = \frac{[(1+\frac{b}{d})^3 - 1]\, c_{22}^{\theta} + c_{22}^{90}}{(1+\frac{b}{d})^3} \tag{8.13}$$

σ_0 is the specified interfacial strength and D_0 is the value of $\overline{D}$ when $\theta = 0^0$. α and γ are tolerance factors on the stress gain and stiffness loss, respectively.

Since the expressions relating $\Psi(1)$ and the interfacial principal tensile stress to the geometry and stiffness properties of the layers are quite complicated, sensitivity of the objective with

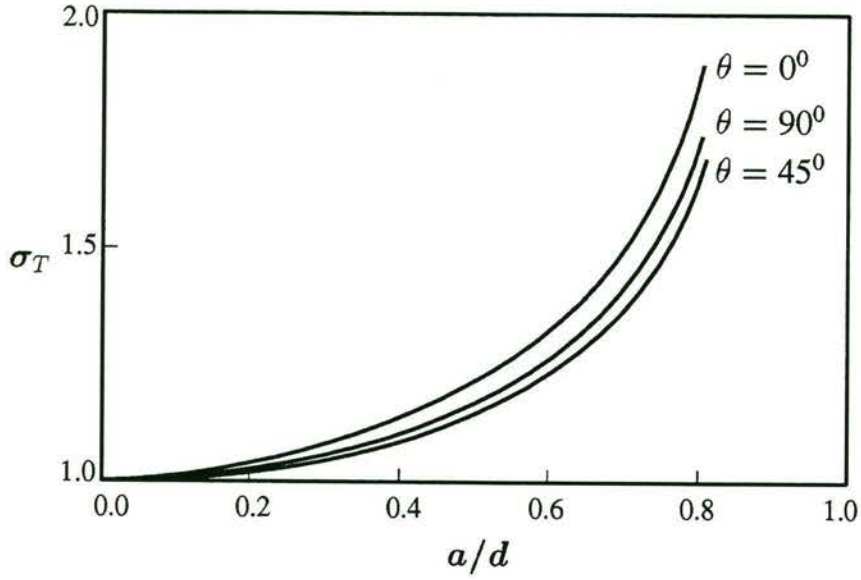

Figure 8.5: The largest interfacial principal tensile stress normalized by τ for $y/d = 0.0$ and $b/d = 2.0$

respect to design variables is calculated by a mixed analytical/numerical procedure. The integral equation (4.124) is discretized into a set of linear equations

$$[A][\Psi] = [B] \tag{8.14}$$

where $[A] = [a_{ij}]$, $[\Psi] = [\Psi(\xi_j)]^T$, $[B] = [\sqrt{\xi_i}]^T$, $(i, j = 1, ..., n)$. $n = 10$ resulted in sufficient accuracy. Then the sensitivity with respect to the design variables x_i is given by

$$\frac{\partial[\Psi]}{\partial x_i} = -[A]^{-1}\frac{\partial[A]}{\partial x_i}[\Psi] \tag{8.15}$$

where, x_i stand for c_{ij}^{θ} $(i, j = 1, 2)$, θ and b/d.

The sensitivities of the constraint (8.9) are calculated numerically, whereas that of (8.10) are calculated analytically (see Appendix C).

The above minimization problem was solved by nonlinear mathematical programming techniques (§ 3.8), viz. sequential linear programming (SLP) with move-limits (Pedersen, 1981), sequential quadratic programming, SQP (Powell, 1978) and sequential convex programming, SCP (Fleury & Braibant, 1986) which are available in the general purpose structural optimization package ADS (Vanderplaats, 1987). The number of functional and gradient evaluations for the above problem and an alternative formulation to be considered below, are given in Table 8.1. It was found that among the three strategies, SLP and SCP terminated with fewer functional evaluations but more gradient calculations than SQP. However, when the objective function was

somewhat flat near the optimum point, the SLP and SQP could sometimes terminate prematurely. It seems therefore for the present problem SQP produces the most precise results with fewer gradient calculations, but more functional evaluations.

Table 8.1: Functional (fe) and gradient (ge) evaluations

	Min $\Psi(1)$		Min $\overline{\sigma}$	
Method	fe	ge	fe	ge
SLP	7	7	10	10
SQP	12	3	26	6
SCP	7	7	8	8

The results of the optimization design problem for the laminate properties of Table 6.1 are shown in Figure 8.6.

It was found that for small a/d, the active constraints were the lower limit on θ and the upper limit on b/d. When $\theta = 0^0$, the outer sublaminates have the strongest effect on the arrest of central layer crack. The minimum of $\Psi(1)$ always occurred at $\theta = 0^0$, no matter what initial θ was chosen.

The relative thickness of the outer sublaminates also plays an important role in arresting the crack growth. The relatively thicker the constraint sublaminates, the smaller the crack driving force and hence the stronger the $(90^0)_{n_1}$ layer.

When a/d is large, the interfacial stress constraint becomes critical to the design. For the satisfaction of this constraint the design angle θ takes a non-zero value. It was found that for $\alpha = 0.5$, $\gamma = 0.15$ and $\overline{b} = 4.0$, when a/d is greater than $0.7\underline{3}$, no optimum design is possible because of the violation of the constraint on interfacial strength. For this reason an alternative formulation of optimization problem was considered in which the largest interfacial tensile stress was minimized subject to the constraint that $\Psi(1)$ not exceed 1.0 and that the flexural stiffness be adequate. The corresponding minimization problem is as follows:

$$\underset{c_{ij}^{\theta}, \frac{b}{d}, \theta}{\text{Min}} \quad \sigma_T \left(c_{ij}^{\theta}, \frac{b}{d}, \theta; \frac{a}{d}\right) \tag{8.16}$$

subject to

$$\Psi(1) < 1.0 \tag{8.17}$$

$$\overline{D} \geq (1-\gamma)\, D_0 \tag{8.18}$$

$$\underline{b} \leq \frac{b}{d} \leq \overline{b} \tag{8.19}$$

$$0 \leq \theta \leq \frac{\pi}{2} \tag{8.20}$$

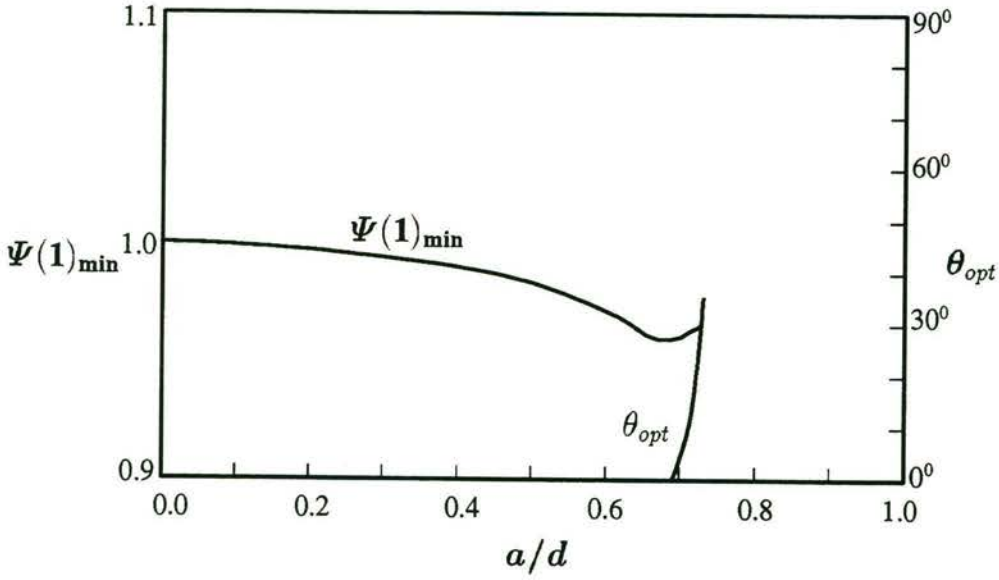

Figure 8.6: Minimization of $\Psi(1)$: $(b/d)_{opt} = \bar{b}$

The results of the above minimization problem are shown in Figure 8.7. In this case, σ_T reaches its minimum when $\theta = 50^0$ and $b/d = \bar{b}$. The reason that the laminate has sufficient flexural stiffness at such large θ is the high value of the transverse in-plane (with respect to laminate) Poisson's ratio of the $(\pm\theta^0)_{n_2}$ sublaminates and the use of plane strain stiffness parameters.

Besides the intralaminar crack problem under out-of-plane (with respect to laminate, but in-plane with respect to crack) shear loading, the analyses for in-plane (with respect to laminate) tensile and shear loadings are needed for a more comprehensive understanding of laminate strength and delamination characteristics. These problems will be considered in Chapter 9. The lamination effect on the stress field and particularly on its singular behaviour when the crack tip touches the interface was studied in the preceding Chapter.

8.4 Multicriterion Optimization

It is noted that the values of α and γ in the constraints (8.9), (8.10) and (8.18) will influence the solution of the single-criterion optimization problems, if they are active in the optimization process. When they are not properly chosen, it is likely that there is no feasible solution. It raises the difficult task of choice of these parameters and the possibility of multiple solutions. This difficulty can be overcome if we use a multicriterion optimization formalism – the so-called

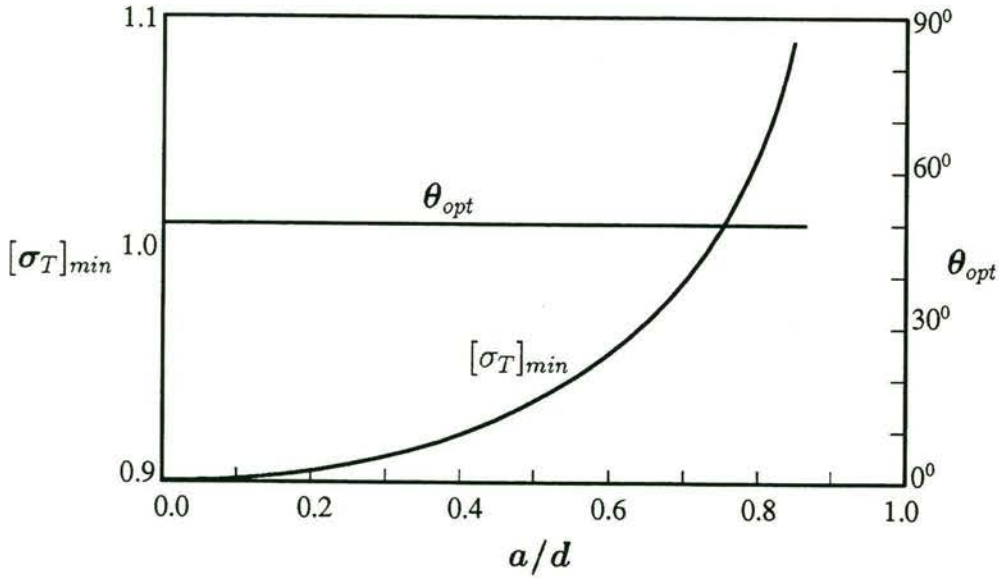

Figure 8.7: Minimization of σ_T: $(b/d)_{opt} = \overline{b}$

Pareto-type optimization. Let us denote

$$f_1(\mathbf{x}) = \sigma_T \tag{8.21}$$

$$f_2(\mathbf{x}) = F_{II} \tag{8.22}$$

$$f_3(\mathbf{x}) = \overline{D} \tag{8.23}$$

where $\mathbf{x}$ is the design vector. With these functions, the objective is to minimize f_1 and f_2 and at the same time, to maximize f_3 (or to minimize $-f_3$). Figure 8.8 shows the three objective functions $f_1(\mathbf{x})$, $f_2(\mathbf{x})$ and $f_3(\mathbf{x})$.

The microstructural parameters (the design variables) that can be altered are the fibre orientations $\pm\theta^o$ in the outer sublaminate, and the thicknesses of the sublaminates b and d, such that the design vector is $\mathbf{x} \equiv [\pm\theta^o \; b \; d]^T$. The crack length a is a parameter of the problem. As noted above (Figure 8.1), the analytical model chosen to establish the relations $f_1(\mathbf{x})$, $f_2(\mathbf{x})$ and $f_3(\mathbf{x})$ requires that $a < d$. By varying $\pm\theta^o$ and the thickness ratio b/d it is desired to minimize the crack driving force $f_2(\mathbf{x})$ and the maximum interfacial principal tensile stress $f_1(\mathbf{x})$ and to maximize simultaneously the flexural stiffness $f_3(\mathbf{x})$ (*i.e.* to minimize -$f_3(\mathbf{x})$), subject to $-90^0 \leq \theta \leq +90^0$, and $(b/d)_{min} \leq b/d \leq (b/d)_{max}$. The limits on design variables are dictated by physical and practical considerations.

For this multicriterion optimization problem, a preference function (the metric) is constructed

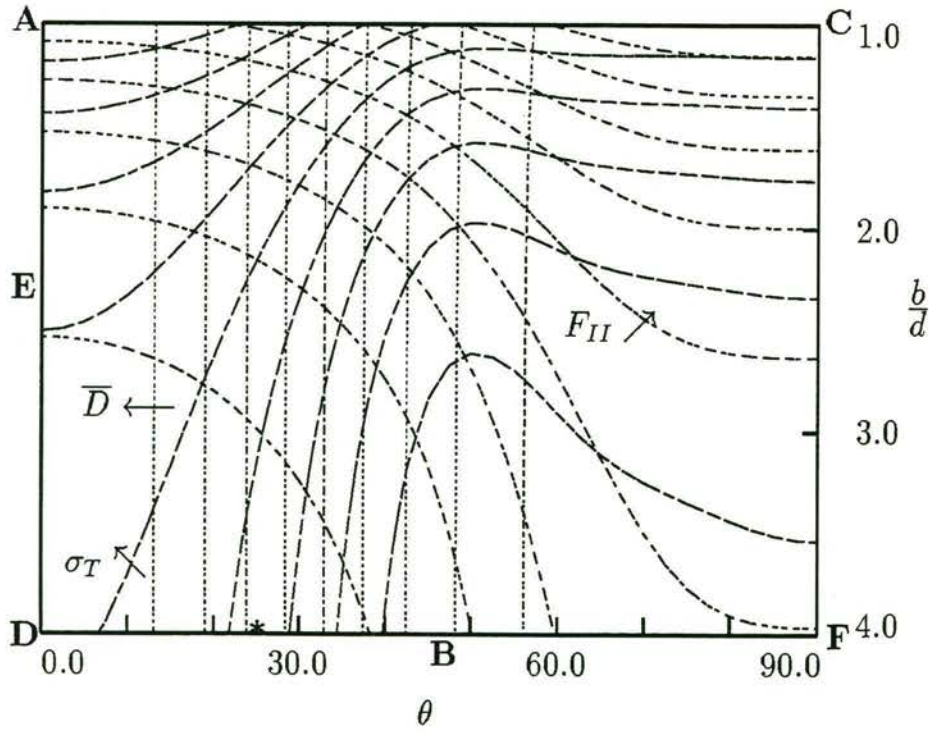

Figure 8.8: Contours of the objective functions $f_1(\mathbf{x}) = \sigma_T$, $f_2(\mathbf{x}) = F_{II}$ and $f_3(\mathbf{x}) = \overline{D}$ for $a/d = 0.4$. Arrows indicate the direction in which the functions increase. The Pareto optimal design corresponding to $\rho = 50$ is indicated by an asterisk ($*$). Maxima and minima of the three objective functions considered in isolation are also shown. **A**: max f_1, **B**: min f_1; **C**: max f_2, **D**: min f_2, **E**: max f_3, **F**: min f_3

as follows

$$F^{(\rho)}(\mathbf{x}) = \left\{ \sum_{j=1}^{m} \left| \frac{f_j(\mathbf{x}) - \min f_j}{\min f_j - \max f_j} \right|^{\rho} \right\}^{\frac{1}{\rho}}, \tag{8.24}$$

where m is the number of objective functions (here equal to 3) and min f_j and max f_j are the minimum and maximum values of each objective function considered in isolation from the others (Figure 8.8). The preferable solution is now found by minimizing the metric function $F^{(\rho)}(\mathbf{x})$. Its solution depends on the chosen parameter ρ. The Pareto optimal design for $\rho = 50$ is indicated by an asterisk in Figure 8.8. Table 8.2 shows the minimized metric function $F^{(\rho)}(\mathbf{x})$ for various values of ρ. It is seen that the min $F^{(\rho)}(\mathbf{x})$ tends to a constant value as ρ is increased. The table also gives the optimum values of the microstructural parameters (design variables $\mathbf{x}$) and the corresponding objective functions $f_j(\mathbf{x})$ which have been appropriately normalized.

Table 8.2: Minimum metric function $F^{(\rho)}(\mathbf{x})$ with corresponding optimum microstructural variables $(\theta, b/d)$ for two crack lengths (a/d) and various exponents (ρ); the upper half for $a/d = 0.4$ and the lower for $a/d = 0.7$. The corresponding values of objective functions $f_1(\mathbf{x})$, $f_2(\mathbf{x})$ and $f_3(\mathbf{x})$ are also given

a/d	ρ	θ	$\frac{b}{d}$	$f_1(\mathbf{x})$	$f_2(\mathbf{x})$	$f_3(\mathbf{x})$	$F^{(\rho)}$
0.40	2	19.15	4.00	1.1127	0.9894	0.8144	0.474
0.40	4	24.48	4.00	1.1098	0.9900	0.7143	0.408
0.40	10	25.53	4.00	1.1091	0.9902	0.6938	0.371
0.40	16	25.69	4.00	1.1090	0.9902	0.6907	0.360
0.40	25	25.67	3.95	1.1091	0.9903	0.6905	0.357
0.40	50	25.64	3.98	1.1091	0.9902	0.6912	0.353
0.70	2	19.01	4.00	1.4844	0.9637	0.8198	0.468
0.70	4	23.95	4.00	1.4729	0.9652	0.7251	0.404
0.70	10	25.44	4.00	1.4687	0.9657	0.6951	0.366
0.70	16	25.23	4.00	1.4694	0.9656	0.6994	0.358
0.70	25	25.71	4.00	1.4680	0.9658	0.6899	0.352
0.70	50	25.46	3.98	1.4689	0.9658	0.6947	0.350

Chapter 9

Optimum *In Situ* Strength Design of Composite Laminates

9.1 Introductory Remarks

It has been widely observed in tests that the transverse tensile and shear strengths of a fibre-reinforced unidirectional lamina, when it is situated in an angle-ply laminate, are functions of the thickness of the lamina itself and the ply angles of its neighbouring laminae (Parvizi *et al.*, 1978; Flaggs & Kural, 1982; Crossman & Wang, 1982; Yamada & Sun, 1979; Chang & Chen, 1987). As a consequence, it is recognized that the transverse and in-plane shear strengths of a lamina cannot be regarded as its intrinsic property. The experiments on $[0^0_m/90^0_n]_s$ cross-ply and/or $[\pm\theta/90^0_n]_s$ angle-ply laminates in these works showed that the failure stress (strain) at the onset of the transverse cracks in the 90^0_n layer under unidirectional tension is a function of n and θ of an angle-ply laminate. If the strength of the 90^0_n layer is assumed to be that corresponding to the onset of transverse cracks in it, then at first sight it would appear to be of a statistical nature. Such an argument based on the size effect has in fact been advanced by Zweben (1994), but it is questionable (Edge, 1994) in that it cannot explain the dependence of the strength of a 90^0 lamina on its thickness. Similarly, based on the experimental measurement of the strength of 90^0_n lamina in $[\pm\theta/90^0_n]_s$ angle-ply laminates, it was found by Flaggs & Kural (1982) that a simple two-parameter Weibull distribution could not adequately describe the thickness effect of the 90^0_n lamina on its strength. Even if one accepted the 'size effect' argument or any other statistical explanation, the well-known dependence of the strength on the ply angle θ of the neighbouring sublaminates could still not be explained.

Since the in-plane normal and shear strengths of a unidirectional lamina form the basis of the failure criteria for general angle-ply laminates and since the transverse cracks are deleterious to the integrity of laminates, much effort has been spent on the prediction of the failure condition

for a lamina in cross-ply (e.g. Garrett & Bailey, 1977; Parvizi *et al.*, 1978; Bailey *et al.*, 1979) and angle-ply laminates (e.g. Tan & Nuismer, 1989). These works examined the conditions at which a through-thickness transverse crack appears in a unidirectional lamina in cross- and angle-ply laminates. Although the strengths were correlated with the thickness of the lamina under consideration and properties of neighbouring laminae, the resulting relationships were not formulated in a manner suitable for a general strength calculation of multidirectional laminates. An exception being the set of concise formulae proposed by Chang & Lessard (1991) for calculating the *in situ* transverse and in-plane shear strengths of a unidirectional lamina in multidirectional laminates. Some of the parameters in these formulae are deduced from experimental results, while others are obtained by curve fitting, thus restricting their applicability. In this Chapter, we shall first provide analytical results from the solution of the problem of a cracked angle-ply laminate. These results clearly show the constraining effect of neighbouring laminae upon a unidirectional lamina, resulting in an enhancement of its *in situ* strength. The analytical calculations are mostly in accord with the formulae of Chang & Lessard (1991) within their range of applicability. Outside of this range, modifications will be made to these in accordance with the present analytical calculations. The basic *in situ* strength parameters will then be used in a failure criterion which judges how close the stress state of a lamina in a multidirectional laminate is to its failure state.

Many failure criteria for unidirectional fibre-reinforced laminae have been proposed (e.g. Hoffman, 1967; Tsai & Wu, 1970; Hashin, 1980; Chang & Lessard, 1991). Rowlands (1985) reviewed the commonly used composite failure criteria and compared them with experimental observations. Some of these give the condition of the matrix failure in laminae; others take into account the fibre breakage, as well. When multidirectional laminates are subjected to loads, it is generally the matrix that fails first due to transverse cracking along the fibre direction (Herakovich, 1982; Crossman & Wang, 1982; Talreja, 1987). This results in the degradation of the laminate stiffness. Transverse cracking is also known to be a direct cause of delamination of neighbouring laminae, as discussed in Chapter 8. The growth of interlaminar delamination and/or fibre breakage result in the final collapse of the laminates (Herakovich, 1982; Crossman & Wang, 1982). In the present work, the *in situ* strengths will be incorporated into a failure criterion which characterizes the onset of transverse cracking in laminates.

The closeness of the stress state in a lamina to its failure point is determined by the laminate configuration, i.e. the ply angles, thicknesses, and stacking sequence of the laminae in the laminate, and by the applied load. It is evident, that under a given load condition, the stress state in a lamina can be altered by varying the configuration of the laminate. Given the choice offered by the composites, it is even likely that there exists an optimum configuration which maximizes the load bearing capacity of the laminate. As we are only considering the situation

at the onset of growth of the transverse cracks in laminates, it is clear that the maximum load so determined will still be a lower bound to the ultimate load carrying capacity of the optimally designed angle-ply laminate.

Traditionally the optimum configuration has been sought by trial and error relying on experience and rules of thumb. Here, the search for the optimum configuration will be put on firm mathematical foundation for symmetric angle-ply laminates under any combination of in-plane loads. In the parlance of mathematical optimization theory, the optimization problem under consideration is a minimax non-differentiable one. It is a minimax problem because the design objective is to minimize the maximum stress norm of the laminae, i.e. to maximize the *in situ* strength of each lamina in the laminate and to bring the strength of the whole laminate as close to the ultimate failure strength as possible. It will be shown that the *in situ* strength of a lamina depends on the differences in the ply angles and thicknesses between this lamina and its immediate neighbours. As the gradients of these differences are not continuous, the optimization problem is non-differentiable.

The optimization problem will be first reduced to a differentiable one (to the first order gradients) by the introduction of a novel smoothing function, and then the differentiable minimax problem will be solved by the bound-formulation method (Olhoff, 1989) and mathematical programming. The gradients of the objective and constraint functions required in this method, will be obtained by a mixed analytical/numerical procedure. The solution shows that the incorporation of the *in situ* strength parameters into the optimum design formalism has great potential for increasing the load bearing capacity of angle-ply laminates. In fact, an optimally designed laminate can carry several times more load than a conventionally designed one. A part of the work described in this Chapter has been published in the paper by Wang & Karihaloo (1995c). Another part has been submitted for publication (Wang & Karihaloo, 1995d).

9.2 Development of *In Situ* Strength Theory

9.2.1 Analysis of a Cracked Laminate

We shall examine the mutual constraining effect in composite laminates through the model of a cracked $[(\pm\theta^0)_{n_2}/(90^0)_{n_1}]_s$ angle-ply laminate shown in Figure 9.1. This model is an asymptotic case of the multicracked angle-ply laminate studied in Chapter 6 when the crack spacing $\lambda \to +\infty$. The solution to this single crack problem is available from Chapter 4. Here, we shall concentrate on the derivation of a set of *in situ* strengths based upon the detailed examination of the constraining effect in this laminate. This single crack approximation is a good model for microcracks or defects existing in the 90^0 lamina in the early stage of their

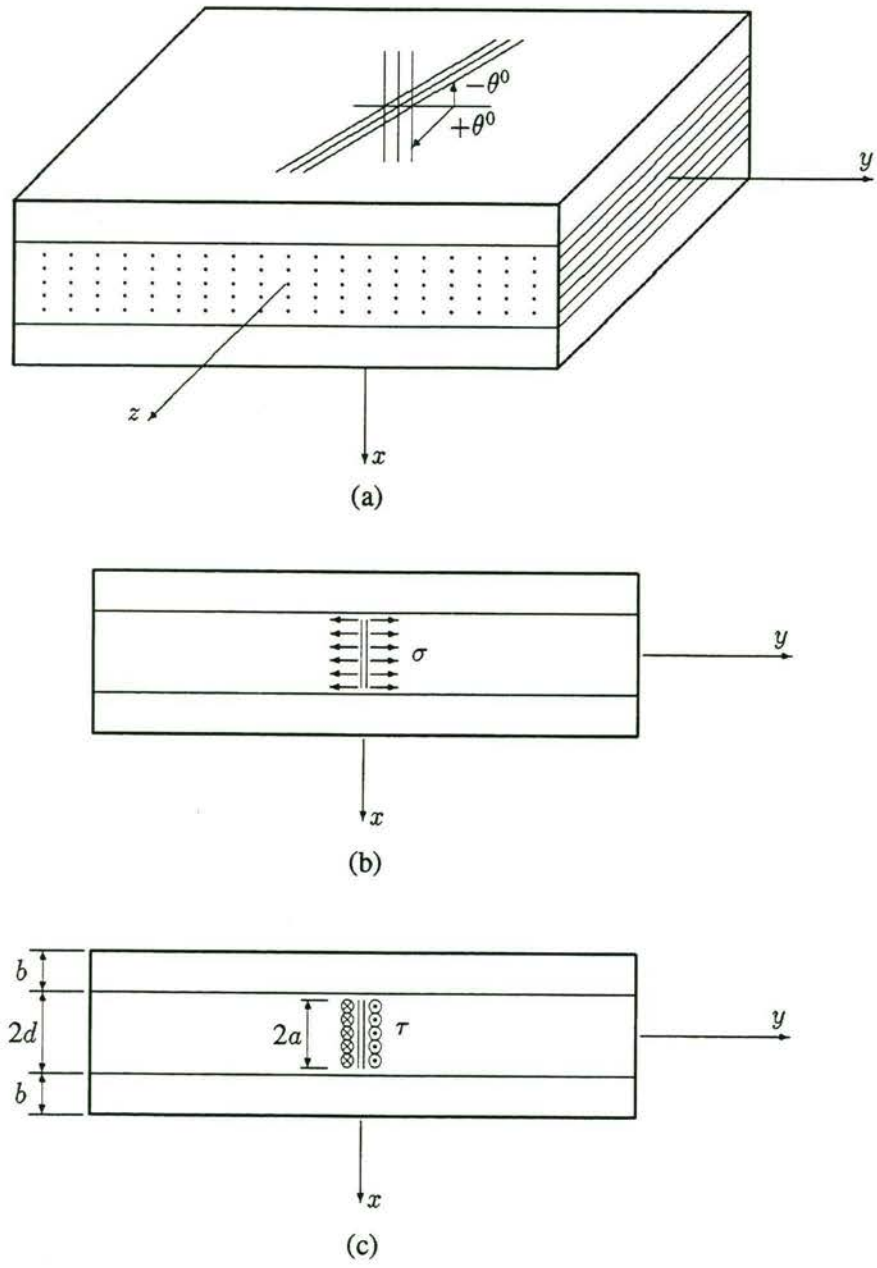

Figure 9.1: A cracked composite laminate, showing the laminate configuration (a), and the opening (b) and anti-plane shear (c) modes of crack face loading

appearance in $[0^0/90^0]_s$ cross-ply and $[\pm\theta/90^0]_s$ angle-ply laminates. Although multiple cracks appear even at early stages, they are usually well separated so that their mutual interactions can be ignored. Experiments show that the density of transverse cracks increases with increasing external load and reaches a saturation level. For a $[0^0/90_n^0]_s$ cross-ply laminate, the saturation spacing between the cracks is found to be about two times the half thickness of the 90_n^0 layer (Highsmith & Reifsnider, 1982). In a $[\pm 25^0/90_n^0]_s$ angle-ply laminate, Crossman & Wang (1982) found that a saturation spacing of $8nt$ (where t is the thickness of ply) using shear-lag model and energy analysis. This prediction appears to agree with the experimental data for $n = 6$. For $n = 4$, a saturation spacing of $4nt$ was found. Thus, it is evident that multiple transverse cracks are well apart at the early stage of their appearance. Theoretical analysis shows that when the spacing between the cracks is several times the half thickness of the 90_n^0 lamina, their mutual interaction is insignificant (Chapter 6). For a multicracked $[0_m^0/90_n^0]_s$ laminate with through-thickness transverse cracks in the 90_n^0 lamina, Hashin (1985) evaluated the stress field by a variational approach. The crack interaction was found to be insignificant when the distance between the cracks was larger than eight times the half thickness of the 90_n^0. A recent study of a cracked $[0^0/\pm 45^0/90^0]_s$ angle-ply laminate with a single transverse crack in the 90^0 lamina (Li *et al.*, 1994) showed that the perturbation of the stress caused by the transverse crack tends to vanish at distances larger than seven times the half thickness of the 90^0 lamina. Therefore, the single crack approximation is quite adequate for studying the constraining effect of the neighbouring sublaminates upon its propagation. Experiments also show (Garrett & Bailey, 1977; Highsmith & Reifsnider,1982; Crossman & Wang, 1982) that the cracks are more or less equally spaced, so that there is no need to consider a random distribution of cracks. Since the multicracked angle-ply laminates have been analysed in Chapter 6, we shall also discuss briefly later in § 9.2.2 the interaction effect of multiple cracks on the behaviour of the deduced *in situ* strengths.

The idea of modelling inherent flaws in fibre-reinforced composite materials by effective central cracks first appeared in the works of Wang & Crossman (1980), and Wang *et al.* (1984). Experiments had shown (Harrison & Bader, 1983) that some dominant flaws coalesce to form a large plane crack. Detailed experimental observations by Bailey *et al.* (1979), and Bailey & Parvizi (1981) on glass fibre- and carbon fibre-reinforced $[0^0/90^0]_s$ cross-ply laminates have revealed that fibre debonds, matrix failure, and even fibre failure sites in the case of carbon fibre-reinforced composite, form the nuclei for transverse cracks. The final through-thickness transverse cracks develop by the coalescence of these nuclei. However, their propagation is influenced by the thickness of the 90^0 layer. If it is thin, the propagation is stable, while in the case of thick 90^0 layer, the propagation may be instantaneous. Therefore, whilst the source of transverse cracks may lie in the very nature of composite laminates, their behaviour under

external loading is influenced by the constraining effect determined by the thickness of the 90^0 and the outer constraining sublaminates. The study of their behaviour is of primary interest in the present work for two reasons. First, the early growth of these nuclei results in the formation of large cracks in the 90^0 layer and thus determines its *in situ* strength in the laminate. Secondly, through an understanding of how the behaviour of the initial cracks depends on the laminate configuration, it is possible to design the laminates so as to retard or even to prevent their failure.

As we will only consider the situation at the onset of growth of the transverse crack(s) in the 90^0 sublaminate, it is sufficient to superimpose the conditions from the two planar modes I and III (Figure 9.1), when the crack is essentially in one plane. The crack will however grow out of its plane so that the growth process will require a proper three-dimensional description. This will not be attempted in the present work.

It was shown in Chapter 4 that when the cracked laminate is subjected to uniform in-plane tension perpendicular to the crack faces (Figure 9.1(b)), the mode I stress intensity factor at each of the crack tips is

$$K_I = \Phi(1)\,\sigma\sqrt{a} \equiv F_I\,\sigma\sqrt{a} \tag{9.1}$$

where F_I is calculated from the solution of the integral equation (4.66), and σ is the in-plane stress applied to the $(90^0)_{n_1}$ sublaminate.

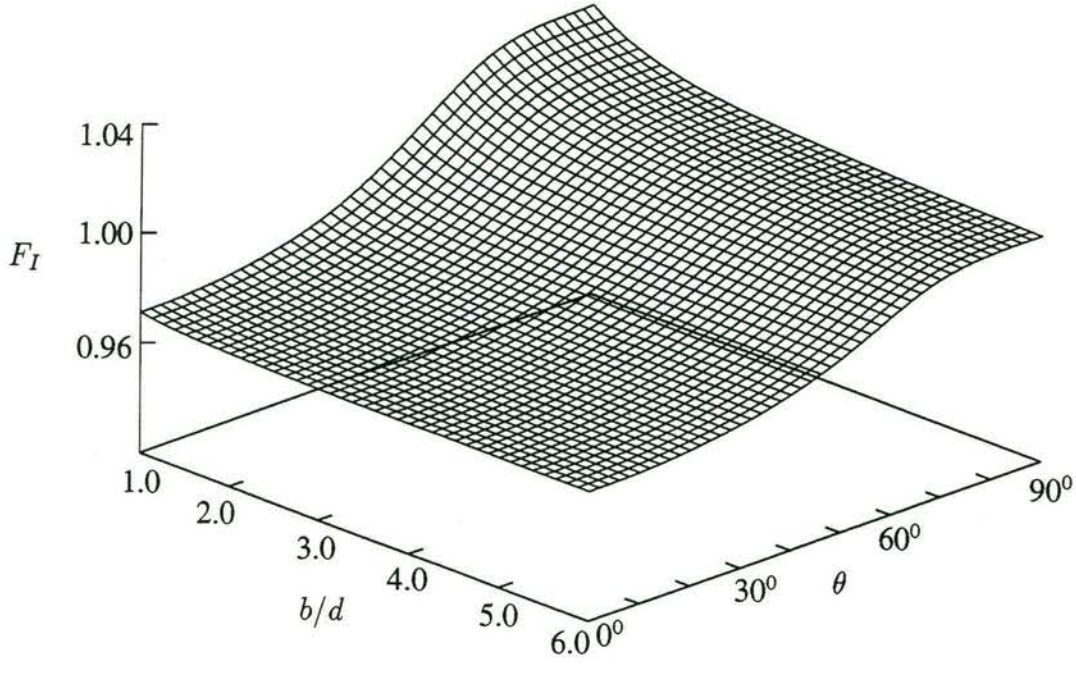

Figure 9.2(a): Variation of F_I with b/d and θ for half crack length $a = 0.4d$

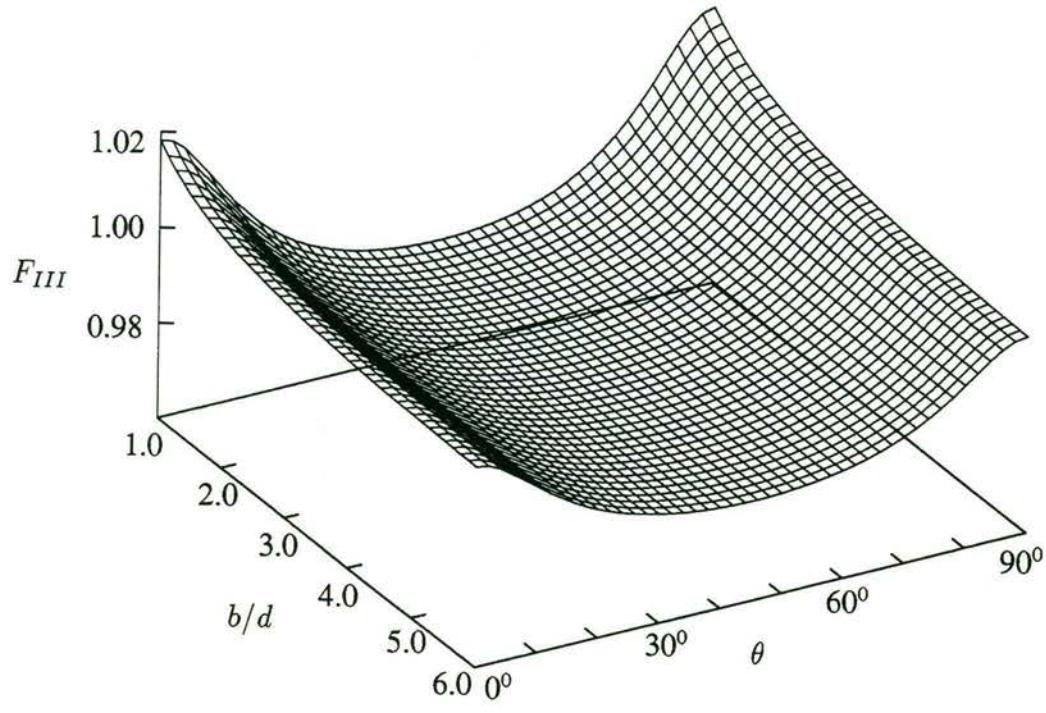

Figure 9.2(b): Variation of F_{III} with b/d and θ for half crack length $a = 0.4d$

Likewise, when the laminate is subjected to in-plane (laminate plane) shear, the mode III stress intensity factor at each of the crack tips is

$$K_{III} = \Omega(1)\,\tau\,\sqrt{a} \equiv F_{III}\,\tau\,\sqrt{a} \tag{9.2}$$

where F_{III} is obtained from the integral equation (4.156), and τ is the shear stress applied to the $(90^0)_{n_1}$ sublaminate.

From the expressions for K_I (9.1) and K_{III} (9.2), it is seen that the crack driving forces depend on the laminate configuration through F_I and F_{III}. For a given crack length, the latter are determined by the stiffnesses, ply angle θ and thicknesses of the inner and outer sublaminates.

The influence of the ply angle θ upon F_I and F_{III} may be judged from Figure 9.2. The material properties used for these calculations were for a graphite/epoxy composite (material 1 in Table 7.1). Figures 9.2(a) and (b) show the variations of F_I and F_{III} with the ply angle θ and the relative thickness of the outer sublaminates. F_I and F_{III} depict completely different dependence on θ; F_I increases monotonically when θ increases from 0^0 to 90^0. This means that the outer sublaminates provide progressively less constraint on the crack propagation. This is in agreement with the experimental results of Flaggs & Kural (1982) who found that the stress at the onset of the transverse cracks in 90^0_n laminae in $(\pm\theta/90_n)_s$ laminates decreases

with increasing θ. The outer sublaminates have the strongest constraining effect on the crack propagation in mode I when $\theta = 0^0$, i.e. in cross-ply laminates.

F_{III} on the other hand, does not vary monotonically with θ. It reaches a minimum at about $\theta = 45^0$. This is because the in-plane shear stiffness of $[(\pm\theta)_{n_2}]$ sublaminate is at its maximum at $\theta = 45^0$. From the material properties of the graphite/epoxy composite, it is seen that G_{LT} is almost equal to G_{TT}, so that F_{III} is nearly symmetric with respect to $\theta = 45^0$. This suggests that under in-plane shear, a lamina has the strongest constraining effect on the crack propagation in the adjacent lamina when the difference of the ply angles of the two laminae is 45^0, instead of 90^0 under in-plane tensile stress. It also suggests that the 0^0 lamina in a $(0^0/90^0)_s$ cross-ply laminate does not provide any constraint on the mode III crack propagation in the 90^0 lamina, if G_{LT} is less than, or almost equal to, G_{TT}. Thus, the experimentally observed enhancement of the *in situ* shear strength of a unidirectional lamina in a cross-ply laminate (Yamada & Sun, 1979; Chang & Chen, 1987) is likely to be a result of crack arrest at the interface between laminae which occurs at a late stage in the failure process of the lamina. The thickness of the outer sublaminates does not have a significant influence upon F_I and F_{III}. But calculations show that this influence is the more significant, the larger the crack length $2a$.

Figures 9.3(a) and (b) demonstrate the influence of the thickness d of the inner $(90^0)_{n_1}$ sublaminate upon F_I and F_{III} for different θ. Both F_I and F_{III} reach constant values at $d/b = 2.0$ for the crack length under consideration.

It is however worth noting that when the crack length is fixed, F_I increases with d/b provided θ is less than about 70^0, with a consequent decrease in the *in situ* tensile strength. For $\theta > 70^0$, F_I decreases smoothly with d/b, as in a centrally cracked isotropic strip. The influence of the ply angle θ weakens with increasing thickness of the inner sublaminate, d. These characteristics of the mode I stress intensity factor agree well with the trend in the *in situ* transverse tensile strength measured by Flaggs & Kural (1982). They found that the thicker the 90^0_n lamina in $(\pm\theta/90^0_n)_s$ ($\theta \leq 60^0$) laminate, the smaller its transverse tensile strength. F_{III} also increases with increasing thickness of the inner $(90^0)_{n_1}$ sublaminate when θ is close to 45^0. It shows a similar variation to that in an isotropic centrally cracked strip, when θ is close to 0^0 or 90^0.

Figures 9.4(a) and (b) show the influence of the relative size of the crack on normalized mode I and mode III stress intensity factors $F_I\sqrt{a/d} = K_I/(\sigma\sqrt{d})$ and $F_{III}\sqrt{a/d} = K_{III}/(\tau\sqrt{d})$, respectively. In mode I, when $\theta \lesssim 70^0$, $F_I\sqrt{a/d}$ increases first with a/d but then decreases. Theoretically, it will eventually become 0 with $a \to d$. For $\theta > 70^0$, $F_I\sqrt{a/d}$ always increases with a/d just as it does in a homogeneous isotropic medium of finite width. We can therefore regard the ply angles θ less than about 70^0 as active ply angles and those above 70^0 as inactive, in that they offer no constraining effect. In mode III, the active angle is around 45^0, while the inactive angles are in the ranges close to 0^0 and 90^0, respectively. When θ lies in the active

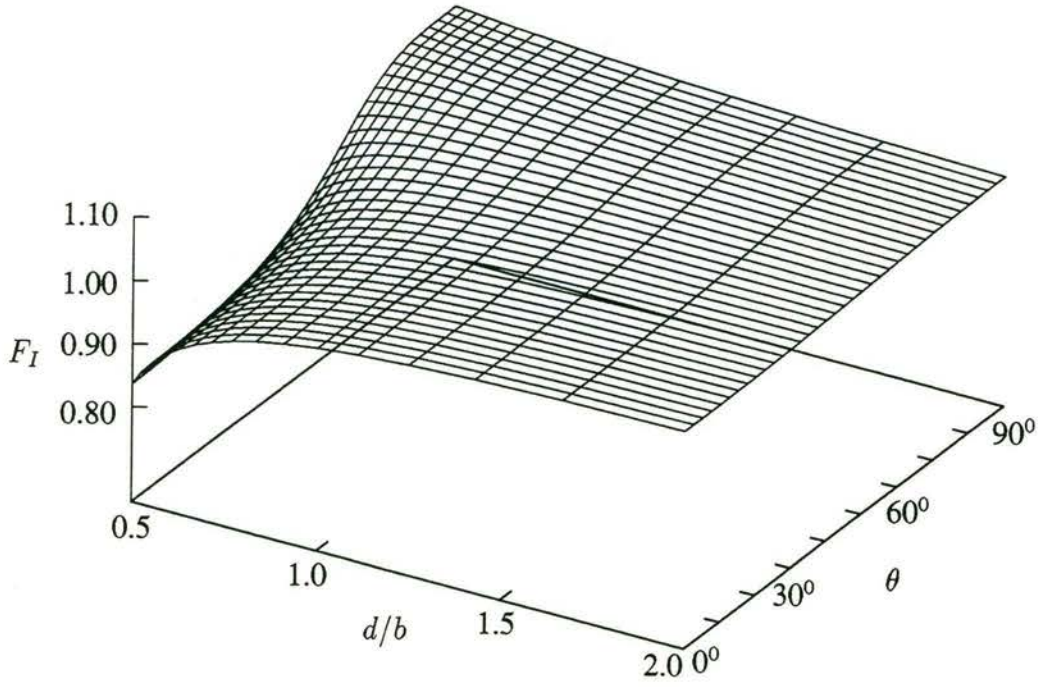

Figure 9.3(a): Variation of F_I with d/b and θ for half crack length $a = 0.4b$

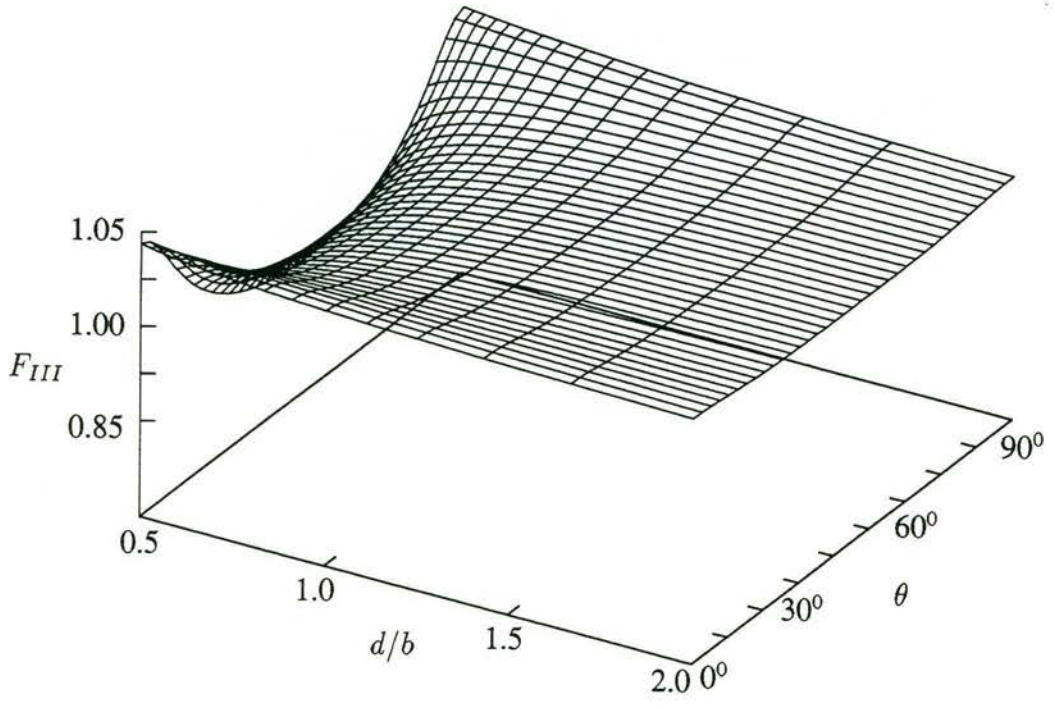

Figure 9.3(b): Variation of F_{III} with d/b and θ for half crack length $a = 0.4b$

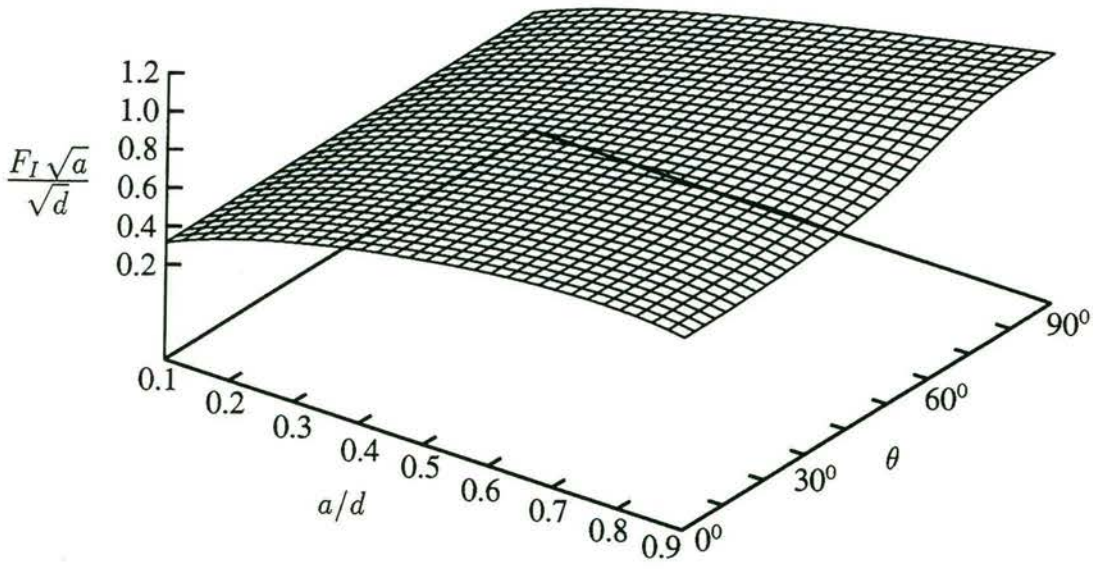

Figure 9.4(a): Variation of the mode I stress intensity factor with half crack length a and θ for $b/d = 2.0$

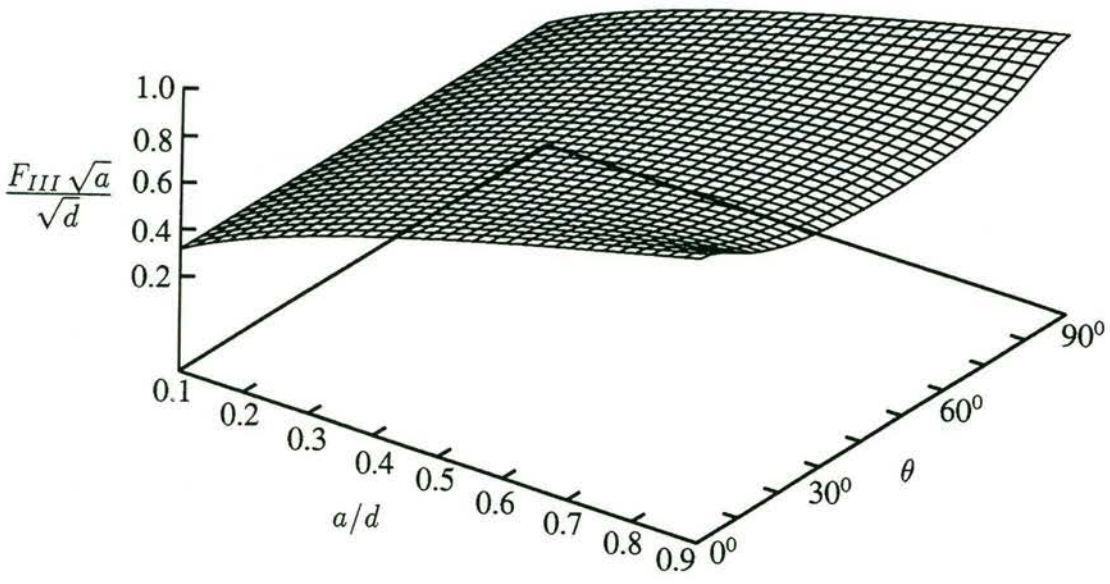

Figure 9.4(b): Variation of the mode III stress intensity factor with half crack length a and θ for $b/d = 2.0$

range, there is a upper limit on the stress intensity factor (SIF). For example, when $\theta = 0^0$, the mode I SIF reaches a maximum value at $a/d \approx 0.78$, and when $\theta = 45^0$ the mode III SIF reaches a maximum value at $a/d \approx 0.83$. When a/d is larger than these values, the SIFs decrease. However, if the ply angle is in the inactive ranges, the crack driving forces will increase rapidly with the relative size of the crack. From the viewpoint of the stability of crack propagation, the former laminate configuration is favourable, whereas the latter should be avoided.

9.2.2 Calculation of *In Situ* Strength Parameters

From a micromechanical point of view, the fibre-reinforced composite material is heterogeneous in the transverse direction. The application of fracture mechanics concepts from isotropic and homogeneous materials such as the critical energy release rate, will therefore inevitably involve certain approximations. Parvizi *et al.* (1978) using work-of-fracture method, as well as the linear elastic fracture mechanics (LEFM) based method, measured the fracture surface energy at initiation γ_I in the transverse direction of unidirectional glass fibre-reinforced epoxy composites. They found that γ_I from both tests was the same, and what is more important, was independent of the initial crack size. This fracture surface energy has been incorporated into the energy balance criterion advanced by Aveston & Kelly (1973) to judge when a through-thickness transverse crack will form in the laminate (Parvizi *et al.*, 1978; Bailey *et al.*, 1979). A similar criterion for transverse cracking was also presented by Tan & Nuismer (1989), who used it to predict the *in situ* crack strain (first-ply-failure strain, FPF) of the 90_n^0 sublaminate in cross-ply and $[\pm 30^0/90_n^0]_s$ angle-ply laminates. Good agreement with experimental data was obtained. An energy criterion for the description of the local behaviour of stresses at the tips of the transverse cracks in cross-ply laminates was used by Wang & Crossman (1980), and Wang *et al.* (1984) to establish the moment at which the initial transverse cracks are about to propagate

$$G(\overline{\sigma}, a_0) = G_c. \tag{9.3}$$

Here $G(\overline{\sigma}, a_0)$ is the energy release rate at the tip of an initial transverse crack of half length a_0 at a stress level $\overline{\sigma}$, and G_c is the material's critical energy release rate ($= 2\gamma_I$).

When the laminate shown in Figure 9.1 is loaded by an in-plane (yz-plane) load, it experiences stresses σ_{yy}, σ_{zz} and τ_{yz}. For the configuration of an intralaminar transverse crack shown in Figure 9.8, Dvorak & Laws (1987) specified relations among these stresses and modes of deformation associated with the two crack fronts designated T and L in Figure 9.8. It is noted that the "mode II" deformation in that paper associated with L-type crack front is mode III with respect to T-type crack front. Therefore, for the crack in the central lamina in Figure 9.1, the crack tip is under mixed mode I and mode III stress state. Thus, following Dvorak &

Laws (1987), the fracture criterion advanced by Hahn & Johnnesson (1983) for fibre-reinforced composites can be used to judge the propagation of the crack under a mixed mode stress state

$$(1-g)\left(\frac{G_I}{G_{Ic}}\right)^{1/2} + g\left(\frac{G_I}{G_{Ic}}\right) + \left(\frac{G_{III}}{G_{IIIc}}\right) \geq 1 \tag{9.4}$$

where G_I and G_{III} are the energy release rates in modes I and III, respectively, and G_{Ic} and G_{IIIc} are the corresponding critical values. $g = G_{Ic}/G_{IIIc}$. The values of G_{Ic} and G_{IIIc} are very rare. However, we shall see that since we are only interested in the influence of the configuration of the laminate on the crack driving force, the absolute values of G_{Ic} and G_{IIIc} are not important.

Under mixed mode conditions a crack cannot propagate in its own plane but must deviate from it. However, if we are only interested in the instant at which the pre-existing cracks are about to grow and not in their growth regime, the stress intensity factors at the original crack tip may be used as a first approximation (Karihaloo, 1982).

For the special loading when only $\sigma_{yy} = \sigma$ exists, following Dvorak & Laws (1987), the failure stress at the propagation of the crack can be calculated from the relation

$$G_I = G_{Ic} \tag{9.5}$$

Substituting

$$G_I = \frac{K_I^2}{E'} = \frac{F_I^2 \sigma^2 a}{E'} \tag{9.6}$$

into (9.5), we get

$$Y_t \equiv \sigma_{cr} = \frac{\sqrt{G_{Ic} E'}}{F_I \sqrt{a}} \tag{9.7}$$

where $E' = E$ (Young's modulus) in plane stress, and $E' = E/(1-\nu^2)$ in plane strain.

Similarly, for the loading when only $\tau_{yz} = \tau$ exists, the failure stress at the propagation of the crack can be calculated from the relation

$$G_{III} = G_{IIIc} \tag{9.8}$$

Substituting

$$G_{III} = \frac{K_{III}^2}{2\mu} = \frac{F_{III}^2 \tau^2 a}{2\mu} \tag{9.9}$$

into (9.8), we get

$$S_c \equiv \tau_{cr} = \frac{\sqrt{2 G_{IIIc} \mu}}{F_{III} \sqrt{a}} \tag{9.10}$$

where μ is the shear modulus.

It is noted that in eqns (9.7) and (9.10), the stresses σ_{cr} and τ_{cr} at the propagation of the crack are regarded as the *in situ* strengths Y_t and S_c (in the notation of Chang & Lessard (1991)) of the

transverse lamina. However, if σ_{cr} or τ_{cr} does not result in the complete rupture of the transverse lamina, i.e. under σ_{cr} or τ_{cr} the crack does not propagate instantaneously through the whole thickness of the lamina, these stresses cannot be regarded as the *in situ* strengths of the lamina. This problem is concerned with the stability of crack propagation. It is seen from Figure 9.4(a) that for a given thickness of the transverse lamina the crack driving force ($F_I\sqrt{a/d}$) increases with increasing a/d up to a critical value approximately equal to 0.78. When a/d is greater than $\sim$ 0.78, $F_I\sqrt{a/d}$ decreases with increasing a/d when θ is in the active range. Therefore, if the relative size a/d of an initial crack is less than $\sim$ 0.78, as is likely to be the case in most composite materials, once the crack starts to propagate at a certain stress σ_{cr}, it will propagate unstably, resulting in the failure of the transverse lamina. On the other hand, if the relative size a/d of the initial crack is greater than $\sim$ 0.78, the propagation will be stable. This is likely to happen when the transverse lamina is very thin. The same discussion holds also for mode III except that the critical value of a/d is $\sim$ 0.83 for this mode. Therefore, the above definition of the *in situ* strengths is appropriate for the size of transverse cracks observed in practice.

Using the finite element method, Wang & Crossman (1980) calculated the mode I strain energy release rate at the tip of an intralaminar transverse crack in the 90^0 lamina of a $[0^0/90^0]_s$ cross-ply laminate. It is expressed as

$$G_I^\sigma = \frac{g_I^\sigma(a/d)\, d\, \overline{\sigma}^2}{\overline{E}} = \frac{g_I^\sigma(a/d)\,(d/a)\, a\, \overline{\sigma}^2}{\overline{E}} \tag{9.11}$$

where a is the half-length of the transverse crack, and d is the half-thickness of the 90^0 lamina. $\overline{\sigma}$ and $\overline{E}$ are the applied stress and Young's modulus, respectively. $g_I^\sigma(a/d)$ is called the shape function. It is independent of the applied load and is determined only by the geometry of the crack and laminate. The superscript σ indicates that the values of G and g correspond to the applied stress σ, and the subscript I denotes mode I loading.

When only mode I loading is considered, a comparison of eqn (9.6) with eqn (9.11) shows that

$$F_I^2 = g_I^\sigma(a/d)\,(d/a) \tag{9.12}$$

or

$$\left[F_I\sqrt{\frac{a}{d}}\right]^2 = g_I^\sigma(a/d) \tag{9.13}$$

The qualitative variation of $g_I^\sigma(a/d)$ with a/d was shown in above-mentioned paper. It depicts a variation similar to that of $F_I\sqrt{a/d}$ in Figure 9.4(a) when θ lies in the active range. $g_I^\sigma(a/d)$ also increases with a/d, reaching a maximum value, and then decreases. $g_I^\sigma(a/d)$ reaches the maximum value at $a/d \approx 0.85$. This is in good agreement with the location of the maximum of $F_I\sqrt{a/d}$ at $a/d \approx 0.78$, as discussed above.

If the values of Y_t and S_c expressed by eqns (9.7) and (9.10) for the lamina with $\theta = 90^0$, (i.e. the angle-ply laminate degenerates into a unidirectional $(90^0)_{2n}$ $(n = n_1 + n_2)$ laminate), are denoted by Y_t^0 and S_c^0, respectively, then we have the following ratios

$$\frac{Y_t}{Y_t^0} = \frac{F_I^0}{F_I} \equiv F_t(\theta, d, b, a) \tag{9.14}$$

$$\frac{S_c}{S_c^0} = \frac{F_{III}^0}{F_{III}} \equiv F_s(\theta, d, b, a) \tag{9.15}$$

where F_I^0 and F_{III}^0 are the values of F_I and F_{III} when $\theta = 90^0$.

Let us now examine the behaviour of the two functions $F_t(\theta, d, b, a)$ and $F_s(\theta, d, b, a)$. From the discussion of Figures 9.2(a) and (b) we know that the influence of b is not significant for a large range of a. Its effect becomes important only when a is nearly equal to d. Therefore, we may neglect the influence of b upon these two functions. Since F_I^0, F_I, F_{III}^0 and F_{III} all depend on the relative crack length a/d and on θ, the expressions (9.14)–(9.15) can thus be rewritten as

$$\frac{Y_t}{Y_t^0} = \frac{F_I^0}{F_I} = F_t(\theta, a/d) \tag{9.16}$$

$$\frac{S_c}{S_c^0} = \frac{F_{III}^0}{F_{III}} = F_s(\theta, a/d) \tag{9.17}$$

Figures 9.5(a) and (b) depict the variations of F_t and F_s with a/d and θ. For the example material considered above, F_t is always greater than or equal to 1. F_s is also greater than 1 but falls below this value at $\theta = 0^0$. The minimum value of F_s is 0.99 and is attained at $a/d = 0.9$ and $\theta = 0^0$. For a given a/d the typical F_t versus θ and F_s versus θ curves are shown by solid lines in Figures 9.6(a) and (b).

From Figures 9.5(a) and 9.6(a) we can deduce the following properties of F_t. First, it is always greater than or equal to 1 because $F_I|_{\theta \neq 90^0} < F_I|_{\theta = 90^0}$. This means that a lamina in an angle-ply laminate always restricts the growth of a mode I transverse crack in the neighbouring lamina having a different ply angle. This constraining effect reaches its maximum when the difference of the ply angles is 90^0, and it decreases monotonically (i.e. $F_t \to 1$) when the difference of the ply angles decreases from 90^0 to 0^0. Secondly, F_t reduces with increasing thickness of the lamina under consideration, i.e. $\lim_{d \to large} F_t \to 1$. This is in agreement with experimental results which show that as the thickness of the 90^0 lamina increases, its *in situ* strength reaches an asymptotic value. Thirdly, F_t is a periodic function of the difference in the ply angles.

F_s also exhibits the first and third features of F_t. However, it reaches its maximum when the difference in the ply angles is about 45^0. Bearing in mind the above properties of F_t and F_s, we shall demonstrate the merits and drawbacks of the *in situ* in-plane tensile and shear strength formulae proposed by Chang & Lessard (1991)

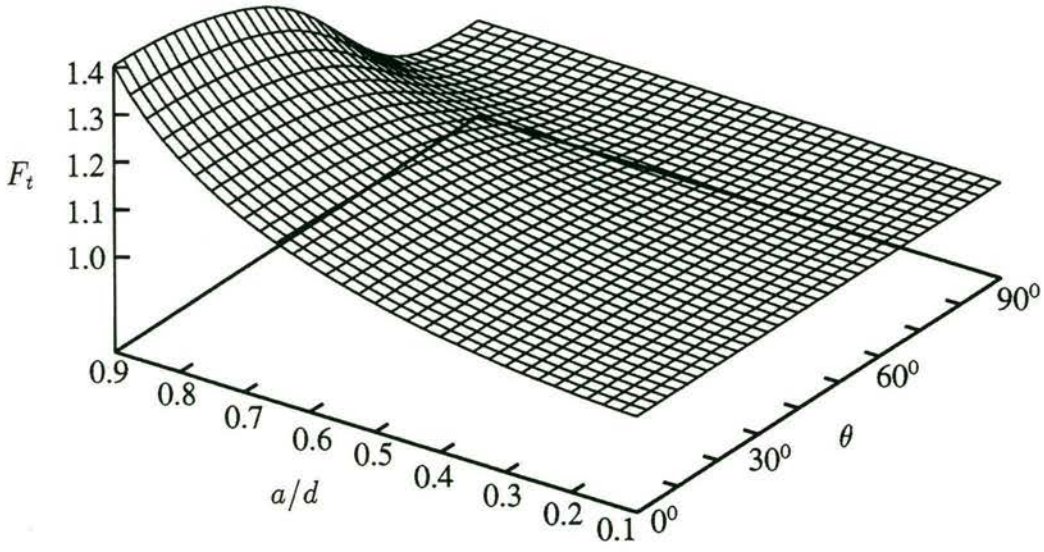

Figure 9.5(a): Variation of F_t with relative crack length a/d and θ for $b/d = 2.0$

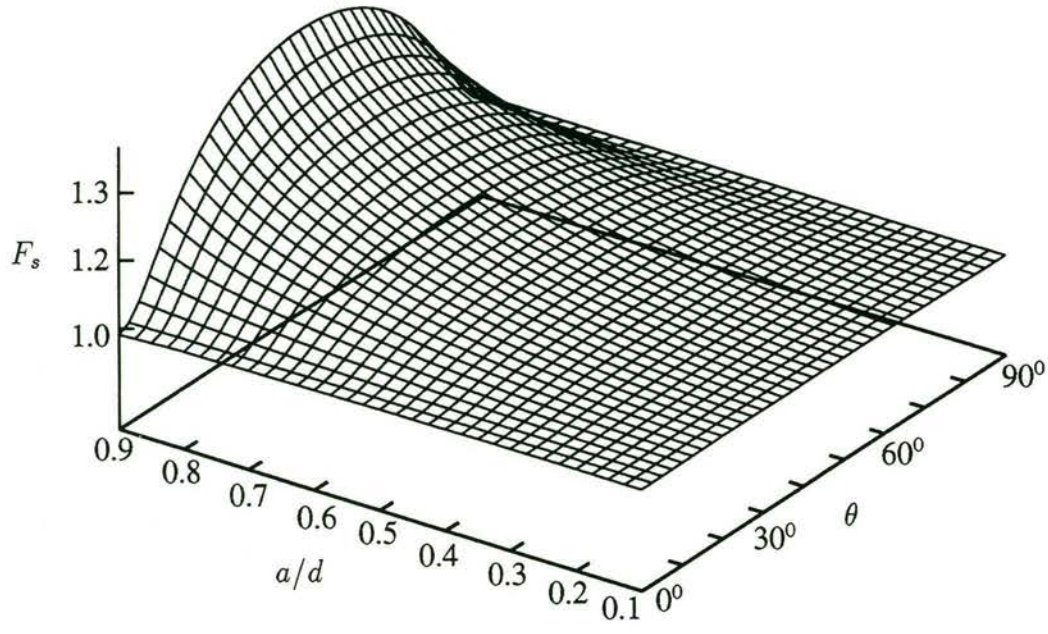

Figure 9.5(b): Variation of F_s with relative crack length a/d and θ for $b/d = 2.0$

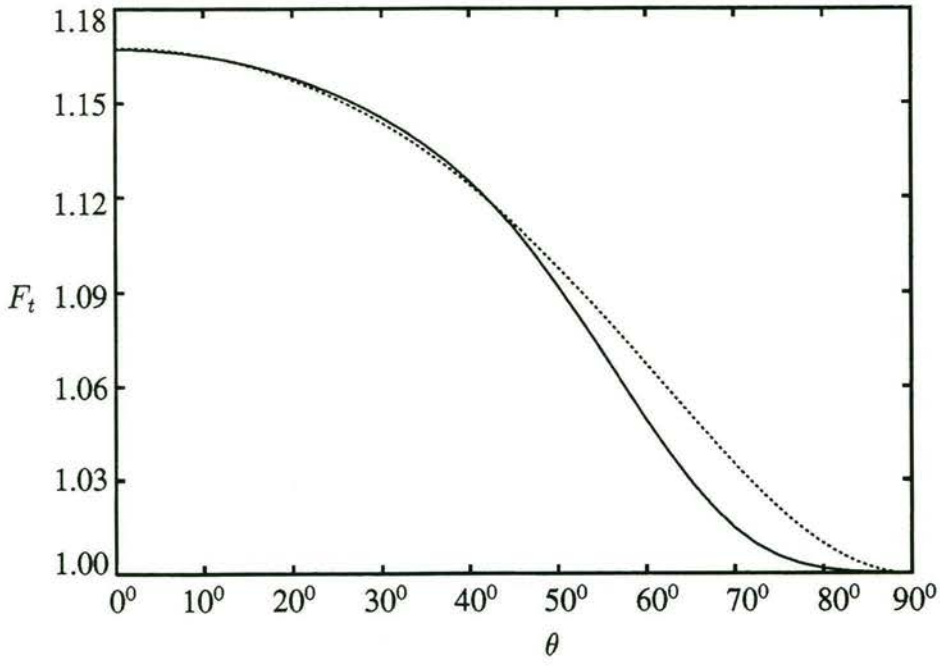

Figure 9.6(a): Typical variation of F_t with θ $(a/d = 0.7)$. The solid line represents the calculated values of F_I^0/F_I from eqn (9.14), and the dotted line the approximate expression (9.20)

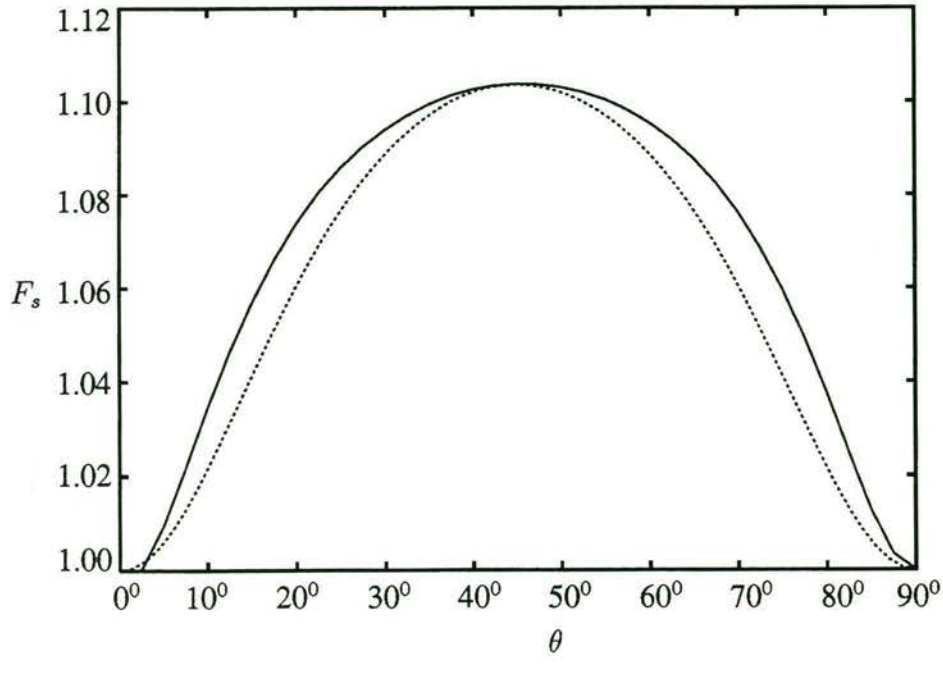

Figure 9.6(b): Typical variation of F_s with θ $(a/d = 0.7)$. The solid line represents the calculated values of F_{III}^0/F_{III} from eqn (9.15), and the dotted line the approximate expression (9.21)

$$\frac{Y_t}{Y_t^0} = 1 + \frac{A}{N^B}\sin(\Delta\theta) \tag{9.18}$$

$$\frac{S_c}{S_c^0} = 1 + \frac{C}{N^D}\sin(\Delta\theta) \tag{9.19}$$

Here, Y_t and S_c are the *in situ* transverse tensile and in-plane shear strengths of a lamina in a laminate, respectively. $\Delta\theta$ is the minimum ply angle difference between the lamina under consideration and laminae immediately above and below it. N is the number of consecutive plies in the lamina under consideration. Y_t^0 and S_c^0 are the reference transverse tensile and in-plane shear strengths of a $[90_n]_s$ unidirectional laminate ($n \geq 6$). A, B, C and D are material parameters which are determined from experiments.

Expressions (9.18) and (9.19) demonstrate the lamination effect on the strengths of a lamina in an angle-ply laminate. The *in situ* transverse tensile strength Y_t for the 90_n lamina in $(\pm\theta/90_n)_s$ laminate ($\theta = 0^0, 30^0, 60^0$) calculated from (9.18) is found to be in good agreement with experimental data (Flaggs & Kural, 1982), when A and B are obtained from curve fitting, as is S_c calculated from (9.19) for cross-ply laminates $(0_{n_1}/90_{n_2})_s$.

The constraining effect of the neighbouring laminae on the strengths of a lamina is determined by the second terms on the right hand side of eqns (9.18) and (9.19). It is seen that the *in situ* strength ratios tend to 1 when the thickness of the lamina becomes large. This agrees with the properties of F_t and F_s deduced above. The variation of Y_t/Y_t^0 with the difference in the ply angles, depicted by $\sin(\Delta\theta)$, also conforms with that of F_t. However, $\sin(\Delta\theta)$ does not seem to describe the observed variation of F_s with the difference in the ply angles. In addition, if we consider the first-order derivative of F_t with respect to θ, we see from the solid line in Figure 9.6(a) that it tends to zero when $\theta = 0^0$ and 90^0, i.e. when the difference between the ply angles of constraining sublaminate and the 90^0 lamina in the considered $[(\pm\theta)_{n_2}/(90^0)_{n_1}]_s$ laminate is equal to 90^0 and 0^0. Expression (9.18) has a zero gradient when $\Delta\theta = 90^0$, but not when $\Delta\theta = 0^0$. Same observations hold also for the behaviour of F_s.

Based upon the above observations and taking into account the merits of the formulae (9.18)–(9.19), we propose a set of modified formulae for calculating the *in situ* strength parameters for a unidirectional lamina when it is placed in a multidirectional angle-ply laminate

$$\frac{Y_t}{Y_t^0} = 1 + \mathcal{A}\, f_t(\Delta\theta) \tag{9.20}$$

$$\frac{S_c}{S_c^0} = 1 + \mathcal{C}\, f_s(\Delta\theta) \tag{9.21}$$

To err on the conservative side, the functions $f_t(\Delta\theta)$ and $f_s(\Delta\theta)$ must only take into account the minimum constraint offered by the neighbouring plies, as in eqns (9.18)–(9.19). In addition,

they must be positive and periodic functions of $\Delta\theta$. These properties and the shapes of F_t and F_s curves in Figures 9.6(a) and (b) suggest that $f_t(\Delta\theta)$ and $f_s(\Delta\theta)$ can be chosen as

$$f_t(\Delta\theta) = \min\left[\frac{\sin^2(\Delta\theta_a)}{1+\sin^2(\Delta\theta_a)}, \frac{\sin^2(\Delta\theta_b)}{1+\sin^2(\Delta\theta_b)}\right] \tag{9.22}$$

$$f_s(\Delta\theta) = \min\left[\frac{\sin^2(2\Delta\theta_a)}{1+\sin^2(2\Delta\theta_a)}, \frac{\sin^2(2\Delta\theta_b)}{1+\sin^2(2\Delta\theta_a)}\right], \tag{9.23}$$

where $\Delta\theta_a$ and $\Delta\theta_b$ denote the ply angle differences between the lamina under consideration and laminae immediately above and below it. The influence of the thicknesses of the neighbouring laminae is neglected.

It will be shown below that the parameters $\mathcal{A}$ and $\mathcal{C}$ in eqns (9.20)–(9.21) play the same role as A/N^B and C/N^D in formulae (9.18)–(9.19) of Chang & Lessard (1991).

The approximations (9.20)–(9.21) to the ratios $Y_t/Y_t^0 = F_I^0/F_I$ and $S_c/S_c^0 = F_{III}^0/F_{III}$ are shown in Figures 9.6(a) and (b) by dotted lines. The values of $\mathcal{A}$ and $\mathcal{C}$ are chosen so that the maxima predicted by (9.20)–(9.21) (at $\theta = 0^0$ for mode I and 45^0 for mode III) coincide with those of F_I^0/F_I and F_{III}^0/F_{III}. This gave $\mathcal{A} = 0.34$ and $\mathcal{C} = 0.207$ for $a/d = 0.7$ of Figure 9.6.

The same matching procedure was used for different values of a/d and the results are shown in Figure 9.7, together with the variation of A/N^B and C/N^D in expressions (9.18)–(9.19) with N. An increase in d is the same as an increase in N.

The size of flaws in a material is unlikely to increase in proportion to its overall size. Therefore, if we assume that a remains more or less constant as d (and also N) increases, the above trend in the variation of $\mathcal{A}$ and $\mathcal{C}$ with d/a surprisingly confirms the inverse exponential decay predicted by the formulae of Chang & Lessard (1991). Of course, there is still a substantial difference in the absolute values of $\mathcal{A}$ and A/N^B, and $\mathcal{C}$ and C/N^D (Figures 9.7(a) and (b)). The cause of this difference needs to be clarified by dedicated experiments and more sophisticated analysis, which is beyond the scope of the present exposition. However, as the formulae (9.18)– (9.19) are deduced from experimental data and they predict accurately the influence of the thickness upon the *in situ* strengths, they will be retained in the modified *in situ* strength parameters of eqns (9.20)–(9.21)

$$\frac{Y_t}{Y_t^0} = 1 + \frac{A}{N^B} f_t(\Delta\theta) \tag{9.24}$$

$$\frac{S_c}{S_c^0} = 1 + \frac{C}{N^D} f_s(\Delta\theta) \tag{9.25}$$

in which $f_t(\Delta\theta)$ and $f_s(\Delta\theta)$ are given by (9.22) and (9.23). Based on the properties of $f_t(\Delta\theta)$ and $f_s(\Delta\theta)$, eqns (9.24)– (9.25) give a conservative estimate of the *in situ* strengths compared with eqns (9.18)–(9.19).

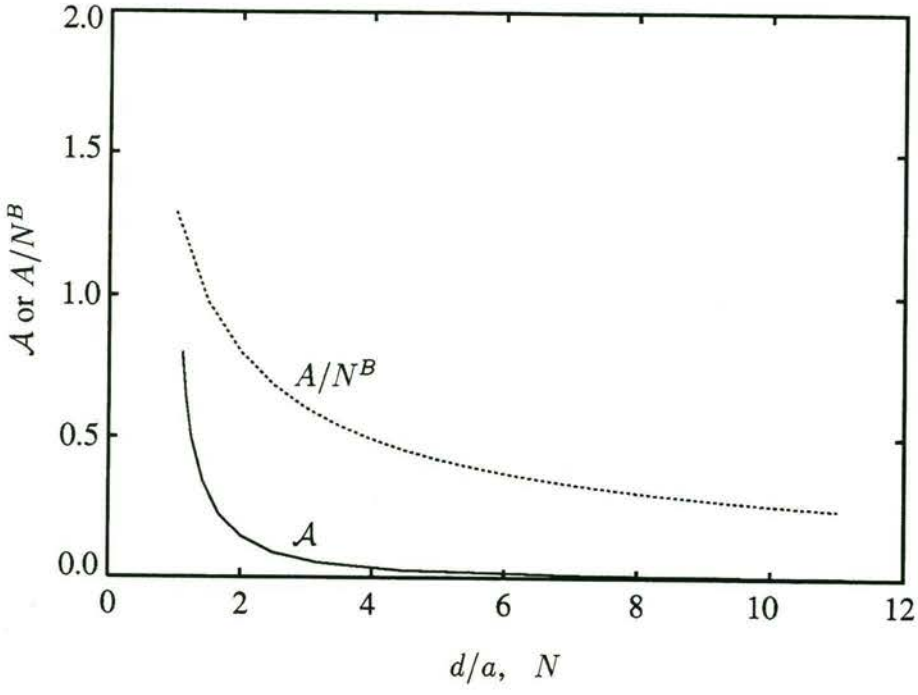

Figure 9.7(a): Variation of $\mathcal{A}$ with d/a, and of A/N^B with N

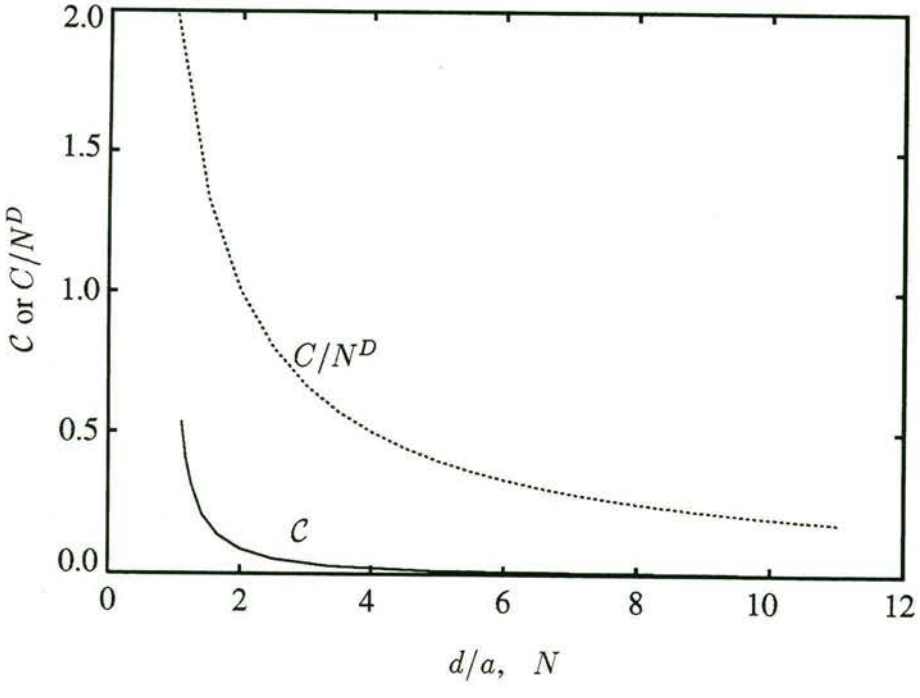

Figure 9.7(b): Variation of $\mathcal{C}$ with d/a, and of C/N^D with N

Let us discuss briefly the influence of multiple transverse cracks on the *in situ* strength parameters (9.24) and (9.25). An examination of Figures 6.3 and 6.7 shows that as the crack spacing reduces, so do $\Phi(1)$ (F_I) and $\Omega(1)$ (F_{III}) for all ply angles θ and crack lengths a/d. Although this reduction is significant, especially when λ/d is small, the ratios F_I^0/F_I and F_{III}^0/F_{III} in eqns (9.16) and (9.17) change little when the crack spacing is reduced. For example, when $b/d = 2.0$ and $a/d = 0.7$, $F_I^0(\theta = 90^0)/F_I(\theta = 0^0)$ is equal to 1.298 and 1.216 for $\lambda/d = 2.0$ and 6.0, respectively. For the same geometry, $F_{III}^0(\theta = 90^0)/F_{III}(\theta = 45^0)$ is equal to 1.126 and 1.106, respectively. For this reason, the interaction of cracks was ignored in the calculation of the *in situ* strengths.

Another problem which has been ignored in most of the research of transverse cracking, including the present work, is the propagation of a transverse crack in the direction of fibres, i.e. z-direction in Figure 9.1 (a). Only the fracture dynamics in the direction perpendicular to the fibres, i.e. x-direction in Figure 9.1 (b), has been taken into account. For brevity, we refer to the former direction of propagation as L (longitudinal) and the latter as T (transverse), following the notation of Dvorak & Laws (1987) as shown in Figure 9.8. If the size of the initial crack in z-direction is (or supposed to be) of the same order as its size in x-direction, then the crack problem must be considered as a three-dimensional one. The present two-dimensional analysis should be regarded as a first approximation to the more difficult three-dimensional problem.

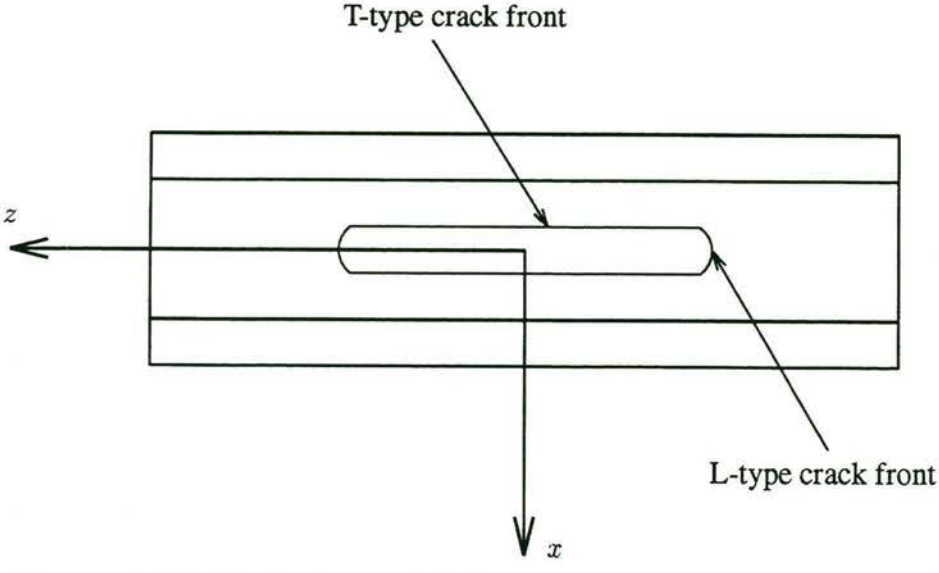

Figure 9.8: An elongated elliptic intralaminar transverse crack in a laminate. The coordinate system follows that in Figure 9.1. The direction of fibres in the central lamina (transverse lamina) is parallel to z-axis. It is assumed that the crack in z-direction is much longer than that in x-direction (After Dvorak & Laws, 1987)

The experimental observations by Parvizi *et al.* (1978) clearly showed the process of

transverse cracking in the 90^0 lamina in a cross-ply laminate under unidirectional tension. There are three basic forms of transverse cracking, depending on the thickness of the 90^0 lamina. When the 90^0 lamina is comparatively thick, the majority of the transverse cracks span the whole width of the specimen and propagate instantaneously. When the thickness is reduced (below $\sim$ 0.4 mm), transverse "edge" cracks are observed. It is important to note that these edge cracks grow very slowly towards the inner area of the specimen under increasing loading. When the thickness is further reduced (to 0.15 mm), transverse cracks are not observed prior to the complete failure of the specimen. From these observations, we may deduce that (i) in the case of thick lamina, the propagation of L- or T-type transverse cracks is indistinguishable, and (ii) in the case of moderately thick lamina, it is likely that an initial transverse crack which spans a certain length along the direction of fibres propagates as a T-type crack to form a through-thickness crack. It is unlikely that a short (measured along the direction of fibres) through-thickness crack appears first and then propagates as an L-type crack, because of the very slow propagation rate of a through-thickness crack towards the inner area of the specimen. It is obvious that such a crack propagation meets strong resistance.

On the theoretical side, the work by Dvorak & Laws (1987) deserves particular attention in that they attempted to predict the propagation of a transverse crack in the direction of the fibres, i.e. L-type propagation in Figure 9.8. They assumed that the intralaminar transverse crack (nucleus) in z-direction is much longer than that in x-direction so that the crack size is not important in the analysis. They calculated the strain energy release rates at the T and L crack fronts. These energy release rates were used to determine the direction in which the crack might propagate. The influence of the outer orthotropic sublaminates on the crack driving force at the tips of the central intralaminar crack was approximated by that for a cracked finite isotropic strip sandwiched between two dissimilar isotropic half-planes considered by Hilton & Sih (1971). Depending upon the size of the crack in x-direction (equivalent to a in Figure 9.1(b)) relative to the thickness of the transverse lamina (equivalent to d in Figure 9.1(b)), Dvorak & Laws (1987) found that three patterns of propagation of the initial crack were possible. When the transverse lamina is relatively thick ($a << d$), the failure is caused by T-type propagation followed by L-type cracking. For transverse lamina of intermediate thickness ($0 < a/d < 1$), the sequence of propagation was not well defined. It is possible however that the crack first propagates in T-direction until it reaches a certain size a_{max} corresponding to the maximum of $F_I\sqrt{a/d}$ (see Figure 9.4(a)), whereafter it begins to propagate in L-direction. It is also possible that propagation happens spontaneously. For thin transverse lamina, Dvorak & Laws (1987) assumed that the initial crack was already a through-thickness crack, i.e. $a/d = 1$, so that the strength of the transverse lamina can only be controlled by propagation of the initial crack in L-direction. This pattern of propagation of the initial crack is different from that being

considered in this Chapter, because a through-thickness crack cannot exist prior to loading. It must form as a consequence of the propagation of an initial crack in T-direction, which is the subject of the present Chapter. We noted in passing that in the work of Dvorak & Laws (1987) the size of the initial crack in z-direction does not play a role in the analysis, irrespective of the lamina thickness. In that sense, their analysis is also a two-dimensional one.

Based upon the above discussion, we conclude that the fracture mechanics analysis in this Chapter is important in determining the *in situ* transverse strength of a unidirectional lamina in laminates. The two-dimensional model which ignores the size of the initial crack in the direction of the fibres is a good approximation of the failure mechanism in laminates judging by both the available experimental evidence and the previous theoretical studies.

9.2.3 Failure Criterion of Lamina in Laminates

A multidirectional angle-ply laminate can fail in a variety of ways. It can fail because of matrix cracking (transverse cracks), fibre breakage, fibre buckling, and delamination (Herakovich, 1982; Chang *et al.*, 1991). However, as mentioned previously, in most laminates the first failure mode is transverse cracking of the laminae along fibre directions. Although the transverse cracks do not directly destroy the overall integrity of the laminates (the failure load of a laminate is much larger than the load at the appearance of transverse cracks), they have the potential to induce other kinds of failure. The growth of transverse cracks results in the redistribution of the stresses in a laminate. They are also known to contribute to the delamination of plies. The eventual failure of a laminate is caused by extensive delamination and/or fibre breakage. Therefore, we shall use the matrix tensile failure criterion (Hashin, 1980; Chang & Lessard, 1991) to judge the appearance of transverse cracks in laminae in a multidirectional laminate. This criterion can be written as

$$\left(\frac{Y}{Y_t}\right)_i^2 + \left(\frac{S}{S_c}\right)_i^2 = 1; \quad (i = 1, ..., L) \tag{9.26}$$

where Y and S are the in-plane transverse and shear stresses in a lamina due to actual in-plane laminate loading; Y_t and S_c are the corresponding *in situ* strengths, and L is the number of laminae in the laminate. This failure criterion traces a supersurface in $2L$-dimension space, if all L laminae have different fibre orientations and thicknesses. If the failure of the laminate is assumed to coincide with that of the first lamina, i.e. the equality in eqn (9.26) is satisfied by the stress state in each of the laminae in the laminate, then (9.26) corresponds to the first-ply-failure (FPF) criterion of Tsai & Hahn (1980).

For a multidirectional laminate subjected to in-plane loads N_1^0, N_2^0 and N_6^0 (in the notation of Tsai & Hahn (1980), see § 3.7), let us denote the left hand term in eqn (9.26) by

$$q_i^2 = \left(\frac{Y}{Y_t}\right)_i^2 + \left(\frac{S}{S_c}\right)_i^2; \quad (i = 1, ..., L) \tag{9.27}$$

q_i can be regarded as a stress norm, if the space of the stresses $\{Y, S\}$ has a variable metric $(1/Y_t, 1/S_c)$. It is similar to the "strain norm" used by Park (1982) in the optimum design of laminates.

9.3 Optimum Design of Multidirectional Laminates

9.3.1 Problem Formulation

For a given composite composition and in-plane loads, the stress distribution in the laminae is determined by the laminate configuration, namely by the ply angles and thicknesses of the constituent laminae. If these design variables are so chosen that the stress state in each lamina is well below the failure state described by (9.26), then the load carried by the laminate will be enhanced. This objective is achieved by minimizing the maximum value of q_i $(i = 1, .., L)$. Suppose that under given in-plane loads $\{N_1^0, N_2^0, N_6^0\}^T$, the values of the stress norm of the laminae are

$$q_i^0 \qquad (i = 1, ..., L). \tag{9.28}$$

When the in-plane loads are increased proportionally by a factor $k > 1$

$$\begin{Bmatrix} N_1 \\ N_2 \\ N_6 \end{Bmatrix} = k \begin{Bmatrix} N_1^0 \\ N_2^0 \\ N_6^0 \end{Bmatrix}, \tag{9.29}$$

the value of q_i will be

$$k\, q_i^0 \qquad (i = 1, ..., L). \tag{9.30}$$

The in-plane loads cannot be increased beyond $\overline{k}$, where

$$\overline{k} = \frac{1}{\max q_i^0}, \quad (i = 1, ..., L) \tag{9.31}$$

From eqns (9.29) and (9.31), it is seen that if the laminate is designed under a given loading so that $\max q_i$ $(i = 1, ..., L)$ is minimized, then the load at which one of the laminae fails can be maximized. If moreover, the laminate is designed to use a fixed volume of material, then the optimum design makes the most effective use of the available composite material.

To achieve the above goal, we formulate the following optimization problem

$$\underset{\theta_i, t_i}{\text{Max}}\, k \equiv \underset{\theta_i, t_i}{\text{Min}} \left\{ \max_i q_i \right\} \tag{9.32}$$

subject to

$$-\frac{\pi}{2} \leq \theta_i \leq \frac{\pi}{2} \tag{9.33}$$

$$\sum_i t_i = h \qquad (i = 1, ..., L) \tag{9.34}$$

$$\underline{t} \leq t_i \leq \overline{t} \tag{9.35}$$

where θ_i and t_i $(i = 1, ..., L)$ are the ply angles and thicknesses, respectively. They form the design variable vector in this optimization problem. h is the prescribed total thickness of the laminate.

The objective function of the above minimax optimization problem (9.32)-(9.35) is not differentiable with respect to the design variables. This is because of the piecewise continuous functions appearing in the stress norm q_i (see relations (9.27), (9.23), (9.22), (9.21), and (9.20)).

9.3.2 Treatment of Non-differentiability of *In Situ* Strength Parameters

As the bound-formulation technique (Olhoff, 1989) that will be used for the solution of the problem (9.32)-(9.35) requires the evaluation of gradients, it is expedient to introduce continuous functions with continuous first order derivatives. For this we proceed as follows. Let

$$F = \text{Min}[f_1, f_2] \tag{9.36}$$

where f_1 and f_2 are scalar functions in $2L$-dimension space. Next, let us construct a function of f_1 and f_2 in such a way that not only is this function as close as possible to F but so are its first derivatives. Such a function could, for instance, be the simple weighted expression

$$\mathcal{F} = \alpha(f_1, f_2)\, f_1 + \beta(f_1, f_2)\, f_2 \tag{9.37}$$

where the functions $\alpha(f_1, f_2)$ and $\beta(f_1, f_2)$ are continuous and at least first-order differentiable. Moreover, they must satisfy the following conditions:

$$f_1 > f_2: \quad \alpha \to 0; \quad \beta \to 1 \tag{9.38}$$

$$f_1 < f_2: \quad \alpha \to 1; \quad \beta \to 0 \tag{9.39}$$

$$f_1 = f_2: \quad \alpha = \beta \tag{9.40}$$

$$\alpha + \beta \equiv 1 \tag{9.41}$$

and

$$f_1 > f_2: \quad \mathcal{F}_x \to f_{2x} \tag{9.42}$$

$$f_1 < f_2: \quad \mathcal{F}_x \to f_{1x} \tag{9.43}$$

where subscript x denotes differentiation with respect to x (a design variable). The conditions (9.38)–(9.43) are met for instance, by the following functions $\alpha(f_1, f_2)$ and $\beta(f_1, f_2)$:

$$\alpha = \frac{1}{2}[1 - \tanh A(f_1 - f_2)] \tag{9.44}$$

$$\beta = \frac{1}{2}[1 + \tanh A(f_1 - f_2)] \tag{9.45}$$

where A is a judiciously chosen large positive number.

Functions (9.44) and (9.45) identically satisfy the conditions (9.40)–(9.41). The satisfaction of conditions (9.38)–(9.39) is dependent on the choice of A. In the numerical computations, where the step length is finite, conditions (9.38)–(9.39) can be satisfied to any desired degree of accuracy. It is easily verified that the functions (9.44) and (9.45), together with the conditions (9.38)–(9.39), if these have been satisfied to the desired accuracy, will lead to the fulfilment of the conditions (9.42) and (9.43). The influence of A on the closeness of the weighted function of the form (9.37) to the original expression (9.36) is examined graphically in Appendix F.

f_t and f_s in (9.22) and (9.23) are now modified to read

$$f_t(\Delta\theta) = \alpha_t \frac{\sin^2(\Delta\theta_a)}{1 + \sin^2(\Delta\theta_a)} + \beta_t \frac{\sin^2(\Delta\theta_b)}{1 + \sin^2(\Delta\theta_b)} \tag{9.46}$$

$$f_s(\Delta\theta) = \alpha_s \frac{\sin^2(2\Delta\theta_a)}{1 + \sin^2(2\Delta\theta_a)} + \beta_s \frac{\sin^2(2\Delta\theta_b)}{1 + \sin^2(2\Delta\theta_b)} \tag{9.47}$$

where α_t, β_t, α_s and β_s are

$$\alpha_t = \frac{1}{2}\left\{1 - \tanh A\left[\frac{\sin^2(\Delta\theta_a)}{1 + \sin^2(\Delta\theta_a)} - \frac{\sin^2(\Delta\theta_b)}{1 + \sin^2(\Delta\theta_b)}\right]\right\} \tag{9.48}$$

$$\beta_t = \frac{1}{2}\left\{1 + \tanh A\left[\frac{\sin^2(\Delta\theta_a)}{1 + \sin^2(\Delta\theta_a)} - \frac{\sin^2(\Delta\theta_b)}{1 + \sin^2(\Delta\theta_b)}\right]\right\} \tag{9.49}$$

$$\alpha_s = \frac{1}{2}\left\{1 - \tanh A\left[\frac{\sin^2(2\Delta\theta_a)}{1 + \sin^2(2\Delta\theta_a)} - \frac{\sin^2(2\Delta\theta_b)}{1 + \sin^2(2\Delta\theta_b)}\right]\right\} \tag{9.50}$$

$$\beta_s = \frac{1}{2}\left\{1 + \tanh A\left[\frac{\sin^2(2\Delta\theta_a)}{1 + \sin^2(2\Delta\theta_a)} - \frac{\sin^2(2\Delta\theta_b)}{1 + \sin^2(2\Delta\theta_b)}\right]\right\} \tag{9.51}$$

We can now use the bound-formulation method to solve the optimization problem (9.32)–(9.35). In this method a new variable γ is introduced as the objective function which is then minimized with respect to the augmented vector of design variables $(\theta_1, ..., \theta_L, t_1, ..., t_L, \gamma)^T$. The original minimax statement of the objective function (9.32) is replaced by constraints $q_i \leq \gamma$. In this way the original optimization problem (9.32)–(9.35) is replaced by the following minimization problem:

$$\underset{\theta_i, t_i, \gamma}{\text{Min}} \quad \gamma \tag{9.52}$$

subject to

$$
\begin{aligned}
q_i - \gamma &\leq 0 && (9.53)\\
-\frac{\pi}{2} \leq \theta_i &\leq \frac{\pi}{2} && (9.54)\\
\sum_i t_i &= h \qquad (i = 1, ..., L) && (9.55)\\
\underline{t} \leq t_i &\leq \bar{t} && (9.56)
\end{aligned}
$$

9.3.3 Sensitivity Analysis

For the solution of the optimization problem (9.52)–(9.56), all the necessary gradients (sensitivities) of the objective function and constraints with respect to γ can be readily calculated analytically. Those of q_i with respect to θ_i and t_i are more complicated. We denote the vector of design variables $(\theta_1, ..., \theta_L, t_1, ..., t_L, \gamma)^T$ as $(x_1, ..., x_{2L}, x_{2L+1})^T$. The derivatives of q_i^2 with respect to the design variables can be expressed as

$$
\begin{aligned}
\frac{\partial q_i^2}{\partial x_j} &= \frac{2Y}{Y_t^2}\frac{\partial Y}{\partial x_j} + \frac{2S}{S_c^2}\frac{\partial S}{\partial x_j} - \\
&\quad -\frac{2Y^2}{Y_t^3}\frac{\partial Y_t}{\partial x_j} - \frac{2S^2}{S_c^3}\frac{\partial S_c}{\partial x_j}, \qquad (i = 1, ..., L; j = 1, ..., 2L) \qquad (9.57)
\end{aligned}
$$

where the derivatives of the stresses Y and S are computed using their appropriate expressions from the classical lamination theory (Tsai & Hahn, 1980, see § 3.7). In principle, these derivatives can also be analytically calculated, but in the optimization procedure used here they will be evaluated numerically to any desired accuracy. The derivatives of the *in situ* strength parameters Y_t and S_c are calculated as follows

$$
\left.
\begin{aligned}
\frac{\partial Y_{ti}}{\partial x_j} &= Y_t^0 A \frac{1}{t_i^B}\frac{\partial f_t(\Delta\theta)}{\partial x_j}\\
\frac{\partial S_{ci}}{\partial x_j} &= S_c^0 C \frac{1}{t_i^D}\frac{\partial f_s(\Delta\theta)}{\partial x_j}
\end{aligned}
\right\} \quad (i, j = 1, ..., L) \qquad (9.58)
$$

$$
\left.
\begin{aligned}
\frac{\partial Y_{ti}}{\partial x_j} &= -A\,B\,Y_t^0 \frac{f_t(\Delta\theta)}{x_j^{B+1}}\delta_{ik}\\
\frac{\partial S_{ci}}{\partial x_j} &= -C\,D\,S_c^0 \frac{f_s(\Delta\theta)}{x_j^{D+1}}\delta_{ik}
\end{aligned}
\right\} \quad (i = 1, ..., L; j = L+1, ..., 2L; k = j - L) \qquad (9.59)
$$

in which $\frac{\partial f_t(\Delta\theta)}{\partial x_j}$ and $\frac{\partial f_s(\Delta\theta)}{\partial x_j}$ are calculated from the expressions (9.46)–(9.51). δ_{ik} is the Kronecker delta, ($\delta_{ik} = 1$, $i = k$; $\delta_{ik} = 0$, otherwise).

9.3.4 Design Examples

The above optimization procedure was applied to the optimum design of a multidirectional laminate shown in Figure 9.9. Figure 9.9(a) shows the in-plane loads, and Figure 9.9(b) shows the detailed configuration of one half of the laminate. This laminate is composed of L laminae of different ply angles and thicknesses. It is physically symmetric with respect to its geometric middle plane, i.e. the laminae are stacked in the order $(\theta_{L/2}/.../\theta_1)_s$. The strength constants used in the calculation of the *in situ* strengths are adapted from Chang & Lessard (1991), i.e. $Y_t^0 = 44.5$ MPa, $S_c^0 = 48.2$ MPa, $A = 1.3$, $B = 0.7$, $C = 2.0$ and $D = 1.0$.

Because of the highly nonlinear nature of the functions q_i and of the fact that they can attain their minima at different combinations of design variables, the above optimization problem can have many local minima. In the computational scheme, the global minimum is sought by a random search technique. The optimization process is begun from different initial design points $(x_j^0)_m^T$ $(j = 1, ..., 2L; m = 1, ..., M)$ (m denotes the mth initial design point) in the space of design variables $\{x_j\}^T$ $(j = 1, ..., 2L)$. These random initial design points are chosen so that they are uniformly distributed in the design space, and the global minimum is sought from among the local minima corresponding to these randomly chosen initial designs. In all cases, M was chosen to be equal to 120. As will be seen later, these initial designs cover the design space with sufficient density to give the global optimum design when the number of unknown ply angles is not excessive ($\theta_{L/2} \leq 5$). When the number of unknown ply angles exceeds this value, the optimization techniques converge to what appears to be a local optimum solution. This will be further discussed below when we consider examples with six or more unknown ply angles.

The optimization problem was solved by standard mathematical programming techniques available in a general-purpose package ADS (automated design synthesis) (Vanderplaats, 1987). In the following, we present three examples of the optimum design of symmetric multidirectional laminates under in-plane loads. Because of symmetry, only one half of the laminate needs to be considered. Therefore, in the sequel the number of the ply angles and/or thicknesses will refer to only one half of the laminate. In the first two examples, the number of ply angles θ_i varies between four and eight. The thickness of each lamina is however assumed to be constant and equal to 0.140 mm so that the total number of design variables ranges between four and eight. In the third example, the number of the ply angles is 4, and both the ply angles θ_i and thicknesses t_i are chosen as variables. Solution of each example problem required numerous calls to ADS.

(i) **A Symmetric Laminate of 4 or 5 Ply Angles**

The change of the load factor k during the optimization process for four in-plane loading combinations is shown in Figures 9.10 and 9.11, respectively. The initial guesses to ply angles (chosen pseudo-randomly) and their final optimum values, and the optimum load factor $\overline{k}$, i.e.

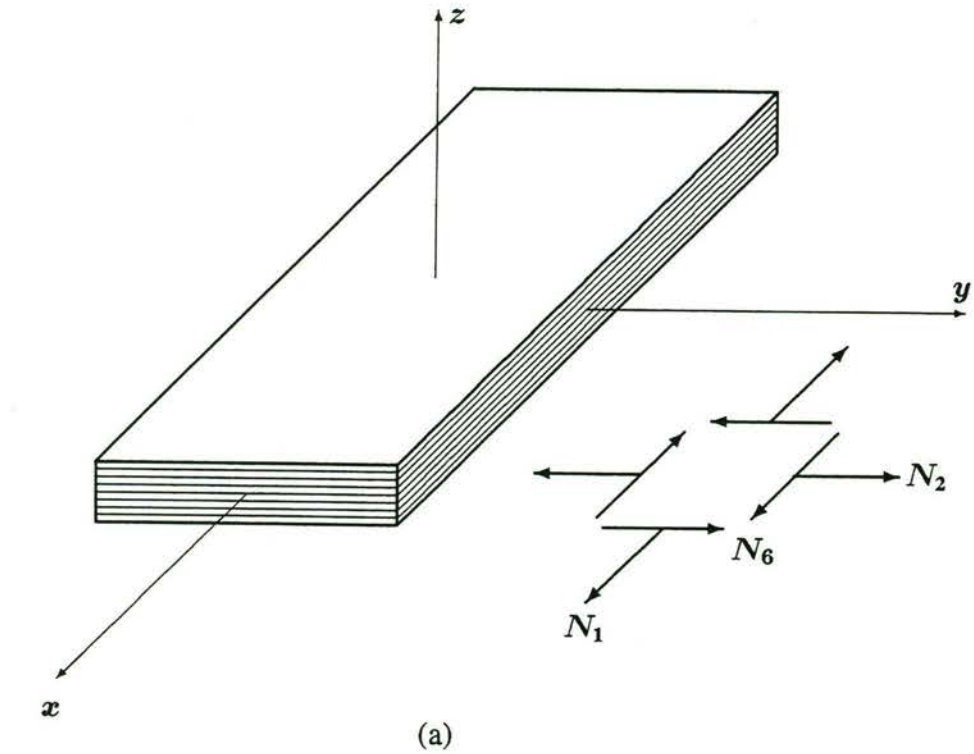

(a)

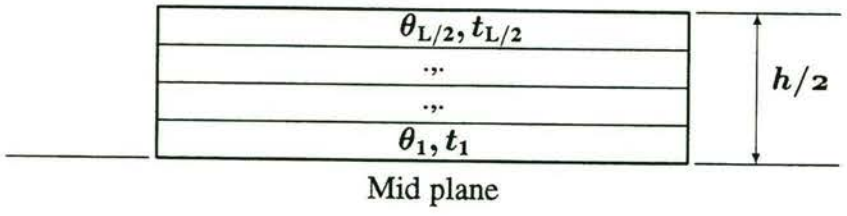

(b)

Figure 9.9: The laminate configuration. The in-plane loading shown represents the resultant forces over the thickness

k_{max}, are given in Tables 9.1 and 9.2, respectively.

Table 9.1: Summary of optimized ply angles in a symmetric laminate of 4 ply angles

In-plane loading	Initial design $\theta_1, \theta_2, \theta_3, \theta_4$	Final design $\theta_1, \theta_2, \theta_3, \theta_4$	k_{max}	$\frac{k_{max}}{k_{in}}$
a	27.04,-32.26,63.31,11.40	62.68,-54.20,81.23,-1.96	1.59	2.18
b	20.00,-46.46,40.55,45.62	32.30,-56.61,-7.78,33.87	1.86	1.98
c	-46.92,73.43,-80.42,47.62	-27.46,57.58,-43.61,20.11	1.34	4.06
d	63.77,79.07,26.81,84.40	45.45,51.72,43.38,39.58	10.21	13.43

Table 9.2: Summary of optimized ply angles in a symmetric laminate of 5 ply angles

In-pl. load.	Initial design $\theta_1, \theta_2, \theta_3, \theta_4, \theta_5$	Final design $\theta_1, \theta_2, \theta_3, \theta_4, \theta_5$	k_{max}	$\frac{k_{max}}{k_{in}}$
a	79.77,-34.34,24.31,-22.12,-64.08	45.90,-22.64,30.14,-19.74,-80.81	1.64	1.55
b	22.82,-60.60,-53.47,-70.64,-40.37	31.38,-58.89,28.50,-31.42,28.62	2.19	4.76
c	-71.85,67.20,38.61,71.85,64.68	-29.80,55.69,-44.26,42.20,-2.68	1.37	7.00
d	80.14,33.04,57.99,35.35,86.63	48.06,42.09,45.25,42.58,47.18	21.50	19.91

The in-plane load vector $[N_1^0, N_2^0, N_6^0]^T$ was chosen so that the values of q_i $(i = 1, .., 4)$ were of the order 1 during most of the optimization process. Figures 9.10 and 9.11 clearly show the significant improvement in the load carrying capacity of the laminate achieved through optimization. For the loading case d, the improvement is particularly dramatic. Intuitively, the best configuration of the laminate for this loading would appear to be the one in which all ply angles are equal to $+45^0$ (Figure 9.12). When all ply angles are equal to $+45^0$, the stress norm q_i for each ply in the laminate (eqn (9.27)) will be identically equal to zero, that is to say, the optimum value of the objective function γ (9.52) will be exactly equal to zero. Although this design is obviously the global solution, the numerical optimization techniques have difficulty in reaching this exact solution because of round-off errors. For the case of 5 unknown ply angles under loading case d, the optimum value of the objective function γ is 0.01, and the values of q_i^2 are $(q_1^2, q_2^2, q_3^2, q_4^2, q_5^2)^T = (0.0022, 0.0015, 0.0002, 0.0011, 0.0013)^T$. It is seen that the values of q_i are very small but not exactly zero. Therefore, the optimization process may be regarded to have converged to the global optimum solution within the accuracy of numerical calculations.

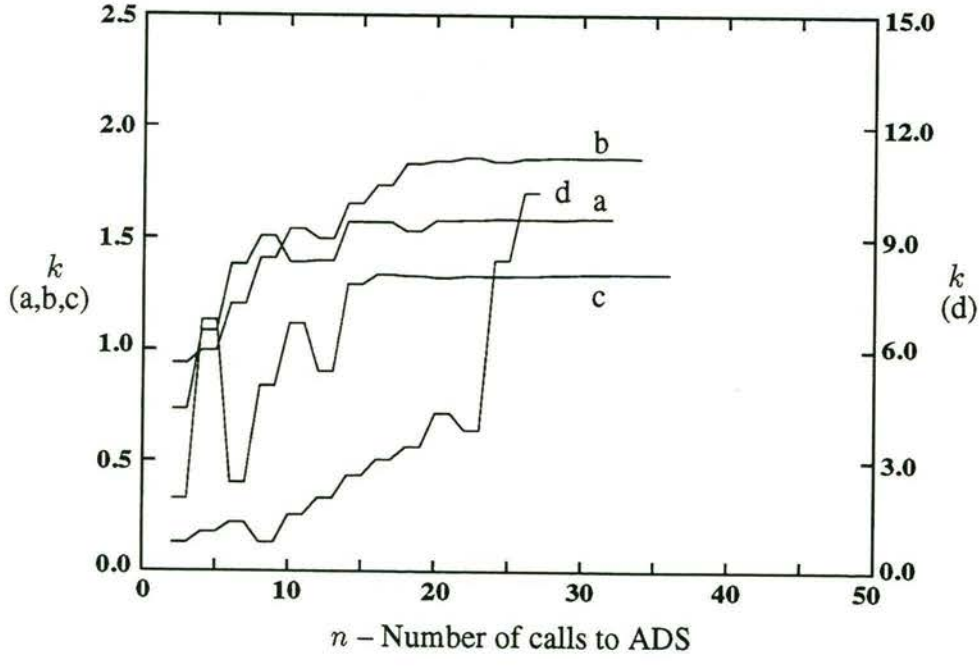

Figure 9.10: Evolution of load factor k for a symmetric laminate of 4 ply angles during optimization for four loading cases: (a) $[N_1^0, N_2^0, N_6^0]^T = [200, 200, 0]^T$ kN/m; (b) $[200,0,200]^T$ kN/m; (c) $[400,200,0]^T$ kN/m; and (d) $[200,200,200]^T$ kN/m

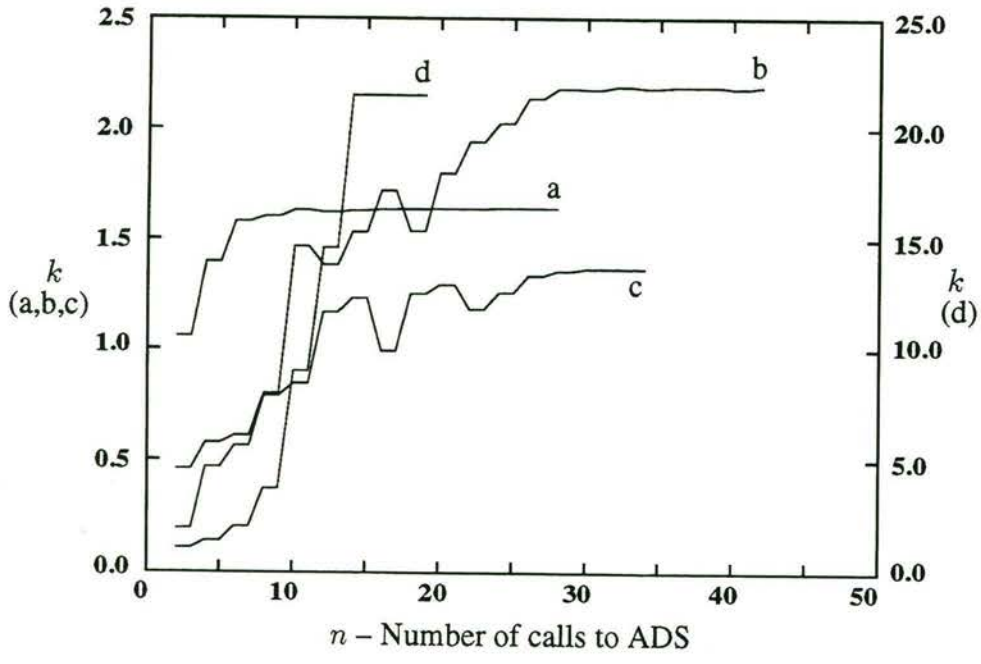

Figure 9.11: Evolution of load factor k for a symmetric laminate of 5 ply angles during optimization for four loading cases: (a) $[N_1^0, N_2^0, N_6^0]^T = [250, 250, 0]^T$ kN/m; (b) $[250,0,250]^T$ kN/m; (c) $[500,250,0]^T$ kN/m; and (d) $[250,250,250]^T$ kN/m

On the other hand, from a strength point of view, the configuration of identical ply angles is not plausible because of the "clustering effect" that reduces the strength of the unidirectional lamina in the laminate. It is also noted that there is a difference between the ply angles of the surface lamina and the lamina immediately beneath it. Such a design prevents a crack in the interior lamina from running through the thickness of the laminate and reaching the surface.

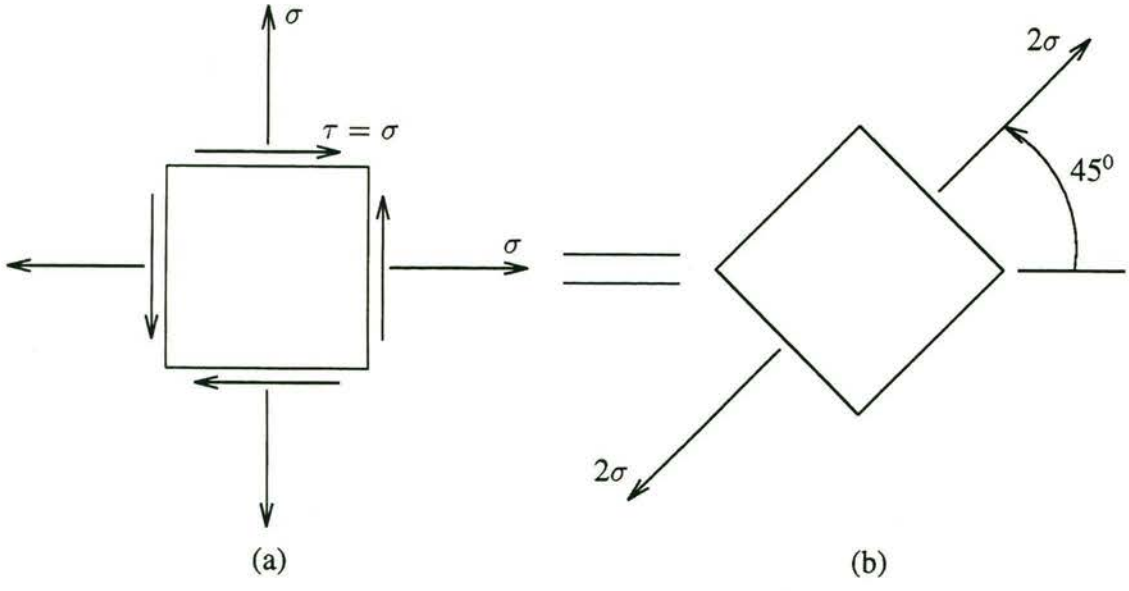

Figure 9.12: The stress state (a) referred to as loading case d in Figures 9.10–9.11, 9.13–9.16 and Tables 9.1–9.9 is equivalent to the unidirectional tension (b)

In Tables 9.1 and 9.2, k_{in} is the load factor corresponding to the initial design and k_{max} the optimum design. The ratio k_{max}/k_{in} indicates the relative enhancement in the loading carrying capacity of the optimally designed laminate. The effect of optimization is manifested in two ways. First, as the optimization procedure aims at reducing the transverse in-plane and shear stresses appearing in the failure criterion (9.26) of the lamina, a considerably large stress is directed along the fibre direction of every lamina in the optimally designed laminate. Secondly, the stress norms q_i $(i = 1, .., 4 \text{ or } 5)$ of individual unidirectional laminae in the laminate have almost the same value. For example, for 5 unknown ply angles under load case c, the values of q_i^2 are $(q_1^2, q_2^2, q_3^2, q_4^2, q_5^2)^T = (0.532, 0.533, 0.532, 0.532, 0.536)^T$. These two observations, although based on numerical computations, would indicate that optimization is tending to create a 'smart' composite. In an anisotropic composite it aims at distributing the stresses (in magnitude and direction) according to the strengths of the material in different locations and directions, i.e. "the strongest carries the largest share". It also aims at achieving a uniform stress norm for all laminae. This should not however be confused with the uniform average strain energy density criterion well-known in structural optimization (Venkayya *et al.*, 1968; Venkayya, 1971).

(ii) A symmetric laminate of 6, 7 or 8 ply angles

In minimizing the compliance of a symmetric angle-ply laminate subjected to flexural loading, Cheng (1986) found that the number of different angles of unidirectional laminae in an optimum laminate is no more than 4. The present example is intended to study the influence of the number of different ply angles on the results of optimization. The evolution of the load factor k is shown in Figures 9.13, 9.14 and 9.15, respectively when the number of unknown ply angles is 6, 7 or 8. The numerical results are given in Tables 9.3, 9.4 and 9.5, respectively. The thickness of the laminate here is larger than that in example (i). In order to maintain q_i at approximately the same value as in example (i), the prescribed loadings $[N_1^0, N_2^0, N_6^0]^T$ used in this example are increased in proportion to the thickness of the laminate.

Table 9.3: Summary of 6 optimized ply angles in symmetric laminate

In-plane loading	Initial design $\begin{pmatrix} \theta_1 & \theta_2 & \theta_3 \\ \theta_4 & \theta_5 & \theta_6 \end{pmatrix}$	Final design $\begin{pmatrix} \theta_1 & \theta_2 & \theta_3 \\ \theta_4 & \theta_5 & \theta_6 \end{pmatrix}$	k_{max}	$\frac{k_{max}}{k_{in}}$
a	88.32,-76.59,36.77 -56.06,60.07,-1.93	46.95,-54.49,69.92 -53.13,69.67,-4.31	1.66	1.57
b	87.94,-60.29,83.41 10.39,-52.10,23.43	34.78,-58.20,37.73 21.99,-57.66,33.42	2.40	3.23
c	72.46,-24.38,59.52 -25.12,40.38,-37.48	29.59,-48.53,39.02 -48.37,34.27,-17.85	1.40	1.97
d	23.03,66.31,89.44 -64.13,68.94,67.41	46.74,48.75,49.28 17.54,49.28,48.36	4.31	5.16

The 8 optimized angles in the third column in Table 9.5 do not exactly merge into only 4 different values. Nevertheless, they show a trend towards the selection of a finite set of angles. For example, the 8 optimized angles for loading case a are roughly from a set of four angles, i.e. $(-90^0, -30^0, 0^0, 40^0)$. Those for loading cases b, c and d are basically from the sets $(-57^0, 30^0, 37^0, 90^0)$, $(-40^0, -25^0, 11^0, 40^0, 50^0)$ and $(12^0, 27^0, 50^0)$. Besides Cheng's prediction mentioned above, Miki (1985) also showed that in designing an angle-ply laminate for a required flexural stiffness, two groups of ply angles, i.e. $(+\theta_1/-\theta_1)$ and $(+\theta_2/-\theta_2)$, are enough. The difference between the strength design dealt with in this Thesis and the stiffness design of Miki (1985) is that the strength depends on the size and location of the lamina in the laminate, whereas stiffness is a global (integral) characteristic of the laminate as a whole.

It is noted that not all the optimum ply angles for loading case d are close to 45^0 in each of the three cases (θ_i, $i = 1, ..., 6$ or 7 or 8). As discussed in example (i), the global optimum

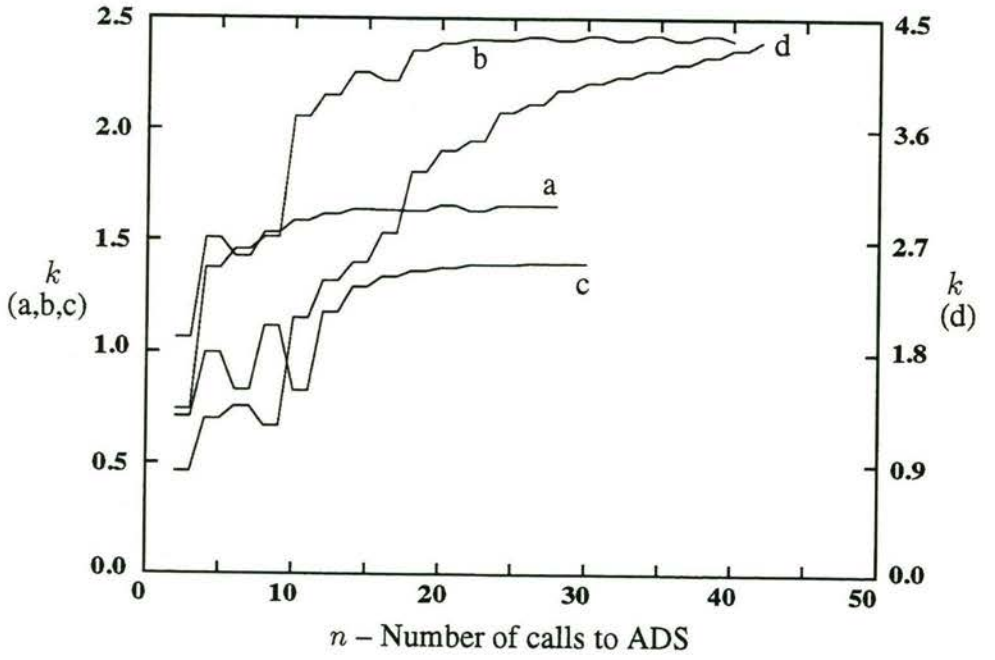

Figure 9.13: Evolution of load factor k for a symmetric laminate of 6 ply angles during optimization for four loading cases: (a) $[N_1^0, N_2^0, N_6^0]^T = [300, 300, 0]^T$ kN/m; (b) $[300,0,300]^T$ kN/m; (c) $[600,300,0]^T$ kN/m; and (d) $[300,300,300]^T$ kN/m

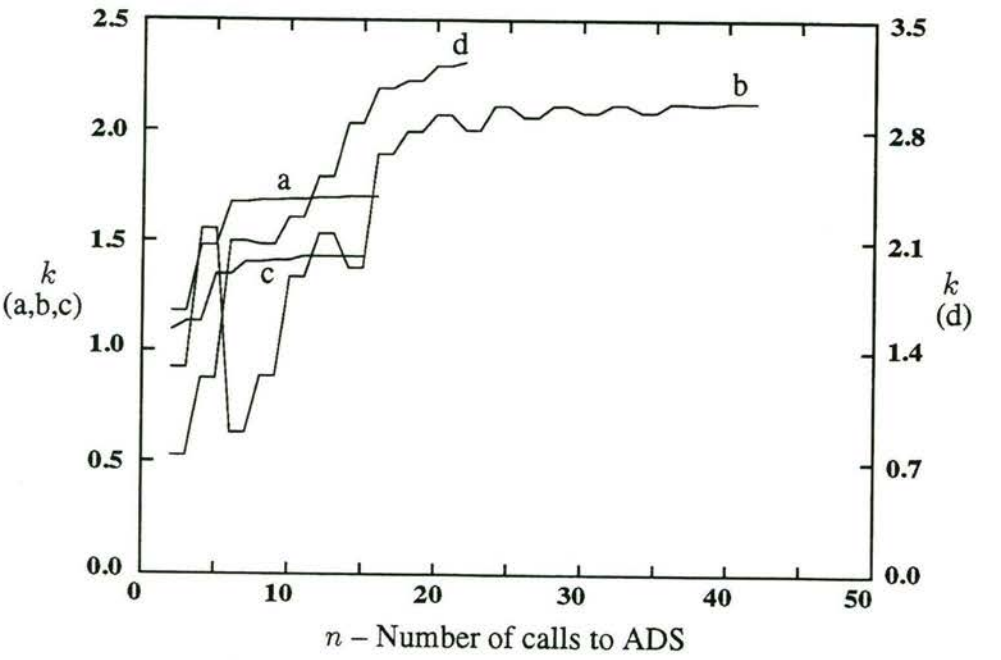

Figure 9.14: Evolution of load factor k for a symmetric laminate of 7 ply angles during optimization for four loading cases: (a) $[N_1^0, N_2^0, N_6^0]^T = [350, 350, 0]^T$ kN/m; (b) $[350,0,350]^T$ kN/m; (c) $[700,350,0]^T$ kN/m; and (d) $[350,350,350]^T$ kN/m

solution for loading case d is that all the ply angles are 45^0, no matter how many ply angles are chosen. Therefore, the solutions for loading case d for the cases when $\theta_{L/2} > 5$ must be local optima. The major reason for the presence of local optima is the multi-modal nature of the problem as a result of the high nonlinearity of the stress norm q_i with respect to the ply angles θ_i. When the number of the ply angles is large, the pseudo-randomly chosen initial designs do not cover the design space sufficiently densely as to lead to the global optimum solution. The situation did not improve even when 400 initial designs were chosen pseudo-randomly.

Table 9.4: Summary of 7 optimized ply angles in symmetric laminate

In-plane loading	Initial design $\begin{pmatrix} \theta_1 & \theta_2 & \theta_3 \\ \theta_4 & \theta_5 & \theta_6 \ \theta_7 \end{pmatrix}$	Final design $\begin{pmatrix} \theta_1 & \theta_2 & \theta_3 \\ \theta_4 & \theta_5 & \theta_6 \ \theta_7 \end{pmatrix}$	k_{max}	$\frac{k_{max}}{k_{in}}$
a	72.46,-24.38,59.52 -25.12,40.38,-37.48,-67.93	60.16,-16.97,41.23 -18.45,39.75,-22.47,-76.01	1.70	1.44
b	88.32,-76.59,36.77 -56.06,60.07,-1.93,34.64	28.68,-56.33,29.18 -56.90,30.39,-4.72,35.35	2.13	2.32
c	-48.38,52.77,-80.81 26.09,-23.17,40.63,-5.19	-30.71,45.93,-40.31 46.31,-40.14,38.67,-3.47	1.43	1.31
d	17.30,-7.85,29.16 44.80,30.50,14.37,36.08	46.10,-1.31,46.15 48.99,49.91,47.91,49.30	3.23	4.38

Table 9.5: Summary of 8 optimized ply angles in symmetric laminate. The prescribed loadings $[N_1^0, N_2^0, N_6^0]^T$ are twice those of example (i)

In-plane loading	Initial design $\begin{pmatrix} \theta_1 & \theta_2 & \theta_3 & \theta_4 \\ \theta_5 & \theta_6 & \theta_7 & \theta_8 \end{pmatrix}$	Final design $\begin{pmatrix} \theta_1 & \theta_2 & \theta_3 & \theta_4 \\ \theta_5 & \theta_6 & \theta_7 & \theta_8 \end{pmatrix}$	k_{max}	$\frac{k_{max}}{k_{in}}$
a	-44.11,87.56,33.79,71.26 -45.26,-60.16,-52.71,28.82	-3.08,-90.00,-28.51,88.00 -28.49,-90.00,-27.59,40.05	1.70	2.17
b	39.13,-13.67,54.59,87.60 26.93,8.42,-52.88,76.60	36.66,-57.68,36.47,90.00 37.31,24.58,-57.77,31.65	2.22	2.64
c	-48.36,52.77,-80.79,26.07 -23.15,40.62,-5.16,38.39	-26.94,49.26,-37.54,40.09 -42.78,55.36,-24.16,10.86	1.40	1.75
d	80.21,56.30,79.78,-66.57 61.31,5.17,84.22,17.93	49.29,49.27,49.29,26.60 49.42,11.91,50.14,49.33	3.62	4.04

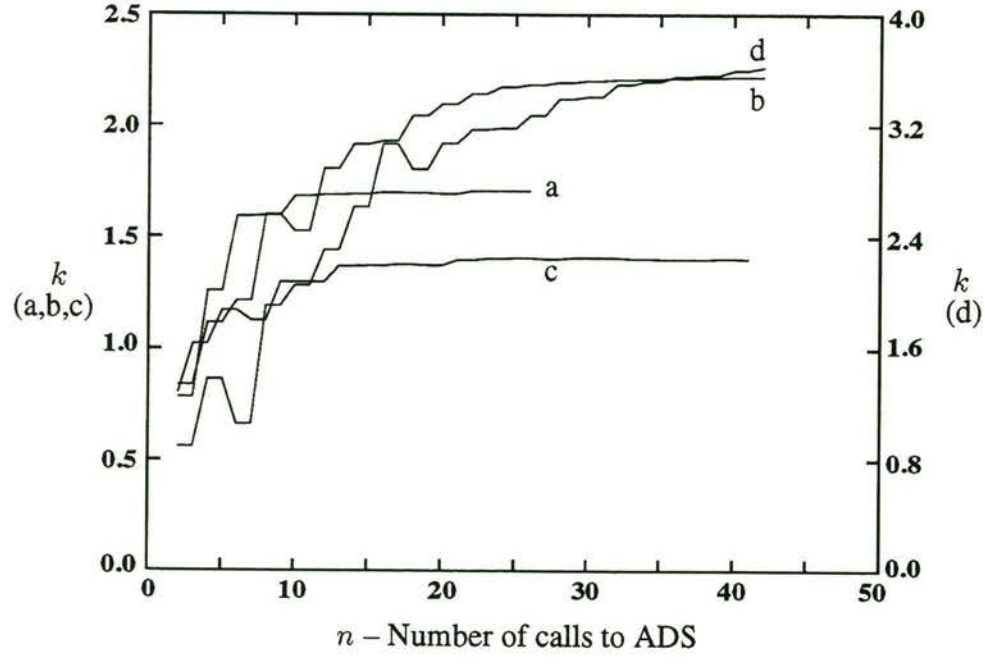

Figure 9.15: Evolution of load factor k for a symmetric laminate of 8 ply angles during optimization for four loading cases: (a) $[N_1^0, N_2^0, N_6^0]^T = [400, 400, 0]^T$ kN/m; (b) [400,0,400]^T kN/m; (c) [800,400,0]^T kN/m; and (d) [400,400,400]^T kN/m

(iii) A symmetric 4-ply laminate with variable angles and thicknesses

In this example, we allow both the ply angles θ_i and thicknesses t_i $(i = 1, 2, 3, 4)$ of the laminae to vary in the optimization process. The half thickness $h/2$ of the laminate is set equal to $20\,t_0$. The lower and upper bounds of t_i are set equal to t_0 and $h/2$, respectively. The evolution of the load factor k during the process of optimization is shown in Figure 9.16. The numerical results are given in Table 9.6. The prescribed loadings $[N_1^0, N_2^0, N_6^0]^T$ are 5 times those in the first example. The thicknesses of the laminae seem to change significantly from the initial values which were pseudo-randomly chosen. It is noted that the sum of the initial ply thicknesses is less than the prescribed half thickness $h/2$ of the laminate. However, the sum of the optimized ply thicknesses is always equal to $h/2$ for the four loading cases. The optimized ply angles are different from those of example (i) when the thicknesses were fixed. Another feature is that the relative enhancement of the load factor k_{max}/k_{in} in this example is much larger than that in the first example. This can be attributed to the small initial ply thicknesses which result in a small initial load factor k_{in} and to the flexibility offered by the large number of design variables (eight instead of four or five in example (i)).

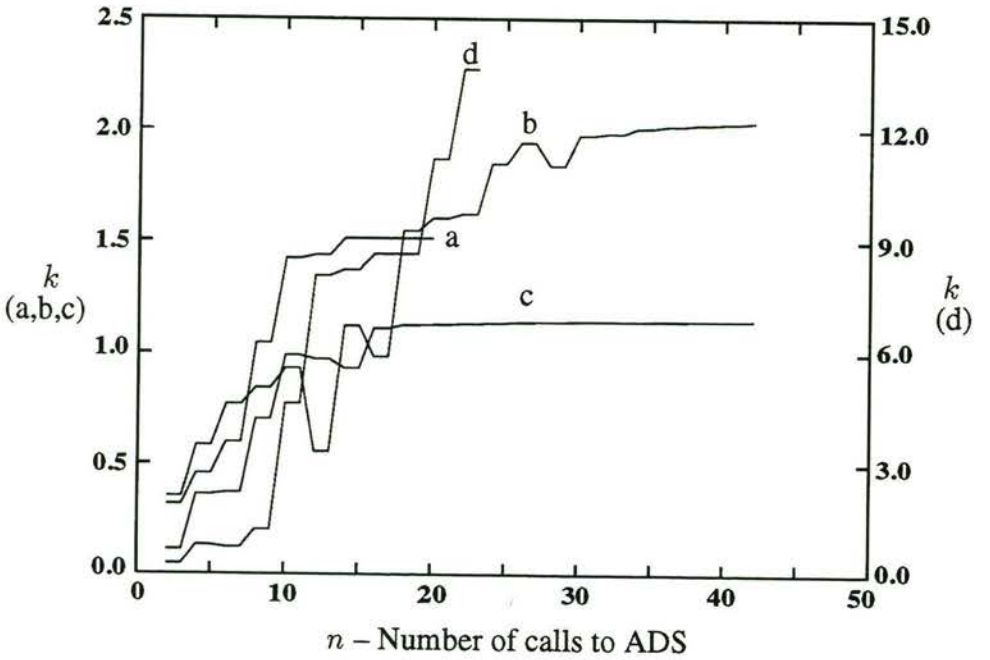

Figure 9.16: Evolution of load factor k for a symmetric laminate when ply angles and thicknesses are design variables during optimization for four loading cases: (a) $[N_1^0, N_2^0, N_6^0]^T = [1000, 1000, 0]^T$ kN/m; (b) [1000,0,1000]^T kN/m; (c) [2000,1000,0]^T kN/m; and (d) [1000,1000,1000]^T kN/m

9.3.5 Sensitivity of Optimum Design

From a mathematical point of view, the solution (i.e. the optimum design variables) of a constrained optimization problem may fall at a point corresponding to an extremum of the objective function or at the boundary of the feasible region. In both cases, the optimum design can become quite sensitive to changes in the design variables. If this is the case for the optimum design of the composite laminates, then a minor deviation of the ply angles and/or thicknesses from the theoretical optimum design can result in a dramatic loss of the load carrying capacity of the laminates. Therefore, it is prudent to check the sensitivity of the optimum design with respect to design variables. This can be done by rounding off the optimum ply angles to the nearest commonly used values 0^0, 30^0, 45^0, 60^0 and 90^0, and the optimum thicknesses of laminae to the nearest multiples of the thickness of a single ply (0.14 mm), that is, the optimum design is compared with a nearly-optimum design. The results of three sensitivity analyses are given in Tables 9.7, 9.8 and 9.9, respectively.

A comparison of the mathematical optimum design with the nearly-optimum design shows that the load factors k_{max} for the latter are always less than those for the former under loading

Table 9.6: Summary of optimized ply angles and thicknesses in symmetric laminate. The prescribed loadings $[N_1^0, N_2^0, N_6^0]^T$ are 5 times those of example (i)

In-plane loading	Initial design $\begin{pmatrix} \theta_1 & \theta_2 & \theta_3 & \theta_4 \\ t_1 & t_2 & t_3 & t_4 \end{pmatrix}$	Final design $\begin{pmatrix} \theta_1 & \theta_2 & \theta_3 & \theta_4 \\ t_1 & t_2 & t_3 & t_4 \end{pmatrix}$	k_{max}	$\frac{k_{max}}{k_{in}}$
a	40.74,-76.20,80.44,-3.55 0.189,0.424,0.255,0.140	38.39,-58.61,47.95,-9.85 0.524,1.175,0.738,0.363	1.51	4.78
b	-72.14,-60.56,42.46,7.85 0.364,0.677,0.189,0.521	28.72,-56.54,35.02,30.41 0.541,0.768,0.398,1.094	2.04	5.77
c	66.41,75.63,-83.31,28.59 0.624,0.356,0.268,0.291	-35.20,35.11,-59.54,15.51 0.924,0.982,0.399,0.496	1.15	10.45
d	79.35,19.19,79.18,51.39 0.144,0.306,0.384,0.147	48.13,43.64,48.14,38.59 0.426,0.901,1.042,0.432	13.64	49.30

Table 9.7: Nearly-optimum ply angles in a symmetric laminate of 4 ply angles. The mathematically optimized ply angles are given in Table 9.1

In-plane loading	Nearly-Optimum Design θ_1	θ_2	θ_3	θ_4	k_{max}
a	60	-60	90	0	1.35
b	30	-60	0	30	1.51
c	-30	60	-45	30	0.99
d	45	45	45	45	∞

cases a, b, and c, but the difference is not large. This indicates that the design near the optimum solution is fairly stable and not very sensitive to changes in the design variables. The situation for loading case d is quite different. The nearly-optimum design in which all the laminae are oriented at 45^0 will carry as much load as possible. The reason for this is simple. First, under this loading condition, the laminate is actually subjected to a unidirectional tension along the 45^0 direction (Figure 9.11). Secondly, the strength criterion (9.26) does not take into account the stress along the direction of the fibre in a unidirectional laminae. As long as there is no normal stress in the transverse direction and no in-plane shear stress, the lamina is safe no matter how much stress is exerted along the longitudinal 45^0 direction. So, if a laminate is subjected only to a unidirectional tension along the direction 45^0, the best laminate is the one in which

the fibres in all laminae point in this direction. However, such a laminate cannot be subjected to any transverse and in-plane shear stresses at all.

Table 9.8: Nearly-optimum ply angles in a symmetric laminate of 5 ply angles. The mathematically optimized ply angles are given in Table 9.2

In-plane loading	Nearly-Optimum Design θ_1	θ_2	θ_3	θ_4	θ_5	k_{max}
a	45	-30	30	-30	-90	1.54
b	30	-60	30	-30	30	2.14
c	-30	45	-45	45	0	1.24
d	45	45	45	45	45	∞

Table 9.9: Nearly-optimum ply angles and thicknesses in symmetric laminate. The prescribed loadings $[N_1^0, N_2^0, N_6^0]^T$ are 5 times those in example (i). The mathematically optimized ply angles and thicknesses are given in Table 9.6

In-plane loading	Nearly optimum design $\begin{pmatrix} \theta_1 & \theta_2 & \theta_3 & \theta_4 \\ t_1 & t_2 & t_3 & t_4 \end{pmatrix}$				k_{max}
a	45 0.56	-60 1.12	45 0.70	0 0.42	1.39
b	30 0.56	-60 0.70	30 0.42	30 1.12	1.70
c	-30 0.98	30 0.98	-60 0.42	30 0.42	1.00
d	45 0.42	45 0.98	45 0.98	45 0.42	∞

9.4 Concluding Remarks

This exposition presented a three-stage procedure for the optimum design of multidirectional laminates. In the first stage, a fracture mechanics analysis was performed on a cracked angle-ply laminate. The results of this analysis revealed the mutual constraining effect of the unidirectional

laminae in a laminate, so that the *in situ* strength of each lamina is enhanced. In the second stage, the above results and experimental observations were used to propose a set of *in situ* strength parameters and a failure criterion. Finally, an optimization problem was formulated in which the load bearing capacity of symmetric laminates was maximized. This minimax optimization problem was solved by using bound-formulation approach and nonlinear mathematical programming. The results demonstrate that the load bearing capacity of multidirectional laminates can be significantly increased through optimization.

It must however be mentioned that in the present work all the design variables, i.e. the ply angles and thicknesses were assumed to be continuous variables. The continuity of thickness also meant that the number of plies was treated as a continuous variable. From a fabrication point of view, it may be expedient to use certain discrete values of ply angles and integer number of plies. Haftka & Walsh (1992) have used discrete ply angles in the optimum design of composite laminate with respect to buckling. The consideration of discrete ply angles and integer ply numbers in the optimum *in situ* strength design of laminates can also be attempted by integer programming. Another factor which depends on the configuration of a laminate and influences its load carrying capacity is the thermal stress induced in the process of manufacturing. This effect may alter the optimum design obtained by considering the external loads only. However, it is easy to incorporate the thermal effect into the procedure of optimization described in this exposition using the lamination theory.

When the number of unknown ply angles is large, the high nonlinearity of the stress norm with respect to the ply angles causes difficulty in reaching the global optimum solution. Therefore, there is a need to use a proper treatment to overcome this difficulty. The nonlinearity may be reduced by using indirect design variables such as the "lamination parameters" of Miki (1982) or the "transformed design variables" $x_i = \cos 2\theta_i$ or $x_i = \sin 2\theta_i$ of Fukunaga & Vanderplaats (1991).

Chapter 10

Conclusions

The large difference in the strengths of unidirectional fibre-reinforced composites along different directions makes their load carrying capacity very sensitive to the direction of loading. Transverse cracks are the most commonly observed damage in these materials. Therefore, in the analysis of the mechanical behaviour of composites, we inevitably have to solve complicated boundary-value problems of cracked bodies. Moreover, the many interfacial areas between the constituent phases in a composite can both be sources of defects and serve as crack arrestors, depending on how we design the microstructure of the composites. Given the many choices of composition available, the materials technologists are faced with the difficult task of designing these materials without any sound guidelines. They often resort to empirical rules of thumb or design the material to suit a specific application utilising one of the performance indicators, e.g. high strength. In order to exploit the full potential of composite materials in different applications, guidelines based upon sound mechanical and mathematical knowledge are needed to assist the materials technologist.

Optimization techniques have shown their potential in the strength design of composite materials. But at the same time it was also observed that most of the explicit optimum designs were obtained at the structural level that did not take into account the microstructural characteristics of the composites. For instance, the high sensitivity of fibre-reinforced composite materials to defects such as cracks in the transverse direction was not considered in the prediction of the strength of the material. On the other hand, the recent developments in both the stress analysis of the heterogeneous materials and in the optimization techniques have provided us with effective tools which can be used to the benefit of the materials technologist.

In view of the fact that fibre-reinforced composites are prone to cracking, the first part of this Thesis presented elastostatic solutions to the boundary-value problems of cracked composite regions using Fourier transforms. These regions were made of three subregions in which the central one was assumed to be a cracked transversely-isotropic medium and outer ones were orthotropic. The generalized expressions for the stresses and displacements in the outer

subregions (layers) included the degenerate case when they were also isotropic, but dissimilar from the central subregion (layer). The three-layer composite problems were solved when the central subregion contained a single intralaminar crack (the crack was wholly within the central subregion) in all three modes of loading - modes I, II and III in the terminology of fracture mechanics. When the central subregion contained a periodic distribution of intralaminar cracks, solutions were given for mode I and mode III loading cases. When the central subregion contained a single interlaminar crack (the tips of the crack touched the interfaces between the central and outer subregions), the interfacial stress singularities and the corresponding *in situ* stress intensity factors were calculated, again under all three modes of loading. It was found that although there are six material constants which characterize the transversely-isotropic central layer and the orthotropic outer layers, the mode I and mode II stress singularities were determined by only two mixed material parameters, respectively. The mode III stress singularity was determined by only one mixed material parameter. The stress intensity factors were functions of the stiffnesses and geometry of the subregions. For the degenerate case when the outer subregions were a dissimilar isotropic medium from the central one, the results for mode I were compared with those available in the literature and were found to be in total agreement.

Although the above boundary-value problems were motivated by the failure characteristics of fibre-reinforced composite laminates, the solutions can be applied to crack problems for any finite regions made up of dissimilar subregions. Many of these solutions were not available in the literature prior to the work described in this Thesis, except the solution for a single intralaminar crack under mode I loading case. These solutions are theoretically significant because of their potential in revealing the failure mechanisms of advanced composites.

In the second part of the Thesis, the elastostatic solutions for cracked transversely isotropic-orthotropic bonded layers obtained in the first part were specialized to glass or carbon fibre-reinforced composite laminates. The ever-increasing range of application of these materials was the main motivation of the study, while the numerous experimental studies on these materials provided a proper frame of reference. In order to render the basic solutions given in the first part applicable to the problems in fibre-reinforced composite laminates, the classical lamination theory and homogeneity assumption were used to evaluate the stiffness parameters of the sublaminates.

First, a fibre-reinforced symmetric angle-ply laminate containing multiple intralaminar cracks was studied under mode I and mode III loading cases. Such cracking is often observed in experiments. The influence of the ply angles and crack spacing upon the stress intensity factors was thoroughly examined. This examination revealed the constraining effect of one sublaminate on the crack driving force in its neighbouring unidirectional lamina, in

agreement with experimental observations. In mode I loading, it was found that transverse cracks could induce high interfacial stresses, the more so when these cracks were close to the interfaces. This is thought to be a major cause of the *crack-induced* delamination in angle-ply laminates. Secondly, a laminate containing a single interlaminar transverse crack was studied. The influence of the ply angles and thicknesses upon the stress singularities and intensities was investigated under all three modes of loading. In each of the three modes, the stress singularity and intensity showed opposite variations with the stiffnesses of the constraining sublaminates. The stiffer the constraining sublaminates, the weaker the stress singularity but the stronger the stress intensity. In mode I loading, the stress singularity reached its minimum value when the ply angle θ of the outer constraining sublaminates was 0^0 for the considered four fibre-reinforced composites. It increased monotonically to the usual square-root type when θ varied from 0^0 to 90^0. On the other hand, the stress intensity decreased as θ increased. The mode II and mode III stress singularities reached their minimum value when the ply angle θ of the constraining sublaminates was around 45^0, whereas the stress intensities in these two modes reached their maximum value at this value of θ. Due to the closeness of the magnitudes of G_{LT} and G_{TT} in all the materials studied, the mode III singularity varied almost symmetrically about $\theta = 45^0$.

In a $[(\pm\theta^0)_{n_2}/(90^0)_{n_1}/(\mp\theta^0)_{n_2}]$ fibre-reinforced laminate, the outer $(\pm\theta^0)_{n_2}$ sublaminates were shown to reduce the mode II stress intensity factor at the tips of a crack in the central $(90^0)_{n_1}$ layer under out-of-plane (laminate plane) shear loading. The degree of reduction depends on the stiffness of the plies, the ply angle θ and the thickness of the outer sublaminates. However, whilst the stress intensity factor decreases, the *crack-induced* largest interfacial principal tensile stress increases. The high interfacial stress would inevitably lead to interfacial delamination. Thus, an optimization problem was formulated with a view to choosing the design variables of the laminate, viz. the ply angle θ, relative ply stiffness and thickness, in such a way as to minimize the stress intensity factor at the crack tips in the $(90^0)_{n_1}$ layer without exceeding the interfacial bond strength. A constraint was also placed on the minimum flexural stiffness of the laminate. An alternative optimization problem in which the largest interfacial principal tensile stress was minimized subject to a limit on the stress intensity factor was also formulated and solved. It was found that the parameters in these single-criterion optimization problems influenced the solutions. If they are not properly chosen, it is likely that there is no feasible solution. To avoid the possibility of multiple or infeasible solutions, a multicriterion optimization problem, in which the crack driving force and *crack-induced* interfacial principal tensile stress are minimized, while the flexural stiffness is maximized, was also formulated and solved. All optimization problems were solved by several techniques of nonlinear mathematical programming. The sensitivities with respect to the design variables required in these techniques were calculated by a mixed analytical/numerical approach.

In the first optimization problem (that of the minimization of crack driving force subject to a limit on the *crack-induced* interfacial principal tensile stress), when the crack length relative to the thickness of the 90^0 sublaminate was small, the active constraints were the lower limit on θ and the upper limit ($\overline{b}$) on the relative thickness b/d of the constraining sublaminates. The minimum of the stress intensity factor always occurred at $\theta = 0^0$ and $b/d = \overline{b}$, no matter what initial θ and b/d were chosen. When the crack was large, the interfacial stress constraint became critical to the design. For the satisfaction of this constraint the design angle θ took on a non-zero value. The transition of the optimal θ from 0^0 to a non-zero value depended on the interfacial stress constraint. In the alternative optimization problem (that of the minimization of *crack-induced* interfacial principal tensile stress subject to a limit on crack driving force), the largest interfacial principal tensile stress reached its minimum when $\theta = 50^0$ and $b/d = \overline{b}$. In the multicriterion optimization problem, the optimum design was reached at a non-zero θ and $b/d = \overline{b}$.

The last Chapter presented a three-stage procedure for the optimum design of multidirectional laminates. In the first stage, a fracture mechanics analysis was performed on a cracked angle-ply laminate. The influence of the configuration of the laminate on the strain energy release rates at the tips of the transverse crack was quantitatively investigated. The results of this analysis revealed the mutual constraining effect of the unidirectional laminae in a laminate, so that the *in situ* transverse tensile and in-plane shear strengths of a lamina were enhanced. This enhancement primarily depended on the differences in the ply angles between this lamina and its immediate neighbours and on the thickness of the lamina itself. In the second stage, the above results and experimental observations were used to propose a set of *in situ* transverse tensile and in-plane shear strength parameters. These parameters were then incorporated into a failure criterion to judge the appearance of transverse cracks in unidirectional laminae in a multidirectional laminate. Finally, an optimization problem was formulated in which the load bearing capacity of multidirectional symmetric laminates under any combination of in-plane (membrane) loads was maximized. The optimum design was sought through minimizing the maximum stress norm which characterized the closeness of the stress state in a lamina to its failure point. The design variables were the ply angles and/or thicknesses.

In the parlance of mathematical optimization theory, the optimization problem under consideration was a minimax non-differentiable one. It was first reduced to a differentiable one (to the first order gradients) by the introduction of a novel smoothing function, and then the differentiable minimax problem was solved by the bound-formulation method and mathematical programming. The gradients of the objective and constraint functions required in this method, were obtained by a mixed analytical/numerical procedure. The results demonstrated that the load bearing capacity of multidirectional laminates could be significantly increased through op-

timization. The sensitivity of the optimum design with respect to changes in the design variables was checked. It was found that the optimum design was fairly stable and not very sensitive to changes in the design variables. Therefore, a nearly-optimum design could be a substitute for the mathematically optimum design. The nearly-optimum design was obtained by rounding off the optimum ply angles to the nearest commonly used discrete values and the thicknesses to the nearest multiples of the lamina thickness.

In the present work, all the design variables, i.e. the ply angles and thicknesses were assumed to be continuous variables. The continuity of thickness also meant that the number of plies was treated as a continuous variable. From a fabrication point of view, it is expedient to use certain discrete values of ply angles and integer number of plies. Discrete/integer programming techniques are needed in considering discrete ply angles and integer ply numbers in the optimum *in situ* strength design of laminates. When the number of unknown ply angles is large, the high nonlinearity of the stress norm with respect to the ply angles causes difficulty in reaching the global optimum solution. There is thus a need to use proper analytical techniques to overcome this difficulty. The nonlinearity may be reduced by using indirect design variables instead of the ply angles. The *in situ* strengths in the present work were defined with reference to the onset of transverse cracks. The composite laminates can still carry additional loads after the occurrence of transverse cracks in its constituent laminae. It will fail at an ultimate load which is larger than that corresponding to the occurrence of transverse cracks. The optimum design that maximizes the load for transverse cracks may not be the design that maximizes the ultimate load. More sophisticated stress analysis and optimization techniques are needed for obtaining the maximum ultimate strength design.

Bibliography

[1] Adali, S. 1985 Optimization of fibre reinforced composite laminates subject to fatigue loading. In *Composite structures (Proc. Third Int. Conf. Composite Structures)* Vol. 3 (ed. I. H. Marshall), pp. 43–55. London: Elsevier Applied Science Publishers Ltd.

[2] Ahmad, J. 1991 A micromechanics analysis of cracks in unidirectional fiber composites. *J. Appl. Mech.* **58**, 964–972.

[3] Arin, K. 1974 A note on a broken layer in an orthotropic laminate composite. *NASA Technical Report TR-74-4, Lehigh University, IFSM-74-59*, Pennsylvania.

[4] Arin, K. 1977 An orthotropic laminate composite containing a layer with a crack. *Int. J. Engng. Sci.* **15**, 545–559.

[5] Ashbaugh, N. E. 1973 Stress in laminated composites containing a broken layer. *J. Appl. Mech.* **40**, 533–540.

[6] Atkinson, C. 1975 On the stress intensity factors associated with cracks interacting with an interface between two elastic media. *Int. J. Solids Structures* **13**, 489–504.

[7] Aveston, J. & Kelly, A. 1973 Theory of multiple fracture of fibrous composites. *J. Mater. Sci.* **8**, 352–362.

[8] Bai, J. M. 1989 Stiffness reduction analysis of cracked cross-ply laminates by using integral equation approach. *Engng. Fract. Mech.* **34**, 245–251.

[9] Bai, J. M. & Loo, T. T. 1989 Strength of stress singularity and stress-intensity factors for a transverse crack in finite symmetric cross-ply laminates under tension. In *Fracture mechanics: perspectives and directions (Twentieth Symposium)*, ASTM STP 1020 (ed. R. P. Wei & R. P. Gangloff), pp. 641–658.

[10] Bailey, J. E., Curtis, P. T. & Parvizi, A. 1979 On the transverse cracking and longitudinal splitting behaviour of glass and carbon fibre reinforced epoxy cross-ply laminates and the effect of Poisson and thermally generated strain. *Proc. Roy. Soc. London* A**366**, 599-623.

[11] Bailey, J. E. & A. Parvizi. 1981 On fibre debonding effects and the mechanism of transverse-ply failure in cross-ply laminates. *J. Mater. Sci.* **16**, 649–659.

[12] Becker, W. 1994 Closed-form analysis of the free edge effect in angle-ply laminates. *J. Appl. Mech.* **61**, 209–211.

[13] Bogy, D. B. 1973 The plane elastostatic solution for a symmetrically loaded crack in a strip composite. *Int. J. Engng. Sci.* **11**, 985–996.

[14] Brandmaier, H. E. 1970 Optimum filament orientation criteria. *J. Compos. Mater.* **4**, 422–425.

[15] Budiansky, B., Hutchinson, J. W. & Evans, A. G. 1986 Matrix fracture in fiber-reinforced ceramics. *J. Mech. Phys. Solids* **34**, 167–189.

[16] Chang, F. K. & Chen, M. H. 1987 The in situ ply shear strength distributions in graphite/epoxy laminated composite. *J. Compos. Mater.* **21**, 708–733.

[17] Chang, F. K. & Lessard, L. B. 1991 Damage tolerance of laminated composites containing an hole and subjected to compressive loadings: Part I – analysis. *J. Compos. Mater.* **25**, 2–43.

[18] Chang, K-Y., Liu, S. & Chang, F. K. 1991 Damage tolerance of laminated composites containing an open hole and subjected to tensile loadings. *J. Compos. Mater.* **25**, 274–301.

[19] Chao, C. C., Sun, C. T. & Koh, S. L. 1975a Strength optimization for cylindrical shells of laminated composites. *J. Compos. Mater.* **9**, 53–66.

[20] Chao, C. C., Koh, S. L. & Sun, C. T. 1975b Optimization of buckling and yield strengths of laminated composites. *AIAA J* **13**, 1131–1132.

[21] Chatterjee, S. N., Pipes, R. B. & Blake, R. A. Jr. 1984 Criticality of disbonds in laminated composites. In *Effect of defects in composite materials*, ASTM STP 836, pp. 161–174.

[22] Cheng, K. 1986 Sensitivity analysis and a mixed approach to the optimization of symmetric layered composite plates. *Engng. Optimiz.* **9**, 233–247.

[23] Christensen, R. M. & DeTeresa, S. J. 1992 Elimination/minimization of edge-induced stress singularities in fiber composite laminates. *Int. J. Solids Structures* **29**, 1221–1231.

[24] Cook, T. S. & Erdogan, F. 1972 Stresses in bonded materials with a crack perpendicular to the interface. *Int. J. Engng. Sci.* **10**, 677–697.

[25] Copson, E. T. 1961 On certain dual integral equations. *Proc. Glasgow Math. Association* **5**, 19–24.

[26] Crossman, F. W. & Wang, A. S. D. 1982 The dependence of transverse cracking and delamination on ply thickness in graphite/epoxy laminates. In *Damage in composite materials*, ASTM STP 775 (ed. K. L. Reifsnider), pp. 118–139.

[27] Dakin, R. J. 1965 A tree search algorithm for mixed integer programming problems. *Comput. J.* **8**, 250–255.

[28] Delale, F. & Erdogan, F. 1979 Bonded orthotropic strips with cracks. *Int. J. Fract.* **15**, 343–364.

[29] Doxsee, L. E., Rubbrecht, P., Li, L., Verpoest, I. & Scholle, M. 1993 Delamination growth in composite plates subjected to transverse loads. *J. Compos. Mater.* **27**, 764–781.

[30] Dundurs, J. 1969 Edge-bonded dissimilar orthogonal elastic wedges. *J. Appl. Mech.* **36**, 650–652.

[31] Dvorak, G. J. & Laws, N. 1987 Analysis of progressive matrix cracking in composite laminates II – first ply failure. *J. Compos. Mater.* **21**, 309–329.

[32] Edge, E. C. 1994 Is there a size effect in composites? Comments on designer's corner by Carl Zweben. *Composites* **25**, 957–958.

[33] Enie, R. B. & Rizzo, R. R. 1969 Three-dimensional laminate moduli. *J. Compos. Mater.* **4**, 150–154.

[34] Erdelyi, A. 1953 *Tables of integral transforms*. Vol. 1. New York: McGraw-Hill.

[35] Erdogan, F. & Gupta, G. 1971 The stress analysis of multi-layered composites with a flaw. *Int. J. Solids Structures* **7**, 39–61.

[36] Erdogan, F., Gupta, G. D. & Cook, T. S. 1973 Numerical solution of singular integral equations. In *Mechanics of fracture – methods of analysis and solutions of crack problems* (ed. G. C. Sih), pp. 368–425. Leyden: Noordhoff International Publishing.

[37] Erdogan, F. & Bakioglu, M. 1976 Fracture of plates which consist of periodic dissimilar strips. *Int. J. Fract.* **12**, 71–84.

[38] Erdogan, F., Kaya, A. C. & Joseph, P. F. 1991a The crack problem in bonded nonhomogeneous materials. *J. Appl. Mech.* **58**, 410–418.

[39] Erdogan, F., Kaya, A.C. & Joseph, P. F. 1991b The mode III crack problem in bonded materials with a nonhomogeneous interfacial zone. *J. Appl. Mech.* **58**, 419–427.

[40] Erdogan, F. & Wu, B. 1991 The surface and through crack problems in layered orthotropic plates. *NASA Technical Report NASA-CR-188188*, Lehigh University.

[41] Erdogan, F. & Kadioglu, S. 1994 T-shape crack problem for bonded orthotropic layers. *Int. J. Fract.* **67**, 273–300.

[42] Fan, F., Dong, W. & Wang, J. 1989 A study on the *in situ* transverse tensile lamina strength and the solution of the opening mode crack in $0^0/90^0/0^0$ laminate. *Acta Mechanica Sinica* **21**, 450–458.

[43] Fiacco, A. V. & McCormick, G. P. 1968 *Nonlinear programming: sequential unconstrained minimization techniques*. New York: John Wiley & Sons.

[44] Fish, J. C. & Lee, S. W. 1990 Three-dimensional analysis of combined free-edge and transverse-crack-tip delamination. In *Composite materials: testing and design (Ninth Conference), ASTM STP 1059* (ed. S. P. Garbo), pp. 271–286.

[45] Flaggs, D. L. & Kural, M. H. 1982 Experimental determination of *in situ* transverse lamina strength in graphite/epoxy laminates. *J. Compos. Mater.* **16**, 103–116.

[46] Fleury, C. & Braibant, V. 1986 Structural optimization: a new dual method using mixed variables. *Int. J. Num. Meth. Engng.* **23**, 409–428.

[47] Folias, E. S. 1992 Boundary layer effects of interlaminar stresses adjacent to a hole in a laminated composite plates. *Int. J. Solids Structures* **29**, 171–186.

[48] Foye, R. 1968 Advanced design concepts for advanced composite frames, Vol. **I-II** Air Force Materials Laboratory, Wright Patterson Air Force Base, Ohio, AFML-TR-68-91.

[49] Fukunaga, H. & Chou, T-W. 1988 On laminate configurations for simultaneous failure. *J. Compos. Mater.* **22**, 271–286.

[50] Fukunaga, H. & Vanderplaats, G. N. 1991 Strength optimization of laminated composites with respect to layer thickness and/or layer orientation angle. *Computers & Structures* **40**, 1429–1439.

[51] Fukunaga, H. & Sekine, H. 1993 Optimum design of composite structures for shape, layer angle and layer thickness distributions. *J. Compos. Mater.* **27**, 1479–1492.

[52] Gao, Y. C. & Mai, Y. W. 1989 Optimal design of fiber-reinforced materials. In *Proc. 7th Int. Conf. Composite Materials* Vol. 3 (ed. Y. Wu, Z. Gu & R. Wu), pp. 377-381. Beijing: International Academic Publishers.

[53] Garfinkel, R. S. & Nemhauser, G. L. 1974 *Integer programming*. New York: John Wiley & Sons.

[54] Garrett, K. W. & Bailey, J. E. 1977 Multiple transverse fracture in 90^0 cross-ply laminates of a glass fibre-reinforced polyester. *J. Mater. Sci.* **12**, 157–168.

[55] Gradshteyn, I. S. & Ryzhik, I. M. 1965 *Tables of integrals, series, and products*. New York: Academic Press Inc.

[56] Gudmundson, P. & Zang, W. 1993 An analytic model for thermoelastic properties of composite laminates containing transverse matrix cracks. *Int. J. Solids Structures* **30**, 3211–3231.

[57] Gupta, G. D. 1973 A layered composite with a broken laminate. *Int. J. Solids Structures* **9**, 1141–1154.

[58] Gupta, V., Argon, A. S., & Suo, Z. 1992 Crack deflection at an interface between two orthotropic media. *J. Appl. Mech.* **59**, S79–S87.

[59] Gürdal, Z. & Haftka, R. T. 1991 Optimization of composite laminates. In *Lecture notes on optimization of large structural systems*, NATO/DFG ASI, Vol. I, pp. 201–215. Berchtesgaden, Germany, September, 1991.

[60] Haftka, R. T. & Walsh, J. L. 1992 Stacking-sequence optimization for buckling of laminated plates by integer programming. *AIAA J* **30**, 814–819.

[61] Hajela, P. & Shih, C. J. 1989 Optimal design of laminated composites using a modified mixed integer and discrete programming algorithm. *Computers & Structures* **32**, 213–221.

[62] Hahn, H. T. & Johnnesson, T. 1983 Fracture of unidirectional composites, theory and applications. In *Mechanics of composite materials – 1983* AMD-Vol. 58 (ed. G. J. Dvorak), p. 135.

[63] Harrison, R. P. & Bader, M. G. 1983 Damage development in CFRP laminates under monotonic and cyclic stressing. *Fibre Sci. Tech.* **18**, 163–180.

[64] Hashin, Z. & Rotem, A. 1973 A fatigue failure criterion for fibre-reinforced materials. *J. Compos. Mater.* **7**, 448–464.

[65] Hashin, Z. 1980 Failure criteria for unidirectional fibre composites. *J. Appl. Mech.* **47**, 329–334.

[66] Hashin, Z. 1985 Analysis of cracked laminates: a variational approach. *Mech. Mater.* **4**, 121–136.

[67] He, M. & Hutchinson, J. W. 1989 Crack deflection at an interface between dissimilar elastic materials. *Int. J. Solids Structures* **25**, 1053–1067.

[68] Herakovich, C. T. 1982 Influence of layer thickness on the strength of angle-ply laminates. *J. Compos. Mater.* **16**,216–227.

[69] Highsmith, A. L. & Reifsnider, K. L. 1982 Stiffness-reduction mechanisms in composite laminates. In *Damage in composite materials*, ASTM STP 775 (ed. K. L. Reifsnider), pp. 103–117.

[70] Hilton, P. D. & Sih, G. C. 1971 A laminate composite with a crack normal to the interfaces. *Int. J. Solids Structures* **7**, 913–930.

[71] Hoffman, O. 1967 The brittle strength of orthotropic materials. *J. Compos. Mater.* **1**, 200–206.

[72] Horii, H. & Nemat-Nasser, S. 1985 Elastic fields of interacting inhomogeneities. *Int. J. Solids Structures* **21**, 731–745.

[73] Ikegami, K., Yoshihiro, N., Yasunaga, T. & Shiratori, E. 1982 Failure criterion of angle ply laminates of fibre reinforced plastics and applications to optimise the strength. *Fibre Sci. Tech.* **16**, 175–190.

[74] Imai, K. & Schmit, L. A. 1981 Configuration optimization of trusses. *ASCE J. Structural Division* **107**, 745–756.

[75] Jones, R., Heller, M., Sparrow, J. G. & Ryall, T. G. 1990 A new approach to structural optimization. *Composite Structures* **16**, 1–32.

[76] Jones, R. M. 1975 *Mechanics of composite materials*. Washington, D. C.: Scripta Book Company.

[77] Karihaloo, B. L. 1982 Crack kinking and curving. *Mech. Mater.* **1**, 189–201.

[78] Karihaloo, B. L. 1993 Most efficient NLP techniques in optimum structural frame design. *Engng. Optimiz.* **20**, 261–272.

[79] Kassapoglou, C. 1990 Determination of interlaminar stresses in composite laminates under combined Loads. *J. Reinf. Plas. Compos.* **9**, 33–58.

[80] Kaw, A. K. & Besterfield, G. H. 1992 Mechanics of multiple periodic brittle matrix cracks in unidirectional fiber-reinforced composites. *Int. J. Solids Structures* **29**, 1193–1207.

[81] Kaw, A. K. 1992 Private communication.

[82] Kelly, J. E. 1960 The cutting plane method for solving convex programs. *J. SIAM*, 703–712.

[83] Kim, R. Y. 1989 Experimental observations of free-edge delamination. In *Interlaminar response of composite materials* (ed. N. J. Pagano), pp. 111–160. Amsterdam: Elsevier.

[84] Konishi, Y. & Atsumi, A. 1973 Crack problem of transversely isotropic strip. *Int. J. Engng. Sci.* **11**, 9–20.

[85] Lee, J-W., Allen, D. H. & Harris, C. E. 1989 Internal state variable approach for predicting stiffness reductions in fibrous laminated composites with matrix cracks. *J. Compos. Mater.* **23**, 1273–1291.

[86] Li, S., Reid, S. R. & Soden, P. D. 1994 A finite strip analysis of cracked laminates. *Mech. Mater.* **18**, 289–311.

[87] Liu, S., Kutlu, Z. & Chang, F. K. 1993 Matrix cracking and delamination in laminated composite beams subjected to a transverse concentrated line load. *J. Compos. Mater.* **27**, 436–470.

[88] Liu, S. & Chang, F. K. 1994 Matrix cracking effect on delamination growth in composite laminates induced by a spherical indenter. *J. Compos. Mater.* **28**, 940–977.

[89] McCartney, L. N. 1992 Theory of stress transfer in a $0^0 - 90^0 - 0^0$ cross-ply laminate containing a parallel array of transverse cracks. *J. Mech. Phys. Solids* **40**, 27–68.

[90] Markenscoff, X. 1993 On the Dundurs correspondence between cavities and rigid inclusions. *J. Appl. Mech.* **60**, 260–264.

[91] Mesquita, L. & Kamat, M. P. 1987 Optimization of stiffened laminated composite plates with frequency constraints, *Engng. Optimiz.* **11**, 77–88.

[92] Miki, M. 1982 Material design of composite laminates with required in-plane elastic properties. In *Progress in science and engineering of composites (Proc. 4th Int. Conf. Composite Materials)* (ed. T. Hayashi, K. Kawata & S. Umekawa), pp. 1725–1731.

[93] Miki, M. 1985 Design of laminated fibrous composite plates with required flexural stiffness. In *Recent advances in composites in the United States and Japan*, ASTM STP 864 (ed. J. R. Vinson & M. Taya), pp. 387–400.

[94] Miravete, A. 1989 Optimization of symmetrically laminated composites rectangular plates. In *Proc. 7th Int. Conf. Composite Materials* Vol. 3 (ed. Y. Wu, Z. Gu & R. Wu), pp. 289–294. Beijing: International Academic Publishers.

[95] Miravete, A. 1990 Analysis and optimization of simple composite structures. In *Composite materials–design and analysis* (ed. W. P. de Wilde & W. R. Blain), pp. 529–547. Southampton: Computational Mechanics Publications & Springer-Verlag.

[96] Moses, F. 1964 Optimum structural design using linear programming. *Proc. ASCE* **90**, ST 6, 89–104.

[97] Murri, G. B. & Guynn, E. G. 1988 Analysis of delamination growth from matrix cracks in laminates subjected to bending loads. In *Composite materials: testing and design (Eighth Conference)*, ASTM STP 972 (ed. J. D. Whitcomb), pp. 322–339.

[98] Murthy, P. L. N. & Chamis, C. C. 1987 Free-edge delamination–laminate width and loading conditions effects. *NASA–TM–100238*, Lewis Research Center, Cleveland.

[99] Muskhelishvili, N. I. 1953 *Singular integral equations*. Groningen: P. Noordhoff.

[100] Nairn, J. A. 1989 The strain energy release rate of composite microcracking: a variational approach. *J. Compos. Mater.* **23**, 1106–1129.

[101] Nakamura, T. & Kamath, S. M. 1992 Three-dimensional effects in thin film fracture mechanics. *Mech. Mater.* **13**, 67–77.

[102] Nied, H. F. 1987 Periodic array of cracks in a half-plane subjected to arbitrary loading. *J. Appl. Mech.* **54**, 642–648.

[103] O'Brien, T. K. 1985 Analysis of local delaminations and their influence on composite laminate behavior. In *Delamination and debonding of materials*, ASTM STP 876 (ed. W. S. Johnson), pp. 282–297.

[104] Olhoff, N. 1989 Multicriterion structural optimization via bound formulation and mathematical programming. *Struct. Optimiz.* **1**, 11–17.

[105] Pagano, N. J. 1971 The influence of stacking sequence on laminate strength. *J. Compos Mater.* **5**, 50–57.

[106] Pagano, N. J. 1975 Distortional energy of composite materials. *J. Compos. Mater.* **9**, 67–72.

[107] Pagano, N. J. & Soni, S. R. 1983 Global-local laminate variational model. *Int. J. Solids Structures* **19**, 207–228.

[108] Park, W. J. 1982 An optimal design of simple symmetric laminates under the first ply failure criterion. *J. Compos. Mater.* **16**, 341–355.

[109] Parvizi, A., Garrett, K. W. & Bailey, J. E. 1978 Constrained cracking in glass fibre-reinforced epoxy cross-ply laminates. *J. Mater. Sci.* **13**, 195–201.

[110] Pedersen, P. 1981 The integrated approach to FEM-SLP for solving problems of optimal design. In *Optimization of distributed parameter systems* (ed. E. J. Haug & J. Cea), vol. I, pp. 739–756.

[111] Pedersen, P. 1991 On thickness and orientational design with orthotropic materials. *Struct. Optimiz.* **3**, 69–78.

[112] Pedersen, P., Tobiesen, L. & Jensen, S. H. 1991 Shapes of orthotropic plates for minimum energy concentration. *Technical Report, The Danish Center for Applied Mathematics and Mechanics*, The Technical University of Denmark, Lyngby, Denmark.

[113] Pierre, D. A. & Lowe, M. J. 1975 *Mathematical programming via augmented Lagrangians.* Applied Mathematics and Computation Series, Addison-Wesley.

[114] Powell, M. J. D. 1978 A fast algorithm for nonlinear constrained optimization calculations. *Proc. Dundee Conf. Num. Analysis, Lecture Notes in Mathematics*, Springer-Verlag.

[115] Powell, M. J. D. 1981 Algorithms for nonlinear constraints that use Lagrangian functions. *Mathematical Programming* **14**, 224–248.

[116] Rao, K. P., Issac, J. C., Viswanath, S. & Murthy, S. S. 1991 Optimum design of composite laminates for strength by ranking. *J. Reinf. Plas. Compos.* **10**, 477–494.

[117] Reddy, A. D., Rehfield, L. W. & Haag, R. S. 1984 Influence of prescribed delamination on stiffness controlled behaviour of composite laminates. In *Effect of defects in composite materials*, ASTM STP 836, pp. 84–103.

[118] Reddy, J. N. 1984 A simple higher-order theory for laminated composites. *J. Appl. Mech.* **51**, 745–752.

[119] Reddy, J. N. & Robbins, D. H. 1994 Theories and computational models for composite laminates. *Applied Mechanics Review* **47**, 147–169.

[120] Rockafellar, R. T. 1973 The multiplier method of Hestenes and Powell applied to convex programming. *J. Optimiz. Theory Appl.* **12**, 555–562.

[121] Rotem, A. & Hashin, Z. 1976 Fatigue failure of angle-ply laminates. *AIAA J* **14**, 868–872.

[122] Rowlands, R. E. 1985 Strength (failure) theories and their experimental correlation. In *Handbook of composites* (ed. A. Kelly & Yu. N. Rabotnov) Vol. 3 – *Failure mechanics of composites* (ed. G. C. Sih & A. M. Skudra), pp. 71–125. Amsterdam: Elsevier.

[123] Salamon, N. J. 1978 Interlaminar stresses in a layered composite laminate in bending. *Fibre Sci. Tech.* **11**, 305–317.

[124] Sandhu, R. S. 1969 Parametric study of Tsai's strength criterion for filamentary composites. TR-68-168, Air Force Flight Dynamic Laboratory, Wright-Patterson AFB, Ohio.

[125] Savage, T. 1991 Materials research role for YARD. *Aircraft Engineering and Aerospace Technology* **63**, No. 4, p. 13.

[126] Schapery, R. A. 1981 Research on composite material for structural design. *Mechanics of Composite Review*, Dayton, OH, Oct. 1981.

[127] Schrage, L. 1989 *User's manual for LINDO*, 4th edn. Redwood City: The Scientific Press.

[128] Shiau, L. & Chue, Y. 1991 Free-edge stress reduction through fiber volume fraction variation. *Composite Structures* **19**, 145–165.

[129] Shin, D. K., Gürdal, Z. & Griffin, O. H. 1990 A penalty approach for nonlinear optimization with discrete design variables. *Engng. Optimiz.* **16**, 29–42.

[130] Sih, G. C. & Chen, E. P. 1981 *Mechanics of fracture – cracks in composite materials.* The Hague: Martinus Nijhoff Publisher.

[131] Sneddon, I. N. 1951 *Fourier transforms*: Chapter 9 Two-dimensional stress analysis. New York: McGraw-Hill.

[132] Sneddon, I. N. & Lowengrub, M. 1969 *Crack problems in the classical theory of elasticity.* New York: John Wiley & Sons.

[133] Sneddon, I. N. & Ejike, U. B. C. O. 1969 The stress intensity factors for a Griffith crack whose surfaces are loaded asymmetrically. *Int. J. Solids Structures* **5**, 513–523.

[134] Sneddon, I. N. & Srivastav, R. P. 1971 The stress field in the vicinity of a Griffith crack in a strip of finite width. *Int. J. Engng. Sci.* **9**, 479–488.

[135] Sokolnikoff, I. S. 1956 *Mathematical theory of elasticity.* New York: McGraw-Hill.

[136] Tada, H., Paris, P. C. & Irwin, G. R. 1985 *The stress analysis of cracks handbook.* St Louis: Del Research Corporation.

[137] Talreja, R. 1985 Transverse cracking and stiffness reduction in composite laminates. *J. Compos. Mater.* **19**, 355–375.

[138] Talreja, R. 1987 *Fatigue of composite materials*. Lancaster: TECHNOMIC Publishing Co. Inc.

[139] Talreja, R. 1991 Transverse cracking and stiffness reduction in cross ply laminates of different matrix toughness. *Report 428, The Danish Center for Applied Mathematics and Mechanics*. Lyngby: The Technical University of Denmark.

[140] Tan, S. C. & Nuismer, R. J. 1989 A theory for progressive matrix cracking in composite laminates. *J. Compos. Mater.* **23**, 1029–1047.

[141] Tang, S. 1976 Interlaminar stresses of uniformly loaded rectangular composite plates. *J. Compos. Mater.* **10**, 69–78.

[142] Tauchert, T. R. & Adibhatla, S. 1985 Design of laminated plates for maximum bending strength. *Engng. Optimiz.* **8**, 253–263.

[143] Ting, T. C. T. & Hoang, P. H. 1984 Singularities at the tip of a crack normal to the interface of an anisotropic layered composite. *Int. J. Solids Structures* **20**, 439–454.

[144] Tsai, S. W. 1968 Strength theories of filamentary structures. In *Fundamental aspects of fibre reinforced plastic composites* (ed. R. T. Schwartz & H. S. Schwartz), pp. 3–12. New York: Interscience Publishers.

[145] Tsai, S. W. & Wu, E. M. 1970 A general theory of strength for anisotropic materials. *J. Compos. Mater.* **5**, 58–80.

[146] Tsai, S. W. & Hahn, H. T. 1980 *Introduction to composite materials*. Westport: TECHNOMIC Publishing Co. Inc.

[147] Vanderplaats, G. N. 1987 *ADS-A FORTRAN program for automated design synthesis.* Santa Barbara: Engineering Design Optimization Inc.

[148] Venkayya, V. B., Khot, N. S. & Reddy, V. S. 1968 Optimization of structures based on the study of strain energy distribution. TR-68-150, Air Force Flight Dynamic Laboratory, Wright-Patterson AFB, Ohio.

[149] Venkayya, V. B. 1971 Design of optimum structures. *Computers & Structures* **1**, 265–309.

[150] Vinson, J. R. & Chow, T. W. 1975 *Composite materials and their use in structures.* London: Applied Science Publishers Ltd.

[151] Waddoups, M. E. 1969 Structural airframe application of advanced composite materials – analytical methods. Vol. IV, AFML-TR-101, Air Force Materials Laboratory, Wright-Patterson AFB, Ohio.

[152] Wang, A. S. D. 1980 Growth mechanism of fracture cracks and ply delaminations in composite materials. In *Proc. of the Third Int. Conf. on Composite Materials*, pp. 170–185. Paris.

[153] Wang, A. S. D. & Crossman, F. W. 1980 Initiation and growth of transverse cracks and edge delamination in composite laminates: Part I – an energy method. *J. Compos. Mater. Supplement* **14**, 71–87.

[154] Wang, A. S. D., Chou, P. C. & Lei, S. C. 1984 A stochastic model for the growth of matrix cracks in composite laminates. *J. Compos. Mater.* **18**, 239–254.

[155] Wang, S. S. & Choi, I. 1982a Boundary-layer effects in composite laminates: Part 1 – free-edge stress stress singularities. *J. Appl. Mech.* **49**, 541–548.

[156] Wang, S. S. & Choi, I. 1982b Boundary-layer effects in composite laminates: Part 2 – free-edge stress solutions and basic characteristics. *J. Appl. Mech.* **49**, 549–560.

[157] Webber, J. P. H. 1988 Some laminated plate optimum design studies using an interactive computer programme. *Aeronautical J.* March, 1988, 107–114.

[158] Wu, B. & Erdogan, F. 1993 Fracture mechanics of orthotropic laminated plates – II. the plane strain crack problem for two bonded orthotropic layers. *Int. J. Solids Structures* **30**, 2379–2391.

[159] Yamada, S. E. & Sun, C. T. 1979 Analysis of laminate strength and its distribution. *J. Compos. Mater.* **12**, 275–284.

[160] Zak, A. R. & Williams, M. L. 1963 Crack point stress singularities at a bi-material interface. *J. Appl. Mech.* **30**, 142–143.

[161] Zweben, C. 1994 Is there a size effect in composites? *Composites* **25**, 451–454.

Appendix A

A.1 Determination of the Unknown Functions in Mode I

The two unknown functions $A(s/a)$ and $B(s/a)$ in the dual integral equations (4.38)–(4.39) can be expressed as functions of $E(s/a)$ by using the continuity and free-surface conditions (4.30)–(4.35). When doing so, it is noted that ρ can take the value 1 or 0. Therefore, these equations have to be solved separately for $\rho = 1$ and $\rho = 0$. In the following we shall demonstrate the procedure on $\rho = 0$. The case for $\rho = 1$ can be similarly dealt with and will not be reproduced here. This procedure also appeared in the work of Erdogan & Wu (1991) for dealing with the continuity and free-surface conditions of stresses and displacements which arose in the solution of the boundary-value problem of a cracked composite laminate of finite thickness. The treatment of free-surface conditions in the framework of Fourier transforms for a cracked strip dates from the work of Sneddon & Lowengrub (1969).

When $\rho = 0$, by substituting the expressions for the stresses and displacements (4.4), (4.6), (4.8),(4.10), (4.11), (4.13), (4.14) and (4.15) into (4.30)–(4.35), we have

$$
\begin{aligned}
&-\frac{2}{\pi}\int_0^{+\infty}\left[A(t)\cosh(td)+B(t)td\sinh(td)\right]\cos(ty)\,dt+\\
&+\frac{2}{\pi}\int_0^{+\infty}E(t)(1-ty)\,e^{-ty}\cos(td)\,dt=\frac{2}{\pi}\int_0^{+\infty}t[Q_1A_1(t)+Q_2A_2(t)]\cos(ty)\,dt \qquad \text{(A.1)}
\end{aligned}
$$

$$
\begin{aligned}
&\frac{2}{\pi}\int_0^{+\infty}\left\{A(t)\sinh(td)+B(t)[\sinh(td)+td\cosh(td)]\right\}\sin(ty)\,dt+\\
&+\frac{2}{\pi}\int_0^{+\infty}E(t)ty\,e^{-ty}\sin(td)\,dt=\frac{2}{\pi}\int_0^{+\infty}t[L_1B_1(t)+L_2B_2(t)]\sin(ty)\,dt \qquad \text{(A.2)}
\end{aligned}
$$

$$
\begin{aligned}
&-\frac{2}{\pi}\frac{1}{4\mu}\int_0^{+\infty}\frac{1}{t}\left\{2A(t)\sinh(td)+B(t)[(1-\kappa)\sinh(td)+2td\cosh(td)]\right\}\cos(ty)\,dt-\\
&-\frac{2}{\pi}\frac{1}{4\mu}\int_0^{+\infty}\frac{1}{t}E(t)(1-\kappa+2ty)\,e^{-ty}\sin(td)=\frac{2}{\pi}\int_0^{+\infty}[B_1(t)+B_2(t)]\cos(ty)\,dt \qquad \text{(A.3)}
\end{aligned}
$$

$$\frac{2}{\pi}\frac{1}{4\mu}\int_0^{+\infty}\frac{1}{t}\{2A(t)\cosh(td)+B(t)[(1+\kappa)\cosh(td)+2td\sinh(td)]\}\sin(ty)\,dt -$$

$$-\frac{2}{\pi}\frac{1}{4\mu}\int_0^{+\infty}\frac{1}{t}E(t)(1+\kappa+2ty)\,e^{-ty}\cos(td)\,dt =$$

$$=\frac{2}{\pi}\int_0^{+\infty}[Z_1A_1(t)+Z_2A_2(t)]\sin(ty)\,dt \tag{A.4}$$

$$\frac{2}{\pi}\int_0^{+\infty}tQ_1[A_1(t)\cosh(\beta_1bt)+B_1(t)\sinh(\beta_1bt)]\cos(ty)\,dt +$$

$$+\frac{2}{\pi}\int_0^{+\infty}tQ_2[A_2(t)\cosh(\beta_2bt)+B_2(t)\sinh(\beta_2bt)]\cos(ty)\,dt=0 \tag{A.5}$$

$$\frac{2}{\pi}\int_0^{+\infty}tL_1[A_1(t)\sinh(\beta_1bt)+B_1(t)\cosh(\beta_1bt)]\sin(ty)\,dt +$$

$$+\frac{2}{\pi}\int_0^{+\infty}tL_2[A_2(t)\sinh(\beta_2bt)+B_2(t)\cosh(\beta_2bt)]\sin(ty)\,dt=0 \tag{A.6}$$

In obtaining the above equations, we have used the identities

$$\cosh\beta_i(x-d)t\,|_{x=d}=1 \tag{A.7}$$

$$\sinh\beta_i(x-d)t\,|_{x=d}=0 \tag{A.8}$$

Eqns (A.1)–(A.6) can be rewritten as

$$\int_0^{+\infty}[A(t)\cosh(td)+B(t)td\sinh(td)+tQ_1A_1(t)+tQ_2A_2(t)]\cos(ty)\,dt =$$

$$=\int_0^{+\infty}E(\eta)(1-\eta y)\,e^{-\eta y}\cos(\eta d)\,d\eta \tag{A.9}$$

$$-\int_0^{+\infty}\{A(t)\sinh(td)+B(t)[\sinh(td)+td\cosh(td)]+tL_1B_1(t)+$$

$$+tL_2B_2(t)\}\sin(ty)\,dt=\int_0^{+\infty}E(\eta)\eta y\,e^{-\eta y}\sin(\eta d)\,d\eta \tag{A.10}$$

$$\int_0^{+\infty}\left\{\frac{1}{4\mu t}[2A(t)\sinh(td)+B(t)\,((1-\kappa)\sinh(td)+2td\cosh(td))]+B_1(t)+\right.$$

$$\left.+B_2(t)\right\}\cos(ty)\,dt=-\frac{1}{4\mu}\int_0^{+\infty}\frac{1}{\eta}E(\eta)(1-\kappa+2\eta y)\,e^{-\eta y}\sin(\eta d)\,d\eta \tag{A.11}$$

$$\int_0^{+\infty}\left\{\frac{1}{4\mu t}[2A(t)\cosh(td)+B(t)((1+\kappa)\cosh(td)+2td\sinh(td))]-Z_1A_1(t)-\right.$$

$$\left.-Z_2A_2(t)\right\}=\frac{1}{4\mu}\int_0^{+\infty}\frac{1}{\eta}E(\eta)(1+\kappa+2\eta y)\,e^{-\eta y}\cos(\eta d)\,d\eta \tag{A.12}$$

$$\int_0^{+\infty} t\,\{Q_1[A_1(t)\cosh(\beta_1 bt) + B_1(t)\sinh(\beta_1 bt)] +$$
$$+ \quad Q_2[A_2(t)\cosh(\beta_2 bt) + B_2(t)\sinh(\beta_2 bt)]\}\,\cos(ty)\,dt = 0 \tag{A.13}$$

$$\int_0^{+\infty} t\,\{L_1[A_1(t)\sinh(\beta_1 bt) + B_1(t)\cosh(\beta_1 bt)] +$$
$$+ \quad L_2[A_2(t)\sinh(\beta_2 bt) + B_2(t)\cosh(\beta_2 bt)]\}\,\sin(ty)\,dt = 0 \tag{A.14}$$

Applying inversion formulae for Fourier sine and cosine transforms to the above equations and using the following integrals

$$\int_0^{+\infty} e^{-\eta y}\,\sin(ty)\,dy = \frac{t}{\eta^2 + t^2} \tag{A.15}$$

$$\int_0^{+\infty} e^{-\eta y}\,\cos(ty)\,dy = \frac{\eta}{\eta^2 + t^2} \tag{A.16}$$

$$\int_0^{+\infty} e^{-\eta y}\,\eta\, y\,\sin(ty)\,dy = \frac{2t\eta^2}{(\eta^2 + t^2)^2} \tag{A.17}$$

$$\int_0^{+\infty} e^{-\eta y}\,\eta\, y\,\cos(ty)\,dy = \frac{\eta^3 - t^2\eta}{(\eta^2 + t^2)^2} \tag{A.18}$$

we get a system of linear equations for the unknown functions

$$\cosh(td)A(t) + td\sinh(td)B(t) + A_1(t) + A_2(t) = F_1' \tag{A.19}$$

$$-\sinh(td)A(t) - [\sinh(td) + td\cosh(td)]B(t) + tL_1\,B_1(t) + tL_2\,B_2(t) = F_2' \tag{A.20}$$

$$\frac{1}{2\mu}\sinh(td)A(t) + \frac{1}{4\mu}[(1-\kappa)\sinh(td) + 2td\cosh(td)] +$$
$$+ \quad B(t) + tB_1(t) + tB_2(t) = F_3' \tag{A.21}$$

$$\frac{1}{2\mu}\cos(td)A(t) + \frac{1}{4\mu}[(1+\kappa)\cosh(td) + 2td\sinh(td)]B(t) -$$
$$- \quad tZ_1A_1(t) - tZ_2A_2(t) = F_4' \tag{A.22}$$

$$tQ_1\cosh(\beta_1 bt)\,A_1(t) + tQ_1\sinh(\beta_1 bt)\,B_1(t) +$$
$$+ \quad tQ_2\cosh(\beta_2 bt)\,A_2(t) + tQ_2\sinh(\beta_2 bt)\,B_2(t) = 0 \tag{A.23}$$

$$tL_1\sinh(\beta_1 bt)\,A_1(t) + tL_1\cosh(\beta_1 bt)\,B_1(t) +$$
$$+ \quad tL_2\sinh(\beta_2 bt)\,A_2(t) + tL_2\cosh(\beta_2 bt)\,B_2(t) = 0 \tag{A.24}$$

where

$$F_1' = \frac{2}{\pi}\int_0^{+\infty} \frac{2\eta t^2}{(\eta^2+t^2)^2} E(\eta)\,\cos(\eta d)\,d\eta \tag{A.25}$$

$$F_2' = \frac{2}{\pi}\int_0^{+\infty} \frac{2\eta^2 t}{(\eta^2+t^2)^2} E(\eta)\,\sin(\eta d)\,d\eta \tag{A.26}$$

$$F_3' = \frac{2}{\pi}\int_0^{+\infty} \frac{(\kappa-3)\eta^2 t+(\kappa+1)t^3}{4\mu(\eta^2+t^2)^2} E(\eta)\,\sin(\eta d)\,d\eta \tag{A.27}$$

$$F_4' = \frac{2}{\pi}\int_0^{+\infty} \frac{(\kappa+5)\eta^2 t^2+(\kappa+1)t^4}{4\mu\eta(\eta^2+t^2)^2} E(\eta)\,\cos(\eta d)\,d\eta \tag{A.28}$$

The six unknown functions $A(t)$, $B(t)$, $A_i(t)$ and $B_i(t)$ $(i=1,2)$ can be solved in terms of t and $F_j'(t)$ $(j=1,2,3,4)$ from eqns (A.19)–(A.24). Since only $A(t)$ and $B(t)$ are needed in the solution of the dual integral equations (4.38)–(4.39), we only give the corresponding expressions but for both values of the switching factor ρ. Using the normalized variables

$$t = \frac{s}{a} \tag{A.29}$$

$$\eta = \frac{\xi}{a} \tag{A.30}$$

we have

$$A\left(\frac{s}{a}\right) = \frac{1}{\Delta(\frac{s}{a})}\left[K_{11}F_1+K_{12}F_2+K_{13}F_3+K_{14}F_4\right] \tag{A.31}$$

$$B\left(\frac{s}{a}\right) = \frac{1}{\Delta(\frac{s}{a})}\left[K_{21}F_1+K_{22}F_2+K_{23}F_3+K_{24}F_4\right] \tag{A.32}$$

where

$$\begin{aligned}
\Delta(\tfrac{s}{a}) &= \left[s\tfrac{d}{a}+\sinh(s\tfrac{d}{a})\cosh(s\tfrac{d}{a})\right]M_1+\left[-\frac{\kappa+1}{4\mu}\sinh^2(s\tfrac{d}{a})\right]M_2+\\
&\quad+\left[\frac{1}{2\mu}s\frac{d}{a}-\frac{\kappa-1}{4\mu}\sinh(s\tfrac{d}{a})\cosh(s\tfrac{d}{a})\right](M_3+M_4)+\\
&\quad+\left[-\frac{\kappa+1}{4\mu}\cosh^2(s\tfrac{d}{a})\right]M_5+\left[-\frac{1}{4\mu^2}s\frac{d}{a}+\frac{\kappa}{4\mu^2}\sinh(s\tfrac{d}{a})\cosh(s\tfrac{d}{a})\right]M_6 \qquad \text{(A.33)}\\
K_{11} &= \left[\sinh(s\tfrac{d}{a})+s\frac{d}{a}\cosh(s\tfrac{d}{a})\right]M_1-\left[-\frac{1}{2\mu}s\frac{d}{a}\cosh(s\tfrac{d}{a})+\right.\\
&\quad\left.+\frac{\kappa-1}{4\mu}\sinh(s\tfrac{d}{a})\right]M_4-\left[\frac{\kappa+1}{4\mu}\cosh(s\tfrac{d}{a})+\frac{1}{2\mu}s\frac{d}{a}\sinh(s\tfrac{d}{a})\right]M_5\\
K_{12} &= s\frac{d}{a}\sinh(s\tfrac{d}{a})M_1+\left[-\frac{1}{2\mu}s\frac{d}{a}\cosh(s\tfrac{d}{a})+\frac{\kappa-1}{4\mu}\sinh(s\tfrac{d}{a})\right]M_2+
\end{aligned}$$

$$
\begin{aligned}
&+\left[\frac{\kappa+1}{4\mu}\cosh(s\frac{d}{a})+\frac{1}{2\mu}s\frac{d}{a}\sinh(s\frac{d}{a})\right]M_3\\
K_{13} &= -\left[\sinh(s\frac{d}{a})+s\frac{d}{a}\cosh(s\frac{d}{a})\right]M_2-s\frac{d}{a}\sinh(s\frac{d}{a})M_4+\\
&+\left[\frac{\kappa+1}{4\mu}\cosh(s\frac{d}{a})+\frac{1}{2\mu}s\frac{d}{a}\sinh(s\frac{d}{a})\right]M_6\\
K_{14} &= \left[\sinh(s\frac{d}{a})+s\frac{d}{a}\cosh(s\frac{d}{a})\right]M_3+s\frac{d}{a}\sinh(s\frac{d}{a})M_5+\\
&+\left[-\frac{1}{2\mu}s\frac{d}{a}\cosh(s\frac{d}{a})+\frac{\kappa-1}{4\mu}\sinh(s\frac{d}{a})\right]M_6\\
K_{21} &= -\sinh(s\frac{d}{a})\,M_1-\frac{1}{2\mu}\sinh(s\frac{d}{a})\,M_4+\frac{1}{2\mu}\cosh(s\frac{d}{a})\,M_5\\
K_{22} &= -\cosh(s\frac{d}{a})\,M_1+\frac{1}{2\mu}\sinh(s\frac{d}{a})\,M_2-\frac{1}{2\mu}\cosh(s\frac{d}{a})\,M_3\\
K_{23} &= \sinh(s\frac{d}{a})\,M_2+\cosh(s\frac{d}{a})M_4-\frac{1}{2\mu}\cosh(s\frac{d}{a})\,M_6\\
K_{24} &= -\sinh(s\frac{d}{a})\,M_3-\cosh(s\frac{d}{a})\,M_5+\frac{1}{2\mu}\sinh(s\frac{d}{a})\,M_6
\end{aligned}
\tag{A.34}
$$

$$
\begin{aligned}
F_1 &= \frac{2}{\pi}\int_0^{+\infty}\frac{2\xi s^2}{(\xi^2+s^2)^2}E(\xi/a)\cos(\xi\frac{d}{a})d\xi\\
F_2 &= \frac{2}{\pi}\int_0^{+\infty}\frac{2s\xi^2}{(\xi^2+s^2)^2}E(\xi/a)\sin(\xi\frac{d}{a})d\xi\\
F_3 &= \frac{2}{\pi}\int_0^{+\infty}\frac{(\kappa-3)s\xi^2+(\kappa+1)s^3}{4\mu(\xi^2+s^2)^2}E(\xi/a)\sin(\xi\frac{d}{a})d\xi\\
F_4 &= \frac{2}{\pi}\int_0^{+\infty}\frac{(\kappa+5)s^2\xi^2+(\kappa+1)s^4}{4\mu\xi(\xi^2+s^2)^2}E(\xi/a)\cos(\xi\frac{d}{a})d\xi
\end{aligned}
\tag{A.35}
$$

$$
\begin{aligned}
M_1 &= (1-\rho)\big[Z_1Q_2L_2+Z_2Q_1L_1+(Z_1Q_1L_2+Z_2Q_2L_2)\sinh t_1\sinh t_2-\\
&\quad-(Z_1Q_2L_1+Z_2Q_1L_2)\cosh t_1\cosh t_2\big]+\\
&\quad+\rho\big[-Q_0(P_3Q_1\cosh t_1-P_1L_1\sinh t_1)+Z_1(P_1P_4-P_2P_3)\big]\\
M_2 &= (1-\rho)\big[Q_1L_2(Z_2Q_1-Z_1Q_2)\sinh t_1\cosh t_2+\\
&\quad+Q_2L_1(Z_1Q_2-Z_2Q_1)\cosh t_1\sinh t_2\big]+\\
&\quad+\rho\big[Q_1Q_0(P_3Q_1\sinh t_1-P_1L_1\cosh t_1)+\\
&\quad+Z_1(c_{11}\beta_0-c_{12}Q_0)(P_4Q_1\sinh t_1-P_1L_1\cosh t_1)\big]\\
M_3 &= (1-\rho)\big[Q_1Q_2(L_1+L_2)(1-\cosh t_1\cosh t_2)+\\
&\quad+(Q_1^2L_2+Q_2^2L_1)\sinh t_1\sinh t_2\big]+\\
&\quad+\rho\big[Q_1(P_1P_4-P_2P_3)+(c_{11}\beta_0-c_{12}Q_0)(P_3Q_1\cosh t_1-P_1L_1\sinh t_1)\big]
\end{aligned}
$$

$$
\begin{aligned}
M_4 &= (1-\rho)\Big[L_1L_2(Z_1Q_2+Z_2Q_1)(1-\cosh t_1\cosh t_2)+\\
&\quad +(Z_1Q_1L_2L_2+Z_2Q_2L_1L_1)\sinh t_1\sinh t_2\Big]+\\
&\quad +\rho\Big[Z_1L_1(P_1P_4-P_2P_3)-Q_0L_1(P_3Q_1\cosh t_1-P_1L_1\sinh t_1)+\\
&\quad +c_{66}Z_1\beta_0(Q_0-Z_0)(P_4Q_1\sinh t_1-P_2L_1\cosh t_1)-\\
&\quad -c_{66}Q_1L_1\beta_0Q_0(Q_0-Z_0)\Big]\\
M_5 &= (1-\rho)\Big[Q_1L_2(L_2-L_1)\cosh t_1\sinh t_2+Q_2L_1(L_1-L_2)\sinh t_1\cosh t_2\Big]+\\
&\quad +\rho\Big[c_{66}\beta_0(Q_0-Z_0)(P_4Q_1\cosh t_1-P_2L_1\sinh t_1)\Big]\\
M_6 &= (1-\rho)\Big[2Q_1Q_2L_1L_2\,(\cosh t_1\cosh t_2-1)-\\
&\quad -(Q_1^2L_2^2+Q_2^2L_1^2)\sinh t_1\sinh t_2\Big]+\\
&\quad +\rho\Big\{L_1\Big[Q_1(P_2P_3-P_1P_4)-(c_{11}\beta_0-c_{12}Q_0)(P_3Q_1\cosh t_1-\\
&\quad -P_1L_1\sinh t_1)\Big]-c_{66}\beta_0(Q_0-Z_0)\Big[Q_1(P_4Q_1\sinh t_1-\\
&\quad -P_2L_1\cosh t_1)+Q_1L_1(c_{11}\beta_0-c_{12}Q_0)\Big]\Big\}
\end{aligned}
\tag{A.36}
$$

$$
\begin{aligned}
\left\{\begin{array}{c}P_1\\P_2\end{array}\right\} &= (c_{11}\beta_0-c_{12}Q_0)\left\{\begin{array}{c}\sinh t_0\\\cosh t_0\end{array}\right\}+(c_{11}\beta_0+c_{12}Z_0)\,t_0\left\{\begin{array}{c}\cosh t_0\\\sinh t_0\end{array}\right\}\\
\left\{\begin{array}{c}P_3\\P_4\end{array}\right\} &= -c_{66}\beta_0(Q_0-Z_0)\left\{\begin{array}{c}\cosh t_0\\\sinh t_0\end{array}\right\}-c_{66}(1-\beta_0Z_0)\,t_0\left\{\begin{array}{c}\sinh t_0\\\cosh t_0\end{array}\right\}
\end{aligned}
\tag{A.37}
$$

In the above expressions

$$
t_l=\beta_l\frac{b}{a}s\qquad(l=0,1,2)
\tag{A.38}
$$

$\Delta(\frac{s}{a})$ is the determinant of a matrix encountered during the solution of a system of linear equations. It is a function of the variable s. Similar determinants also appeared in the works of Bogy (1973), Sih & Chen (1981), and Erdogan & Wu (1991). Here, we discuss briefly its behaviour for $\rho=0$. For convenience of the numerical computation, let us denote

$$
\delta_s=\Delta(\frac{s}{a})\times e^{-2s\frac{d}{a}}\,e^{-(t_1+t_2)}
\tag{A.39}
$$

From an asymptotic analysis similar to that in § 5.2, we can get the exact asymptotic value of the above expression

$$
\lim_{s\to+\infty}\delta_s=\frac{1}{16}\,\delta\,(Q_1L_2-Q_2L_1)
\tag{A.40}
$$

where δ is given by (5.60), and L_i and Q_i $(i=1,2)$ are given by (4.19) and (4.21), respectively.

Bogy (1973) showed analytically that the determinant in the solution of an centrally cracked isotropic strip bonded to two dissimilar half planes is never equal to zero when the variable

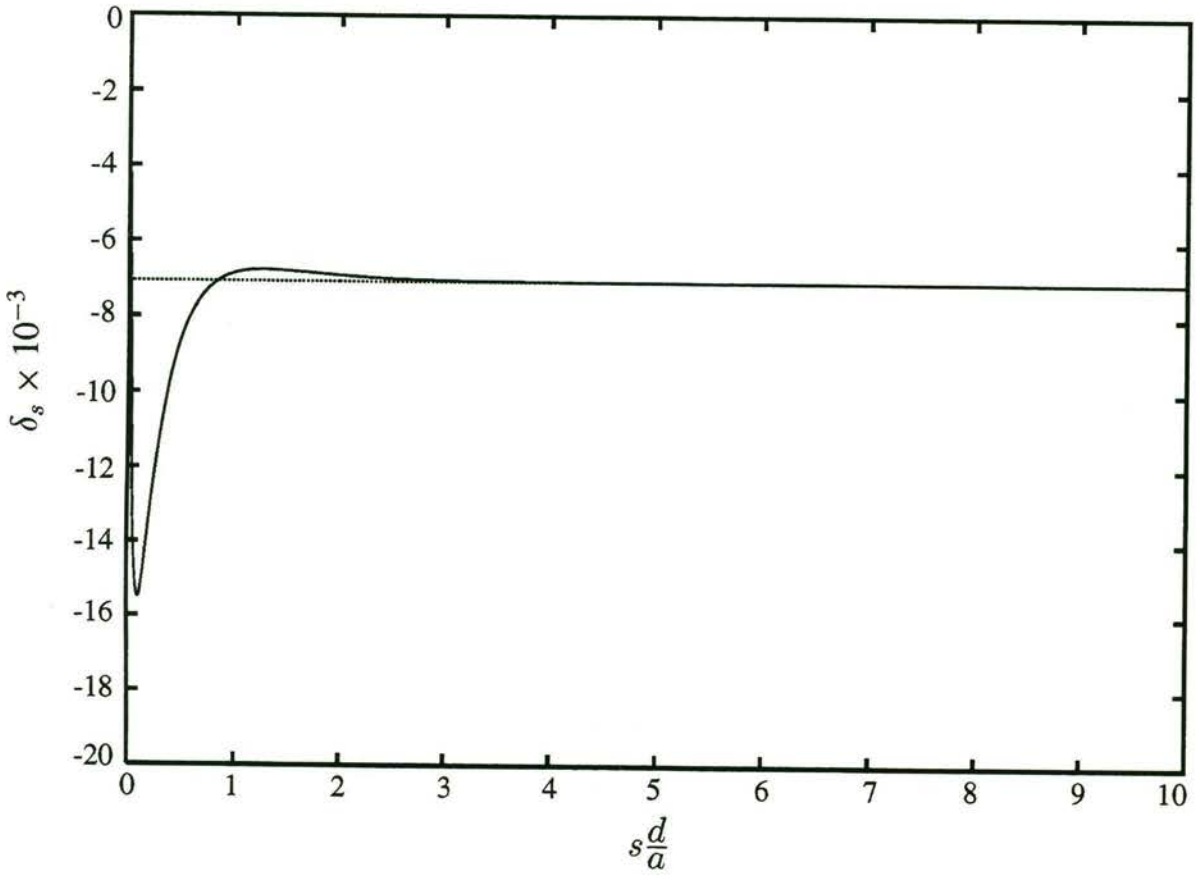

Figure A1. Variation of $\delta_s \times 10^{-3}$ with $s\frac{d}{a}$ for the material in Table 6.1 when $\theta = 0^0$, $b/d = 2.0$ and $a/d = 0.7$. The dotted line denotes its exact asymptotic value when $s \to +\infty$ (A.40)

(which is equivalent to s here) varies between $(0,+\infty)$. Here, because of the complexity of $\Delta(\frac{s}{a})$, it is hard to show analytically that it does not vanish when s varies between $(0,+\infty)$. However, numerical calculation of δ_s at discrete points with fine step lengths for numerous combinations of material properties shows that it never vanishes up to a large finite value of s. A typical variation of δ_s with $s\frac{d}{a}$ is shown in Figure A1. The data used to draw this curve are calculated for $s\frac{d}{a} \in [0, 10]$ in steps of 0.005. The value of $\delta_s \times 10^{-3}$ at $s\frac{d}{a} = 10$ is equal to -7.0639491 which is already close to the exact asymptotic value -7.0639497 obtained from (A.40). The asymptotic value δ given by (5.60) is found never to vanish for the materials considered in this Thesis. From a physical viewpoint, if $1/\Delta(\frac{s}{a})$ has a non-integrable singularity in the interval $(0, +\infty)$ for certain laminate configurations, the two constraining sublaminates will lead to an infinite perturbation in the stress field of the cracked central sublaminate (Figure 4.1). This cannot be true for the materials under consideration. The same discussion holds also for the

case $\rho = 1$, and also for mode II. The corresponding $\Delta(\frac{s}{a})$ for mode III given by (4.150) has been shown analytically in § 4.5 never to vanish.

A.2 Determination of the Unknown Functions in Mode II

Following the above procedure for mode I problem, we can solve the two unknown functions $A(s/a)$ and $B(s/a)$ in the expression (4.115) for mode II case

$$A(\frac{s}{a}) = \frac{1}{\Delta(\frac{s}{a})}\Big[K_{11}F_1 + K_{12}F_2 + K_{13}F_3 + K_{14}F_4\Big] \tag{A.41}$$

$$B(\frac{s}{a}) = \frac{1}{\Delta(\frac{s}{a})}\Big[K_{21}F_1 + K_{22}F_2 + K_{23}F_3 + K_{24}F_4\Big] \tag{A.42}$$

Here

$$\begin{aligned}
\Delta(\frac{s}{a}) \;=\; & -\left[\frac{1}{4\mu^2}\,s\frac{d}{a} - \frac{\kappa}{4\mu^2}\sinh(s\frac{d}{a})\cosh(s\frac{d}{a})\right] M_1 - \\
& -\left[\frac{1}{2\mu}\,s\frac{d}{a} + \frac{\kappa-1}{4\mu}\sinh(s\frac{d}{a})\cosh(s\frac{d}{a})\right] M_2 + \\
& +\left[\frac{\kappa+1}{4\mu}\cosh^2(s\frac{d}{a})\right] M_3 - \left[\frac{\kappa+1}{4\mu}\sinh^2(s\frac{d}{a})\right] M_4 + \\
& +\left[\frac{1}{2\mu}\,s\frac{d}{a} + \frac{\kappa-1}{2\mu}\sinh(s\frac{d}{a})\cosh(s\frac{d}{a})\right] M_5 + \\
& +\left[s\frac{d}{a} - \sinh(s\frac{d}{a})\cosh(s\frac{d}{a})\right] M_6
\end{aligned} \tag{A.43}$$

$$\begin{aligned}
K_{11} &= -\frac{1}{2\mu}\cosh(s\frac{d}{a})\,M_2 + \frac{1}{2\mu}\sinh(s\frac{d}{a})\,M_4 + \cosh(s\frac{d}{a})\,M_6 \\
K_{12} &= \frac{1}{2\mu}\cosh(s\frac{d}{a})\,M_3 - \frac{1}{2\mu}\sinh(s\frac{d}{a})\,M_5 - \sinh(s\frac{d}{a})\,M_6 \\
K_{13} &= -\frac{1}{2\mu}\sinh(s\frac{d}{a})\,M_1 - \sinh(s\frac{d}{a})\,M_2 + \cosh(s\frac{d}{a})\,M_3 \\
K_{14} &= \frac{1}{2\mu}\cosh(s\frac{d}{a})\,M_1 + \sinh(s\frac{d}{a})\,M_4 - \cosh(s\frac{d}{a})\,M_5 \\
K_{21} &= \left[\frac{1}{2\mu}\,s\frac{d}{a}\sinh(s\frac{d}{a}) - \frac{\kappa-1}{4\mu}\cosh(s\frac{d}{a})\right] M_2 + \\
&\quad -\left[\frac{1}{2\mu}\,s\frac{d}{a}\cosh(s\frac{d}{a}) + \frac{\kappa+1}{4\mu}\sinh(s\frac{d}{a})\right] M_4 - \\
&\quad -\left[\cosh(s\frac{d}{a}) + s\frac{d}{a}\sinh(s\frac{d}{a})\right] M_6
\end{aligned}$$

$$
\begin{aligned}
K_{22} &= \left[-\frac{1}{2\mu}\, s\frac{d}{a}\sinh(s\frac{d}{a}) + \frac{\kappa-1}{4\mu}\cosh(s\frac{d}{a})\right] M_3 - \\
&+ \left[\frac{1}{2\mu}\, s\frac{d}{a}\cosh(s\frac{d}{a}) + \frac{\kappa+1}{4\mu}\sinh(s\frac{d}{a})\right] M_5 + s\frac{d}{a}\cosh(s\frac{d}{a})\, M_6 \\
K_{23} &= \left[\frac{\kappa+1}{4\mu}\sinh(s\frac{d}{a}) + \frac{1}{2\mu}\, s\frac{d}{a}\cosh(s\frac{d}{a})\right] M_1 + \\
&+ s\frac{d}{a}\cosh(s\frac{d}{a})\, M_2 - \left[\cosh(s\frac{d}{a}) + s\frac{d}{a}\sinh(s\frac{d}{a})\right] M_3 \\
K_{24} &= \left[-\frac{1}{2\mu}\, s\frac{d}{a}\sinh(s\frac{d}{a}) + \frac{\kappa+1}{4\mu}\cosh(s\frac{d}{a})\right] M_1 - \\
&- s\frac{d}{a}\cosh(s\frac{d}{a})\, M_4 + \left[\cosh(s\frac{d}{a}) + s\frac{d}{a}\sinh(s\frac{d}{a})\right] M_5
\end{aligned}
\tag{A.44}
$$

$$
\begin{aligned}
F_1 &= \frac{2}{\pi}\int_0^\infty \frac{2s^3}{(\xi^2+s^2)^2} E(\frac{\xi}{a})\sin(\xi\frac{d}{a})\, d\xi \\
F_2 &= \frac{2}{\pi}\int_0^\infty \frac{2\xi s^2}{(\xi^2+s^2)^2} E(\frac{\xi}{a})\cos(\xi\frac{d}{a})\, d\xi \\
F_3 &= \frac{2}{\pi}\frac{1}{4\mu}\int_0^\infty \frac{(\kappa+1)\, s^4 + (\kappa-3)\, s^2\xi^2}{\xi(\xi^2+s^2)^2} E(\frac{\xi}{a})\cos(\xi\frac{d}{a})\, d\xi \\
F_4 &= \frac{2}{\pi}\frac{1}{4\mu}\int_0^\infty \frac{(\kappa+1)\, s\xi^2 + (\kappa-3)\, s^3}{(\xi^2+s^2)^2} E(\frac{\xi}{a})\sin(\xi\frac{d}{a})\, d\xi
\end{aligned}
\tag{A.45}
$$

$$
\begin{aligned}
M_1 &= (1-\rho)\,\{2c_{66}(Z_1+\beta_1)(Z_2+\beta_2)Q_1Q_2(1-\cosh t_1\cosh t_2) \\
&+ c_{66}\left[Q_2^2(Z_1+\beta_1)^2 + Q_1^2(Z_2+\beta_2)^2\right]\sinh t_1\sinh t_2\Big\} + \\
&+\rho\,\{-c_{66}(Z_1+\beta_1)Q_1(P_1P_4 - P_2P_3) - c_{66}(\beta_0-T_0)Q_1\,[Q_1P_3\sinh t_1 - \\
&-(Z_1+\beta_1)P_1\cosh t_1] + c_{11}c_{66}\beta_0(Z_1+\beta_1)(Z_0-T_0)\,[Q_1P_4\cosh t_1 - \\
&-(Z_1+\beta_1)P_2\sinh t_1] - c_{11}c_{66}\beta_0(Z_0-T_0)(Z_1+\beta_1)(\beta_0-T_0)Q_1\} \\
M_2 &= (1-\rho)\,\{c_{66}(Z_1+\beta_1)(Z_2+\beta_2)(Q_1+Q_2)(\cosh t_1\cosh t_2 - 1) - \\
&-c_{66}[(Z_1+\beta_1)^2Q_2 + (Z_2+\beta_2)^2Q_1]\sinh t_1\sinh t_2\Big\} + \\
&+\rho\,\{c_{66}(\beta_0-T_0)[Q_1P_3\sinh t_1 - (Z_1+\beta_1)P_1\cosh t_1] + \\
&+ c_{66}(Z_1+\beta_1)(P_1P_4 - P_2P_3)\} \\
M_3 &= (1-\rho)\,\{Q_1(Z_2+\beta_2)(Q_2-Q_1)\sinh t_1\cosh t_2 + \\
&+ Q_2(Z_1+\beta_1)(Q_1-Q_2)\cosh t_1\sinh t_2\} \\
&+\rho\,\{-c_{11}\beta_0(Z_0-T_0)[Q_1P_4\sinh t_1 - (Z_1+\beta_1)P_2\cosh t_1]\}
\end{aligned}
$$

$$
\begin{aligned}
M_4 &= (1-\rho)\left\{c_{66}[Z_1Q_1(Z_2+\beta_2)^2\cosh t_1\sinh t_2 + Z_2Q_2(Z_1+\beta_1)^2\sinh t_1\cosh t_2]-\right.\\
&\quad -c_{66}(Z_1+\beta_1)(Z_2+\beta_2)[Z_1Q_2\sinh t_1\cosh t_2 + Z_2Q_1\cosh t_1\sinh t_2]\}+\\
&\quad +\rho\{-c_{66}(Z_1\beta_0+\beta_1T_0)[Q_1P_3\cosh t_1-(Z_1+\beta_1)P_1\sinh t_1]\}\\
M_5 &= (1-\rho)\{Q_1Q_2[Z_1(Z_2+\beta_2)+Z_2(Z_1+\beta_1)](1-\cosh t_1\cosh t_2)+\\
&\quad \left.+[Z_1Q_2^2(Z_1+\beta_1)+Z_2Q_1^2(Z_2+\beta_2)]\sinh t_1\sinh t_2\right\}+\\
&\quad +\rho\{c_{11}\beta_0(Z_0-T_0)Z_1[Q_1P_4\cosh t_1-(Z_1+\beta_1)P_2\sinh t_1]-\\
&\quad -Z_1Q_1(P_1P_4-P_2P_3)+T_0Q_1[Q_1P_3\sinh t_1-(Z_1+\beta_1)P_1\cosh t_1]+\\
&\quad +c_{11}\beta_0T_0(Z_1+\beta_1)(Z_0-T_0)Q_1\}\\
M_6 &= (1-\rho)\{[Z_1Q_1(Z_2+\beta_2)+Z_2Q_2(Z_1+\beta_1)]\cosh t_1\cosh t_2-\\
&\quad -[Z_1Q_2(Z_1+\beta_1)+Z_2Q_1(Z_2+\beta_2)]\sinh t_1\sinh t_2-\\
&\quad -[Z_1Q_2(Z_2+\beta_2)+Z_2Q_1(Z_1+\beta_1)]\}+\\
&\quad +\rho\{-T_0[Q_1P_3\sinh t_1-(Z_1+\beta_1)P_1\cosh t_1]+Z_1(P_1P_4-P_2P_3]\}
\end{aligned}
\tag{A.46}
$$

$$
\begin{aligned}
\left\{\begin{array}{c}P_1\\P_2\end{array}\right\} &= Q_0t_0\left\{\begin{array}{c}\sinh t_0\\\cosh t_0\end{array}\right\}+c_{11}\beta_0(Z_0-T_0)\left\{\begin{array}{c}\cosh t_0\\\sinh t_0\end{array}\right\}\\
\left\{\begin{array}{c}P_3\\P_4\end{array}\right\} &= (Z_1+\beta_1)t_0\left\{\begin{array}{c}\cosh t_0\\\sinh t_0\end{array}\right\}+(\beta_0-T_0)\left\{\begin{array}{c}\sinh t_0\\\cosh t_0\end{array}\right\}
\end{aligned}
\tag{A.47}
$$

In the above expressions

$$
t_l = \beta_l\frac{b}{a}s \quad (l=0,1,2) \tag{A.48}
$$

Appendix B

Solution of the Dual Integral Equations

The contents of this Appendix follow closely the paper by Wang & Karihaloo (1994a). For the dual integral equations

$$\int_0^\infty A(s)\, J_\nu(rs)\, ds \;=\; 0 \quad r > a \tag{B.1}$$

$$\int_0^\infty s^{2\alpha} A(s)\, J_\nu(rs)\, ds \;=\; f(r) \quad r < a \tag{B.2}$$

Copson (1961) showed the solution to be

$$A(s) = s^{1-\alpha} \int_0^a \phi(t)\, J_{\nu+\alpha}(st)\, dt \tag{B.3}$$

provided that

$$0 \;<\; \alpha < 1 \tag{B.4}$$

$$\nu \;>\; -\alpha \tag{B.5}$$

$$\lim_{t\to 0^+} [t^{\nu+\alpha-1}\, \phi(t)] \;=\; 0 \tag{B.6}$$

The function $\phi(t)$ may be determined from

$$\phi(t) = \frac{2^{1-\alpha}}{\Gamma(\alpha)}\, t^{1-\nu-\alpha}\, \phi(t) = \frac{2^{1-\alpha}}{\Gamma(\alpha)}\, t^{1-\nu-\alpha} \int_0^t \frac{r^{1+\nu} f(r)}{(t^2 - r^2)^{1-\alpha}}\, dr \tag{B.7}$$

Equation (B.7) was derived by assuming that the function $r^\nu f(r)$ and its first derivative are continuous in the interval $[0, a]$. The above solution procedure was also cited by Sih & Chen (1981) in relation to crack problems in composite materials.

In the crack problems under consideration (e.g. (4.44)–(4.45)), $\alpha = 1/2$ and $\nu = -1/2$, so that the condition (B.5) is not satisfied. We will show below that the solution of

$$\int_0^\infty A(s)\, J_{-\frac{1}{2}}\, ds \;=\; 0 \quad r > a \tag{B.8}$$

$$\int_0^\infty sA(s)\, J_{-\frac{1}{2}}\, ds \;=\; f(r) \quad r < a \tag{B.9}$$

is also given by (B.3) and (B.7), thereby extending the range of applicability of Copson's procedure to include the equality sign in (B.5), i.e. $\nu \geq -\alpha$.

To this end, we rewrite first (B.8)–(B.9) in the following form

$$\int_0^\infty \frac{1}{s} E(s)\cos(sr)\,ds = 0 \quad r > a \tag{B.10}$$

$$\int_0^\infty E(s)\cos(sr)\,ds = (\frac{\pi}{2})^{\frac{1}{2}} r^{\frac{1}{2}} f(r) \quad r < a \tag{B.11}$$

where we have made use of the definition

$$J_{-\frac{1}{2}}(sr) = (\frac{\pi sr}{2})^{-\frac{1}{2}} \cos(sr) \tag{B.12}$$

and denoted

$$E(s) = s^{\frac{1}{2}} A(s) \tag{B.13}$$

In order to solve eqns (B.10)–(B.11), eqn (B.11) is further rewritten (Sneddon & Srivastav, 1971) as

$$\frac{d}{dr}\int_0^\infty \frac{1}{s} E(s)\,\sin(sr)\,ds = (\frac{\pi}{2})^{\frac{1}{2}} r^{\frac{1}{2}} f(r) \quad r < a \tag{B.14}$$

Next, we introduce a new unknown function $\phi(t)$ as follows

$$\frac{1}{s} E(s) = \int_0^a \phi(t)\, J_0(st)\, dt \tag{B.15}$$

which automatically satisfies eqn (B.10). Inserting eqn (B.15) into eqn (B.14) gives

$$\frac{d}{dr}\int_0^\infty \int_0^a \phi(t)\, J_0(st)\,\sin(sr)\, dt\, ds = (\frac{\pi}{2})^{\frac{1}{2}} r^{\frac{1}{2}} f(r) \tag{B.16}$$

Changing the order of integration and noting that

$$\begin{aligned} \int_0^\infty J_0(st)\,\sin(sr)\,ds &= \frac{1}{\sqrt{r^2 - t^2}} \quad 0 \leq t < r \\ &= 0 \qquad r < t < \infty \end{aligned} \tag{B.17}$$

reduces eqn (B.16) to

$$\frac{d}{dr}\int_0^r \frac{\phi(t)}{\sqrt{r^2 - t^2}}\, dt = (\frac{\pi}{2})^{\frac{1}{2}} r^{\frac{1}{2}} f(r) \tag{B.18}$$

The solution of this Abel-type integral equation is

$$\phi(t) = (\frac{2}{\pi})^{\frac{1}{2}} t \int_0^t \frac{r^{\frac{1}{2}} f(r)}{\sqrt{t^2 - r^2}}\, dr \tag{B.19}$$

Then from eqns (B.13) and (B.15) we get the solution of eqns (B.8)–(B.9)

$$A(s) = s^{\frac{1}{2}} \int_0^a \phi(t)\, J_0(st)\, dt \tag{B.20}$$

The solution (B.20), with $\phi(t)$ given by (B.19), could be directly written from (B.3) and (B.7) with $\alpha = 1/2$ and $\nu = -1/2$, thus extending the range of applicability to include the equality sign in (B.5), i.e. $\nu \geq -\alpha$.

In § 4.6, we encountered dual integral equations (4.185)–(4.186), which are slightly different from (B.1)–(B.2)

$$\int_0^\infty A(s)J_\nu(rs)\,ds = 0 \quad r > a \tag{B.21}$$

$$\int_o^\infty s^{2\alpha} F(s)A(s)J_\nu(rs)\,ds = f(r) \quad r < a \tag{B.22}$$

These may however be formally given the form of (B.1)–(B.2)

$$\int_0^\infty A(s)J_\nu(rs)\,ds = 0 \quad r > a \tag{B.23}$$

$$\int_0^\infty s^{2\alpha} A(s)J_\nu(rs)ds = f^*(r) \quad r < a \tag{B.24}$$

where

$$f^*(r) = f(r) - \int_0^\infty s^{2\alpha}[F(s) - 1]A(s)J_\nu(rs)\,ds \tag{B.25}$$

The solution (B.7) now becomes

$$\phi(t) + \int_0^c \phi(\xi)\,K(\xi,\eta)\,d\eta = \frac{2^{1-\alpha}}{\Gamma(\alpha)}\,t^{1-\nu-\alpha}\int_0^t \frac{r^{1+\nu}f(r)}{(t^2-r^2)^{1-\alpha}}\,dr \tag{B.26}$$

in which the additional kernel $K(\xi,\eta)$ is

$$K(\xi,\eta) = t\int_0^\infty s[F(s) - 1]J_{\alpha+\nu}(s\xi)J_{\alpha+\nu}(st)\,ds \tag{B.27}$$

Appendix C

Stiffness Parameters and Their Gradients

In this Appendix, we evaluate the stiffnesses of the sublaminate $(\pm\theta)_{n_2}$ in the symmetric angle-ply $[(\pm\theta)_{n_2}/(90^0)_{n_1}]_s$ laminate considered in Chapter 6. The stiffnesses of the constraining sublaminates considered in Chapter 7, and those of the $(\pm\theta)_{n_2}$ sublaminate in the antisymmetric angle-ply $[(\pm\theta)_{n_2}/(90^0)_{n_1}/(\mp\theta)_{n_2}]$ laminate considered in Chapter 8 are also calculated. The stiffnesses of all these sublaminates are approximated by those of an antisymmetric angle-ply $[(\pm\theta)_{n_2}/(\mp\theta)_{n_2}]$ laminate. Because it has an identical in-plane (laminate plane) matrix of average stiffnesses to that of a symmetric $[(\pm\theta)_{n_2}]_s$ laminate (cf. (3.157) and (3.158)), some of the relations are also applicable to the latter. The procedure is approximate and is based upon homogenisation and classical lamination theory. The exposition in this Appendix follows closely the contents of Appendix A in the paper by Wang & Karihaloo (1994a).

Using the notation of Tsai & Hahn (1980) (see also § 3.7), and denoting

$$
\begin{aligned}
Q_{xx} &= \frac{E_L}{1-\nu_{LT}\,\nu_{TL}} \\
Q_{xy} &= \frac{E_L\,\nu_{TL}}{1-\nu_{LT}\,\nu_{TL}} \\
Q_{yy} &= \frac{E_T}{1-\nu_{LT}\,\nu_{TL}} \\
Q_{ss} &= G_{LT} \\
U_1 &= \frac{1}{8}\left[3Q_{xx}+3Q_{yy}+2Q_{xy}+4Q_{ss}\right] \\
U_2 &= \frac{1}{2}\left[Q_{xx}-Q_{yy}\right] \\
U_3 &= \frac{1}{8}\left[Q_{xx}+Q_{yy}-2Q_{xy}-4Q_{ss}\right] \\
U_4 &= \frac{1}{8}\left[Q_{xx}+Q_{yy}+6Q_{xy}-4Q_{ss}\right]
\end{aligned}
$$

$$
\begin{aligned}
U_5 &= \frac{1}{8}\left[Q_{xx} + Q_{yy} - 2Q_{xy} + 4Q_{ss}\right] \\
Q_{11} &= U_1 + U_2\cos 2\theta + U_3\cos 4\theta \\
Q_{22} &= U_1 - U_2\cos 2\theta + U_3\cos 4\theta \\
Q_{12} &= U_4 - U_3\cos 4\theta \\
Q_{66} &= U_5 - U_3\cos 4\theta
\end{aligned} \tag{C.1}
$$

the in-plane (with respect to laminate) stiffness matrix of a symmetric $[(\pm\theta)_{n_2}]_s$ and an anti-symmetric $[(\pm\theta^0)_{n_2}/(\mp\theta^0)_{n_2}]$ laminate may be written as (cf. § 3.7.2)

$$
[Q] = \begin{bmatrix} Q_{11} & Q_{12} & 0 \\ Q_{12} & Q_{22} & 0 \\ 0 & 0 & Q_{66} \end{bmatrix} \tag{C.2}
$$

with the compliance matrix as

$$
[S] = [Q]^{-1} = \begin{bmatrix} a_{11} & a_{12} & 0 \\ a_{12} & a_{22} & 0 \\ 0 & 0 & a_{66} \end{bmatrix} \tag{C.3}
$$

In the coordinate system of Figure 6.2(a), we have

$$
\begin{aligned}
E_x &= E_T \\
E_y &= \frac{1}{a_{11}} \\
E_z &= \frac{1}{a_{22}} \\
\nu_{yz} &= -\frac{a_{12}}{a_{11}} \\
\nu_{zy} &= E_z\frac{\nu_{yz}}{E_y}
\end{aligned} \tag{C.4}
$$

The modulus E_x is evaluated using a series model (Enie & Rizzo, 1970). It can also be calculated from the formula

$$
\frac{1}{E_x} = S_{33} - \frac{S_{36}^2}{S_{66}} \tag{C.5}
$$

where

$$
\begin{aligned}
S_{33} &= \frac{1}{E_T} \\
S_{36} &= \left(\frac{\nu_{TT}}{E_T} - \frac{\nu_{LT}}{E_L}\right)\sin 2\theta \\
S_{66} &= G_{LT}
\end{aligned} \tag{C.6}
$$

Eqn (C.5) takes into account the shear-normal stress coupling between the laminae. If this coupling is ignored, E_x reduces to E_T. For the material properties used in Chapter 8, it was found that the maximum deviation of E_x (C.5) from E_T is 5.8%. The changes in the stress intensity factor and the stresses are smaller still. In order to maintain consistency with the parameters calculated using the lamination theory, $E_x = E_T$ is used in this Thesis.

To calculate the out-of-plane (in xy-plane) Poisson's ratios, we invoke the assumption of homogeneity and orthotropy of $[(\pm\theta^0)_{n_2}/(\mp\theta^0)_{n_2}]$ laminate, and write

$$\nu_{yx} = \nu_{LT}\cos^2\theta + \nu_{TT}\sin^2\theta \tag{C.7}$$

$$\nu_{zx} = \nu_{LT}\sin^2\theta + \nu_{TT}\cos^2\theta \tag{C.8}$$

The out-of-plane (in xy-plane) shear modulus is taken as (Vinson & Chow, 1975)

$$c_{66} = G_{LT}\cos^2\theta + G_{TT}\sin^2\theta \tag{C.9}$$

From the above engineering constants and plane strain condition, we get the constitutive equations of $[(\pm\theta^0)_{n_2}/(\mp\theta^0)_{n_2}]$ laminate

$$\begin{bmatrix} \epsilon_{xx} \\ \epsilon_{yy} \\ \gamma_{xy} \end{bmatrix} = \begin{bmatrix} s_{11} & s_{12} & 0 \\ s_{21} & s_{22} & 0 \\ 0 & 0 & s_{66} \end{bmatrix} \begin{bmatrix} \sigma_{xx} \\ \sigma_{yy} \\ \tau_{xy} \end{bmatrix} \tag{C.10}$$

in which s_{ij} $(i,j = 1,2,6)$ are the compliance coefficients. They can be expressed as

$$\begin{aligned} s_{11} &= \frac{1}{E_x} - \frac{\nu_{zx}^2}{E_z} \\ s_{12} &= s_{21} = -\frac{\nu_{yx} + \nu_{zx}\,\nu_{yz}}{E_y} \\ s_{22} &= \frac{1}{E_y} - \frac{\nu_{zy}^2}{E_z} \\ s_{66} &= \frac{1}{c_{66}} \end{aligned} \tag{C.11}$$

Inverting the above compliance matrix $[s_{ij}]$ gives the stiffness matrix $[c_{ij}]$ $(i,j = 1,2,6)$ of the $[(\pm\theta^0)_{n_2}/(\mp\theta^0)_{n_2}]$ laminate

$$\begin{bmatrix} c_{11} & c_{12} & 0 \\ c_{21} & c_{22} & 0 \\ 0 & 0 & c_{66} \end{bmatrix} \tag{C.12}$$

Once the stiffness parameters have been obtained, the normalized flexural modulus, eqn (8.13), of the laminate can be calculated using the lamination theory (Tsai & Hahn, 1980). For ease of

gradient calculation, it is expedient to rewrite the constraint (8.10) as

$$(1-\gamma) - \frac{\overline{D}}{D_0} \leq 0 \tag{C.13}$$

where, by definition (8.13),

$$\frac{\overline{D}}{D_0} = \frac{[(1+\frac{b}{d})^3 - 1]\, c_{22}^{\theta} + c_{22}^{90}}{[(1+\frac{b}{d})^3 - 1]\, c_{22}^{0} + c_{22}^{90}} \tag{C.14}$$

The gradients of $\overline{D}/D_0$ with respect to θ and b/d are easily written

$$\frac{\partial}{\partial\theta}\left(\frac{\overline{D}}{D_0}\right) = \frac{[(1+\frac{b}{d})^3 - 1]}{[(1+\frac{b}{d})^3 - 1]\, c_{22}^{0} + c_{22}^{90}} \frac{\partial}{\partial\theta} c_{22}^{\theta} \tag{C.15}$$

$$\frac{\partial}{\partial(\frac{b}{d})}\left(\frac{\overline{D}}{D_0}\right) = 3(1+\frac{b}{d})^2 \frac{(c_{22}^{\theta} - c_{22}^{0})\, c_{22}^{90}}{\left\{[(1+\frac{b}{d})^3 - 1]\, c_{22}^{0} + c_{22}^{90}\right\}^2} \tag{C.16}$$

in which $\partial c_{22}^{\theta}/\partial\theta$ can be calculated analytically from (C.12) and (C.11).

When the angle-ply fibre-reinforced laminate is considered in mode III in § 6.3, the necessary shear stiffnesses for the outer constraining sublaminate $[(\pm\theta^0)_{n_2}]$ are evaluated from the following expressions

$$c_{44} = U_5 - U_3 \cos 4\theta \tag{C.17}$$

$$c_{55} = G_{TT}\cos^2\theta + G_{LT}\sin^2\theta \tag{C.18}$$

where U_3 and U_5 given by (C.1).

Appendix D

Expressions for M_i When β_i Are Complex Conjugate

For the $[(\pm\theta^0)_{n_2}/(90^0)_{n_1}/(\mp\theta^0)_{n_2}]$ laminate and the commonly used materials, when $0^0 \leq \theta < \theta_c$, the roots β_i $(i = 1, 2)$ of the eqn (3.113) are distinct real numbers; whereas for $\theta_c < \theta \leq 90^0$, the roots are complex conjugate. θ_c depends on the material properties. With real roots β_i $(i = 1, 2)$, the results are given in Appendix A. On the other hand, when β_i $(i = 1, 2)$ are complex conjugate, M_i $(i = 1, ..., 6)$ in eqns (A.36) and (A.46) would seem at first sight to require modifications. However, it will be shown below that irrespective of whether β_i $(i = 1, 2)$ are real or complex conjugate, M_i $(i = 1, ..., 6)$ are always real. Thus the entire procedure described in Appendix A is applicable to any configuration of $[(\pm\theta^0)_{n_2}/(90^0)_{n_1}/(\mp\theta^0)_{n_2}]$ laminates.

If the roots β_i $(i = 1, 2)$ of eqn (3.113) are complex conjugate, they may be written as

$$\beta_1 = r + t\,i \qquad \beta_2 = r - t\,i = \overline{\beta_1} \tag{D.1}$$

where

$$r = \sqrt{\frac{1}{2}(\sqrt{B_2} + B_1)} \qquad t = \sqrt{\frac{1}{2}(\sqrt{B_2} - B_1)} \tag{D.2}$$

The other constants are

$$Z_1 = A + B\,i \quad Z_2 = A - B\,i = \overline{Z_1} \tag{D.3}$$

$$Q_1 = R + T\,i \quad Q_2 = R - T\,i = \overline{Q_1} \tag{D.4}$$

in which

$$A = \frac{c_{22}r - c_{66}r(r^2 - t^2) - 2c_{66}rt^2}{(r^2 + t^2)(c_{12} + c_{66})}$$

$$
\begin{aligned}
B &= \frac{c_{66}(r^2-t^2)t - 2c_{66}r^2t - c_{22}t}{(r^2+t^2)(c_{12}+c_{66})} \\
R &= c_{11}(Ar - Bt) - c_{12} \\
T &= c_{11}(At + Br)
\end{aligned} \tag{D.5}
$$

Denoting the various combinations of hyperbolic functions appearing in eqns (A.36) and (A.46) through

$$
\begin{aligned}
\cosh t_1 \cosh t_2 &= \frac{1}{2}\cosh(2r\frac{b}{a}s) + \frac{1}{2}\cos(2t\frac{b}{a}s) \equiv CC \\
\sinh t_1 \sinh t_2 &= \frac{1}{2}\cosh(2r\frac{b}{a}s) - \frac{1}{2}\cos(2t\frac{b}{a}s) \equiv SS \\
\sinh t_1 \cosh t_2 &= \frac{1}{2}\sinh(2r\frac{b}{a}s) + \frac{1}{2}\sin(2t\frac{b}{a}s)\,i \equiv D + H\,i \\
\cosh t_1 \sinh t_2 &= \frac{1}{2}\sinh(2r\frac{b}{a}s) - \frac{1}{2}\sin(2t\frac{b}{a}s)\,i \equiv D - H\,i,
\end{aligned} \tag{D.6}
$$

M_i $(i = 1, ..., 6)$ of (A.46) may be rewritten as

$$
\begin{aligned}
M_1 &= 2c_{66}[(A+r)^2 + (B+t)^2](R^2+T^2)(1-CC) + \\
&\quad +2c_{66}\{(R^2-T^2)[(A+r)^2 - (B+t)^2] + 4RT(A+r)(B+t)\}SS \\
M_2 &= 2c_{66}R[(A+r)^2 + (B+t)^2](CC-1) - \\
&\quad -2c_{66}\{R[(A+r)^2 - (B+t)^2] + 2T(A+r)(B+t)\}SS \\
M_3 &= 4T[(DT+HR)(A+r) + (HT-DR)(B+t)] \\
M_4 &= 2c_{66}\{[(A+r)^2 - (B+t)^2][D(AR-BT) + H(AT+BR)] + \\
&\quad +2(A+r)(B+t)[D(AT+BR) - H(AR-BT)]\} - \\
&\quad -2c_{66}[(A+r)^2 + (B+t)^2][D(AR+BT) - H(BR-AT)] \\
M_5 &= 2(R^2+T^2)[A(A+r) + B(B+t)](1-CC) + \\
&\quad +2\{(A+r)[A(R^2-T^2) + 2RTB] - \\
&\quad -(B+t)[B(R^2-T^2) - 2RTA]\}SS \\
M_6 &= 2[(A+r)(AR-BT) + (B+t)(AT+BR)]CC - \\
&\quad -2[(A+r)(AR+BT) - (B+t)(BR-AT)]SS - \\
&\quad -2[(A+r)(AR+BT) + (B+t)(BR-AT)]
\end{aligned} \tag{D.7}
$$

which are all real.

In a similar manner it can be shown that M_i $(i = 1, ..., 6)$ appearing in (A.36) are also real.

Appendix E

Finiteness of $\frac{d}{d\xi}\left[\frac{\Phi(\xi)}{\xi^{1/2}}\right]$

In this Appendix, we shall examine the behaviour of $K^*(\xi,\eta)$ in the expression (4.75) with respect to ξ alone. For this, we shall omit the details of the influence of η but only keep in mind that $0 \leq \eta \leq 1$. Therefore, all the expressions up to (E.12) inclusive are valid for any $\eta \in [0,1]$. For the sake of conciseness and convenience of the exposition in this Appendix, we rewrite the expression (4.75) as follows

$$K^*(\xi,\eta) = \int_0^{+\infty} f(\xi,\eta,s)\,ds \tag{E.1}$$

where

$$f(\xi,\eta,s) = \sqrt{\eta}\,\frac{se^{-s\frac{d}{a}}}{\Delta(\frac{s}{a})}\left\{I_0(s\xi)\sum_{j=1}^{4}K_{1j}E_j + [2I_0(s\xi) + s\xi I_1(s\xi)]\sum_{j=1}^{4}K_{2j}E_j\right\}ds \tag{E.2}$$

Following the discussion from (4.69) to (4.72), we know that the integral (E.1) is convergent for any ξ.

In the following, we shall show that

$$\int_0^{+\infty}\frac{\partial}{\partial\xi}f(\xi,\eta,s)\,ds \tag{E.3}$$

is uniformly convergent with respect to $\xi \in [0,1]$. For this, we perform the differentiation in (E.3) and write

$$\frac{\partial}{\partial\xi}f(\xi,\eta,s) = \sqrt{\eta}\,s^2\left\{I_1(s\xi)\sum_{j=1}^{4}\frac{K_{ij}E_j}{\Delta(\frac{s}{a})} + [2I_1(s\xi) + s\xi\, I_0(s\xi)]\sum_{j=1}^{4}\frac{K_{2j}E_j}{\Delta(\frac{s}{a})}\right\}e^{-s\frac{d}{a}} \tag{E.4}$$

where we have used the formulae

$$\frac{d}{dx}I_0(x) = I_1(x) \tag{E.5}$$

$$\frac{d}{dx}I_1(x) = I_0(x) - \frac{1}{x}I_1(x) \tag{E.6}$$

For any $\xi \in [0,1]$ and $s \in [0,+\infty)$, we have

$$\begin{aligned}
\left|\frac{\partial}{\partial\xi} f(\xi,\eta,s)\right| &\leq \sqrt{\eta}\, s^2 \left\{ I_1(s\xi) \left|\sum_{j=1}^{4} \frac{K_{1j}E_j}{\Delta(\frac{s}{a})}\right| + [2I_1(s\xi) + s\xi\, I_0(s\xi)] \left|\sum_{j=1}^{4} \frac{K_{2j}E_j}{\Delta(\frac{s}{a})}\right| \right\} e^{-s\frac{d}{a}} \\
&\leq s^2 \left\{ I_1(s) \left|\sum_{j=1}^{4} \frac{K_{1j}E_j}{\Delta(\frac{s}{a})}\right| + [2I_1(s) + sI_0(s)] \left|\sum_{j=1}^{4} \frac{K_{2j}E_j}{\Delta(\frac{s}{a})}\right| \right\} e^{-s\frac{d}{a}} \\
&\leq s^2 \left\{ \frac{1}{2}s \left|\sum_{j=1}^{4} \frac{K_{1j}E_j}{\Delta(\frac{s}{a})}\right| + 2s \left|\sum_{j=1}^{4} \frac{K_{2j}E_j}{\Delta(\frac{s}{a})}\right| \right\} e^{-s(\frac{d}{a}-1)} \equiv h(s,\eta) \qquad \text{(E.7)}
\end{aligned}$$

where we have used the properties of $I_0(x)$ and $I_1(x)$, i.e.

$$\begin{aligned}
I_0(x_1) &\leq I_0(x_2) \\
I_1(x_1) &\leq I_1(x_2)
\end{aligned} \qquad \text{if} \quad 0 \leq x_1 \leq x_2 \qquad \text{(E.8)}$$

and

$$\begin{aligned}
I_0(x) &\leq e^x \\
I_1(x) &\leq \frac{1}{2} x e^x
\end{aligned} \qquad 0 \leq x < +\infty \qquad \text{(E.9)}$$

These properties are easily derived from the integral expression of the deformed Bessel function

$$I_\nu(x) = \frac{\left(\frac{x}{2}\right)^\nu}{\Gamma(\nu+\frac{1}{2})\,\Gamma(\frac{1}{2})} \int_{-1}^{+1} (1-t^2)^{\nu-\frac{1}{2}} \cosh(xt)\, dt \quad \text{Re}(\nu) > -\frac{1}{2} \qquad \text{(E.10)}$$

Considering the behaviour of $\frac{K_{ij}}{\Delta(\frac{s}{a})}$ (eqn (4.69)) and $I_\nu(\eta s)$ ($\nu = 0, 1$) in E_j (eqns (4.55)–(4.58)), it is seen that $h(s,\eta)$, which does not depend ξ, is integrable in the interval $[0,+\infty)$. Therefore, Weierstrass's criterion ensures that

$$\int_0^{+\infty} \frac{\partial}{\partial\xi} f(\xi,\eta,s)\, ds \qquad \text{(E.11)}$$

is uniformly convergent with respect to ξ. Based upon this conclusion, we can differentiate $f(\xi,\eta,s)$ with respect to ξ under the integral sign when we differentiate $K^*(\xi,\eta)$ in eqn (E.1) with respect to ξ, i.e.

$$\frac{\partial}{\partial\xi} K^*(\xi,\eta) = \frac{\partial}{\partial\xi}\left[\int_0^{+\infty} f(\xi,\eta,s)\, d\xi\right] = \int_0^{+\infty} \frac{\partial}{\partial\xi} f(\xi,\eta,s)\, d\xi \qquad \text{(E.12)}$$

which is finite and a continuous function of ξ. Therefore, from (4.74), we have

$$\frac{d}{d\xi}\left[\frac{\Phi(\xi)}{\sqrt{\xi}}\right] = \frac{d}{d\xi}\left[1 - \int_0^1 K^*(\xi,\eta)\, \Phi(\eta)\, d\eta\right] = -\int_0^1 \frac{\partial}{\partial\xi} K^*(\xi,\eta)\ \Phi(\eta)\, d\eta \qquad \text{(E.13)}$$

We now show that $\frac{\partial}{\partial\xi}K^*(\xi,\eta)$ is also a continuous function of η for any $\xi \in [0,1]$. For this, we use eqn (E.7) and eqns (4.55)–(4.58) to get

$$\begin{aligned}\left|\frac{\partial}{\partial\xi}f(\xi,\eta,s)\right| &\leq s^2\left\{\frac{1}{2}s\sum_{j=1}^{4}\left|\frac{K_{1j}}{\Delta(\frac{s}{a})}e^{s\frac{d}{a}}\right|E'_j + 2s\sum_{j=1}^{4}\left|\frac{K_{2j}}{\Delta(\frac{s}{a})}e^{s\frac{d}{a}}\right|E'_j\right\}e^{-2s(\frac{d}{a}-1)} \\ &\equiv g(s) \end{aligned} \tag{E.14}$$

in which

$$E'_1 = \left|(1-s\frac{d}{a})\right| + \frac{1}{2}s^2 \tag{E.15}$$

$$E'_2 = \left|(2-s\frac{d}{a})\right| + \frac{1}{2}s^2 \tag{E.16}$$

$$E'_3 = \frac{1}{4\mu}\left|(\kappa-3+2s\frac{d}{a})\right| + \frac{1}{2\mu}s^2 \tag{E.17}$$

$$E'_4 = \frac{1}{4\mu}\left|(\kappa+3-2s\frac{d}{a})\right| + \frac{1}{2\mu}s^2 \tag{E.18}$$

Noting the behaviour of $\frac{K_{ij}}{\Delta(\frac{s}{a})}$ (eqn (4.69)) and that $\frac{d}{a} > 1$, the integral $\int_0^{+\infty} g(s)\,ds$, which does not depend on η, is convergent. Thus, the integral (E.11) is also uniformly convergent with respect to η. $\frac{\partial}{\partial\xi}K^*(\xi,\eta)$ is a finite and continuous function of η via eqn (E.12). Therefore, the integral in eqn (E.13) exists, i.e. $\frac{d}{d\xi}\left[\frac{\Phi(\xi)}{\sqrt{\xi}}\right]$ is finite.

Following the same procedure as used to obtain eqn (E.7), it can be shown that the improper integrals of $K(\xi,\eta)$ in eqn (4.62) and of $K^*(\xi,\eta)$ in eqn (4.75) are uniformly convergent with respect to ξ for any $\eta \in [0,1]$, and they are also uniformly convergent with respect to η for any $\xi \in [0,1]$.

Appendix F

Behaviour of the Smoothing Function

Here, we shall show the closeness of the two functions expressed in eqns (9.36) and (9.37), i.e. the original $F = \min(f_1, f_2)$ and the weighted smoothing approximation $\mathcal{F}$.

As an example, let us assume

$$f_1 = \sin^2 x \tag{F.1}$$

$$f_2 = \sin^2 2x \tag{F.2}$$

which are similar to the trigonometric functions appearing in f_t and f_s of eqns (9.22)–(9.23).

Using the expressions for α and β (eqns (9.44)–(9.45))

$$\alpha = \frac{1}{2}[1 - \tanh A(f_1 - f_2)] \tag{F.3}$$

$$\beta = \frac{1}{2}[1 + \tanh A(f_1 - f_2)] \tag{F.4}$$

we get

$$\mathcal{F} = \alpha f_1 + \beta f_2 \tag{F.5}$$

The variations of F and $\mathcal{F}$ with x for $A = 100$ and $A = 2000$ are shown in Figures F1 and F2, respectively. At the scale used in Figures F1(a) and F2(a), the difference between these two functions can hardly be seen. A deviation at the corner in Figure F1(a) can be seen in Figure F1(b) on a magnified scale. But when $A = 2000$, no deviation is seen even on the magnified scale in Figure F2(b). The two curves are practically indistinguishable.

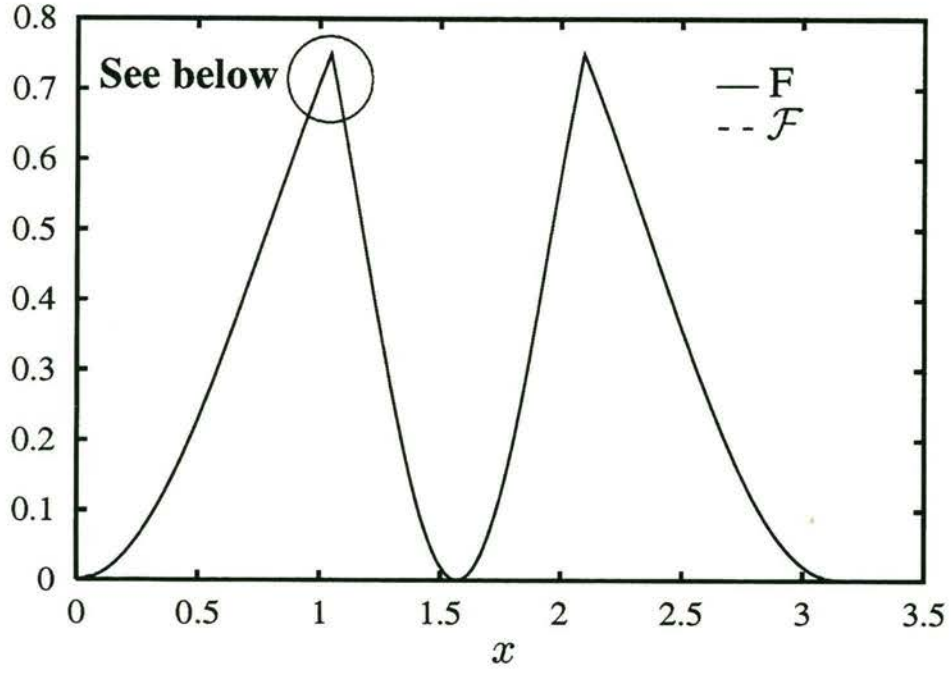

Figure F1(a): Comparison of F and $\mathcal{F}$ when A=100

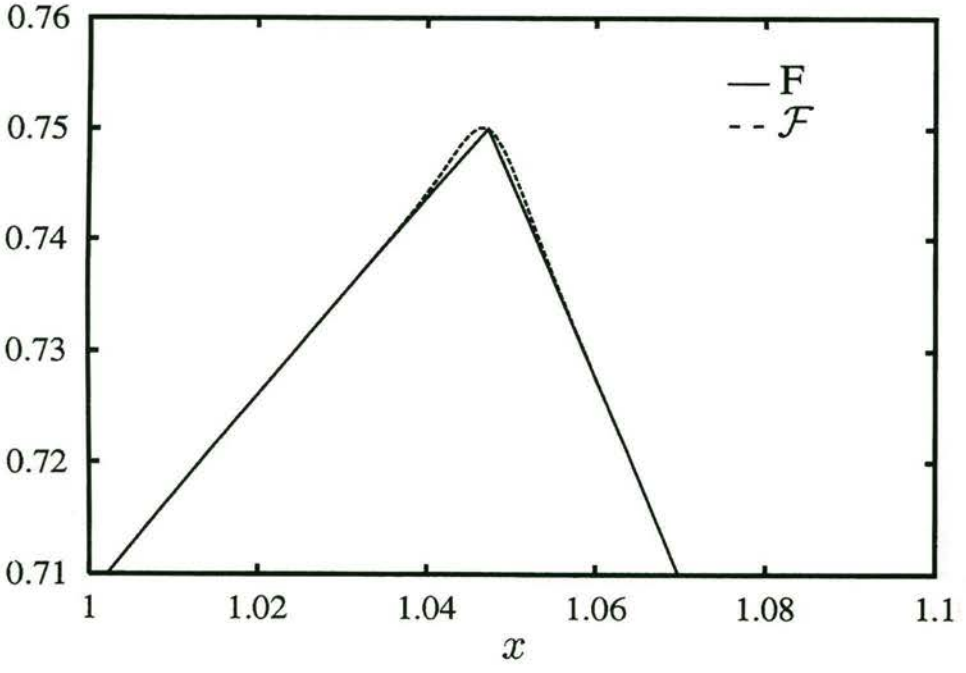

Figure F1(b): Comparison of F and $\mathcal{F}$ near a corner when A=100 on a magnified scale

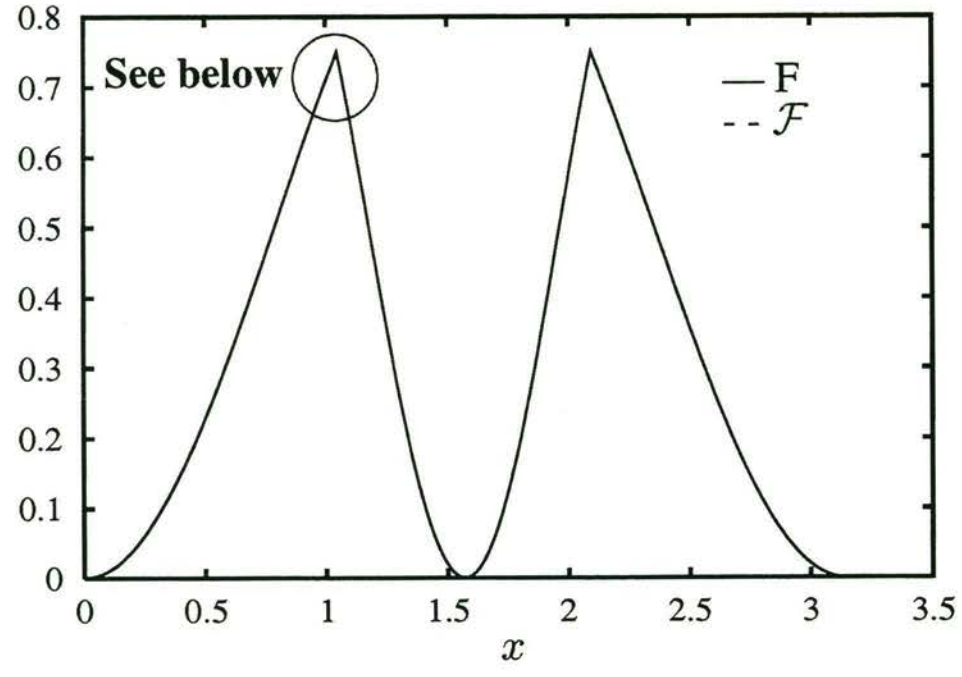

Figure F2(a). Comparison of F and $\mathcal{F}$ when A=2000

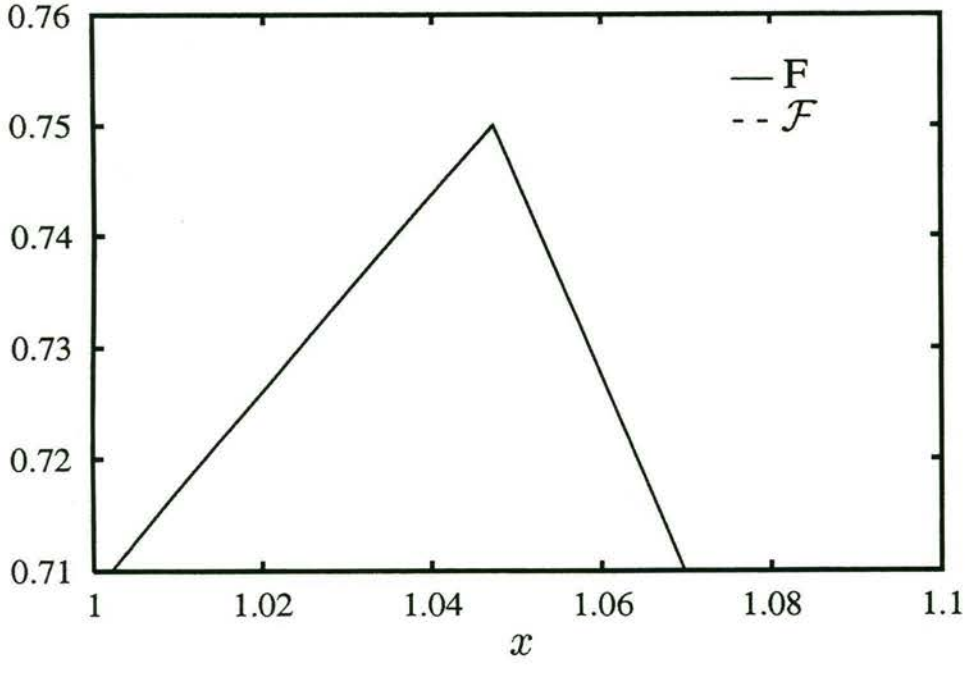

Figure F2(b). Comparison of F and $\mathcal{F}$ near a corner when A=2000 on a magnified scale